DEVELOPMENT OF A PROBABILISTIC SEISMIC RISK ASSESSMENT FRAMEWORK FOR CRITICAL INFRASTRUCTURE IN WEST AFRICA (PSRA CIWA)

A thesis submitted to

THE UNIVERSITY OF MANCHESTER

for the degree of

DOCTOR OF PHILOSOPHY (PhD)

In the Faculty of Sciences and Engineering

2022

Irinyemi A. Stephen

School of Mechanical, Aerospace and Civil Engineering

(This page is intentionally left blank)

Irinyemi A. Stephen
PhD in Geotechnical Earthquake Engineering (2021)
University of Manchester (UK)

TABLE OF CONTENTS

Irinyemi A. Stephen
PhD in Geotechnical Earthquake Engineering (2021)
University of Manchester (UK)

Irinyemi A. Stephen
PhD in Geotechnical Earthquake Engineering (2021)
University of Manchester (UK)

Irinyemi A. Stephen
PhD in Geotechnical Earthquake Engineering (2021)
University of Manchester (UK)

Irinyemi A. Stephen
PhD in Geotechnical Earthquake Engineering (2021)
University of Manchester (UK)

LIST OF TABLES

Irinyemi A. Stephen
PhD in Geotechnical Earthquake Engineering (2021)
University of Manchester (UK)

LIST OF FIGURES

Irinyemi A. Stephen
PhD in Geotechnical Earthquake Engineering (2021)
University of Manchester (UK)

Irinyemi A. Stephen
PhD in Geotechnical Earthquake Engineering (2021)
University of Manchester (UK)

LIST OF PUBLICATIONS

Journal Publications

1. *Paper title:- Probabilistic seismic hazard assessment for West Africa region*
   Authors:- Irinyemi A. Stephen, Lombardi, D., & Syed M, A.
   Journal Name:- Georisk
   Status:- Published Online, 15 July 2021.
   DOI:10.1080/17499518.2021.1952608

2. *Paper title:- Seismic risk analysis for large dams in West Coast basin, southern Ghana*
   Authors:- Irinyemi A. Stephen, Lombardi, D., & Syed M, A.
   Journal Name:- Journal of Seismology
   Status:- Published Online, 29 September 2021.
   DOI:10.1007/s10950-021-10045-w

3. *Paper title:- Dynamic response and stability analyses of Akosombo dam using numerical analysis*
   Authors:- Irinyemi A. Stephen, Lombardi, D., & Syed M, A.
   Journal Name:- International Journal of Advanced Research
   Status:- Published Online, 19 October 2021.
   DOI: 10.21474/IJAR01/13588

4. *Paper title:- Seismic risk analysis for large dams in West Africa Region*
   Authors:- Irinyemi A. Stephen, Lombardi, D., & Syed M, A.
   Journal Name:- Earth Science
   Status:- In Press

5. *Paper title:- Seismic hazard assessment in Guinea, West Africa*
   Authors:- Irinyemi A. Stephen, Lombardi, D., & Syed M, A.
   Journal Name:- Scientific Reports
   Status:- Published online, 16 February 2022.

DOI: https://doi.org/10.1038/s41598-022-06222-7

Peer-reviewed Conference Publications

1. *Paper title:- Seismic risk analyses for southern part of Ghana*
   Authors:- Irinyemi A. Stephen, Lombardi, D., & Syed M, A.
   Conference Name:- MACE PGR Conference 2021. 25th – 27th May 2021
   Status:- Accepted

ABSTRACT

Dams are essential infrastructures for human activities and the economic development of a region. Therefore, dam safety is a priority, particularly regarding natural events like earthquakes. Furthermore, since past seismic activities revealed damage to dams and their host environments, it is required to perform a seismic risk assessment to identify the criticalities and prevent damage consequences. The research illustrates a probabilistic framework for seismic risk assessment of critical infrastructure in West Africa for such reasons.

West Africa is a stable continental with a few reported earthquake magnitudes greater than 5, mainly the 1939 M_w 6.4 Accra (Ghana) and 1983 M_w 6.3 Northwest Guinea earthquakes. Earlier studies tried to assess the region's seismic hazard but only focused on the narrow area close to the Gulf of Guinea. Their assessments produced seismic hazard maps for a 475-year, but the current study examined a wider area based on updated earthquake catalogue of West Africa with higher return periods. Deaggregation was also introduced to identify the dominant earthquake scenario for Accra. It was observed that the prevalent scenario is dominated by seismic events between magnitudes 5.5-6.0 and at a distance less than 60 km. However, despite the encouraging results from earlier hazard assessments, it was limited to old-outdated ground motion prediction equations (GMPEs). Also, the seismic hazard assessments (SHA) obtained was only for a 475-year return period; thereby, the outcome can only be used for building code. Consequently, a probabilistic seismic hazard assessment (PSHA) was developed using R-CRISIS software to build seismic codes for the region and critical infrastructures such as large dams, lifelines, and power plants.

Assessing the potential seismic risk for large dams across the region of West Africa was done to determine the dams' most vulnerable based on the method proposed by Bureau (2003). The assessed dams are based on the seismicity within the dam sites and their physical properties and locations risks. The development of the Bureau (2003) method requires different factors and weighing points of the types of dams, age, reservoir capacity, downstream risk potential, and vulnerability. Hence, this was achieved by combining the probabilistic seismic hazard assessment (PSHA) at the dam sites and the risk rating of the dam structures to estimate the total risk factor (TRF) of the dams.

A non-linear time history recorded data was used to implement non-linear numerical procedures to estimate the region's most critical dam (Akosombo dam) behaviour. Nineteen real accelerograms were obtained from the Pacific Earthquake Engineering Research Center (PEER) ground motion website and European strong-motion (ESM) database and processed by SeismoSignal. In addition, PLAXIS 2D is used for numerical analysis. As a result, dynamic deformations and factors of safety were obtained for the dam.

Irinyemi A. Stephen
PhD in Geotechnical Earthquake Engineering (2021)
University of Manchester (UK)

DECLARATION

I hereby declare that no portion of the work referred to in the thesis has been submitted in support for another degree or qualification of this or any other university or other institutes of learning.

Irinyemi A. Stephen
PhD in Geotechnical Earthquake Engineering (2021)
University of Manchester (UK)

COPYRIGHT STATEMENT

I. The author of this thesis (including any appendices and/or schedules to this thesis) owns certain copyright or related rights in it (the "Copyright") and he has given The University of Manchester certain rights to use such Copyright, including for administrative purposes.

II. II. Copies of this thesis, either in full or in extracts and whether in hard or electronic copy, may be made only in accordance with the Copyright, Designs and Patents Act 1988 (as amended) and regulations issued under it or, where appropriate, in accordance with licensing agreements which the University has from time to time. This page must form part of any such copies made.

III. The ownership of certain Copyright, patents, designs, trademarks and other intellectual property (the "Intellectual Property") and any reproductions of copyright works in the thesis, for example graphs and tables ("Reproductions"), which may be described in this thesis, may not be owned by the author and may be owned by third parties. Such Intellectual Property and Reproductions cannot and must not be made available for use without written permission of the owner(s) of the relevant Intellectual Property and/or Reproductions.

IV. Further information on the conditions under which disclosure, publication and commercialisation of this thesis, the Copyright and any Intellectual Property and/or Reproductions described in it may take place is available in the University IP Policy (see http://documents.manchester.ac.uk/DocuInfo.aspx?DocID=24420), in any relevant Thesis restriction declarations deposited in the University Library, the University Library's regulations (see http://www.library.manchester.ac.uk/about/regulations/) and in the University's policy on Presentation of Theses.

Irinyemi A. Stephen
PhD in Geotechnical Earthquake Engineering (2021)
University of Manchester (UK)

ACKNOWLEDGEMENTS

I am excited to express my most profound gratitude to Dr Domenico Lombardi and Dr Syed M. Ahmad for allowing me to undergo my PhD under their supervision and for such an exciting research topic. I am in debt to them for their thorough and patient care throughout the development of this thesis. My special thanks to Dr Domenico Lombardi for his painstaking efforts in getting my first published paper.

I acknowledge the financial support from Petroleum Technology Development Funds (PTDF), the government of Nigeria under the Presidential Special Scholarship Scheme for Innovation and Development (PRESSID), towards funding this research. I will always reference PTDF for what they have done.

I would also like to thank Professor Mario Ordaz, Institute of Engineering of the Mexican National University (II-UNAM) and Dr Mario Sagado-Gálvez, Disaster risk financing and cat-risk specialist, Greater Barcelona Metropolitan area, for providing the software, R-CRISIS, to perform the seismic hazard calculations.

Special thanks to Iziengbe Inerhunwa for his friendship and encouragement during the PhD research programme. Many thanks to my friends: Abiodun Sholanke, Dr Godstime A. Okudolor and Abdullahi A. Aneco, Mfonobong Moses, Agu Ojugbo Peter who have become my bosom friends in England.

Finally, I want to thank my lovely wife, Mrs Edith Bolanle Irinyemi, for encouraging me throughout my research project. Without her marital, spiritual, and financial support, my dream of completing PhD research programme would not have been possible.

DEDICATIONS

I dedicate this work to my late mother, who died on the 16th of April 2016, my father, my care and loving wife, my children, my friends who supported and encouraged me during this PhD research.

CHAPTER 1

INTRODUCTION

1.1 General overview

A natural hazard such as earthquakes is known for its devastating impact on people, the economy, and the built environment. With climate change, land use act, and increases in population density, poverty, political instability, illiteracy, and poor infrastructure development, West African countries are more vulnerable to damaging potential caused by earthquakes. Though it is almost difficult to prevent the effects of earthquakes, adequate measures and steady preparedness are required to minimize the potential risks of such disasters.

Earthquakes have historically been known to cause the most extensive impact and damage to infrastructure, human casualties, and significant economic losses (Oliveira et al., 2006). Ambraseys and Adams (1986) document several West African earthquakes from 1615 to 1984. In addition to large earthquakes in Ghana, their research also identified a strong earthquake in Guinea (1983) and moderate earthquakes near Abengourou (1879), Djidja (1788), and Tombouctou (1618), all of which have now developed into major cities with more populations. Musson (2004) provides the seismicity of West Africa from 1615 to 2009. Therefore, the risk assessment of critical infrastructure such as dams is one of the essential processes for design, inspecting and continued operation period for the infrastructure. Moreover, the safe operation of critical infrastructure in West Africa is a key for economic development and sustainability since the damage from infrastructure could affect the region's social, cultural, and economic structures.

To fully characterise the seismic risk across the West Africa region, each of the three major components that contribute to the risk needs to be studied in detail:

1. The seismic hazard component involves estimating the levels of shaking intensity that can be expected to occur in the study region and their frequencies of occurrence.
2. The exposure component describes critical infrastructure's geographical distribution and physical characteristics, such as dams.

Irinyemi A. Stephen
PhD in Geotechnical Earthquake Engineering (2021)
University of Manchester (UK)

3. Dam behaviour due to earthquake loading to determine its susceptibility to the excitation of earthquakes.

Seismic hazard assessment requires quantitative analysis of many interrelated factors that may be characterised by significant uncertainties as epistemic and aleatory. The epistemic uncertainty, the dominant source of uncertainty in natural hazard assessment, reflects the incomplete knowledge of the nature of all inputs to the assessment, the variability of the interpretation of available data, and the limitations of the technique applied for the analysis. For example, all parameters of the PSHA input models (location and shape of seismic source zones, size and orientation of earthquake sources, maximum magnitudes, the depth distribution of earthquake sources, recurrence relations, etc.) requires consideration of epistemic uncertainty.

Probabilistic seismic risk assessment is a complex process that involves analysing different parameters, including some degree of uncertainties. Therefore, seismic risk analysis covers a wide area and could be time-consuming during the assessment of West Africa. But this thesis creates the procedure for assessing seismic hazard levels for some important cities and potential seismic risks associated with critical dams in West Africa. Seismic safety is one serious concern for every seismic prone region in the world. However, in many seismically affected regions like China, the USA and Japan, technological and economically feasible programs and procedures have helped to minimise the level of risk in these regions.

According to International Commission on Large Dams (ICOLD) standard, over 150 large dams are built across the West Africa region's rivers (Skinner et al., 2009). These dams have increased water storage capacity and regulated watercourses that have improved the economic development of the region's countries over the years.

Many of these dams are located in Nigeria and Burkina Faso, with some situated in Ghana, Guinea, Côte d'Ivoire, Mali etc. The first large dam built in the region based on ICOLD definition is the Akosombo dam in 1964. The dam was constructed to generate energy for the host environment. The first part of this report reviews the tools and approaches currently in use to estimate the seismic hazard in the region. The second part describes a simplified approach by Bureau (2003) to analyse the seismic risk of large

dams to prioritise the safety of dams in the West Africa region. Finally, numerical analysis is conducted on the Akosombo dam to study the dynamic behaviour of the dam.

PSHA is regarded as the most widely used method for assessing seismic hazards. It is used as input parameters for seismic-resistant structures design and links to risk assessment, evaluation, and seismic risk mitigation, among other applications. Significant improvements to the first proposal of PSHA by Cornell (1968) have been implemented. Kulkarni et al., 1984; Giardini et al., 2004; Deif et al., 2011 introduced the use of logic trees to PSHA. The representation of the hazard results using deaggregation are presented (Bazzurro and Cornell, 1999; Kramer 1996; McGuire, 1995). McGuire (2008) presented a concise and candid historical outline of the early history of PSHA. Although PSHA has been widely used for evaluating seismic hazards, there is some degree of uncertainties in performing and interpreting hazard results in a PSHA framework (Bommer et al., 2015; Bommer and Abrahamson, 2006; Bommer and Scherbaum, 2008). The reasons for this have been explained in their published works.

The first recorded dam failure due to the earthquake occurred during the 1886 Charleston, SC earthquake (Bureau, 2003). The location of dams close to the densely populated area presents a potential risk to the downstream population and properties during earthquake damage. The seismic performance of dams is closely related to the fill material's nature and state of compaction. Well-compacted dams are capable of withstanding substantial earthquake shaking without detrimental effects. For example, (Bureau, 2003) has found out that a compacted dam built of clayey materials on competent foundations and rockfill dams has shown excellent stability under extreme earthquake loading. The bureau (2003) method provides various factors and weighing points that quantify the total risk factor of any selected large dam. The total risk factor depends on three components: (1) dam structure influence, (2) downstream hazard factors, and (3) the dam vulnerability rating. The dam structural component is represented by the sum of the capacity risk factor (CRF), height risk factor (HRF) and the age risk factor (ARF). The downstream hazard factor is based on the population of people, and the public and private properties at the flood paths. The site-dependent seismic and observed performance of similar dams characterised the vulnerability rating. An example of the Bureau method has been demonstrated in China, Turkey, and South

Africa dams to estimate total risk and seismic analysis of large dams across various basins (Chin and Lin, 2018; Tosun et al., 2007; Tosun and Seyrek, 2010; Singh et al., 2011).

Evaluating the effects of earthquakes on embankment dams and the safety of the dams during and after earthquakes remained an important issue when designing earth and rockfill dams. A report by Fell et al. (2005) shows the percentage of failure of some earth dams during earthquake loading. The unexpected behaviour and unknown factors affecting the response of dams during earthquake loading are serious engineering problems (Kan and Taiebat, 2011). Different methods have been proposed to analyse earth/rockfill embankment dams subjected to earthquake; among them is Pseudo static stability analysis, simplify dynamic analysis, complex numerical analysis, etc. In this thesis, numerical modelling of the dynamic performance of the dam to estimate the crest settlement and safety of the dam is presented. In the dynamic analysis, finite element (PLAXIS Software) is used to simulate the non-linear dynamic behaviour of the Akosombo dam. Different researchers have used this software to evaluate the numerical behaviour of dams (Sengupta, 2010; Albano et al., 2012; Afiri and Gabi, 2018; Selçuk and Terzi, 2015).

This thesis aims to explore and use the previously listed methods to develop the framework for the risk assessment in West Africa region.

1.2 Research Objectives

This research work aims to determine the probabilistic level of seismic hazard and seismic risk for the West Africa region and its critical infrastructure to prepare for future seismic activities. Hence, the objectives are listed below:

- ***Objective 1:*** *Estimate seismic hazard levels for some significant cities in West Africa using PSHA.*

- ***Objective 2:*** *Compare the seismic hazard assessment of the West Africa region with already published seismic hazard analysis for some parts of West African cities.*

- ***Objective 3:*** *Prepare seismic hazard maps (475, 2475 and 9975 years) for West Africa region.*

- ***Objective 4:*** *Update earthquake catalogue for the region.*

- ***Objective 5:*** *Prioritise seismic risk for critical dams in the region.*

- ***Objective 6:*** *Determine the dynamic response of the Akosombo dam using numerical simulation.*

1.3 Thesis organisation

The thesis is organised based on the alternative format to a well-known traditional thesis. The main context is presented in published/In Press/submitted research journals and peer-reviewed papers. The PhD thesis collection of papers format requires that all references be compiled and grouped under "References" at the end of all the thesis chapters.

Chapter 2 reviews academic and commercial research works related to the general concepts of probabilistic seismic hazard assessment. As a result of the alternative format presented for this thesis, the literature review conducted throughout Chapter 2 was limited to a general overview of probabilistic seismic hazard assessment. However, each chapter (i.e., Chapters 3-7) contained an additional literature review to be read without reference to the rest of the thesis.

Chapter 3 detailed description of the research methodology used for the estimation of seismic hazard assessment for West Africa are provided which includes research tools adopted for the for collection of data, processing and viewing, editing and analysing the outputs of seismic hazard assessment.

Chapter 4, titled "Probabilistic Seismic Hazard Assessment for West Africa Region", is the first step that connects the other chapters.

It is intended to estimate the seismic hazards for important cities and critical infrastructure based on a probabilistic approach. First, the formulation of the chapter is explained in detail to provide an insight into the probabilistic analysis method for interested readers and the broader societies. The derivations start by assessing the seismic hazard of a larger area within the study region. The next level of complexity is a modified and updated catalogue for West Africa, determined through the combination of published catalogues and online bulletins available for the study region. Next, the seismic source model for this chapter is developed by dividing the study region into fourteen seismic

source zones based on the geological-tectonic features and spatial distribution of historical and instrumental events—another layer of complexity in accounting for uncertainty due to limited knowledge implemented in a logic-tree formation. In the final step, seismic hazard estimates are computed for different return periods in terms of hazard maps, response spectra and hazard curves.

Chapter 5, or "Seismic hazard Assessment in Guinea, West Africa Region", uses the same approach as Chapter 3. This chapter discusses the seismic hazard analyses for ten cities and the Guinea region because of major earthquakes reported within the region. This study provides the seismic hazard levels for the region and ten cities.

Chapter 6, "Seismic risk analysis for large dams in West Africa Region", using a simplifying method proposed by Bureau (2003). Chapter 5 analyses the seismic risk associated with seventeen dams where histories of seismic activities have been reported within a 300 km radius of the dam sites. The seismic hazard assessment is developed using the approach from chapter 3. Different representations of the seismic hazards and seismic risk analyses results are illustrated and discussed in this chapter.

Chapter 7, "Seismic risk analysis for large dams in West Coast basin, Southern Ghana", uses the same method from chapter 5. This chapter estimated the seismic risk for three large dams in Ghana because of their economic advantages. In the first section of this chapter 6, the seismic hazard is computed using area source zones within Ghana as proposed by Ahulu et al. (2018). The seismic hazards and seismic risk analyses results are also presented in this chapter.

Chapter 8 presents the dynamic response and stability analyses of Akosombo dam using numerical analysis. The dynamic response and earthquake resistance of the Akosombo dam using non-linear dynamic time histories is investigated. The dam was first analysed under static conditions and then performed acceleration-time histories using 19 earthquakes. Also, the factor of safety was calculated by the drawdown reduction method. Based on the findings of this chapter, different results of dynamic deformations, factors of safety and recommendations for a site inspection of the dam are presented.

Finally, **Chapter 9** summarises the main findings of the research conducted from Chapters 3 to 7, discussing the conclusions and recommendations for the future.

CHAPTER 2

LITERATURE REVIEW

This chapter commences by presenting a general overview of probabilistic seismic risk assessment (PSRA), including detailed explanations of the vital stages (i.e., Earthquake source catalogue, Seismicity Model and Ground-motion prediction equations (GMPEs)), for estimate risk assessment. The chapter then proceeds to explain PSHA. Finally, reviews of past reported research studies on methods commonly used to estimate seismic hazard and risk analysis are presented.

2.1 Overview of PSRA

PSRA mostly estimates the probability of damage and loss, for critical infrastructure such as dams. The main structures of a PSRA for dams for this research comprises the seismic hazard models (i.e., to get the probability of exceedance for 50 years), the exposure model (location and characteristics of dams within the region) and dam vulnerability (i.e., the behaviour of dam to seismic excitations).

In probabilistic seismic risk assessment, all possible and relevant earthquake scenarios capable of causing ground shaking at the site of interest are considered together with ground probability levels (Crowley, 2014). In research, there are two approaches that are commonly used in practice seismic risk assessment. Both approaches are combined to estimate seismic risk assessment for dams.

1. PSHA (i.e., calculating the rate or probability of exceedance of a set of intensity measure levels (IMLs). More explanations on PSHA are presented in section 2.5.

2. Seismic risk analysis is also known as the Bureau (2003) method. The method was initially developed for earthquake risk and loss estimation programs in the State of Caroline (URS Corporation et al., 2012; Singh et al., 2011). More explanations are shown in section 2.8

2.2 Earthquake catalogue

For accurate seismic hazard assessment (SHA), reliable and homogenous earthquake catalogues are required as input parament. These consist of estimates of past seismic events, characterised by spatial distribution, time of occurrence, the co-ordinate, and the magnitudes of events of a particular region or site of interest (Aldama-Bustos, 2009). In addition, earthquake catalogue is used for different aspects of assessment such as source parameter calculations, delineation, seismotectonic, recurrence, hazard analysis and M_{max} determination (Woessner and Wiemer, 2005; Midzi et al., 2020).The homogeneity of earthquake data reflects the accuracy of SHA results. A specific site's geology, seismo-tectonic setting, and earthquake catalogues are vital factors for constructing the seismicity model, which are elements needed for seismic hazard assessment. A collection of earthquake catalogues should include Paleoseismic, historical and instrumental data available in any region of interest. Compilation of historical catalogue requires interpreting reports of felt and damaging effects and transforming them into macroseismic intensities. Then, empirical relationships based on modern data is used to determine earthquake magnitudes and epicentres from the observed intensity distribution of the seismic events. A compiled catalogue required the conversion of macroseismic data to the magnitude of different scales (Stromeyer, 2004).

Though instrumental seismicity began around 1900, the study of earthquakes was based on the collection of contemporary reports of seismic events from felt areas, diplomatic notes, newspapers, diaries, church records and paintings. In addition, instrumental earthquakes have been reported (Ambraseys and Adams, 1986; Ambraseys and Melville, 1982; Musson, 2004).

The seismic networks required to monitor seismic activities was first established in 1898 by John Milne, an Englishman, where about 30 monitoring stations are situated in different areas. According to (Stoneley, 1970), the first global earthquake catalogue agency, International Seismological Summary (ISS), established in 1922, reported the global earthquake catalogue between 1918 and 1963. In 1964 the ISS was changed to International Seismological Centre (ISC), with a more powerful computer monitoring programme considered the most dependable in earthquake locations. However, much uncertainty remained in-depth estimation of events around this time. In 1928, another reporting agency called the U.S. Coast and Geological Survey (USCGS) started

producing the Preliminary Determination of Epicentres (PDE), which is conducted by the National Earthquake Information Centre (NEIC), part of the United States Geological Survey (USGS). Other agencies that reported earthquake data are Incorporated Research Institutions for Seismology (IRIS) established in 1986, National Oceanic and Atmospheric Administration (NOAA), now National Centers for Environmental Information, which began in 1970. GEM-Global Earthquake Model in 2018. Other agencies with broad knowledge of earthquake coverage are the International Institute of Earthquake Engineering and Seismology (IIEES) established in 1989, and the European Mediterranean Seismological Centre (EMSC), formed in 1975.

The above-listed earthquake catalogues are usually recommended as reliable earthquake data for use in seismic hazard analysis. In addition, improved instrumental earthquake catalogues where about 100,000 seismic events were relocated as reported by Engdahl et al. (1998) and macroseismic based catalogues by Ambraseys et al. (1994) are encouraged use as a reliable earthquake database in the hazard analysis.

2.2.1 Catalogue completeness

A statistical analysis of the earthquake catalogue requires assessing the completeness of the data in the earthquake catalogue. An earthquake catalogue is affected by incompleteness in both location and time due to the paucity of historical and instrumental seismicity data. Catalogues are to be incomplete at various threshold magnitudes and at different time periods. A minimum (Threshold) magnitude (M_O) is considered the magnitude above which all seismic events are reported. Earthquake catalogues may be biased against small events due to the low sensitivity of the recording instruments and sparse recording station density during the past (Stepp, 1972). It is shown that an incomplete catalogue may usually lead to erroneous estimation of the seismicity parameters, and thus, completeness assessment is required (Bashir and Basu, 2018).

The incompleteness of an earthquake mostly depends on the following factors (Aldama-Bustos; 2009):

- Demographic variations
- Historical and socio-economical contexts
- Macroseismic intensity

- Development of seismic networks of a particular region

Estimating the threshold magnitudes at different time periods in an earthquake catalogue has been reported in the literature (Stepp, 1972; Rotondi and Garavaglia, 2002; Woessner and Wiemer, 2005).

2.2.1.1 The Stepp (1971) method

One of the first methods of completion analysis was the Stepp (1972) method which is based on the assumption that a Poisson distribution can model the number of earthquakes (K) within a unit time interval:

$$\bar{\lambda} = \frac{1}{N}\sum_{i=1}^{N} \lambda_i \qquad (2.1)$$

where λ_i and N are rate of occurrence of events per unit time interval for the i*th* subclass of the event set, and the number of sub-classes, respectively. With variance $\sigma_\lambda{}^2 = \bar{\lambda}/T$. Thus, for a sample length T, the standard deviation of the mean can be defined as:

$$\sigma_\lambda = \sqrt{\bar{\lambda}/T} \qquad (2.2)$$

Assuming stationarity, the mean rate of occurrence and variance should remain constant; hence σ_λ behaves as $1/\sqrt{T}$ in the interval where the mean rate of occurrence also remains constant. If the observed departed of σ_λ from the $1/\sqrt{T}$ behaviour explain the incomplete earthquake data of sample reported.

The Stepp (1972) method provides a valuable overview of temporal variation in completeness analysis, but the precise value of the magnitude of completeness (M_c) depends on the magnitude sub-classes adopted.

2.2.1.2 Maximum curvature method

The Maximum Curvature method is one of the simplest methods which provide robust analysis (Wiemer and Wyss, 2000; Woessner and Wiemer, 2005). The method assumed that the cumulative magnitude-frequency follow a power-law distribution whereby the absolute number of events for each magnitude range increases at lower magnitudes,

where the number of events begins to decrease below the magnitude of completeness (Weatherill, 2010). The assumption means that the magnitude of completeness is the magnitude that most frequently occurs. However, this simple method may lead to underestimating or overestimating M_C for some catalogue of events. Figure 2.1 shows the result of Maximum curvature approach by computing the maximum value of the first derivative of the frequency magnitude curve (Woessner and Wiemer, 2005).This assumes that the number of events decreases below M_C, yet the absolute number of events does not necessarily have to decrease to deviate from the power-law behaviour. For example, it may be the case that there is an increasing deficit of more minor earthquakes within the catalogue. This will produce a gradual deviation from the expected power-law without necessarily producing a peak in the absolute number of events of a particular magnitude, thus lowering M_C.

2.2.1.3 Goodness of Fit Test (GFT)

GFT method estimates MC by comparing the observed Gutenberg-Richter relation for the cumulative magnitude-frequency distribution with the synthetic method (Wiemer and Wyss, 2000). The technique is computed as the absolute difference in the number of events in the magnitude bins between synthetic Gutenberg-Richter distribution and observed (Woessner and Wiemer, 2005).

Synthetic distributions estimated using *a*- and *b*-values of the observed dataset for which $M \geq M_{co}$ functions as ascending cut-off magnitudes M_{co}. R-value determines the fit in percentage with observed frequency-magnitude distribution and is computed using the cut-off magnitude(Woessner and Wiemer, 2005). Figure 2.2 shows the model at R-value at which a predefined percentage (90% or 95%) of the observed data was modelled by a straight line.

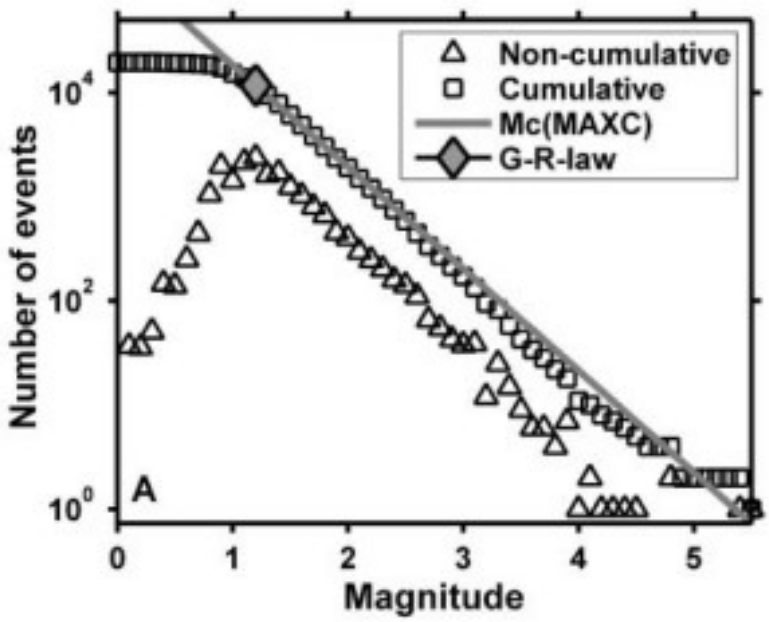

Figure 2.1. Frequency-magnitude distribution of the subset of the Northern California Seismic Network (NCSN) catalogue. The result of the Maximum curvature approach is shown by diamond (Woessner and Wiemer, 2005).

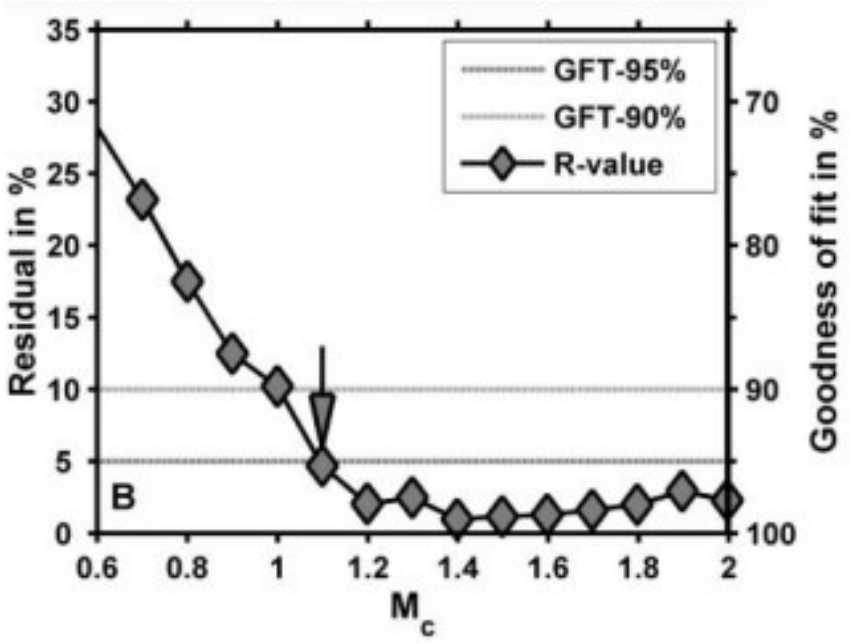

Figure 2.2. Residuals and goodness-of-fit value R for the GFT-method. R is the difference between the observed and synthetic FMDs, in terms of Mc. Dashed horizontal lines displayed magnitudes 90% and 95% of the observed data modelled by a straightline fit (Woessner and Wiemer, 2005).

2.2.1.4 *b*-value stability

A method by Cao and Gao (2002) estimated *M*c using the stability of the *b*-value in terms of cut-off magnitude (M_{co}). This model is based on the assumption that *b*-values ascend for $M_{co} < Mc$, remain constant for $M_{co} \geq M_c$, and which also ascend again for $M_{co} \geq Mc$. However, If $M_{co} \leq M_c$, the resulting *b*-value will be too low (Woessner and Wiemer, 2005).

*M*c is defined as the magnitude at which the change in *b*-value, $\Delta b(M_{co})$ for two successive M_{co}, is believed to be smaller than 0.03. More explanations are presented in Woessner and Wiemer (2005).

2.2.1.5 Cumulative Visual Inspection (CUVI) Method

Another method of estimating M_C is the Cumulative Visual Inspection Method (VCMI) based on plots of the cumulative number of seismic events of different magnitude intervals versus time. The method is efficient for limited event data (Shukla and Choudhury, 2012; Bashir and Basu, 2018). The CUVI method is based on the visual method for assessing catalogue completeness, based on the plot of the cumulative number of events, which is very easy to apply efficiently for limited event data. Shukla and Choudhury (2012) used Cumulative Visual (CUVI) method for catalogue completeness for Gujarat for $M_w \geq 4$.

2.3 Seismicity Models

The seismic model defines the key to making credible estimates and expressing uncertainties about future earthquakes' source properties and effects (McGuire, 2004). The seismicity model identifies the seismic sources and maximum-magnitude events that could occur within each source. It characterises the spatiotemporal distribution of seismic events within a region (Goda et al., 2003). In deterministic seismic hazard analysis (DSHA), the shortest source-to-site distance prefers to use for analysis. Though, on some occasions, the analyst usually defines a "credible" source-to-site distance.

In PSHA, the seismicity model defines and characterises all the earthquake sources as in DSHA but with the difference that the probability distribution of potential future

earthquakes needs to be characterised. PSHA considered the location of the future earthquake equally likely to occur anywhere within the seismic source. In DSHA, the largest earthquake is hypothesised to appear at the worst location for the site. It is essential to highlight that future seismicity may not demonstrate uniformity within a source, not over the short term and might not over a long time. In other words, these assumptions only represent the present understanding of regional seismicity (McGuire, 2004). When enough information exists to justify the non-uniform spatial distribution of the seismicity within a given source, two area sources could represent earthquake occurrence. For example, well-studied faults, like San Andreas Fault, are often divided into segments where rupture recurrence are preferentially restricted in each segment separately. However, multiple segments may rupture in large earthquakes. In addition, PSHA defines the temporal distribution of earthquake occurrence for different magnitudes at the respective seismic source. The temporal distribution of the seismicity is represented by recurrence relationships (Gutenberg and Richter, 1944) that consider an exponential recurrence model consistent with the recurrence statistics for large areas. Seismicity models require a declustering earthquake catalogue of independent events to calculate earthquake rates (Petersen et al., 2010). PSHA is considered in this research over the DSHA for seismic hazard analysis because by following probabilistic method the economic life of most structures can be envisioned at the planning stage, it quantifies uncertainties associated with input parameters for the model and combine them to produce an explicit description of the distribution of future shaking that may occur at a site of interest. PSHA defined as the annual probability of a ground motion being exceeded at a site, while the DSHA defined as the ground motion from individual earthquake that have maximum impacts at a particular site.

Youngs and Coppersmith (1985) propose a characteristic recurrence model that may better represent the seismic activity in subduction zones or major faults in continental regions. In these areas, the largest events occur quasi-periodically with little or no earthquakes expected with magnitudes in the interval immediately below the characteristic earthquake's size; earthquakes with smallest and medium-size magnitudes are expected to follow the Gutenberg and Richter relationship. Figure 2.3 displays the magnitude-frequency plots with characteristic earthquake behaviour. In some seismic hazard analyses, the Gutenberg and Richter (1944) model doubly bounded is used (Cornell and Vanmarcke, 1969) instead of the untruncated method. The two most

commonly used earthquake recurrence models are ones presented by Gutenberg and Richter (1944) and Youngs and Coppersmith (1985).

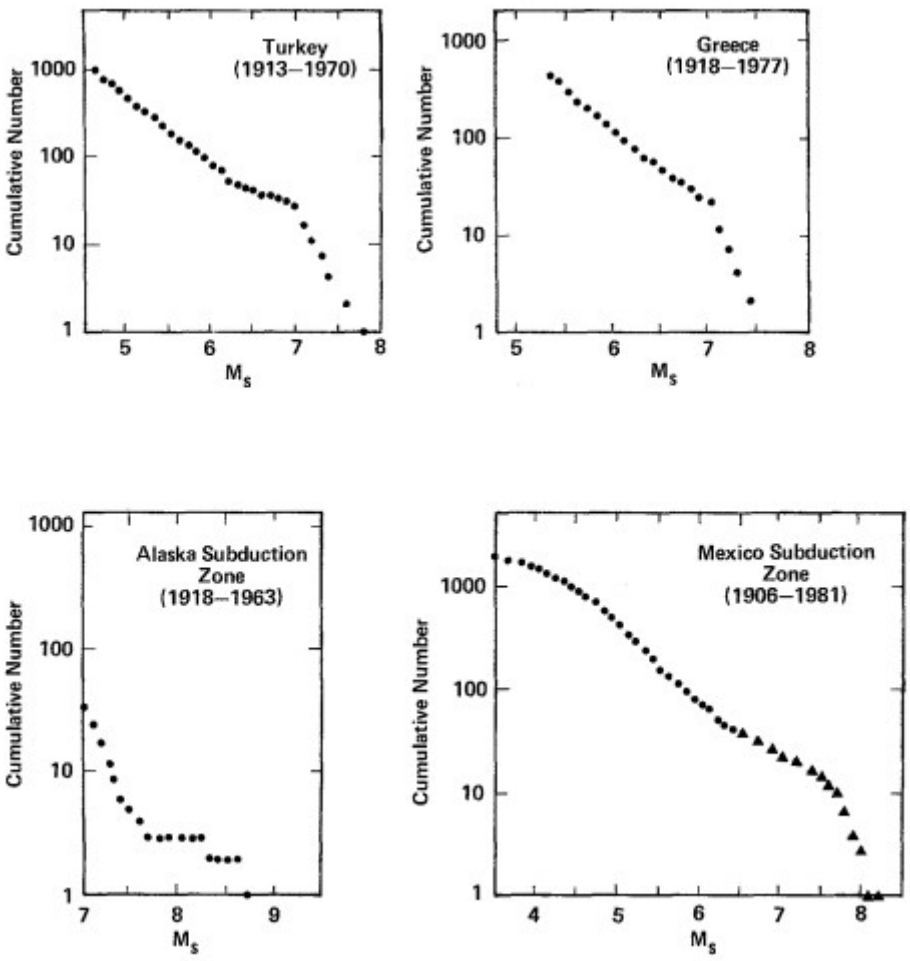

Figure 2.3. Frequency-magnitude plots for seismic sources displaying seismicity with "nonlinear" or "characteristic earthquake" recurrence behaviour presented by Youngs and Coppersmith (1985)

2.3.1 Seismic source characterisation

Characterization of seismic source requires consideration of the spatial feature of the source, distribution of earthquakes, the earthquake size distribution for each source, and distribution of earthquakes with time (Kramer, 1996). All the above-listed characteristics involve some degree of uncertainty. Therefore, the definition of all seismic sources is essential to estimate seismic hazards at any site of interest. The geometry of seismic

sources takes three forms; areal sources, fault sources, and point sources, usually based on the tectonic framework and seismicity. Figure 2.4 shows typical source zone geometries always considered for seismic hazard analysis. When seismicity is concentrated in small, well-defined areas, such as volcanic activity, seismic sources may be point sources. Fault sources are usually individual faults or regions of faulting with clear surface evidence. Faults can be inferred through past earthquake activity, tectonic interpretations of crustal stress and the strain, seismicity patterns, or other indirect evidence when no surface evidence is found. Fault sources can be considered 2D-sources, with a strike and dip, following the mapped geometry of the fault (Figure 2.4b). For simplicity, faults can be modelled as a linear source where this line can be the projection of the fault on the surface or a line along with a seismogenic depth (Figure 2.4a) (Kramer, 1996; Aldama-Bustos, 2009).

Area sources are defined as zones or regions within which future events are expected. Still, geologic or tectonic structures are poorly defined or where faulting is so extensive that it makes it impossible to attribute seismic activity to individual faults. Frequently the geometry is defined based only on historical and instrumental seismicity.

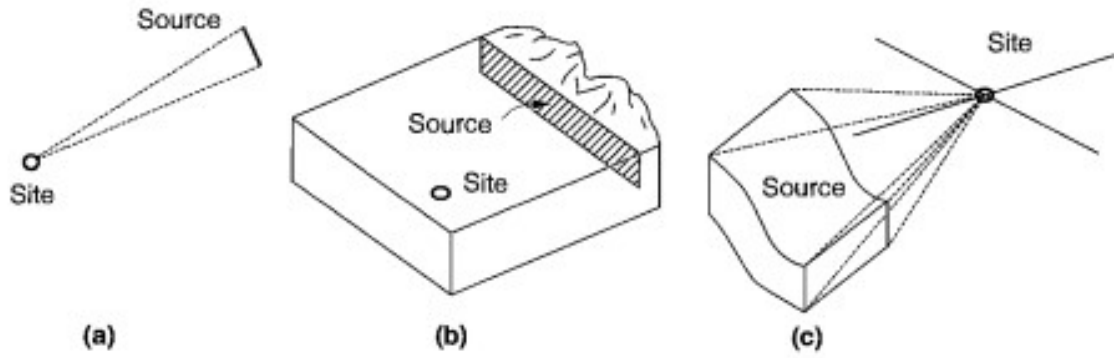

Figure 2.4 (a) short fault modelled as a point source; (b) shallow fault that can be modelled as a 2D plane source; (c) 3D source zone.

However, information from regional crustal geology, tectonic style of crustal deformation, local geology (including observed and inferred intrusive bodies), states of crustal stress, rates of crustal strain, among others, must be considered. Areal sources are modelled as horizontal planes with a fixed depth or as a three-dimensional source when enough data to constrain the variation with depth is available (Figure 2.4c); however, the variation with depth usually is not included in the models. Seismic sources aim to identify

regions with similar seismic activity; thus, if multiple neighbouring faults present identical seismic activity, they might be better modelled as a single area source than multiple individual fault sources.

2.3.2 Exponential recurrence model

The Gutenberg-Richter model, is typically expressed by the Equation 2.3

$$Log_{10}N(M) = a\text{-}bM \qquad (2.3)$$

where N represents earthquakes of magnitude M or greater per unit of time, a is the Log_{10} of the number of events of $M \geq 0$, and b is the relative frequency of occurrence between events of various magnitudes. Ishimoto and Iida (1939) were the first to express the relationship in terms of intensities before Gutenberg and Richter (1944) described this in terms of magnitudes and used it to characterise Californian seismicity. Gutenberg and Richter (1944) found b values close to 1.0 over a reasonable range of magnitudes for Californian seismicity. The relationship applied to other world regions, and only minor deviations from a b value of 1.0 have been observed. In general, a and b were obtained using a maximum likelihood regression on a dataset of seismicity from the seismic source of interest. This dataset is part of the earthquake catalogue compiled for the PSHA and comprises historical and instrumental seismicity. In PSHA calculations, the earthquake catalogue should be declustterd to remove foreshocks and aftershocks. For seismic hazard analysis, Equation 2.4 is expressed below:

$$N(M) = v_o e^{-}\beta M \qquad (2.4)$$

Where v_o represent number of events per unit of time with $M \geq 0$, and $\beta = b*Ln(10) \approx 2.3b$.

The range of magnitudes considered in the hazard analysis is often doubly bounded (Cornell and Vanmarcke, 1969). It is bounded to a minimum threshold magnitude at the lowest magnitude, M_{min} considered the appropriate minimum magnitude for buildings with good design and construction (McCann and Reed, 1989). In the maximum magnitudes, the distribution is truncated at an upper-bound value M_{max}, usually the magnitude of the maximum, also known as “possible” or “credible” earthquake that a seismic source can produce. If Equation 2.4 is modified to incorporate minimum and

maximum threshold magnitudes, then the number of earthquakes, N(M), with magnitude $\geq M$ per unit of time is shown in the equation 2.5 and 2.6.

$$N(M) = v_{M_{min}}[1 - k + ke^{-}\beta(M - M_{min})] \qquad (2.5)$$

$$k = [1 - e^{-}\beta(M - M_{min})]^{-1} \qquad (2.6)$$

Historical and instrumental seismicity are used to estimate $v_{M_{min}}$ and β as published by (Weichert, 1980; Dong et al., 1984; Kijko and Graham, 1999). $M_{\max}$ can be assessed through statistical analysis when adequate data is available in the earthquake catalogue (Kijko, 2004; Pisarenko et al., 1996). Alternatively, this estimation can be based on geological features, slip rate, geophysical data, or the maximum observed magnitude in the worst-case scenario based on expert judgement (Aldama-Bustos, 2009).

2.3.3 Characteristic recurrence model

The exponential model describes recurrence statistics of events in large areas. In some regions, such as subduction zones and major faults, the extrapolation of the recurrence frequency inferred from smaller-magnitude events tends to underestimate the occurrence of large-characteristic events (Figure 2.5). In such situations, a characteristic earthquake recurrence model is usually employed. Paleoseismic evidence has shown that in very well-defined geological structures, individual faults and fault segments move by the same distance in each earthquake. This suggests that these faults repeatedly generate the "same size earthquakes essentially," usually within one-half of a magnitude unit (Youngs and Coppersmith, 1985). A generalized magnitude-frequency density function developed by Youngs and Coppersmith (1985) combined an exponential distribution at lower magnitudes up to magnitude level m' as shown in Figure 2.5. Above this value lies the characteristic component with a uniform distribution about the characteristic event.

The characteristic model, initially proposed by Schwartz and Coppersmith (1984), presents similar distribution for small and moderate magnitude events as the exponential model. However, based on geological data, they suggest a variation in the slope of the recurrence curve to b' at some m' magnitude (Aldama-Bustos, 2009).

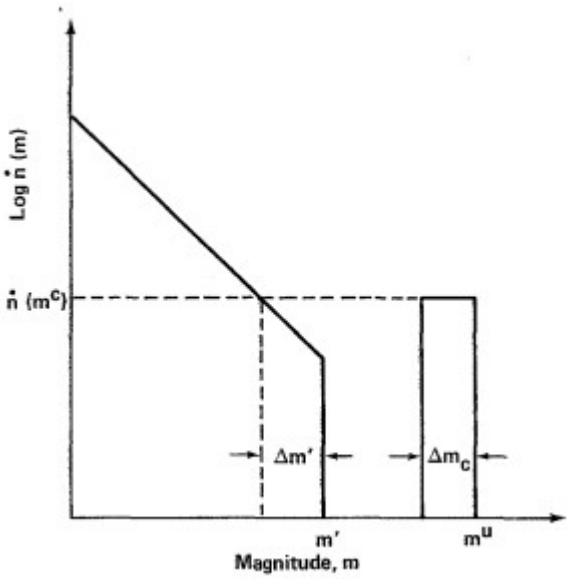

Figure 2.5 Generalized frequency magnitude density function for the characteristic earthquake model by Youngs and Coppersmith (1985).

2.3.4 Time-dependent recurrence model

The average stress and the fault change during an earthquake, dropping an amount $\Delta\sigma$ below the average stress condition before the event. After the earthquake has occurred, elastic energy starts building up in the fault of the surroundings due to the interaction of the tectonic plates (Aldama-Bustos, 2009). Based on the result, the average stress along the fault increases with time, and deformation can be observed on both sides. When the resistance of the fault is exceeded, it ruptures, relaxing the stress in the fault and the cycle re-starts. This theory is called "elastic rebound;" it was initially proposed by Reid (1910) which is been widely accepted.

This process disagrees with time-independent models such as the exponential or characteristic models, which are based on memoryless Poissonian behaviour. Time-dependent models developed by Cramer et al. (2000) and Petersen et al. (2007) encompass the physics behind the earthquake cycle, permitting the statistical "renewal" of the recurrent process.

A range of time- and magnitude-dependent earthquake recurrence models was examined by Cornell and Winterstein (1988) thereby compared their influence upon hazard results against the traditional Poisson model. They conclude that the Poisson

model is adequate in most cases. The notable exception is when a single feature controls the hazard. Since the last significant event, the elapsed time exceeds the average time between such events and the fault exhibits strongly regular, characteristic time behaviour (Aldama-Bustos, 2009).

2.4 Ground-motion prediction equations (GMPEs)

The most fundamental components in PSHA and DSHA are the ground-motion prediction equations (GMPEs) for predicting the expected ground motion at a specific site due to future earthquakes. The models relate a ground-motion parameter such as PGA and elastic response spectral ordinates to some independent variables such as the magnitude, source-site distance, geological conditions, rupture mechanism etc, which describe the earthquake source, local site conditions and wave propagation path (Douglas, 2003; Midzi et al., 2009). In seismicity models, the GMPEs have the most significant influences on the seismic hazard results. However, it is also typically the largest contributor to uncertainties in hazard calculations (Midzi et al, 2009). Various definitions for each parameter are reported in the literature. For example, in earthquake magnitude, different scales are used in ground-motion models. The most common are Surface magnitude (M_s), body magnitude (m_b), local magnitude (M_L), and moment (M_w). The M_w is the most preferred magnitude scale since it directly related to the earthquake's seismic moment (Hanks and Kanamori, 1979).

For this reason, the majority of the most recent ground motion prediction equations use M_w magnitude scale. Many definitions are used for the source-to-site distance. The most common definitions for these variables are:

- The closest horizontal distance to the surface projection of the rupture (R_{jb}).
- The closest distance to the rupture surface (R_{rup}).
- The closest distance to the seismogenic part of the rupture surface (R_{seis}).
- The hypocentral distance (R_{hypo}).

Figure 2.6 shows schematic definitions of different distance used for vertical and dipping faults. For site classification as well, several schemes are found in the literature. Commonly site classification is a broad and qualitative description of surface geology. However, some equations, those recently derived as part of the NGA (Next Generation

of Attenuation) project in the U.S., use a more quantitative description based on the shear-wave velocity corresponding to the uppermost 30m of the soil deposit (V_{s30}). Nevertheless, the use of V_{s30} for describing site conditions goes back to Boore et al. (1993). The influence of the style of faulting on the nature of the strong motion is not included in all ground-motion equations, but among those that do have this factor agree that reverse faulting produces the strongest ground motions.

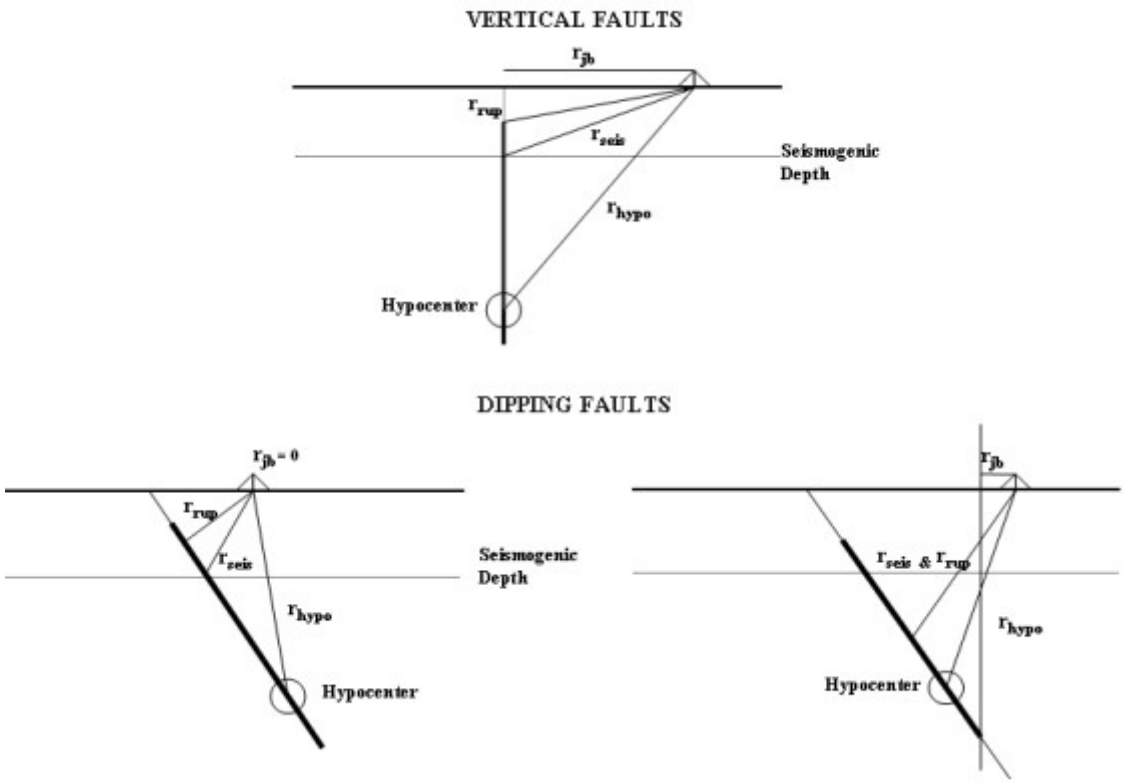

Figure 2.6. Different definitions of source-to-site distance in GMPEs.

In the first published GMPEs (Esteva and Rosenblueth, 1964), a large number of models for predicting ground motion parameters for engineering purposes was developed. A comprehensive summary of ground-motion prediction equations estimating predicting peak ground acceleration (PGA) and spectral amplitudes (SA) is presented in (Douglas, 2006).

Most ground motion prediction equations are based on a statistical analysis of recorded ground motions updated as new information becomes available. These types of equations are better known as empirical ground-motion equations. On the other hand, when insufficient data is available to derive empirical equations, stochastic methods are

applied to derive ground-motion models. However, it is more common to use empirical ground motion prediction equations from some other region. Based on the seismotectonic region, GMPEs can usually be classified into three categories: active shallow crustal, stable continental and subduction zone earthquakes (Ordaz and Sagado-Gálvez, 2017)). Regardless of the methodology applied to derive a particular GMPEs, there is always a variance term representing the uncertainty associated with the predicted ground motion. This variance term represents the scatter in the data used in the regression analysis; however, the most common measure of this scatter is the standard deviation, defined as the square root of the variance. Thus, the variance in a ground-motion equation may not represent the lack of fit of a particular equation. Still, it means the distribution of the ground motion observed in the field given a specific set of predictor variables such as magnitude and distance and site condition. In both PSHA and DSHA, variability in ground-motion prediction has a very relevant position as it defines how likely a ground-motion level is to be reached given a particular earthquake scenario. Usually, the variability in ground-motion predictions and the occurrence of earthquakes within a seismic source are the only aleatory variabilities modelled in PSHA. In DSHA, this variability is considered through an arbitrary decision on the number of standard deviations added to the expected ground motion value. In any case, the proper treatment of ground-motion variability plays an important role in seismic hazard analysis (Bommer and Abrahamson, 2006).

2.5 PSHA

PSHA provides a framework in which uncertainties due to earthquake magnitude, location and rate of occurrence of recurrence of earthquakes are identified, assessed, and combined rationally to give a transparent and comprehensive evaluation of the seismic hazard (Kramer, 1996). PSHA requires the knowledge of a ground-motion model and a seismic source model (Goitom et al., 2017).

The PSHA results are expressed in many ways. For example, one of the most common ways is the maps of seismic hazard curves or seismic zonation maps (Figure 2.7) which show mostly Peak Ground Acceleration (PGA) values for different return periods over a particular region. The maps are frequently incorporated in seismic codes that include the

minimum requirements to design new engineering structures. The hazard maps are constructed by conducting hazard assessments at different locations of seismicity within the region under consideration (Aldama-Bustos, 2009). Also, sensitivity analysis provides additional information about a procedure and various parameters that will significantly influence the results of seismic hazards (Aguilar-Meléndez et al., 2018). Another alternative way to present PSHA results is the seismic hazard curves in terms of the annual frequency of exceedance against selected ground-motion level or as a function of exceedance probability within a fixed period of time (Figure 2.7). A seismic hazard curve provides a convenient way to combine each individual source zone to display the level of hazards at a particular site.

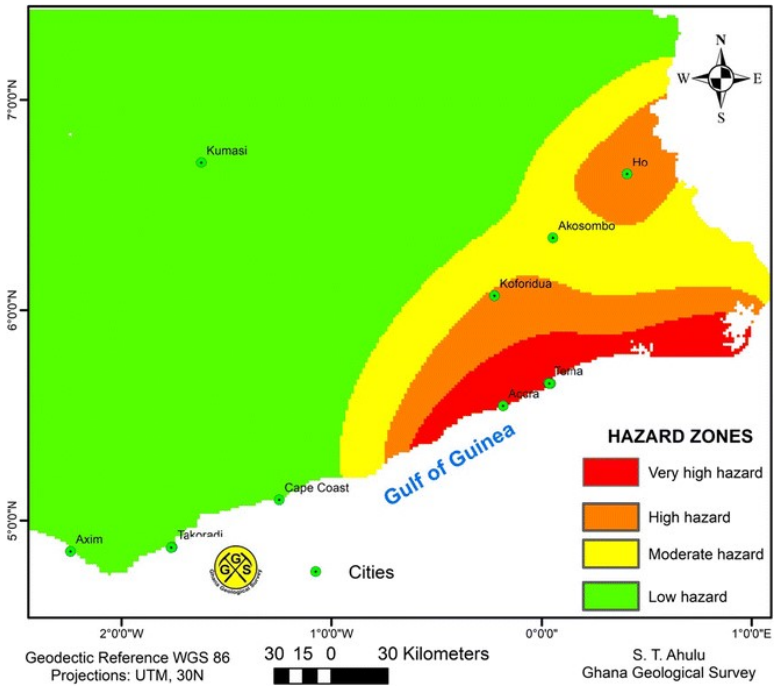

(a)

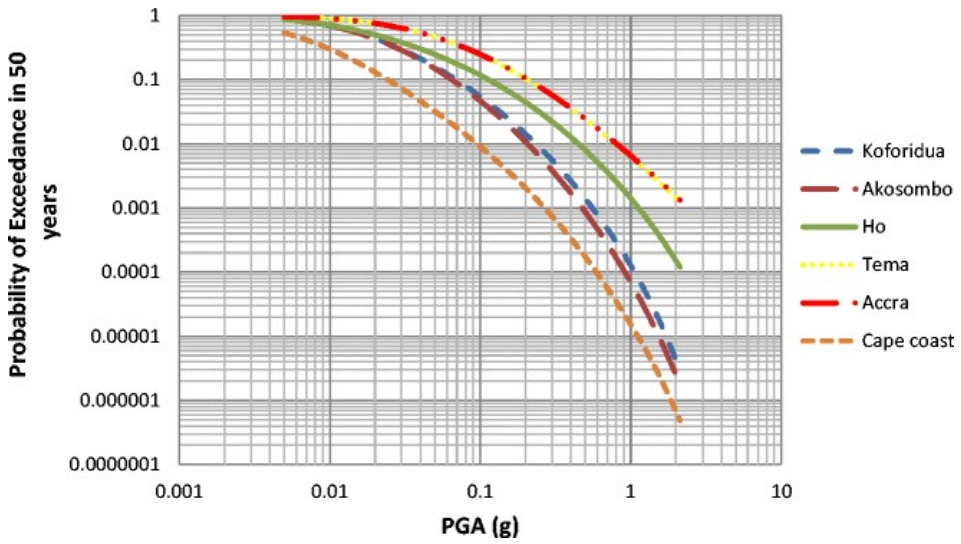

(b)

Figure 2.7. Presentation of PSHA results (a) Hazard curve (b) seismic hazard curves for a specific site (Ahulu et al., 2018)

The seismic hazard is obtained through interpolation, where contours of equal ground motion values are drawn for a given return period. Zonation maps are constructed for a single or more ground-motion parameter and different return periods or exceedance probability. For example, in the past research about PSHA, a PGA of 475 years return period hazard maps has been developed in most studies. However, other return periods are recently considered due to seismic effects of critical infrastructural development in most regions. Therefore, mapping other ground-motion parameters such as spectral acceleration (SA) of different periods is also available for PSHA results. Seismic hazard maps provide parameters for seismic building codes and land-use regulations that show hazards at different locations. Regional or national seismic hazard maps cover the world. According to United Nations International Decade for Natural Disaster Reduction (UN/IDNDR) framework, the Global Seismic Hazard Assessment Project (GSHAP) was launched in 1992. PGA values correspond to a 10% probability of exceedance in 50 years, creating a worldwide seismic hazard map and four regional maps (Giardini, 1999).

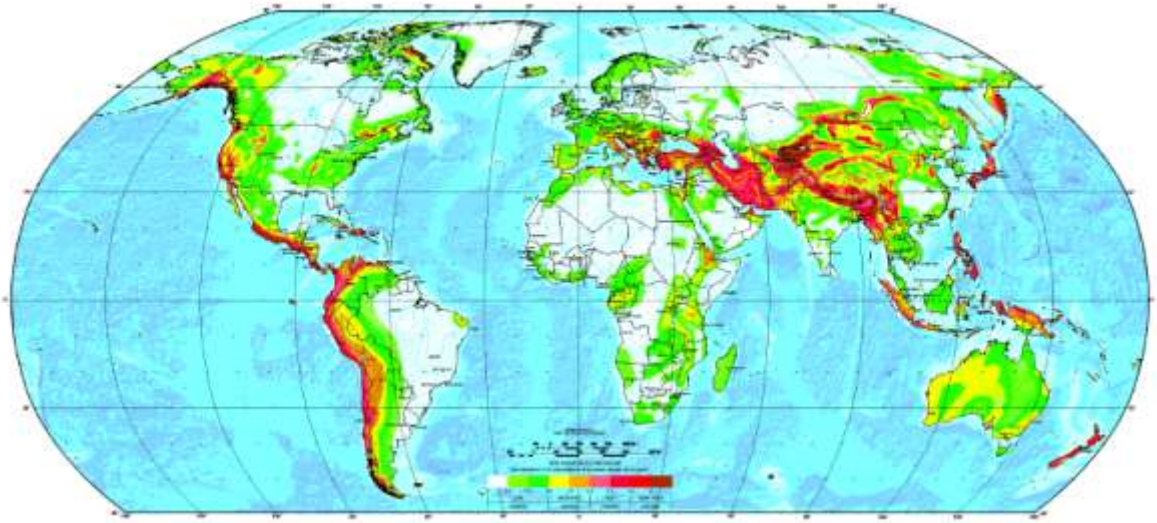

Figure 2.8. The GSHAP global seismic hazard map (Giardini et al., 1999).

The response spectrum ordinates are another way of characterising seismic hazards to use for geotechnical or seismic design. There are two methods to determine the response spectrum as an output of a PSHA. The most efficient is calculating seismic hazard in terms of PGA and then anchoring a standard spectral shape based on geological site conditions reference PGA. However, the determination of uniform hazard spectra (UHS) has significant limitations. For instance, they do not consider the variation in the spectrum's shape with magnitude and distance (Ambraseys et al., 1996).

Additionally, the only ordinate at which the return period is known is zero (PGA), whereas at other response periods is unknown (McGuire, 1977). Hence, a response spectrum estimated for hazard may not be uniform over the spectrum. An improvement to this approach is to get a uniform hazard spectrum by evaluating the hazard assessment many times and producing PGA and the spectral amplitudes (SA) corresponding to each response period for the specified return period. Design spectra obtained is known as uniform hazard spectra since the hazard level is genuinely uniform across the entire range of periods. Figure 2.8 shows an example of UHS for eight sites within Eritrea for different return periods (Baker, 2013). Seismic hazard is also estimated using the Deaggregation by plotting different factors that contributed most to the hazard at the site. The deaggregation is shown in section 2.6.

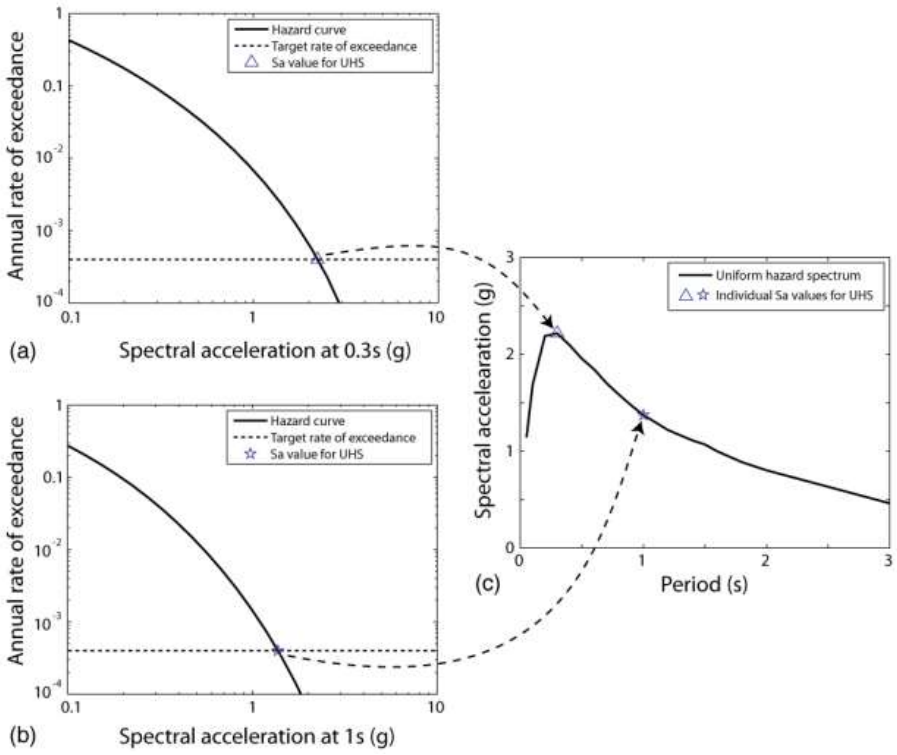

Figure 2.9. Generation of UHS. Hazard curve for SA(0.3s), with UHS point identified. (b) Hazard curve for SA(1s), with UHS point identified. (c) Uniform hazard spectrum, based on a series of calculations like those in (a) and (b) (Baker, 2013).

2.6 Deaggregation

As described in section 2.5, a seismic hazard curve integrates the hazard through magnitude-distance scenarios for possible future earthquakes, as defined by the seismicity model. In this manner, the rate of exceedance that the hazard curve could represent may not be associated with any specific earthquake magnitude or source-to-site distance (Kramer, 1996). One should identify the contribution of magnitude, source-to-distance scenarios, and at time epsilon (e), which measures the deviation of the ground motion from the median value to the total hazard for a particular ground-motion level. Epsilon is the standard deviation of the target ground motion from the median ground motion as predicted by a GMPE. Thus, deaggregation determines the exceedance rates in the hazard curve for magnitude-distance scenarios. In some research, deaggregation is changed to disaggregation, but this depends on the author's choices. In computational terms, this process involves the reordering of terms in Equation 2.7. The rate of exceedance of a given ground-motion level for magnitude-distance scenario is provided by:

$$\gamma(Z > z|\, m_j, r_k) = \sum_{i=1}^{N_{sources}} v_i\, P\left(M = m_j\right) P(R = r_k) \int_{\varepsilon=-\infty}^{\infty} (\varepsilon)\, P(Z > z|m_j, r_k, \varepsilon) d\varepsilon \quad (2.7)$$

where $P\left(M = m_j\right)$ and $P(R = r_k)$ represents the probabilities of an event occurring in the ith seismic source with magnitude (M) at a distance from the site (R), respectively, and $P(Z > z|m_j, r_k, \varepsilon)$ is determined from the ground motion model.

Deaggregation results present the exceedances of the probabilistic ground motion by magnitude-distance scenarios (Harmsen et al., 1999). Still, other factors such as those contributed by seismic sources can also be helpful. A compressive review on seismic hazard disaggregation procedures is presented by Bazzurro and Cornell (1999), which also examine how different assumptions made during the deaggregation process and binning scheme affect the results. Deaggregated seismic hazards define the specific earthquake scenarios that give the maximum contribution to the hazard at a particular site of interest (Weatherill, 2010). Furthermore, other parameters, like the duration of the strong motion, can be derived, and accelerations time-histories can be selected based on the dominant magnitude-distance scenarios. Thus, ground-motion parameters or acceleration time-histories, real, synthetic or artificial, obtained may be compatible with a specific probability of occurrence (Aldama-Bustos, 2009).

2.7 Epistemic uncertainty

In PSHA, uncertainties are grouped into aleatory variability and epistemic uncertainty. Aleatory variability, also known as random variability, is related to an uncertain event in repeated trials or experimental sampling of the outcome. In other words, uncertainty arises because the system under study can potentially behave in many different ways (natural randomness). Aleatory variability, in principle, cannot be reduced through the increase of knowledge (Bommer and Scherbaum, 2008). On the other hand, epistemic uncertainty is related to the belief or confidence in the outcome of an uncertain event, given the state of knowledge when it is assessed. In other words, it is the uncertainty related to the lack of knowledge regarding a specific event (Helton and Oberkampf, 2004; Vick, 2002). Thus, epistemic uncertainty is expected to decrease with time as the relevant data increases and better understand the uncertain event. The most important issue regarding uncertainty in PSHA is to ensure all sources of uncertainty, whether defined as aleatory or epistemic, are included and traceable through the hazard estimation process.

Therefore, it is essential to differentiate between aleatory and epistemic uncertainties. Aleatory variability is integrated into the hazard curves directly and contributes to the shape of the curves. In contrast, epistemic uncertainties lead to alternative hazard curves. Therefore, the distribution corresponding to the full suite of hazard curves captures both aleatory and epistemic uncertainties. However, the differentiation between aleatory and epistemic uncertainties may not always be free of ambiguity (Bommer and Scherbaum, 2008). For example, an extreme hypothesis regarding epistemic uncertainty is the Laplacian view that the world is completely deterministic; under this hypothesis, all uncertainty is epistemic. However, even under this assumption, it is pragmatically convenient to treat the world as if some uncertainties are not limited knowledge but random when enough information is available to determine a probability distribution (McGuire et al., 2005). In any case, probability might still be a good representation of epistemic uncertainty under the understanding that we may not be able to determine the probabilities ideally.

As was previously mentioned, in a logic-tree framework, epistemic uncertainties are represented by the nodes and branches of the tree, and the weight assigned to each branch represents the analyst "s degree of belief or conviction in the outcome. The degree of belief allows the analyst to incorporate the full range of understanding in ways that correspond to how they think. The treatment of this degree-of-belief that the analyst has for each of the considered possibilities, typically described as "weights", as subjective probabilities, is merely a practical matter. The justification for this lies in the purposes of probability, which is to communicate uncertainty to others and to communicate uncertainties associated with events that have not been or cannot be evaluated directly. Therefore, it is required to quantify these uncertainties in numerical form (Vick, 2002).

Logic trees were initially introduced to treat epistemic uncertainties when performing SHA by Kulkarni et al. (1984). Subsequently, logic trees are widely used for seismic hazard analysis and have become a standard feature of PSHA (Bommer et al., 2005). On the other hand, epistemic uncertainties are treated through a logic tree. Each node represents an element of epistemic uncertainty. The branches extending from each node are the different discrete options that reflect the uncertainty through alternative possibilities. It is common practice to place nodes representing assumptions, models or parameters that do not depend on others on the left, while those nodes dependent on

others are placed to the right. This is done to have the sections of the logic tree in the order of execution; however, it is irrelevant to set the logic tree from right to left or from top to bottom or vice versa. They are keeping the logical sequence of the different steps throughout all branches of the logic tree matters.

One of the requirements of logic-tree branches is that they, in theory, must be mutually exclusive and collectively exhaustive (Bommer and Scherbaum, 2008). For each branch added to the logic tree, a cost in terms of additional calculations is paid, and the total number of calculations can rapidly become very large. Hence, it is advisable to avoid branches representing options with minimal difference (Bommer et al., 2005). To satisfy the conditions of mutual exclusivity and collective exhaustiveness in the branches. However, this does not necessarily invalidate the underlying probabilistic framework. Under the most favourable conditions, the weights assigned to the logic-tree branches can be treated as approximate probabilities (Bommer and Scherbaum, 2008). Once the logic tree has been set up, weights representing the analyst's confidence (subjective probabilities) on each branch are assigned.

When setting up branches for different rupture models, it is a common pitfall to consider only one node with different branches, one branch for the non-segmented rupture model and an additional branch for each different segmentation model. This violates the principle of mutual exclusivity since the occurrence of a non-segmented rupture would imply that all the segments of the fault would rupture at the same time (Abrahamson, 2000b). The second of the uncertainties, slip ratio estimation, presents a common situation where the weights are centred on the best estimate. This is the case, for instance, for slip rates, where commonly a set of estimated values is reported, but some tendency to a central value can be observed. In this case, the analyst may give a higher weight to the central value, and lower weights to the upper and lower values of the set of slip rates reported. Finally, the third uncertainty in this example, the ground-motion model, is the most common source of uncertainty that the analyst has to face and the one that incorporates the highest levels of epistemic uncertainty in PSHA (Toro, 2006; Aldama-Bustos; 2009).

Regarding GMPEs in logic trees, it is common to find uniform weights on branches for different ground-motion models representing equal levels of analyst confidence on the other options. However, as previously discussed, if the weights assigned to each branch

are considered subjective probabilities, uniform weights would represent an equiprobability distribution. However, if the analyst "s belief that one of the equations means the seismic attenuation in the region is better than the others, more weight is assigned to it. Frequently, great attention is given to the weights assigned to the logic-tree branches regarding different GMPEs. However, once there are more than a few branches, the hazard is almost insensitive to the weighting process, which has a more significant impact in selecting the GMPEs themselves rather than the relative weights assigned to the models (Sabetta et al., 2005; Scherbaum et al., 2005).

Using a logic tree to assess epistemic uncertainties has many benefits and is technically easy to implement. The most crucial advantage of using logic trees is that they help organise one "s thinking where alternative models or interpretations might apply. However, many dangers can arise from the misuse of logic trees. Additionally, careful considerations must be made to ensure compatibility among the models employed at each branch, for example, when using alternative ground-motion models with different distance definitions (Bommer et al., 2005). Regarding how PSHA is engaged in current engineering practice, different interpretations of the logic-tree outputs have been proposed in recent years (Abrahamson and Bommer, 2005; McGuire et al., 2005; Musson, 2005).

2.8 Seismic risk analysis

The choice of the analysis model to estimate the seismic risk depends on the available information regarding the dam structure (Cosentini et al., 2020). Therefore, a seismic risk assessment study for dams is performed based on the seismic hazard and risk associated with the dam structures. The main aims of risk analysis are to improve the knowledge regarding the risks of dams and the related resilience of the host communities. Seismic risk analysis is a systematic tool that allows the estimation of risks from different types of seismic hazards, thereby facilitating the identification of the most vulnerable elements in the dam inventory and the hazards that contribute to the risk. Thus, the vulnerability of the dam is reduced by strengthening the dam elements. The safety of the existing dams is a crucial aspect of dam engineering. The risk-based method combines the benefits of

the well-established traditional system for both the dam safety analysis and risk assessment (Babu and Srivastava, 2009).

A simplified Bureau (2003) procedures are always employed to assess the most vulnerable dams in the dam inventory. In addition, this risk classification can be used to identify the need for more detailed seismic safety evaluations and establish priorities for such assessments (Singh et al., 2011). Bureau (2003) has been applied for dams in South Africa for ranking large dams; also, for the Euphrates Basin in Turkey (Tosun et al., 2007: 2020), Tosun and Seyrek, 2010 and in Romania (Moldovan and Constantin 2006).

A recent study by Ahulu et al. (2018) adopted a probabilistic framework for assessing the seismic hazard in southern Ghana using OpenQuake software package. The research estimated the highest level of seismic hazard in Accra which is close to Gulf of Guinea. The peak ground acceleration (PGA) obtained was close to 0.2 g at 10% probability of exceedance in 50 years. Study by Grunthal et al. (1999) provided available seismic hazard assessment for West Africa as part of the worldwide "Global Seismic Hazard Assessment Project" (GSHAP), where sixteen independent regional maps were collected, modified, and integrated to produce a global hazard map. A study by Afegbua et al. (2019) which conducted the probabilistic seismic hazard assessment (PSHA) for Nigeria using earthquake catalogue from 1933–2018 computed critical earthquake hazard parameters and peak ground accelerations (PGAs) for the country. The result produced PGA value within the range of 0.01–0.08g for a 10% probability of exceedance in 50 years. A summary of PGA values of some sites obtained from previous studies and compared with this study are shown in Table 2.1.

Table 2.1. Comparison of seismic hazard values evaluated in this study to those obtained in previous studies.

Location	PGA values (g) this study	Previous studies (g)				
Accra	0.10	0.2 Ahulu et al., (2018)	0.15 Kumapley (1996)	0.08-0.16 GSHAP Grunthal et al. (1999)	0.14-0.57 Amponsah et al. (2009)	0.35 CSDCS BRRI, (1990)
Lagos	0.035	0.01-0.08 Afegbua et al. (2019)				

Irinyemi A. Stephen
PhD in Geotechnical Earthquake Engineering (2021)
University of Manchester (UK)

CHAPTER 3

RESEARCH METHODOLOGY

3.1 Background

This method describes various ways for conducting Probabilistic Seismic Hazard Analysis (PSHA) using R-CRISIS software, ZMAP and QGIS Tool for seismic hazard assessment. The following steps are based on the case study PSHA analysis conducted for West Africa region and this can be applied to other site of interest around the world. R-CRISIS is PSHA software that perform seismic hazard calculations using a probabilistic approach. The programme computes seismic hazard results by utilizing the earthquake occurrence probabilities, GMPEs and the spatial and temporal distribution of earthquakes. ZMAP is a research tool used for catalogue data evaluation. ZMAP analysed the earthquake decluttering data and the recurrence parameters such as the *b*-value and magnitude of completion (Mc). The QGIS is geographic information system that was used to viewing, editing and analysing the outputs of seismic hazard assessment.

3.1.1 Location of study area

The shape file of West Africa region was extracted in GIS that comprising the site of interest with respective administrative boundaries. The area of interest in the study considered where earthquake activities have been recorded which assumed to influence seismic hazard in West Africa. Figure 3.1 shows the location of the study region enclosed within latitudes 2°N and 16°N and longitudes 18°W and 15°E.

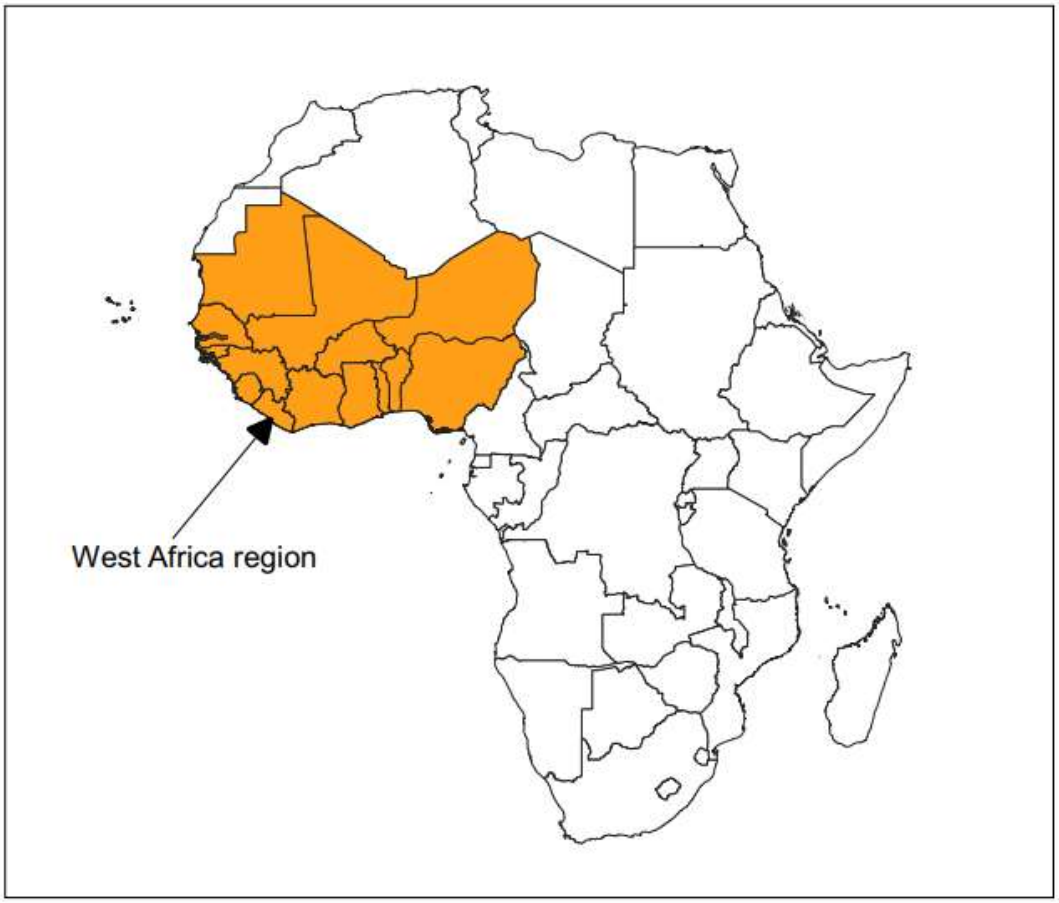

Figure 3.1. location of West Africa region.

3.1.2 Source of Earthquake catalogue

The source of earthquakes involves collection of earthquake catalogue data for processing and development of recurrence models and source input parameters for hazard assessment using ZMap and R-CRISIS software. The following sources can be used to retrieve earthquake catalogue for West Africa region:

- United States Geological Survey (USGS)
- International Seismological Centre (ISC)
- Catalogue of Ambrasey and Adams (1986)
- Musson (2014)
- Catalogue of Amponsah et al., 2012

Out of the five seismic sources compiled, both USGS and ISC sources provided data in either rectangular or circular shape and was adjusted based on area of seismicity within the rectangular shape as shown in Figure 3.2. The inputs used for this study for all the sources are as follow,

Geographic region	South= 2°N West= 18°W North= 16°N East= 15°E
Date	1973-2018
Magnitude	3-7
Depth	0-100 km
Type of Magnitude	Any
Source	All

Figure 3.2. Source option for USGS.

In this study, a total of 19 seismic events of different magnitudes (M_w, M_b, M_s)from USGS source were collected within the period 1973 to 2018 and the output was downloaded using CSV format using http://earthquake.usgs.gov/earthquakes/search/. A total of 95 events are collected and then imported to Excel. These events were from 1939 to 2018 and obtained through http://www.isc.ac.uk/iscbulletin/search/bulletin/.

Ambraseys and Adams (1986) were used for earthquakes starting from the historical period of 1615 to 1976. It provides information on historical earthquakes of the West African region and some parts of Eastern African region compiled by the authors

through different sources, such as libraries, questionnaires, newspapers, and other scholars from international agencies and researchers of that region. It lists and describes earthquakes in terms of probable time of occurrence, coordinate, magnitude, intensity, and felt effects. Their works are noticeable and regard as the most referenced and comprehensive source of earthquakes in terms of historical earthquakes for the West Africa region. Nevertheless, adequate cares are taken, as the locations of the epicentre and focal depths are not accurately recorded.

Musson (2014) covered the period of 1615 to 2009, the report covers earthquake events from different authors and agencies that includes Ambraseys and Adams 1986, ISC and additional data from other researchers.

Amponsah et al., (2012) the event, covered the period from 1615 to 2003. The report covers earthquake events from different authors and agencies that includes Ambraseys and Adams (1986) and additional data from other researchers. It describes earthquakes in terms of magnitude/intensity, location and time of occurrence.

3.1.2.1 Compiled catalogue preparation

After a carefully collection of all the data, a homogeneous catalogue is compiled from the combined catalogue by merging all the data as shown in Figure 3.3. The combined, combined catalogue consisted of 315 earthquakes. The catalogue is listed from oldest to latest. Furthermore, the highlighted events represented the duplicate events from the compiled catalogue. Three catalogues (Ambraseys and Adams, 1986; Amponsah et al., 2012; Musson, 2014) reported similar events. Adequate care was taken to remove duplicate events which occurred in more than one catalogues. We adopted the catalogue which contain the complete record of events in retaining the catalogue. Based on this, 56 events were found to be repeated and harmonised. We unify the different magnitude scales used in the compiled catalogue into a single moment magnitude scale (M_w) using the relationships developed by Scordilis (2006) and Papazachos, (1997) as shown in Table 3.1. To ensure that the earthquakes in the compiled catalogue are independent events, all the foreshocks and aftershocks were removed using the declustering technique by Gardner and Knopoff (1974) which is implemented in the code ZMAP (Wiemer, 2001).

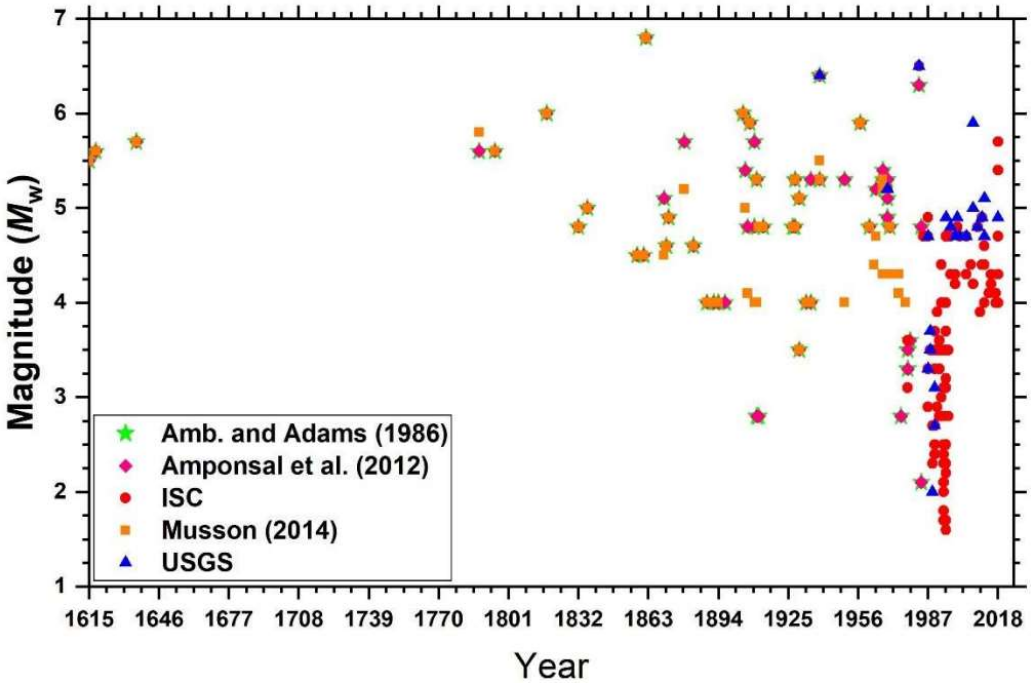

Figure 3.3. Combined Catalogue of the study area from 1615 to 2018.

Table 3.1. Source catalogues for earthquake catalogue (with magnitudes $M_w \geq 3.0$).

S/N	Magnitude range	Conversion Relationship
1	$3.5 \leq m_b \leq 6.2$	$M_w = 0.85m_b + 1.03$
2	$3.0 \leq M_s \leq 6.1$	$M_w = 0.67M_s + 2.07$
3	$3.0 \leq M_s \leq 6.1$	$M_w = 0.85M_L + 0.65$
4	$3.0 \leq M_s \leq 6.8$	$M_w = 1.47M_d - 1.49$

3.2 Definition of seismic sources

Both the historical and instrumental catalogues from the combined catalogues USGS, ISC and other local data and its correlation with tectonic structures are used for the identification of seismic source zones for determination of seismic hazard of the study area. Area source zones in PSHA delineated seismic source zones where a potential location of future earthquakes may likely to occur. For this study, individual fault zones that are seismically active in this study region difficult to identify due to the fact that no existing literature gives details the about the fault geometry, slip rate of faulting during the recent geologic period and fault segmentation length. However, the analyses

of the seismic source model have been divided into seventeen (14) based on tectonics and seismicity of the study area as shown in Figure 3.4.

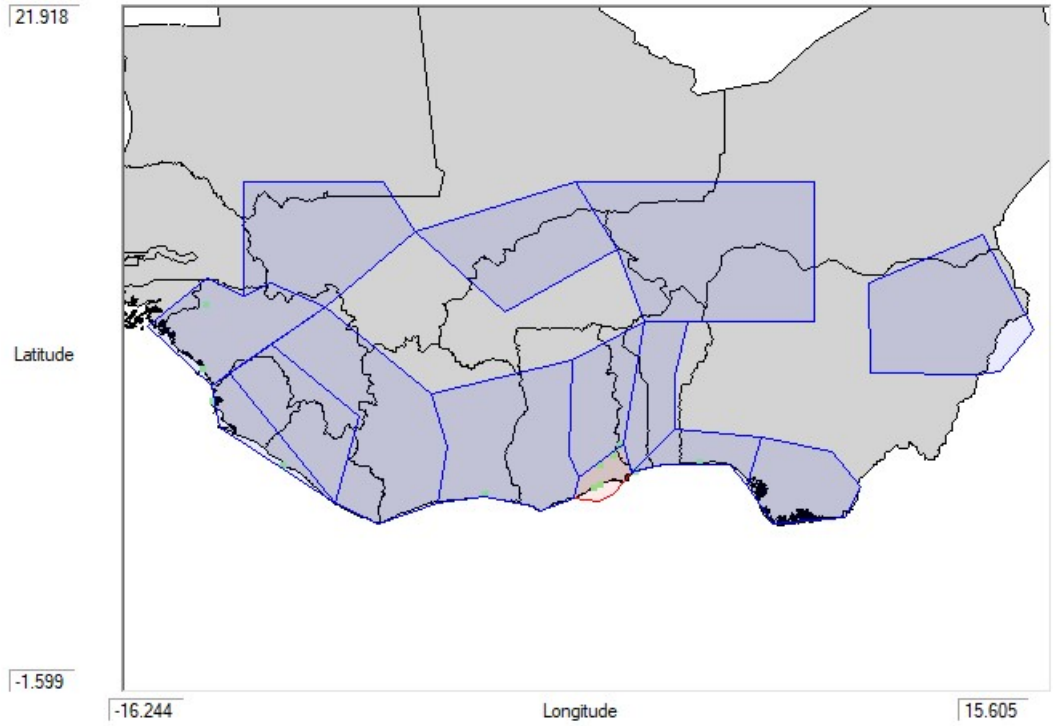

Figure 3.4. Area seismic source zones using R-CRISIS software.

3.2.1 The use of ZMAP for seismic hazard assessment

ZMAP as a research tool is used to analyse the earthquake decluttering data, histogram of magnitude distribution for the compiled catalogue display, the seismicity of the region, calculate recurrence parameters such as the *b*-value and magnitude of completion (M_c) as shown in Figure 3.5.

Earthquake Catalogue data are converted into Z-MAP format as a text file as expressed below,

Longitude, Latitude, Year Month, Day, Mw, Depth Hrs, Min. The ZMAP is run in MATLAB and catalogue is load as follows.

Load, get/load catalogue, from other formatted file, ASCII Columns (txts,. Dat,.csv) and finally Data Import Filter.

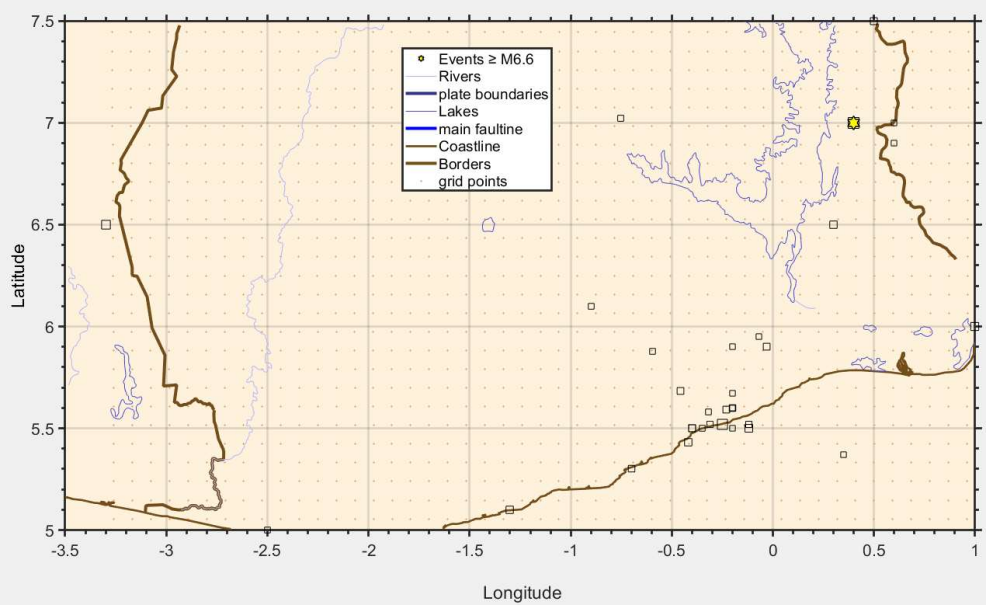
Events ≥ M6.6
Rivers
plate boundaries
Lakes
main faultline
Coastline
Borders
grid points
Latitude
Longitude
7.5
7
6.5
6
5.5
5
-3.5
-3
-2.5
-2
-1.5
-1
-0.5
0
0.5
1

(a)

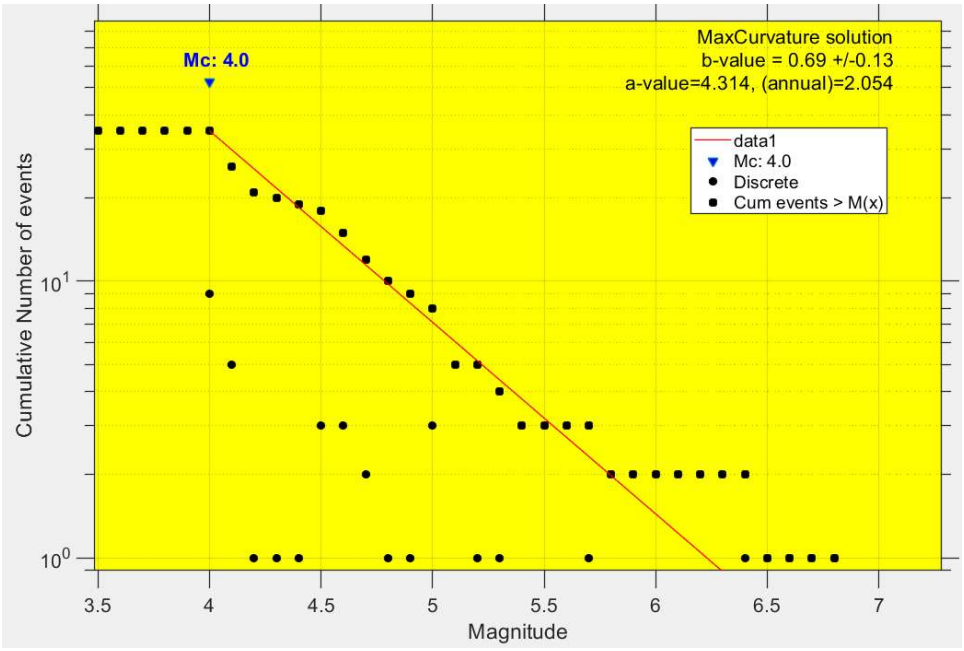
Mc: 4.0
MaxCurvature solution
b-value = 0.69 +/-0.13
a-value=4.314, (annual)=2.054
data1
Mc: 4.0
Discrete
Cum events > M(x)
Cumulative Number of events
Magnitude
10^1
10^0
3.5
4
4.5
5
5.5
6
6.5
7

(b)

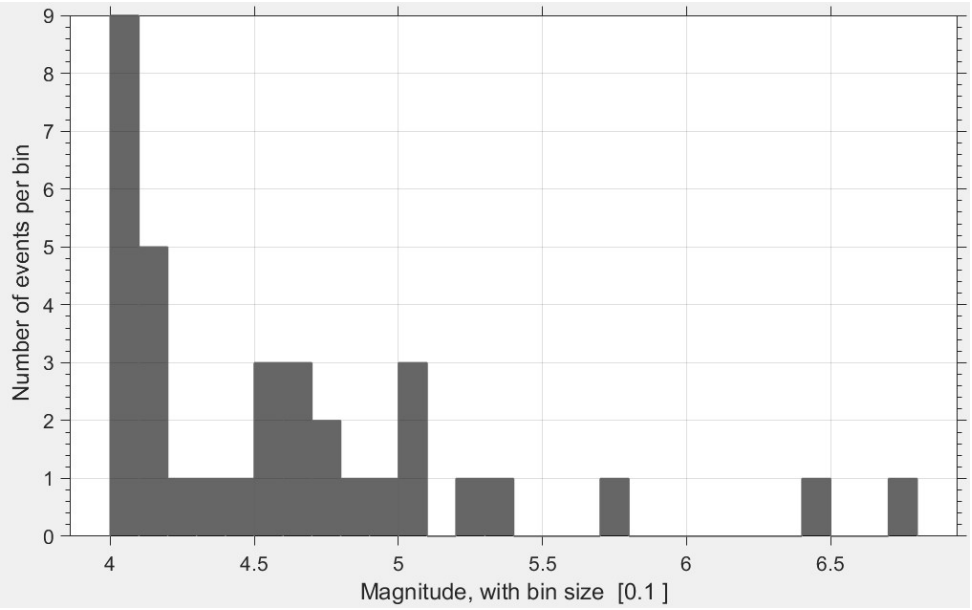

(c)

Figure 3.5. The use of ZMAP for seismic hazard assessment. (a) Spatial distribution of earthquake epicentres; (b) Recurrence parameters using magnitude from 1964-2018. (c) Histogram of magnitude of events.

CHAPTER 4

PROBABILISTIC SEISMIC HAZARD ASSESSMENT FOR WEST AFRICA REGION

Reformatted version of the following paper:

Paper title: **Probabilistic Seismic Hazard Assessment for West Africa Region**

Authors**: Stephen A. Irinyemi, Domenico Lombardi & Syed M. Ahmad**

Published in: Georisk. (2021)

Research output: Contribution to journal › Article › peer-review

DOI:10.1080/17499518.2021.1952608

Author contributions

The author (Irinyemi) conducted the seismic data analysis, designed the work, acquired and analysed the data and drafted the paper. Lombardi and Ahmad supervised the author.

Abstract

This chapter presents the seismic hazard analyses for West Africa region using probabilistic method. West-Africa is a region of low-to-moderate seismicity, with only a few known earthquakes of moment magnitude greater than 5, notably the 1939 Mw 6.4 Accra (Ghana) earthquake. An effort has been made to perform a seismic hazard assessment for the region enclosed within latitudes 2°N and 16°N and longitudes 18°W and 15°E using a probabilistic approach within a logic-tree framework. Ground-motion scaling relationships are selected to account for epistemic uncertainty. The compiled catalogue from 1615 to 2018 and homogenised to moment magnitude (M_w). We present hazard result values on rock site conditions, in terms of seismic hazard curves, peak ground acceleration and uniform hazard spectra, for the study region and four selected cities. We estimate the maximum PGAs of 10%, and 2%, chances over 50 years at 0.10 and 0.26 g respectively, in Accra. Finally, a deaggregation of the Accra site was conducted to identify the dominant earthquake scenario for the chosen site for a 475-year return period. Results showed that the prevalent scenario characterised by seismic events

between magnitudes 5.5-6.0 and at a distance less than 60 km. Findings from these assessments will help to contribute to the safe development of the region.

Keywords: seismic hazard assessment; Ground motion prediction equations; Earthquake catalogue; West Africa region.

4.1 Introduction

West Africa is located within the African plate, the third largest tectonic plate, which extends for approximately 60 million km^2 (Schulte and Mooney, 2005; Meghraoui et al., 2016). The nearest active plate boundaries are the Mid-Atlantic Ridge to the west and the North African margins to the north. The African plate consists of three major Archean cratons, i.e., West African, Congo and Kalahari Cratons, and smaller cratonic fragments. The main structural units were established in the Late Neoproterozoic-Early Palaeozoic Pan-African orogeny (Begg et al., 2009; Celli et al., 2020). Although the African plate has moved slowly for the past 150Ma, its continental interior has experienced rifting, folding and variations in sedimentary basin subsidence, even in areas thousands of kilometres away from its boundaries (Gaina et al., 2013). Intra-continental crustal deformation has been related to local and regional tectonic events (Cloetingh and Burov, 2011), mantle–lithosphere interaction (Heine et al. 2008), and propagation of far field stresses related to changes in plate boundaries (Xie and Heller, 2009). Freeth (1978) studied the plate tectonic forces within West Africa, suggesting that the northward movement of the African plate has been responsible for the limited seismicity of the region.

Geographically, the study region is bordered by the Sahara Desert to the north and by the Atlantic Ocean to the west and southwest. The main structural units include the West African Craton, and the West Africa Mobile Zone (Globig et al., 2016). The West African Craton (Figure 4.1), located in the northwest of the study region, has been stable for 2 Ga, which explains the low seismicity of the northern part of the study area. The higher seismic activity in southern Ghana has been associated to the Paul's and Romanche transform-fracture systems (Bacon and Quaah, 1981), whose intersection is located a few tens of kilometres to the southeast of Accra.

As most of the historical earthquakes have been recorded in Ghana, many available studies have focused primarily on a narrow area of West Africa, especially near Accra, which was heavily damaged by earthquakes in 1636, 1862 and 1939 (Ambraseys and Adams, 1986; Grunthal et al., 1999; Musson, 2014; Ahulu et al., 2018). Fewer studies have provided seismic hazard assessments for a greater area that includes West Africa. Amponsah et al. (2009) adopted a deterministic method to generate synthetic seismic waveforms for Accra. It was found that the peak ground acceleration ranged from 0.14 g to 0.57 g. It should be noted that due to the deterministic nature of this analysis, the results cannot be associate with a particular probability of exceedance, and thus are difficult to be compared with results obtained from probabilistic seismic risk assessments. A recent study by Ahulu et al. (2018) adopted a probabilistic framework for assessing the seismic hazard in southern Ghana. The highest level of seismic hazard was found in Accra and on the Bight of Benin and Atlantic coast of Ghana. The estimated peak ground acceleration was close to 0.2 g for a 10% probability of exceedance in 50 years (i.e., return period of 475 years). The estimated acceleration reduced to 0.05 g moving 140 km south from Accra. The only available seismic hazard assessment for West Africa was part of the worldwide "Global Seismic Hazard Assessment Project" (GSHAP), in which sixteen independent regional maps were collected, modified, and integrated to produce a global hazard map (Grunthal et al., 1999). Although this represents the only available hazard map for West Africa, it lacks detail at the scale of the study region. GSHAP reported peak ground acceleration (PGA) slightly higher than 0.1 g for equatorial West Africa for the 10% probability of exceedance in 50 years.

The present work assesses the seismic hazard of a larger area within West Africa, extending from latitudes 2°N and 16°N and longitudes 18°W and 15°E. The first contribution of this work is a modified and updated catalogue for West Africa, obtained by combining five catalogues and online bulletins. The seismic source model is developed by dividing the study region into a number of seismic source zones, whose limits reflect geological-tectonic features and spatial distribution of historical and instrumental events. The ground motion model is constructed using different ground motion prediction equations (GMPEs). To account for epistemic uncertainty, the GMPEs are used within a logic tree whose weights are computed using the average sample log likelihood method (Delavaud et al., 2009). The use of logic trees provides a convenient form for quantitative treatment of the uncertainties and have widely used by many

researchers in PSHA (Kulkarni et al., 1984; Coppersmith and Youngs, 1986; Reiter, 1990, Midzi, et al., 2020). Due to limited available data the logic tree is based on subjective judgements of scientist knowledges with earthquake phenomena. (Finally, the hazard estimates are computed for return periods of 475, 2475, and 9975 years. The hazard estimates at longer return periods (i.e., return periods of 2475 and 9975 years) are the first to be made available in the literature for this study region. As such, they provide valuable data for risk assessment, land use management, and planning of critical infrastructures, such as dams and nuclear facilities.

4.2 Tectonic setting of the study region

From the Late Jurassic-Early Cretaceous onwards, rifting has been taking place along the line of the proto-South Atlantic, resulting in the separation of South American plate from the African plate and the consequent formation of the West and Central African rift systems (Binks and Fairhead, 1992). The divergent movement of the African Plate and the American plate has formed the Midge Atlantic Ridge, which is spreading at an average rate of about 25 mm/yr (Ahulu et al., 2018). The rate of movement on the western side of the plate, which includes West Africa, is slow, i.e., 2.0–15 mm/year (Hartnady and Benouar, 2007). The study region is part of the West African Rift sub-system (WAS) that extends from north-eastward Nigeria to the Gulf of Guinea. The rift comprises a set of strike-slip fractures that deeply penetrate the African continent before terminating in extensional basins perpendicular to the direction of the strike-slip motion (Binks and Fairhead, 1992).

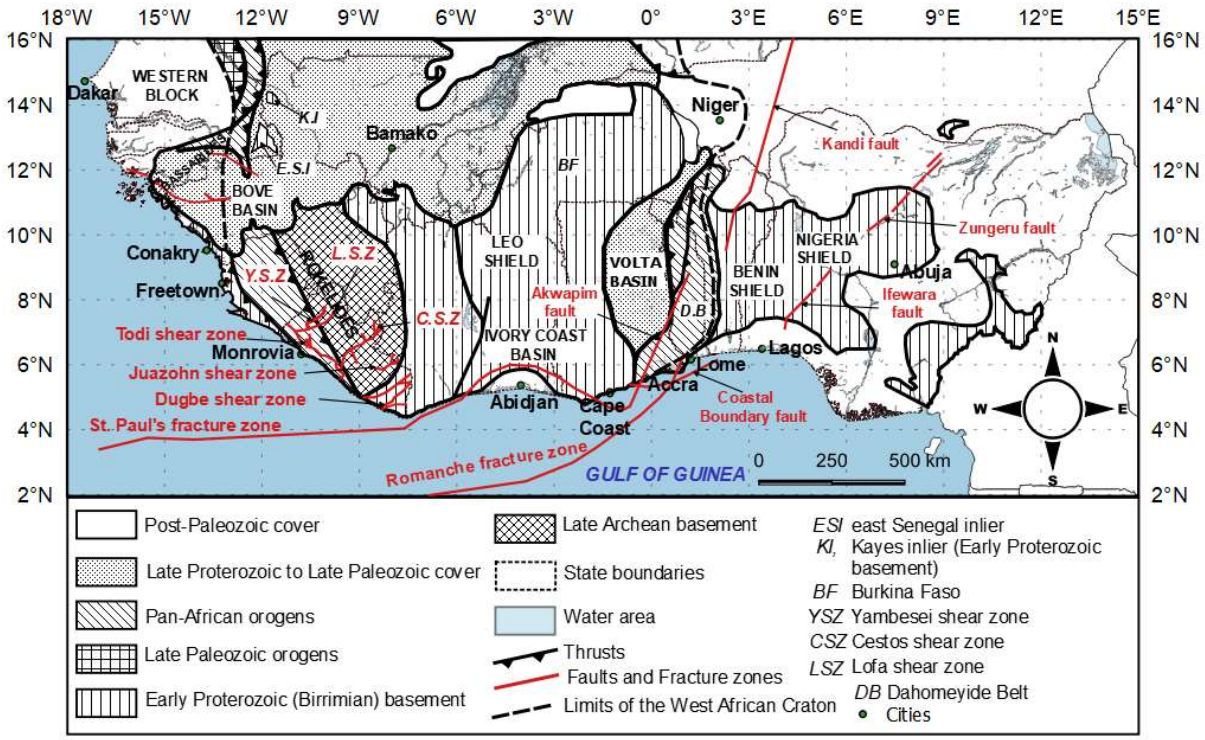

Figure 4.1. Geology and tectonic map of West Africa region.

West Africa is composed of two major tectonic elements, namely the West African Precambrian craton in the north, and the mobile belts in the south (Latil-Brun et al., 1988). The West Africa craton is covered by Upper Proterozoic to Late Palaeozoic sediments and crops out in the Leo shield, which contains Early Proterozoic Birrimian rocks (Figure 3.1). The Volta passive margin basin in Ghana and Burkina Faso formed the foreland of the Dahomeyide orogen (Affaton et al., 1980). The Bove basin in Guinea (Villeneuve and Dallmeyer, 1987) contains Palaeozoic sediments, while the adjacent Benin-Nigeria Shield has been dominated by accretionary tectonics throughout the Proterozoic (Begg et al., 2009). Six major faults found in Liberia, they are: Dugbe, Cestos and Juazohn shear zones in the southeastern, are the northeast-trending faults which are the extensions of regional structure into Côte d'Ivoire. The Lofa Shear Zone in the north-western also trends north-east. The four shear zones are the structural trend of rocks that occurred in Liberia and Eburnean age provinces. Todi shear zone and Yambesei shear zone which trend northwest, marks the boundary of the Pan African province and contains series of south-west-dipping faults that are associated with intense zones of mylonite (Tysdal and Thorman, 1983; Tysdal, 1978).

Two transform-fracture systems are found in the Gulf of Guinea, namely, St. Paul's and Romanche fracture zones (Figure 3.1). The St. Paul's fracture zone comes onshore in the Cote D'Ivoire and turns east to intersect the Romanche fracture zone in Accra. The seismicity of southern Ghana is associated with the fault systems of the Romanche and St. Paul's fracture zones. In particular, the southwestern part of Ghana is affected by tectonic movements of the St. Paul's fault system, and only marginally affected by the Romanche fault zone. Earthquakes recorded in Accra attributed to the reactivation of faults in the Romanche fracture zone, more specifically, the Coastal Boundary fault and Akwapim fault (Kutu, 2013). The Coastal Boundary fault became tectonically active in Jurassic times and is still active. The Akwapim Fault Zone comprises a system of faults trending in a north-easterly direction from just west of Accra, along an ancient line of thrust boundaries in the Dahomeyan belt. Other major faults include Ifewara-Zungeru fault, which trends in the north-northeast to south-southwest directions from the southwestern part of Nigeria (Awoyemi et al., 2017).

4.2.1 History of seismicity of the study region

According to Ambraseys and Adams (1986), the earliest known seismic event occurred in 1615, causing the collapse of the fortress of Sao Jorge on the south coast of Ghana, in the present-day Elmina. In the same century, a second event struck the southwestern part of Ghana, near the border between Ghana and the Ivory Coast, leading to the collapse of a gold mine sited in the present-day Obuasi (Claridge, 1915). In 1795, an earthquake with an estimated magnitude of 5 occurred in southwest Guinea, which caused damage along the coast and inland area Ambraseys and Adams (1986). There are no known records of earthquakes between 1636 and 1858. Ambraseys and Adams (1986) found evidence of an earthquake occurring in Accra in 1858. The first well-documented earthquake was recorded in Accra in 1862. With an estimated 6.5 local magnitude, the event caused significant damage to the castle and some forts in Accra (Junner, 1941), while the shaking was felt along the coast east of Togo and in Benin. Other events with estimated magnitudes of 4.6 and 4.9 were recorded in Accra in 1871 and 1872, respectively (Ambraseys and Adams, 1986). However, Musson (2014) suggested that much of the recorded seismicity around Accra is in fact a very protracted aftershock sequence of the 1862 event.

Instrumental recording of earthquakes in Ghana began in 1914 but ceased in 1933 due to financial constraints (Banson, 1970). A major earthquake struck Accra in 1939. The event was recorded by enough seismic stations to allow for a detailed study of its seismotectonic characteristics (Yarwood and Doser, 1990). In fact, it was found that the event consisted of two consecutive earthquakes, the smaller one with magnitude 6.1 occurring 9.5s before the larger event with magnitude 6.4. The largest earthquake occurred to the north of the intersection of the Akwapim and Coastal Boundary Fault systems (Figure 4.1), along the strike-slip fault that parallels the coastline of Ghana. The 1939 earthquake caused extensive damage and was felt over an area of approx. 780,000 km^2 . In Accra, at least 16 people lost their lives, and over 100 people were severely injured. Continuous instrumental recording resumed in Ghana in 1977 (Quaah, 1980). The strongest earthquake recorded outside Ghana occurred in north-western Guinea in 1983. The epicentre of the 1983 M6.3 Guinea earthquake was located in Gaoual, near the border with Guinea-Bissau. It resulted in approximately 10 km of surface rupture, which extensively damaged buildings, killing over 200 people (Langer et al., 1987). More recent seismic events have been attributed to the reactivation of the Akwapim fault zone (Langer et al., 1987; Kutu, 2013; Musson, 2014; and Ahulu et al., 2018).

4.3 Earthquake catalogue

The first earthquake catalogue for the region was compiled by Ambraseys and Adams (1986) and included events as far back as 1615. Musson (2014) provided a comprehensive earthquake catalogue that included historical and instrumental earthquakes. Amponsah et al., (2012) published an earthquake catalogue of Ghana for the time period 1615–2003. In the present work, we compile a new catalogue based on the earthquake catalogues discussed earlier and including events listed in the online USGS-NEIC catalogue (https://earthquake.usgs.gov/earthquakes/search/) and ISC online bulletin (http://www.isc.ac.uk/ iscbulletin/search/catalogue/), the latter were last accessed in October 2020. The five source catalogues for the updated earthquake catalogue are listed in Table 4.1.

As the five catalogues reported events in local magnitude (M_L), surface magnitude (M_S), body magnitude (m_b) and duration magnitude (M_d), for the compiled catalogue the

Irinyemi A. Stephen
PhD in Geotechnical Earthquake Engineering (2021)
University of Manchester (UK)

different magnitude scales were homogenised to the moment magnitude (M_w) using the following relationships from Scordilis (2006):

$M_w = 0.85m_b + 1.03$ valid for $3.5 \leq m_b \leq 6.2$ (4.1)

$M_w = 0.67M_s + 2.07$ valid for $3.0 \leq M_s \leq 6.1$ (4.2)

$M_w = 0.85M_L + 0.65$ valid for $3.0 \leq M_s \leq 6.1$ (4.3)

$M_w = 1.47M_d - 1.49$ (4.4)

Since different catalogues reported same events, it was necessary to manually remove duplicates using the criteria by Nasir et al. (2013), which include events located within 10 km and recorded within a time period of 2 min. For duplicate events, the following catalogue was given priority for retaining the event in the catalogue: Musson (2014), followed by the USGS-NEIC earthquake catalogue, ISC earthquake catalogue, Amponsah et al. (2012) and finally Ambraseys and Adams (1986). The complete catalogue was finally declustered by removing foreshocks and aftershock, and seismic swarms, using the cluster-based method by Reasenberg (1985), implemented by Wiemer (2001). The declustered catalogue contained 129 events in the moment magnitude range $3 \leq M_w \leq 6.8$. The spatial distribution of the events of the compiled declustered catalogue is shown in Figures 4.2(a). The temporal distribution of magnitudes in the periods 1818–2018 is shown in Figures 3.2(b).

Table 4.1. Source catalogues for earthquake catalogue database (with magnitudes $M_w \geq 3.0$).

Source catalogue	Period (year)	No. of Events
Ambraseys and Adams (1986)	1615-1976	64
Amponsah et al. (2012)	1615-2003	72
ISC Bulletin[a]	1939-2018	95
Musson (2014)	1615-2009	65
(USGS – NEIC)[b]	1939-2018	19

[a]International Seismological Centre (2018)

[b]United States Geological Survey -National Earthquake Information Centre.

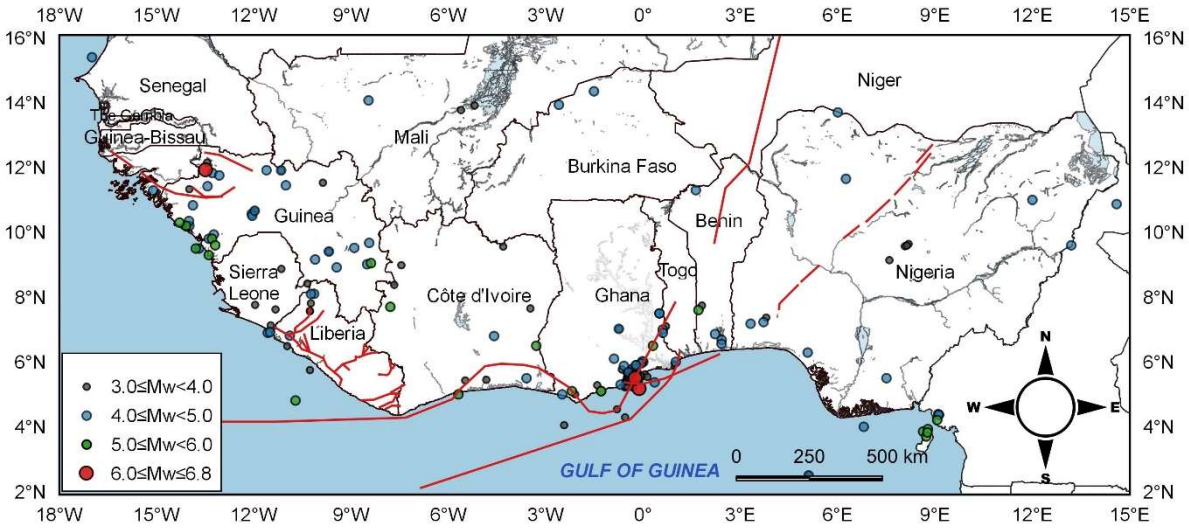

(a)

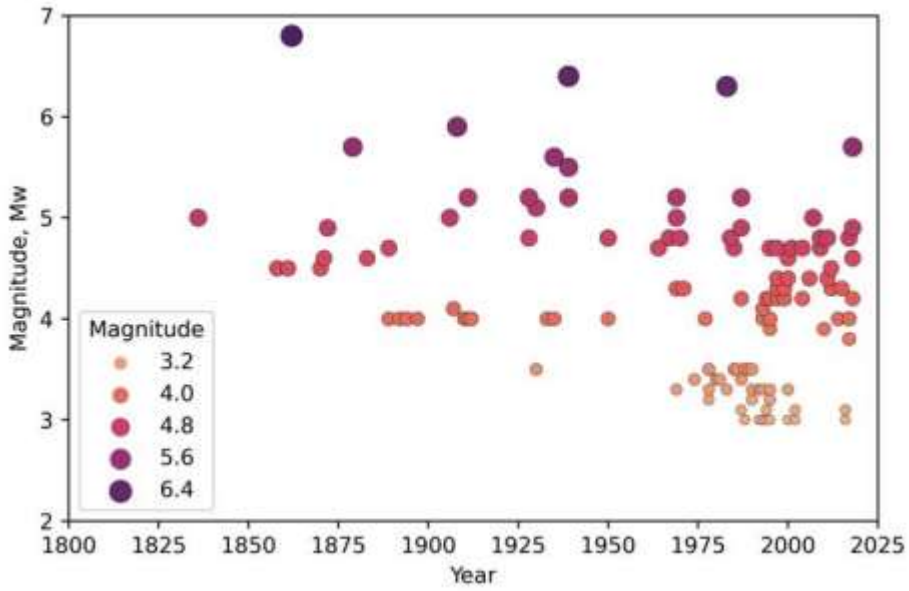

(b)

Figure 4.2. Distribution of seismic events in the compiled declustered catalogue: (a) Spatial distribution of earthquake epicentres; (b) temporal distribution of earthquake magnitudes for the period 1818-2018.

4.3.1 Catalogue completeness analysis

An earthquake catalogue is said to be complete over a certain magnitude range and time period if no earthquakes with magnitudes within that range are thought to be missing from the catalogue. Different completeness analysis methods are available (Rydelek and Sacks, 1989; Woessner and Wiemer, 2005; Nasir et al., 2013). To determine the

completeness of the new compiled catalogue with respect to the magnitude we used the method by Stepp (1972), which relies on the assumption that each magnitude sub-class can be represented as a point process in time and the earthquake occurrence follows a Poisson distribution. The unbiased estimate of the mean rate of occurrence of events per unit time interval is given by

$$\bar{\lambda} = \frac{1}{N}\sum_{i=1}^{N} \lambda_i \qquad (4.5)$$

where λ_i is the rate of occurrence of events per unit time interval for the i*th* subclass of the event set, and *N* is the number of sub-classes.

The standard deviation of the mean rate per unit time interval, taken as one year, and the total time of the sample equal to T is:

$$\sigma_\lambda = \sqrt{\bar{\lambda}/T} \qquad (4.6)$$

If the sample is unbiased and the earthquake process stationary, the plotted relationship between standard deviation σ_λ versus time follows exactly the line with slope $1/\sqrt{T}$ (Figure 4.3). The completeness time interval corresponds to the time interval at which no deviation from that straight line $1/\sqrt{T}$ occurs. The completeness analysis shows that the catalogue is complete for $M_w \geq 4$ for the period between 1818 and 2018 (Table 4.2). All events with magnitude $M_w < 4.0$ were excluded from the complete catalogue, thus leaving 85 events in the working catalogue used for the definition of the recurrence parameters discussed later. The maximum curvature method was used to determine the completeness of the catalogue with respect to time (Wiemer and Wyss, 2001). From the histogram shown in Figure 4.4, it can be concluded that the compiled catalogue is complete for $M_w \geq 4$. The bimodal features in the histogram of Figure 4.4, is due to the inclusion of more data of smaller magnitudes from 1930. Conservatively, we considered that our catalogue can be considered complete for moment magnitude $M_w > 4.0$ and time period after 1818.

Irinyemi A. Stephen
PhD in Geotechnical Earthquake Engineering (2021)
University of Manchester (UK)

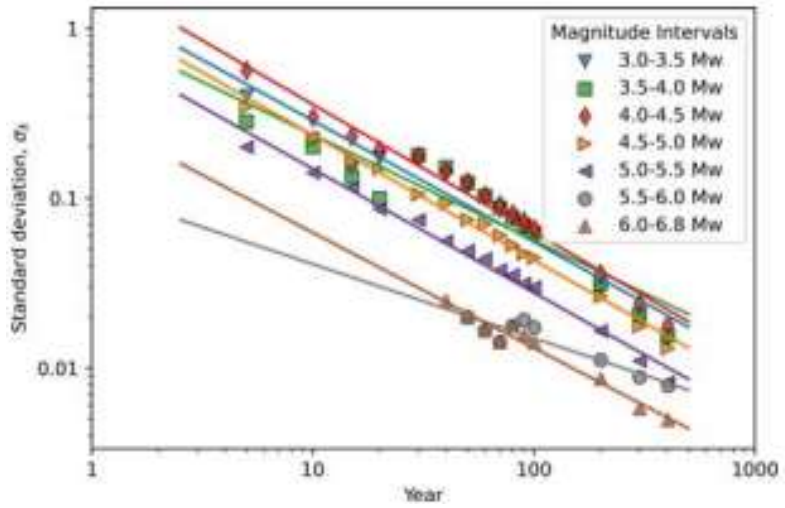

Figure 4.3. Completeness periods for different magnitude ranges using Stepp method (Stepp, 1972).

Table 4.2. Completeness periods for different magnitude classes

Magnitude class (M_w)	Completeness period	Completeness interval (years)
$3.0 \leq M_w < 3.5$	1918-2018	100
$3.5 \leq M_w < 4.0$	1918-2018	100
$4.0 \leq M_w < 4.5$	1818-2018	200
$4.5 \leq M_w < 5.0$	1918-2018	100
$5.0 \leq M_w < 5.5$	1818-2018	200
$5.5 \leq M_w < 6.0$	1718-2018	300
$6.0 \leq M_w \leq 6.8$	1718-2018	300

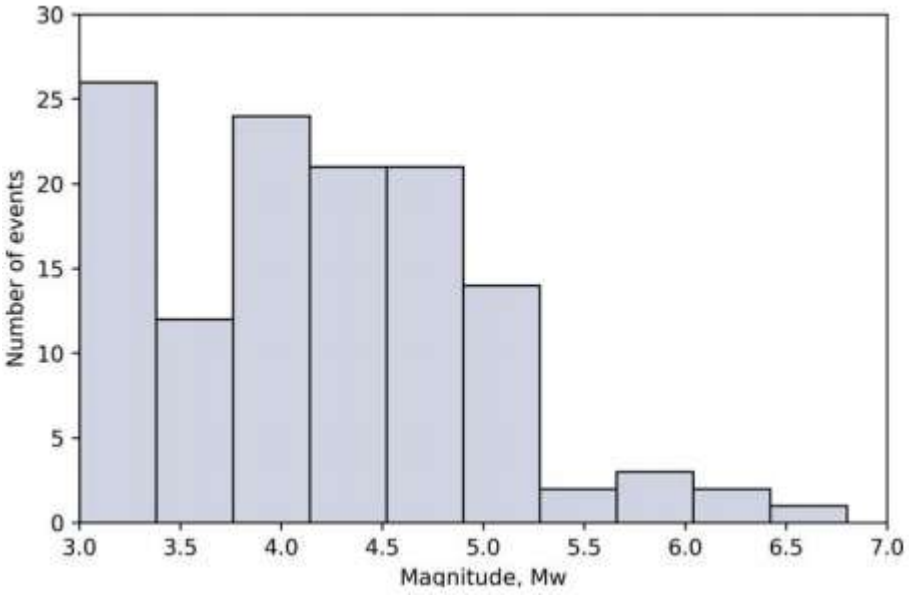

Figure 4.4. Histogram of magnitude distribution for the compiled catalogue.

4.4 Seismic source characterisation

4.4.1 Seismic source zone

The study region was divided into fourteen seismic source zones (Figure 4.5). These were delineated based on the main tectonic features discussed in section 4.2 (see also Figure 4.1) and the spatial distributions of historical and instrumental events (Figure 4.2a).

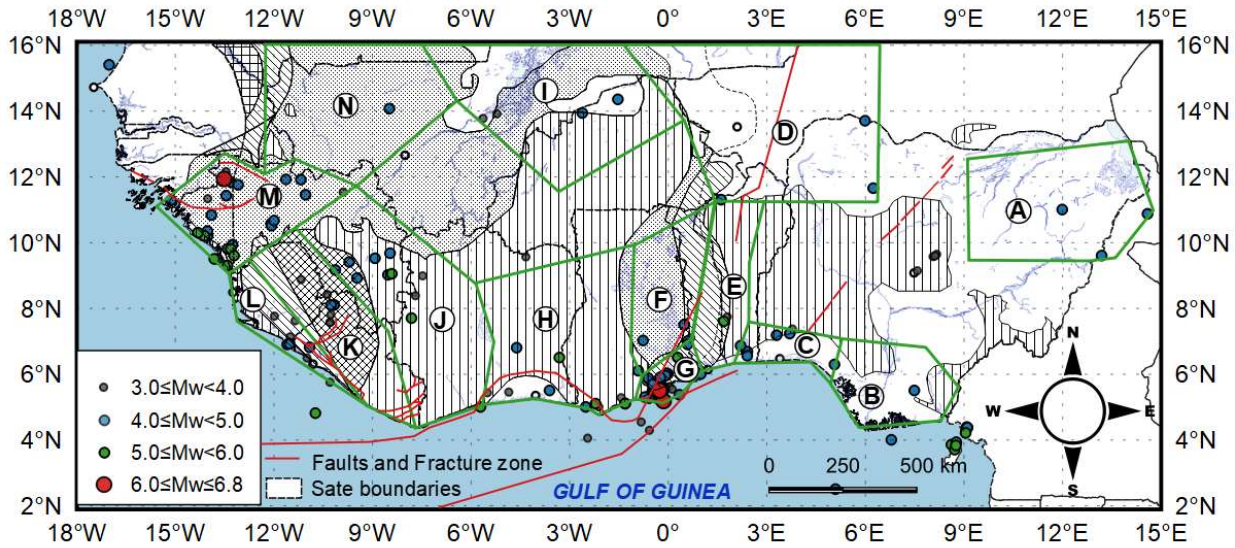

Figure 4.5. Seismic source zones for the study region

4.5 Seismic recurrent parameter (*b*-value)

The seismic characteristics of the seismic source zones are assumed to follow a truncated exponential Gutenberg-Richter distribution. This requires the definition of the recurrence parameters used by the Gutenberg-Richter recurrence law:

$$Log_{10}(N) = a\text{-}bM \qquad (4.7)$$

where N is the number of events with magnitudes equal to, or greater than, M, a-value is the activity rate which defines the intercept of the Gutenberg-Richter relation at M equal zero.

The b-value represents the slope of the Gutenberg-Richter relation and controls the relative frequency of occurrence of earthquakes of different magnitudes. The recurrence parameters b-values and λ were calculated using the maximum-likelihood method implemented in the computer programme ZMAP (Wiemer, 2001). In the low-to-moderate seismicity area, it is common to use a unique b-value for all seismic source zones due to limited recorded data. As a result, the b-value was classified, into three groups with values shown in Table 4.3. The a-value calculated is shown in Table 4.3. The λ-parameter is known to vary from the different zones within a given area, so it was estimated differently for each zone by taking the average of an annual number of earthquakes with magnitude equal to or higher than $M_{min.}$

Different methods are available for the definition of the maximum credible magnitude, M_{max}, (Kijko and Sellevoll, 1989; Kijko and Graham, 1998). In this work due to the paucity of recorded data, M_{max} was determined from the largest observed magnitude M_{obs} using the simple expression by Gupta (2002), which despite its simplicity has been extensively used by other researchers in regions with limited data (Deif et al., 2011; Ahulu et al., 2018; Poggi et al., 2017).

$$M_{max} = M_{obs}+0.5 \qquad (4.8)$$

There is limited available information on the focal depth of earthquakes in this study region, due to sparse seismic station coverage and spacing. However, results from

microseismic studies reported focal depths in the range 1-30km (Ahulu et al., 2018). In this study, hazard analysis is conducted for a constant focal depth of 10km for all zones.

Table 4.3. Seismicity parameters used in the study model.

Group	Zone	M_{obs}	M_{max}	$b \pm \sigma b$	a	λ
(1)	G	6.8	7.3	0.63± 0.13	3.916	0.156
(2)	M	6.3	6.8	0.60± 0.11	3.370	0.165
(3)	A	4.8	5.3	1.12± 0.29	6.584	0.015
	B	4.8	5.3			0.010
	C	4.8	5.3			0.030
	D	4.2	4.7			0.015
	E	5.6	6.1			0.004
	F	4.3	4.8			0.015
	H	5.7	6.2			0.020
	I	4.3	4.8			0.010
	N	4.3	4.8			0.010
	J	5.9	6.4			0.035
	K	4.8	5.3			0.020
	L	4.7	5.2			0.015

4.6 Ground motion prediction equations (GMPEs)

Ground motion prediction equations (GMPEs) are essential for the definition of the ground motion model. Although GMPEs calibrated from local seismic data are preferred, these were not available for the study region owing to limited, and in many zones, lack of recorded strong-ground motions. Consequently, we used five different GMPEs developed for regions with compatible tectonic characteristics. The selected GMPEs are listed in Table 4.4 and presented hereafter.

(1) Pezeshk et al. (2011): this is a hybrid empirical method developed for Eastern North America (ENA), a region with moderate seismicity and sparse ground motions. The method employs the stochastic simulation method to adjust empirical GMPEs developed Western North America (WNA), an area with high seismicity and abundant strong-motion recordings. The adjustments take into account differences in

the earthquake source, wave propagation, and site-response characteristics between the two regions. The resulting model is applicable for moment magnitude range 5-8 and closest distances to the fault rupture up to 1000 km. Ground-motion prediction equations are developed for the 5%-damped response spectra and peak ground acceleration for hard-rock sites.

$$\log(\bar{Y}) = c_1 + c_2 M_w + c_3 M_w^2 + (c_4 + c_5 M_w) \times min\{\log(R), \log(70)\} + (c_6 + c_7 M_w) \times max\left[min\left\{\log\left(\frac{R}{70}\right), \log(140/70)\right\}, 0\right] + (c_8 + c_9 M_w) \times max\{\log(R/140), 0)\} + c_{10} R \quad (4.9)$$

where $(\bar{Y})$ is the median value of PGA or PSA in g, R is the distance computed as

$$R = \sqrt{R_{rup}^2 + c_{11}^2} \quad (4.10)$$

where R_{rup} is the closest distance to fault rupture in km, and c_1 to c_{11} are constants as reported by Pezeshk et al. (2011). Note that $\log(140/70)$ is the geometric spreading, $Z(R)$, used for Eastern North America (ENA). The value of 70 is equal to the hybrid empirical method prediction as reported by Pezeshk et al. (2011).

Table 4.4. Ground motion prediction equations used in the study

GMPE reference source	GMPE	Magnitude	Distance (km)
Pezeshk et al. (2011)	Equation (4.9)	5.0-8.0	$R_{rup} < 1000$
Tavakoli and Pezeshk (2005)	Equation (4.11)	5.0-8.2	$R_{rup} < 1000$
Abrahamson et al. (2014)	Equation (4.13)	3.0-8.5	$R_{rup} \leq 200$
Campbell and Bozorgnia (2014)	Equation (4.14)	3.0-7.9	$R_{rup} \leq 500$
Chiou and Youngs (2014)	Equation (4.15)	3.5-8.5	$R_{rup} \leq 300$

(2) Tavakoli and Pezeshk (2005): this is another hybrid-empirical model developed to predict the ground-motion relationship for eastern North America (ENA) based on data from western North America (WNA). The proposed empirical-stochastic attenuation

relationship provides peak ground acceleration and 5%-damped spectral acceleration. The model applies to earthquakes of with moment magnitude range $5.0 \leq M_w \leq 8.2$ at distances of up to 1000 km.

$$\ln(Y) = f_1(M_w) + f_2(R_{rup}) + f_3(M_w, R_{rup}) \quad (4.11)$$

$$R = \sqrt{R^2{}_{rup} + (C_5 \exp[C_6 M_w + C_7 (8.5 - M_w)^{2.5}])^2} \quad (4.12)$$

where Y is the median value of PGA or PSA in (g), M_w is the moment magnitude, R_{rup} is the rupture and define the distance to the fault rupture in (km). f_1 to f_3 are frequencies (Hz), while and c_5 to c_7 are constants as reported by Tavakoli and Pezeshk (2005).

According to Bacon and Quaah (1981) and Ahulu et al. (2018), prevalent active normal faulting and thrust faulting have experienced within the Akwapim fault zone, which is similar to the active region. For that reason, the equations of Abrahamson et al. (2014), Chiou and Youngs (2014) and Campbell and Bozorgnia (2014), are selected for seismic hazard assessment.

(3) Abrahamson et al. (2014): this is empirical ground motions for the average horizontal component used in shallow crustal earthquakes from tectonic regions derived from PEER NGA-West2 database. The model is applicable to moment magnitudes 3.0–8.5, distances 0–300 km, and spectral periods of 0–10 s

$$\ln Sa(g) = f_1(M, R_{rup}) + f_{RV} f_7(M) + f_N f_8(M) + f_{AS} f_{11}(CR_{jb}) + f_5(\widehat{Sa}_{1180} V_{s30}) + f_{HW} f_4(R_{jb}, R_{rup}, R_x, R_{y0}, W, dip, Z_{TOR}, M) + f_6(Z_{TOR}) + f_{10}(Z_{1.0}, V_{s30}) + Regional + (V_{s30}, R_{rup}) \quad (4.13)$$

Where the functional forms ($f_1, f_4, f_5, f_6, f_7, f_8, f_{10}, f_{11}$), and the regional terms are presented by Abrahamson et al. (2014).

R_{rup} = rupture distance in (km), f_{RV} = flag for reverse faulting earthquakes, f_N = flag for normal faulting earthquakes, f_{AS} = flag for aftershocks, CR_{jb} = centroid of R_{jb}, $\widehat{Sa}_{1180}$ = median peak spectral acceleration (g) for V_{s3} = 1.180 m/s, V_{s30}= Shear-wave

Irinyemi A. Stephen
PhD in Geotechnical Earthquake Engineering (2021)
University of Manchester (UK)

velocity over the top 30 m (m/s), f_{HW} = flag for hanging wall sites, R_{jb},= closest horizontal distance to the surface projection of the rupture (km), R_x = horizontal distance from the top edge of the rupture, measured perpendicular to the fault strike (km), R_{y0} = horizontal distance off the end of the rupture measured parallel to strike (km), W = down-dip rupture width (km), Dip = fault dip degrees, Z_{TOR} = depth to top of rupture (km), M = moment magnitude, $Z_{1.0}$ = depth to V_s = 1.0 km⁄s at the site (m).

(4) Campbell and Bozorgnia (2014): the model used an expanded PEER NGA-West2 database to develop a new GMPE for the average horizontal components of PGA, PGV, and 5% damped linear acceleration response spectra. The model is applicable for moment magnitudes ranging between 3.0 and 7.9 and distances ranging from 0 to 500 km.

$$\ln(Y) = \begin{cases} \ln PGA; & PSA < PGA \text{ and } T < 0.25\ s \\ f_{mag} + f_{dis} + f_{flt} + f_{hng} + f_{site} + f_{sed} + f_{hyp} + f_{dip} + f_{atn}, & otherwise \end{cases} \quad (3.14)$$

where Y = intensity measure of interest and f – terms represent the scaling of ground motion with respect to earthquake magnitude, geometric attenuation, style of faulting, hanging wall geometry, shallow site response, basin response, hypocentral depth, fault dip, and anelastic attenuation, respectively, are presented by Campbell and Bozorgnia (2014).

(5) Chiou and Youngs (2014): this is an updated 2008 NGA model for predicting horizontal ground motion used in shallow crustal earthquakes from tectonic regions derived from expanded PEER NGA-West2 database and numerical simulations. The model is applicable for moment magnitude range 3.0-8.5, and maximum distances up to 300km. The full equation is shown in the Appendix A.

Irinyemi A. Stephen
PhD in Geotechnical Earthquake Engineering (2021)
University of Manchester (UK)

Table 4.5. Computed weights for different ground motion prediction equations for different seismic source zones.

Zone	M_{max}	TP2005	PEAL2011	ASK2014	CB2014	CY2014
G	7.3			0.53	0.37	0.10
M	6.8			0.48	0.41	0.11
A	5.3	0.57	0.43			
B	5.3	0.57	0.43			
C	5.3	0.57	0.43			
D	4.7	0.47	0.53			
E	6.1	0.58	0.42			
F	4.8	0.48	0.52			
H	6.2	0.59	0.41			
I	4.8	0.48	0.52			
N	4.8	0.48	0.52			
J	6.4	0.63	0.37			
K	5.3	0.57	0.43			
L	5.2	0.57	0.43			

To account for epistemic uncertainty, the five GMPEs have been used within a logic tree ((e.g., Kulkarni et al., 1984, Giardini et al., 2004; Deif et al., 2011)). The weight of each branch was estimated using the average sample log likelihood function (Delavaud et al., 2009), whose estimator can be expressed by

$$\text{LLH}\ (g, x_i) \ = \ -\frac{1}{N}\sum_{i=1}^{N} log_2\ [g(x_i)] \qquad (4.15)$$

where x_1, x_2, ..., x_N are samples of the ground motion values obtained using a GMPE model (g, x_i). The estimator LLH (g, x_i) used as a ranking criterion.

Once the LLH_i value of each GMPE model is known, the weight of a (w_i) can be computed as:

$$w_i \ = \ 2^{-LLH_i} \Big/ \sum_{k=1}^{K=M} 2^{-LLH_k} \qquad (4.16)$$

In this study, we used the following parameters: $M = 3$ for group 1 and 2, and $M = 2$ for group 3. The ranking is based on PGA value using each observation of x_i, 1, … ...

Irinyemi A. Stephen
PhD in Geotechnical Earthquake Engineering (2021)
University of Manchester (UK)

… *N,* which are 30km, 60km, 120km, 150km and 200km. We calculated the sample log likelihood of each GMPE model given x_i. The quantities have been averaged (equation 2.15) at (N = 5). The rankings of the GMPEs, are based on mean LLH_i values, and the weight for each GMPE as shown in Table 4.5.

4.7 Seismic hazard calculations

The seismic hazard calculations (Cornell, 1968; McGuire, 1976) in this study region are performed using the software programme R-CRISIS Ver. 18.4 (Ordaz and Sagado-Gálvez, 2017). The analysis is carried out on a grid with dimensions 0.5^0 x 0.5^0. The seismic hazard estimates are computed for rock sites and three return periods, i.e., return periods of 475, 2475 and 9975 years. The main results are presented in terms of hazard maps and 5%-damped elastic response spectra. Results from a deaggregation analysis for Accra is also presented to investigate the earthquake scenarios (expressed by the pair moment-distance) that have the highest contribution for the seismic hazard.

4.7.1 Results

Figure 4.6 shows the seismic hazard maps in terms of mean peak ground acceleration (PGA) for return periods of 475, 2475, and 9975 years. It can be seen that the highest hazard is located in Ghana, more specifically, in Accra and the southern Ghana, where PGA attains maximum value of 0.1g, 0.26 g and 0.45 g for return periods of 475, 2475, and 9975 years, respectively. To provide further estimates for different exceedance probabilities, Figure 4.7 plots the seismic hazard curves for four major cities within West Africa (whose population is listed in Table 4.6). The hazard curves confirm that the highest hazard is concentrated along the southern coast of Ghana and adjacent Togo, including its capital city Lomé. Figure 4.8 shows the 5%-damped elastic response spectra for the four selected cities and different return periods.

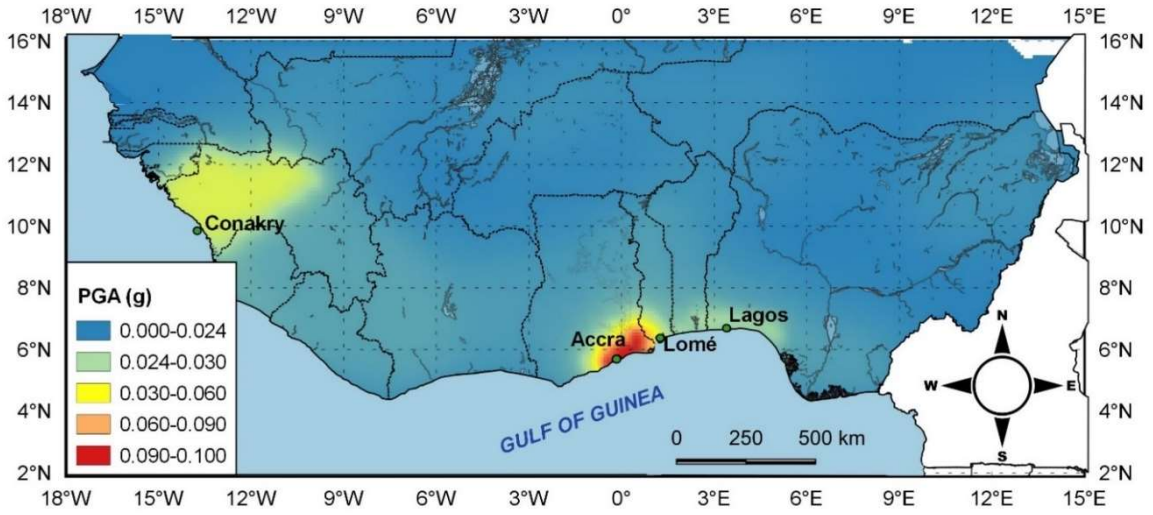

(a)

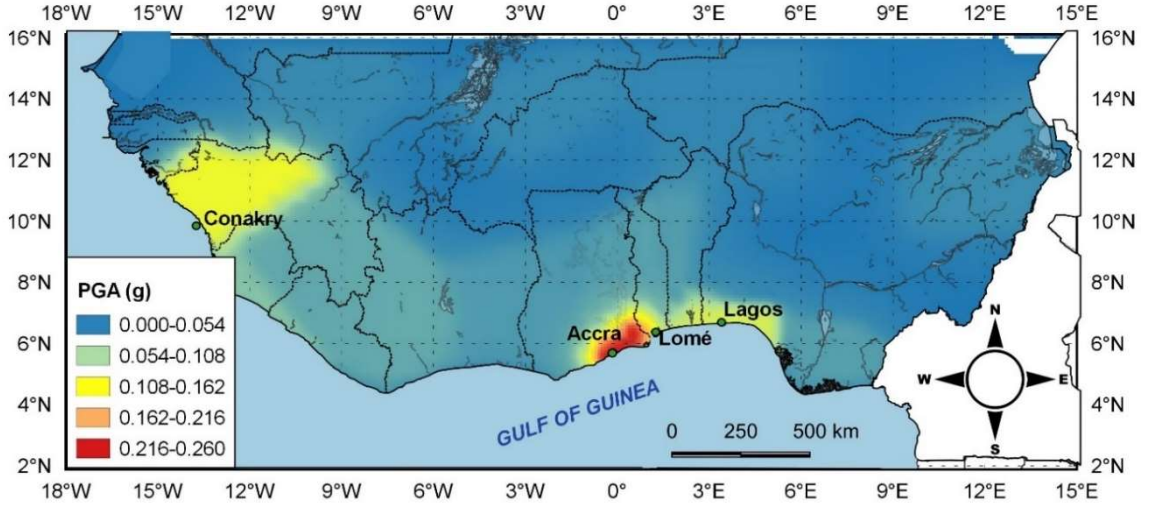

(b)

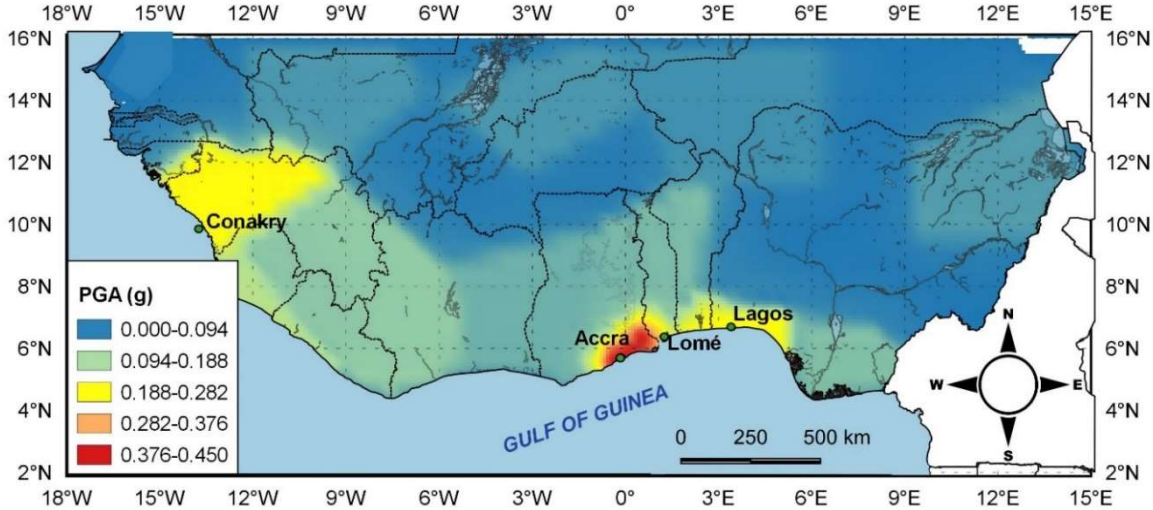

(c)

Figure 4.6. Seismic hazard maps, for a return period of: (a) 475 years; (b) 2475 year; (c) 9975 years.

Table 4.6. The population of major cities in West Africa.

Number	City/Country	Population
1	Lagos/Nigeria	8,029,200
2	Lomé/Togo	675,000
3	Accra/Ghana	1,605,400
4	Conakry/Guinea	1,595,800

(Source: https://namecensus.com/igapo/West_Africa.htm)

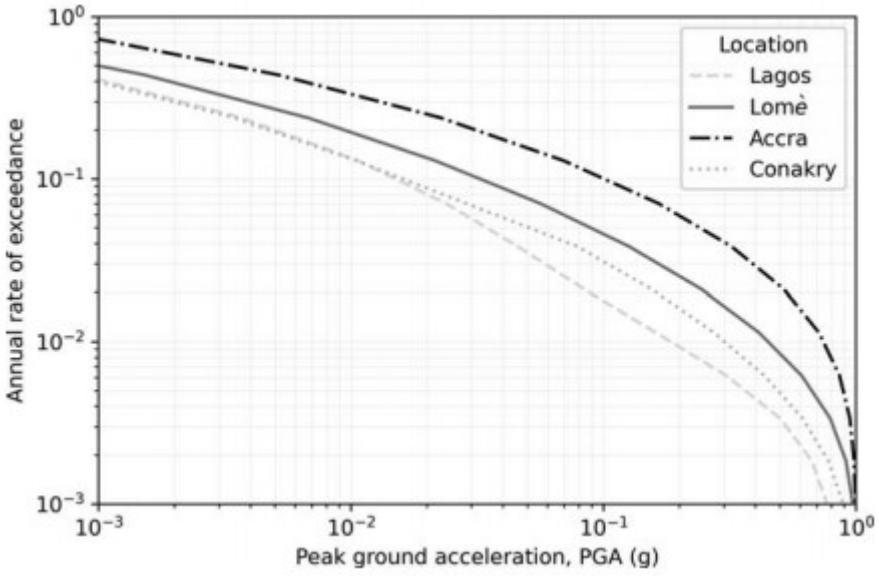

Figure 4.7. Seismic hazard curves for four major cities within West Africa

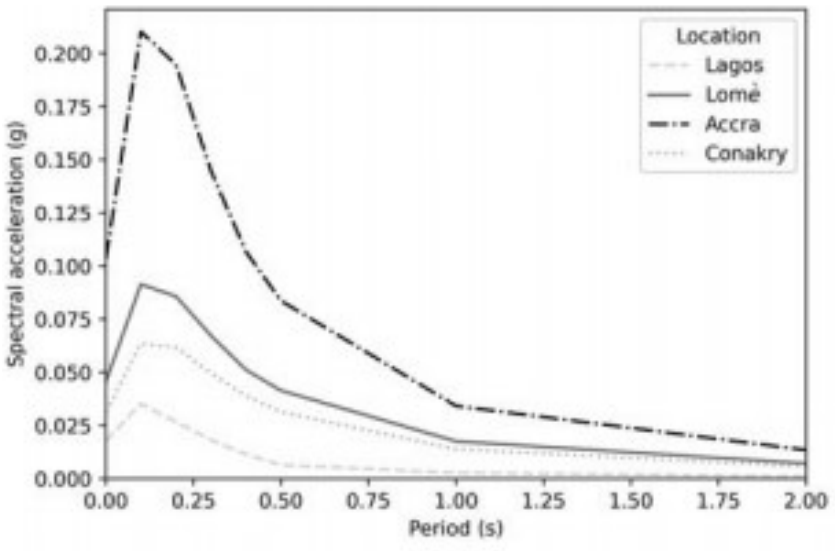

(a)

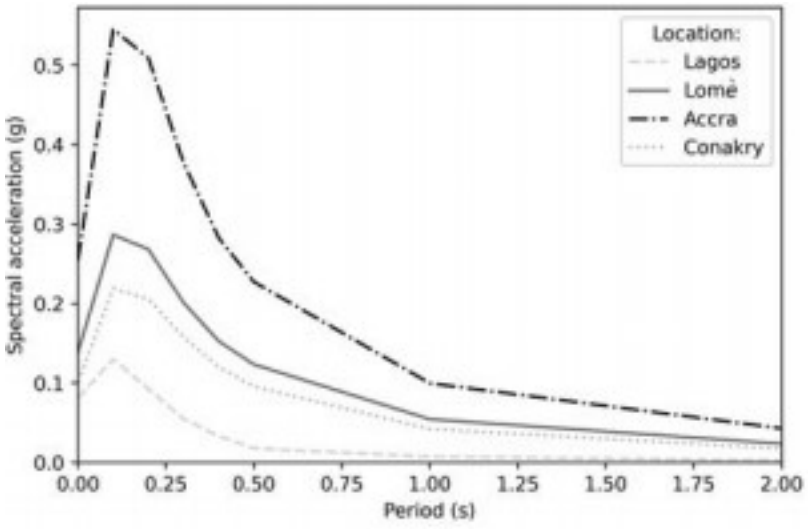

(b)

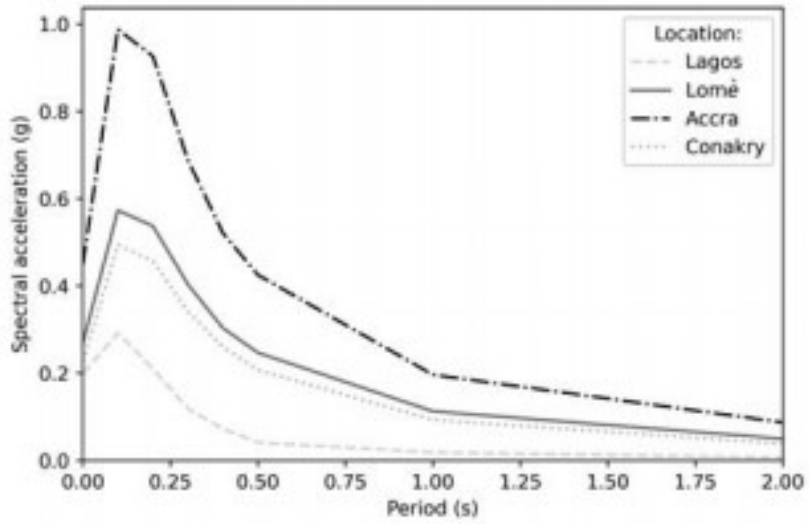

(c)

Figure 4.8. 5%-damped elastic response spectra for four major cities within West Africa for return periods of: (a) 475 years; (b) 2475 years; (c) 9975 years.

Figure 4.9 summarises the results from the deaggregation for Accra at the 475-year return period for vibration periods of 0.1, 0.2, 1.0 and 2.0 s. From Figure 4.9, it can be seen that the hazard is dominated by earthquakes of magnitudes 5.5–6.0 at distances less than 60 km.

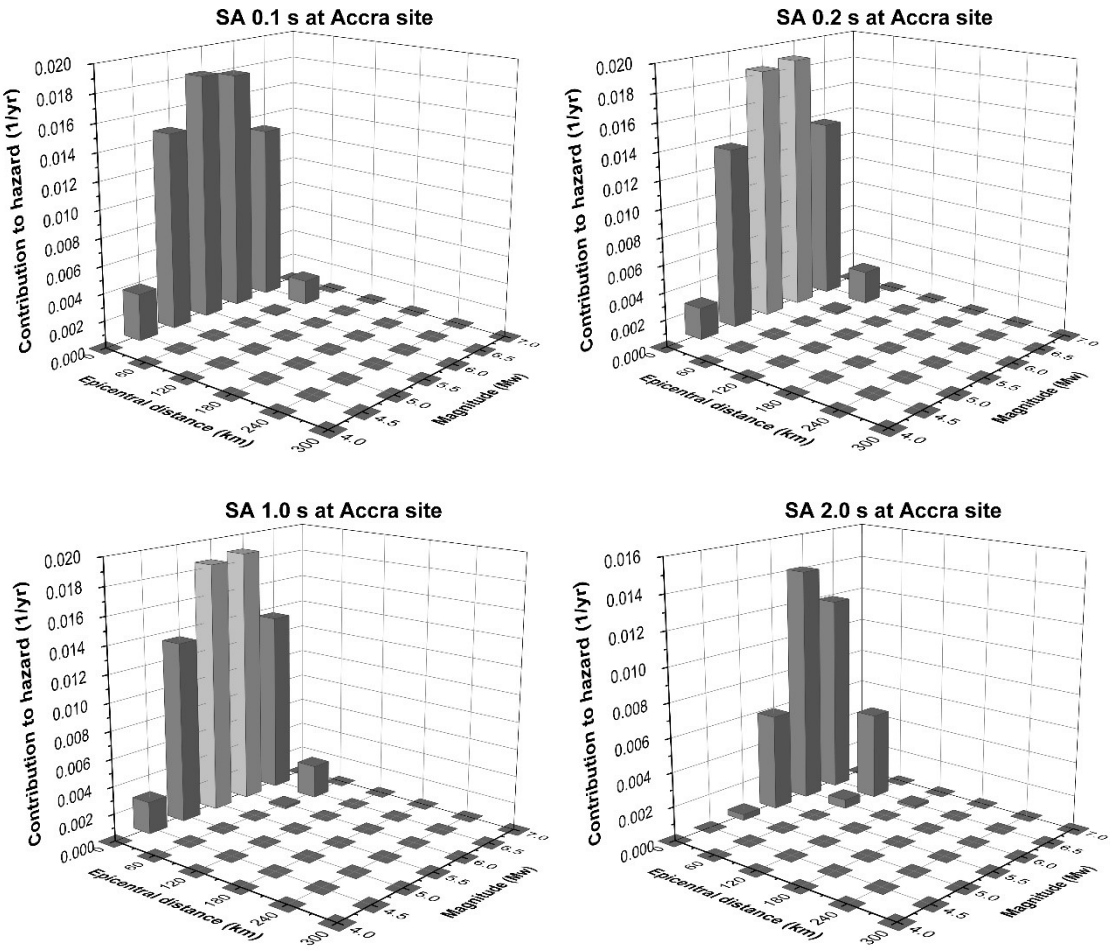

Figure 4.9. Disaggregation results for Accra at the 475-year return period for vibration periods of 0.1, 0.2, 1.0 and 2.0 s.

4.8 Discussion and Summary

The paper presents results of a logic-tree based probabilistic seismic hazard assessment of West Africa. The West African region is known to be of low-to-moderate seismicity, yet historical events suggest that important seismic events with potentially damaging consequences are possible in Accra and southern Ghana. Our approach to the regional seismic hazard assessment was improved by including a longer catalogue of earthquakes (1615-2018), more recent GMPEs, and a combination of two or three relations with different weights, conducted site-specific hazard assessments for important cities within the region, and disaggregated results for Accra site to determine the magnitude and distance range of seismic source that dominate the hazard. The results show that for return periods of 475, 2475 and 9975 years there is a significant seismic hazard within

the Accra region close to the Gulf of Guinea –despite the low-to-moderate seismicity of the region. Similarly, site-specific hazard analysis of four selected sites within the region showed a maximum hazard level (at the period of 0.1 s) in Accra (0.21g) and a minimum hazard level (0.035g) in Lagos at the 475-year return period. The results confirm the high seismicity of these regions, with peak ground acceleration up to 0.1g for rock sites at a return period of 475, that is 10% probability of exceedance in 50 years. The PGA estimates for Accra are lower (0.1g) than those reported by Ahulu et al. (2018) who predicted values close to 0.2g for Accra, and in agreement with those published as part of the GSHAP. The difference in the value of maximum PGA of 0.1 g obtained in the present study compared to the value of 0.2 g reported by Ahulu et al. (2018) may be due to the additional seismic sources and more recent seismic GMPEs used for the assessment. Also, under GSHAP, Grunthal et al. (1999) reported that Africa's western part has a maximum PGA value of around 0.08 g. The equatorial part of West Africa slightly higher, about 0.1 g. These values are comparable with this present study. Furthermore, it is interesting to note that our estimates for Accra for a return period of 9975 years are close to those predicted by the deterministic seismic hazard analysis by Amponsah et al. (2009). The approach of Amponsah et al. (2009) uses the 1939 M_w 6.4 Accra earthquake as the source earthquake and has been conducted for computing the synthetic seismograms for four profiles located in the Greater Accra Metropolitan Area. In such a case, the approach usually used for critical infrastructures (large dams, lifelines, and power plants), which inherently has higher return period – this match with the results obtained from the present study for higher return periods. According to a guideline provided by ICOLD (2010), the results for 475 years, 2475 years and 9975 years return periods can be adopted as design earthquakes for dam infrastructure. From our study, we find that four cities selected within the region (Accra, Conakry, Lagos, and Lomé) fall within the high hazard levels on the new seismic hazard maps. This is a critical result as the four cities are now seeing sizeable infrastructure development (e.g., in the Accra and Lagos regions), and hence according to our study, the seismic risk associated with such development can be significant. Thus, to protect the local population and to sustain the region's economic development, it is critical to mitigate against such risks, which, from designer's perspective can be achieved by designing and building new infrastructure using the seismic hazard maps proposed in this study.

CHAPTER 5

SEISMIC HAZARD ASSESSMENT IN GUINEA, WEST AFRICA REGION

Reformatted version of the following paper:

Paper title**: Seismic hazard Assessment in Guinea, West Africa Region**

Authors**: Stephen A. Irinyemi, Domenico Lombardi & Syed M. Ahmad**

Research output: Contribution to journal › Article › peer-review

Published in: Scientific Reports. (2022)

DOI: https://doi.org/10.1038/s41598-022-06222-7

Author contributions

The author (Irinyemi) conducted the seismic data analysis, designed the work, acquired and analysed the data and drafted the paper. Lombardi and Ahmad supervised the author.

Abstract

Guinea is located in a stable continental region in West Africa, which is characterised by infrequent seismic activities. In this study, the seismic hazard level in Guinea, West Africa was determined by a probabilistic approach for the country and for 10 sites across the region. The calculation was conducted for 10%, 2% and 0.5% probability of exceedance in 50 years (475, 2475 and 9975 years return periods, respectively) using a homogenized 100-year catalogue compiled from different seismic sources. Two ground motion prediction equations, originally developed for Eastern and Central North America, a stable continental region, were used in the hazard calculation presented using the R-CRISIS program. A uniform *b*-value of 0.70 ± 0.12, and individual activity rate (λ) were calculated for the three seismic zones. The levels of hazard estimated were high in the Palaeozoic area of Guinea. The PGA values estimated for the study region are 0.08

g, 0.27 g, and 0.57 g for 475, 2475 and 9975 years return periods, respectively for hard rock conditions. The results of this study will be useful in disaster management and planning for regional infrastructure.

Keywords: Seismic hazard assessment; Guinea; West Africa; Conakry; Peak ground acceleration.

5.1 Introduction

Guinea is located in West Africa far away from any known active plate boundary. The Guinea region is not known to be seismically active and the occurrence of moderate to large earthquakes is infrequent based on available records. The first reported earthquake in Guinea occurred in 1795, with an estimated surface magnitude of 5.2, causing considerable damage in the city of Labé (Ambraseys and Adams, 1986). In 1818 an earthquake of surface magnitude, M_S 5.9 occurred in the Futa Djallon massif in northern Guinea. Another earthquake with a surface magnitude of 4.0 caused panic in the Kakulima region but no damage was reported. In 1928 an earthquake with a surface magnitude of 4.8 struck the western part of Guinea leading to the collapse of some dwellings along the Konkouré river. Aftershocks followed this event in August 1928 triggering a landslide (Ambraseys and Adams, 1986). More earthquakes were reported between 1935 and 1939. On 22nd December 1983, north-western Guinea experienced a strong earthquake of moment magnitude, M_w, 6.3. The epicentre of the event was located in Gaoual, close to the border of Guinea-Bissau. It resulted in approximately 10 km of surface rupture, which extensively damaged buildings, killing over 300 people and destroying more than 4,000 houses (Langer et al., 1987; Langer and Bollinger, 1992). Despite this history of seismicity, no seismic hazard assessment has been conducted for Guinea.

In this study, we develop a seismic source model for the study region using available seismicity and geological information. The ground motion model is constructed using two different strong-motion attenuation equations. Finally, the hazard estimates for the region and for ten cities are computed at different return periods: 475, 2475, and 9975 years. The steady population expansion, types of building materials used for construction, inadequate land planning and development, obsolete construction method and improper systems of infrastructure associated with a high-risk level are major issues in disaster management. The present study provides valuable data for risk assessment and mitigation interventions, land use management, and planning for present and future infrastructures across the study region. This can be demonstrated by preventing and reducing the harmful effects of all hazards to the region through the use of emergency response.

5.2 Geology of the Guinea

Guinea, West Africa, has a total surface area of 245,000 km^2. Figure 5.1 shows the seismo-tectonic and geology of the study region and was generated by QGIS Ver. 3.18.3 software (https://www.qgis.org/en/site/). This is formed by Precambrian crystalline and Palaeozoic Rocks, which spread along the Guinean-Liberian shield. The Fouta Djallon massif is made of Silurian shade. Ordovician sandstone experienced massive arrival in both dolerites' tertiary and a parent rock gigantic bauxitic with laterite deposits (Soumah, 2009). The northwest of the basin's coastal zone consists of an unconsolidated-small outcrop of upper cretaceous to Tertiary sedimentary rocks. The Mesozoic contains some Kimberlite dykes and pipes located in the southern area that is diamond-bearing (Schlüter, 2006). The Western part of the African plate moves at slow rates within 2.0–15 mm/year (Hartnady and Benouar, 2006). The eastern part is primarily underlain by Archaean and Lower Proterozoic rocks, while upper Proterozoic metasedimentary rocks dominate the north. The coastal plains were formed by Quaternary marine and unconsolidated alluvial sediments. Older Palaeozoic overlay the plain, with small

Tertiary and Upper Cretaceous sedimentary rocks. Langer et al. (1987) explained the faults mechanism that resulted in the 1983 northwest Guinea earthquake recorded in the study. Rocks in Guinea are affected by rokelide orogeny like the one in Sierra Leone deformed during the Pan-African tectonothermal (Schlüter, 2006).

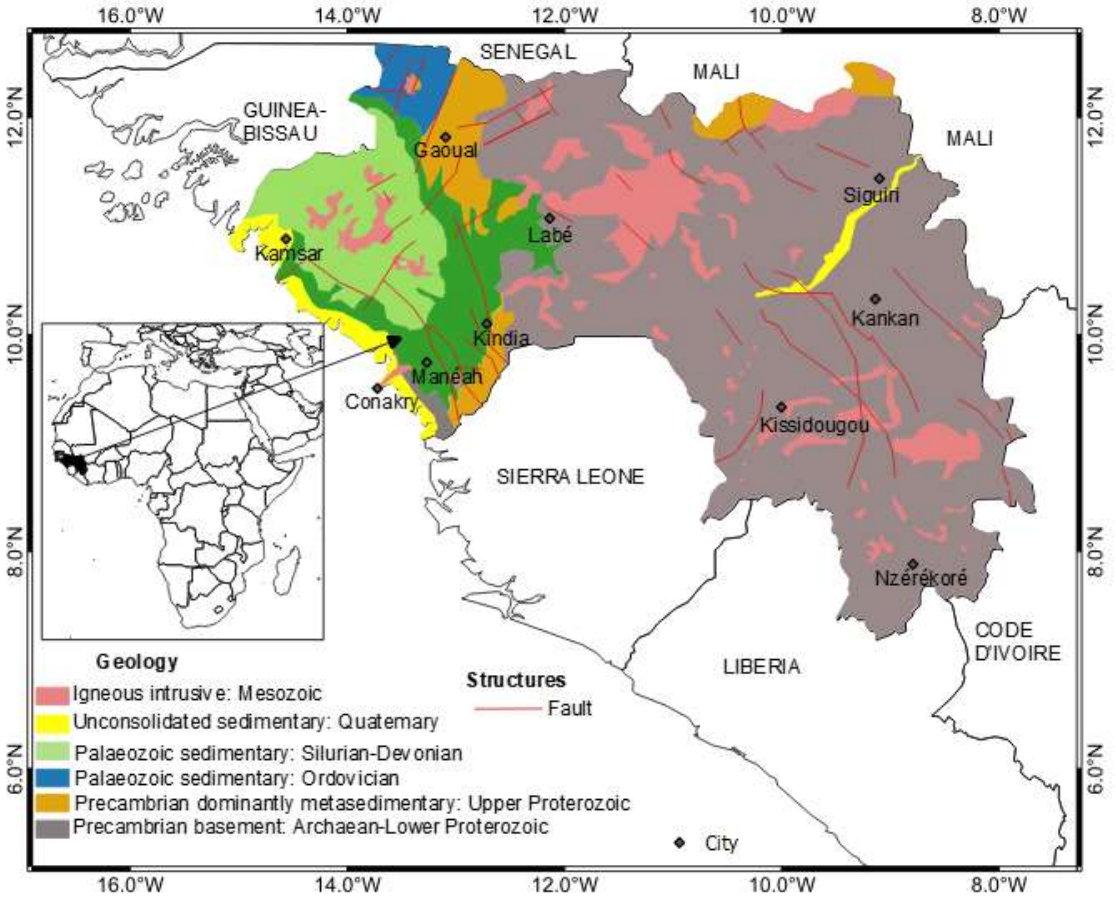

Figure 5.1. Geology and tectonic map of Guinea.

5.3 Compiled Earthquake Catalogue

The historical data sources used for this study were compiled by Ambraseys and Adams (1986) and include events as far back as 1795. The instrumental earthquakes are obtained from international agencies, including: the USGS online catalogue obtained from international agencies, including: the USGS online catalogue (https://earthquake.usgs.gov/earthquakes/search/) and the International Seismological Centre (ISC) (http://www.isc.ac.uk/iscbulletin/search/catalogue/). We unify the different magnitude scales used in the historical and instrumental database into a single moment

magnitude scale (M_w) using the empirical equations given in 1 to 3 (Scordilis, 2006; Papazachos, 1997).

$$M_w = 0.85m_b + 1.03 \; Value \; for \; 3.5 \leq m_b \leq 6.2 \quad (5.1)$$

$$M_w = 0.67M_s + 2.07 \; Value \; for \; 3.0 \leq M_s \leq 6.1 \quad (5.2)$$

$$M_w = 0.97M_L + 0.58 \; Value \; for \; 3.0 \leq M_L \leq 6.0 \quad (5.3)$$

where M_L = local magnitude (M_L), Ms = surface magnitude, and m_b = body magnitude.

As we compile the catalogue from different sources, duplicate events, defined as events with longitude and latitude within 10 km and recorded within a period of 2 minutes (Nasir et al., 2013) We manually remove duplicate events by prioritising events in the ISC earthquake catalogue, followed by the USGS-NEIC earthquake catalogue, and finally by Ambraseys and Adams (1986). To ensure that the earthquakes in the compiled catalogue are independent events, we remove all foreshocks and aftershocks using the declustering technique by Gardner and Knopoff (1974) which is implemented in the code ZMAP (Wiemer, 2001). The compiled catalogue ranges from $4 \leq M_w \leq 6.3$. The spatial and temporal distributions of the harmonised and declustered catalogue are shown in Figure 5.2. Figure 5.2a was generated by graphic and analysis software QGIS Ver. 3.18.3 (https://www.qgis.org/en/site/).

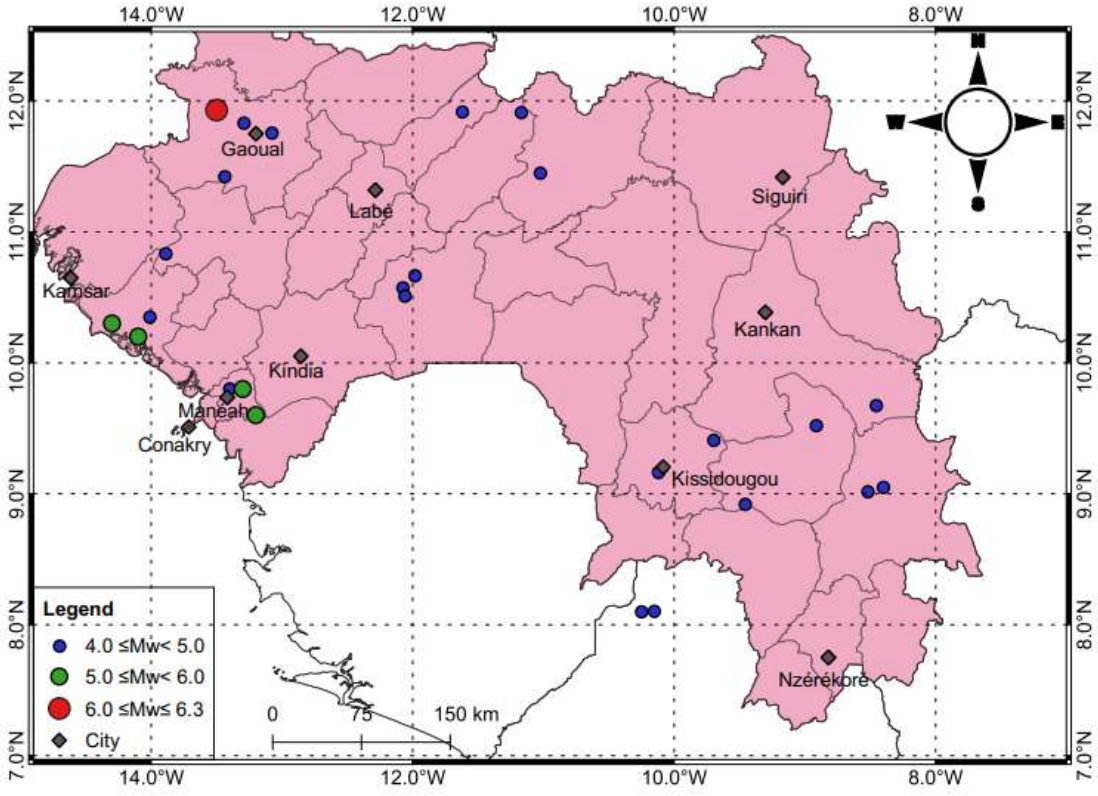

(a)

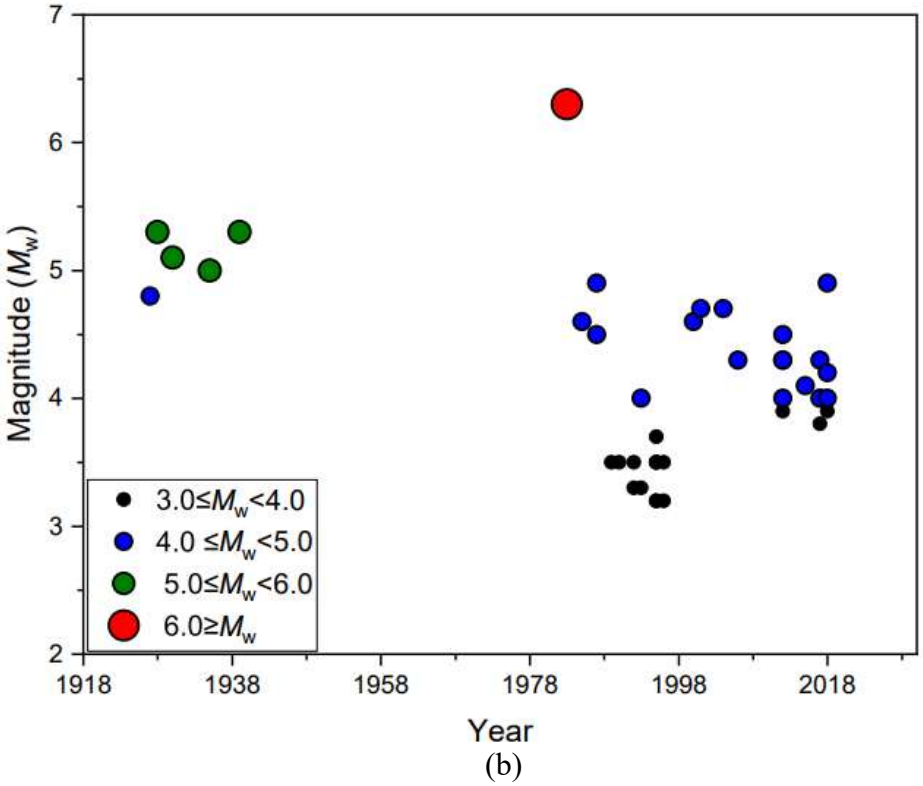

(b)

Figure 5.2. (a) Spatial distribution of earthquake epicentres (b) Time- magnitude distribution of the $M_w \geq 3.0$ for the period 1918-2018.

5.4 Seismic hazard analysis

We use the standard probabilistic framework method (Cornell, 1968; McGuire, 1995) to estimate the seismic hazard for the study region. We first compute the distribution of recurrence parameters for the events in the harmonised declustered catalogue and use the Stepp (1972) method to assess the completeness of catalogue. The process assumes that the magnitude sub-class represents a point process in time and follows a Poisson distribution. The unbiased mean rate of occurrence per unit time interval is shown in the expression,

$$\bar{\lambda} = \frac{1}{N}\sum_{i=1}^{N} \lambda_i \qquad (5.4)$$

$$\sigma_\lambda = \sqrt{\bar{\lambda}/T} \qquad (5.5)$$

where λ_i = rate of occurrence of events per unit time interval for each subclass magnitude, N = number of sub-classes, σ_λ = standard deviation and T = magnitude class time interval.

Table 3.1 and Figure 3.3 show the completeness analysis, which indicates that the catalogue is complete for Mw ≥ 4 between 1918 and 2018. Thus, 27 events having event magnitude $M_w \geq 4.0$ were left on the compiled catalogue. The catalogue is complete for $M_w \geq 3.0$ for the period 1978-2018, for $M_w \geq 4.0$ the complete catalogue from 1948-2018 (Table 5.1). The approach developed by Wiemer and Wyss (2000) determined the completeness of the catalogue with respect to time.

Since information regarding the local faults for this study region is poorly documented; the determination of seismic hazard was based on available information on seismicity and geological setting of the study area. Three area source zones used to estimate the hazard levels are shown in Figure 5.5 using QGIS Ver. 3.18.3 (https://www.qgis.org/en/site/). Zone A represents the Palaeozoic craton, while zone B and zone C, are characteristic of the Archaean and Lower Proterozoic rocks.

Table 5.1. Catalogue completeness for different magnitude sub-classes

Magnitude sub-class	Period of Completeness	Interval (years)
$M_w \geq 3.0$	1978-2018	30
$M_w \geq 3.5$	1948-2018	70
$M_w \geq 4.0$	1948-2018	70
$M_w \geq 4.5$	1948-2018	70
$M_w \geq 5.0$	1918-2018	100
$M_w \geq 6.0$	1918-2018	100

In order to complete the preparation of the seismic source model, the three identified seismic sources need to be characterised in terms of their earthquake recurrence, i.e., the relative frequency of occurrence of earthquakes with different sizes, as well as the maximum expected magnitude for each for each source. The calculations for these parameters were conducted using the declustered catalogue described above. The seismicity of all sources is assumed to follow a truncated exponential (Gutenberg-Richter) distribution characterised by Equation 5.6.

$$Log_{10}(N) = a\text{-}bM \qquad (5.6)$$

where N = number of events with magnitudes equal to, or greater than, M, a-value = activity rate which defines Gutenberg-Richter relation intercept at M equal zero. The b-value indicates the relative number of large and small earthquakes and represents the Gutenberg-Richter relation.

Irinyemi A. Stephen
PhD in Geotechnical Earthquake Engineering (2021)
University of Manchester (UK)

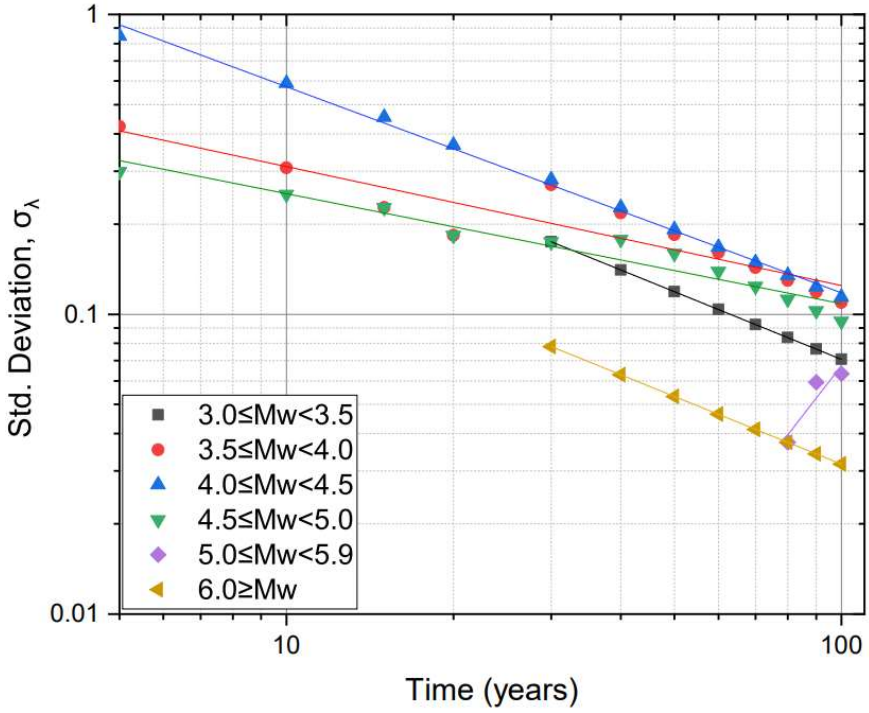

Figure 5.3. Catalogue completeness periods

It is common to use a unique *b*-value for source zones in low-to-moderate seismicity due to limited recorded data (Goitom et al., 2017; Ahulu et al., 2018). As a result, a uniform *b*-value was calculated and adopted for all the zones (Table 5.2 and Figure 5.4). The activity rate, (λ-parameter) is known to vary significantly for the different zones within a given area. It was estimated for each zone by taking the average number of earthquakes for magnitude equal to or higher than the minimum magnitude (M_{min}). Out of the 27 events in the catalogue, 18 events are used for zone A, 5 events for zone B and 4 events for zone C, respectively. We use maximum-likelihood method (Wiemer, 2001) to estimate the recurrence parameters listed in Table 5.2.

Table 5.2. Recurrent parameters for each zone

Zone	M_{min}	M_{max}	$b \pm \sigma b$	a	λ
A	4.0	6.8	0.70± 0.12	4.215	0.18
B	4.0	4.8			0.05
C	4.0	5.2			0.04

Irinyemi A. Stephen
PhD in Geotechnical Earthquake Engineering (2021)
University of Manchester (UK)

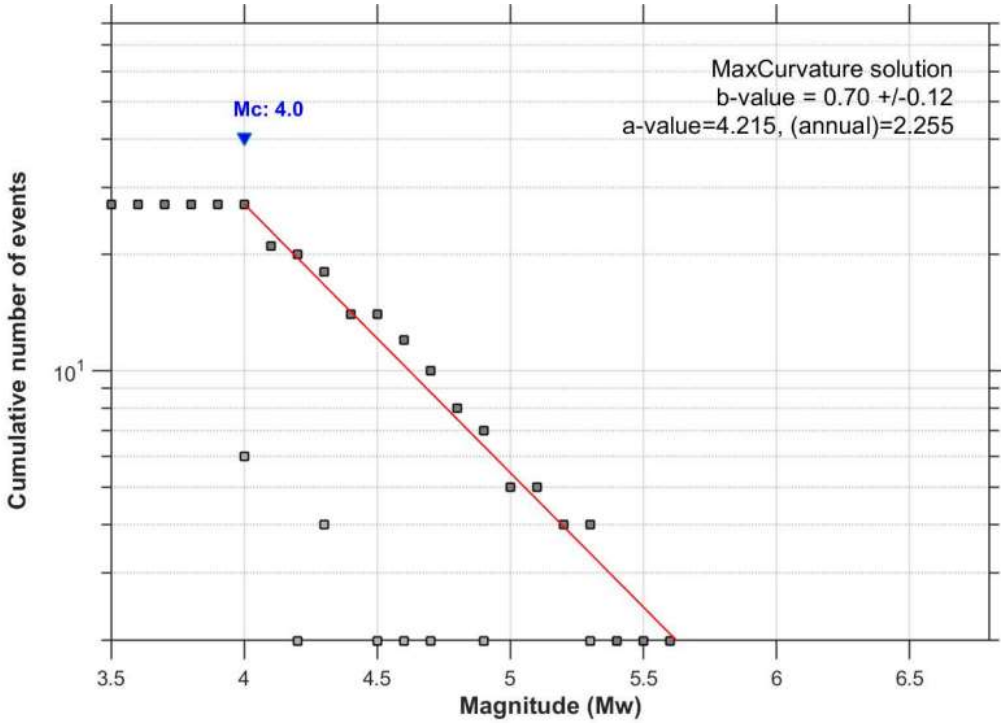

Figure 5.4. Frequency-Magnitude Distribution from 1818-2018 earthquake catalogue.

We estimate maximum possible magnitude, M_{max} for each of the three seismic sources. Many statistical methods are available to compute M_{max} (Kijko and Graham, 1998; Kijko, 2004). Owing to a lack of paleoseismic studies for the study area, characterised by a slow relative movement (~ 2 to ~ 15 mm/year) of the African Plate, which makes the recurrence period of strong earthquakes extremely long and thus unlikely to be included in our catalogue**,** we compute M_{max} by adding half magnitude increment to the maximum magnitude observed from the catalogue, such that M_{max}=0.5 + M_{obs}. This simplified method proposed by Gupta[20] has been extensively used by other researchers for stable continental regions and where paleoseismic studies are limited, including studies focused on the seismicity of the Africa continent (Ahulu et al., 2018; Deif et al., 2011; Basir and Basu, 2018; Poggi et al., 2017).

The accuracy of the focal depths is poor in this study region owing to the limited available information. However, based on the sources catalogue compiled for this study, the earthquake foci are within 10 to 15 km. Consequently, the hazard analyses were conducted using 10 and 15 km for all zones.

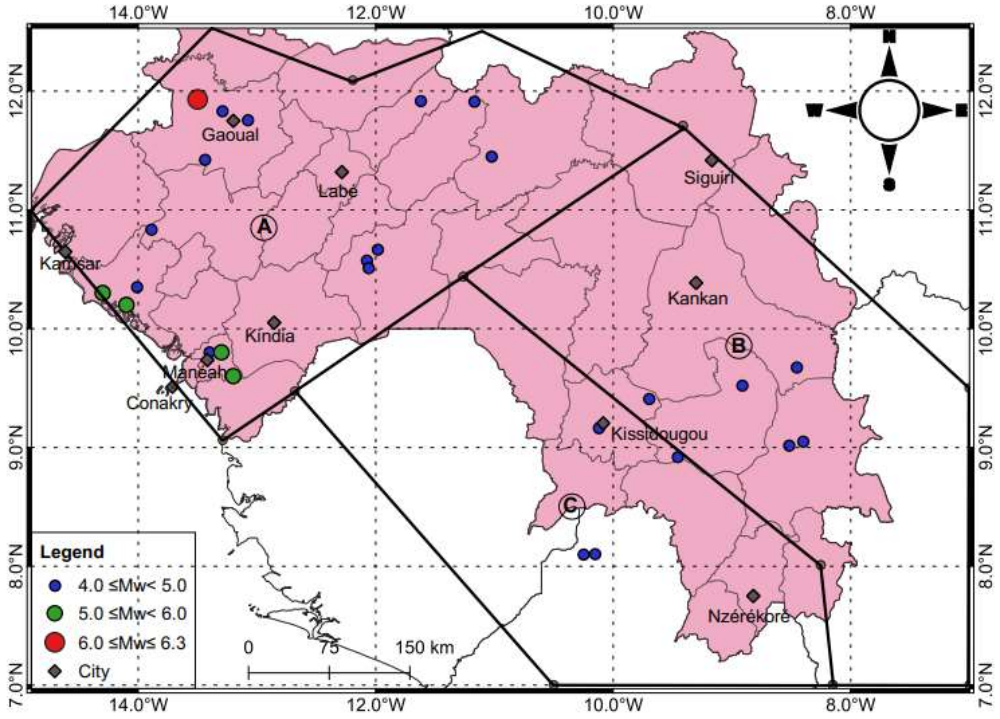

Figure 5.5**.** Seismic source zones for the study region

5.4.1 Ground motion prediction equations

The ground-motion prediction equations (GMPEs) define the attenuation of ground motion amplitudes as a function of source-to-site distance and earthquake magnitude constructed for the different local site conditions and with different frequencies. In general, ground motion prediction equations (GMPEs) are the primary source of epistemic uncertainty with respect to other variables of seismological models. However, the local models describing the observed characteristics of the strong-motion data are not available. Therefore, well-established global predictive models, such as the Next Generation of Ground Motion Attenuation (NGA), capture data from high magnitude events. Also, an alternative approach based on a hybrid-empirical model for Eastern North America (ENA), as is Guinea's target region, was implemented in the calculation in this study. The two GMPEs (Pezeshk et al., 2018; Tavakoli and Pezeshk, 2005) were used for the hazard calculation by assigning weight for each using a logic-tree approach, thereby representing confidence levels in the model. The equations for the GMPEs are listed in Table 5.3.

5.4.1.1 Treatment of epistemic uncertainty

We explicitly consider epistemic uncertainty using the logic tree approach (Giardini et al., 2004; Baro et al., 2018; Delavaud et al., 2009; Kulkarni et al., 1984). Each branch of the logic tree uses a different GMPE. Appropriate weight GMPEs are added using average sample log likelihood (LLH) function[28], expressed as

Appropriate weight GMPEs are added using the approach previously used by Delavaud et al.(2009). The average sample log likelihood (LLH) function is expressed as

$$\text{LLH}\ (g, x_i) \ = \ -\frac{1}{N}\sum_{i=1}^{N} log_2\ [g(x_i)] \qquad (5.7)$$

where x_1, x_2, x_3,....., x_N are samples of the ground motion values determined from a GMPE model $g(x_i)$. The value of LLH (g, x_i) are used as a ranking criterion. The weight of each branch (w_i) can be calculated as:

$$w_i \ = \ {2^{-LLH_i}}\Big/{\sum_{k=1}^{K=M} 2^{-LLH_k}} \qquad (5.8)$$

In this study, the following parameters: $M = 2$ for this study. The ranking is calculated only on PGA value using each observation of x_i, 1, ... N, which are 50km, 100km, 120km, 150km and 200km. The sample log likelihood for the individual GMPE model is given x_i. The quantities have been averaged using Equations (5.7) at (N = 5). The rankings of the GMPEs, are based on mean LLH$_i$ values, and the weight for the individual GMPE is provided in Table 5.4 and Figure 5.6.

Irinyemi A. Stephen
PhD in Geotechnical Earthquake Engineering (2021)
University of Manchester (UK)

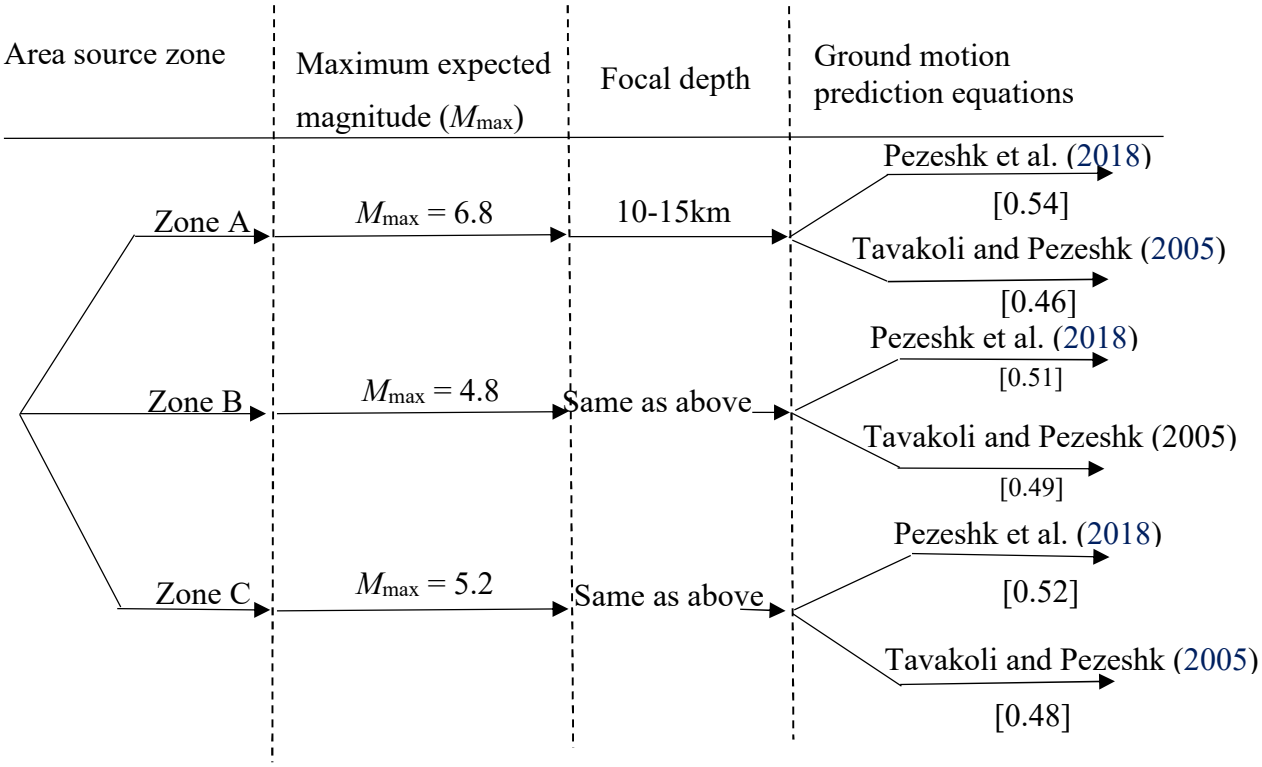

Figure 5.6. Logic-tree used for hazard calculation. The weights are in shown in square parentheses.

Table 5.3 List and conditions of GMPEs used in the study.

References	Ground motion prediction equations (GMPEs)	Salient features
Pezeshk et al. (2018).	$\log(\bar{Y}) = c_1 + c_2 M_w + c_3 M_w^2 + (c_4 + c_5 M_w) \times min\{\log(R), \log(60)\} + (c_6 + c_7 M_w) \times max\left[min\left\{\log\left(\frac{R}{60}\right), \log(120/60)\right\}, 0\right] + (c_8 + c_9 M_w) \times max\{\log(R/120), 0)\} + c_{10} R$ where $(\bar{Y})$ is the median value of PGA or PSA in g, R is the distance computed as $R = \sqrt{R_{rup}^2 + c_{11}^2}$ where R_{Rup} = closest distance to fault rupture in km, and c_1 to c_{11} are regression coefficients as defined in Pezeshk et al. (2018).	Based on hybrid empirical method (HEM). The GMPEs are derived for peak ground acceleration and response spectral ordinates at periods ranging from 0.01 to 10 s. Suitable for moment magnitudes (M_w) from 4.0 to 8.0. Valid for R_{Rup} < 300-400 km. Mean aleatory standard deviation associated with the prediction is given by $\sigma_T = \sqrt{\sigma_{\log\bar{Y}}^2 + \sigma_{\text{Reg}}^2}$ σ_{Reg} is the standard deviation of the regression. $\sigma_{\log\bar{Y}}$ is the total aleatory standard deviation. The values are given in Pezeshk et al. (2018). Hard-rock site condition. V_{S30} = 3000 m/s
Tavakoli and Pezeshk (2005)	$\text{Ln}(Y) = f_1(M_w) + f_2(R_{rup}) + f_3(M_w, R_{rup})$ $R = \sqrt{R^2_{rup} + (C_5 \exp[C_6 M_w + C_7 (8.5 - M_w)^{2.5}])^2}$ where Y = median value of PGA or PSA in (g), M_w = moment magnitude, R_{rup} = rupture distance and means the closest distance to the fault rupture in (km). f_1 to f_3 are frequencies (Hz), while and c_5 to c_7 are regression coefficients listed in Tavakoli and Pezeshk (2005).	Based on a hybrid-empirical model is utilized to predict the ground-motion relationship for eastern North America (ENA). This is an empirical-stochastic attenuation relationship used for horizontal peak ground acceleration and for spectral acceleration. Applicable to M_w 5.0–8.2. R_{Rup} <1000 km. Hard-rock site condition. V_{S30} = 2880 m/s. The aleatory standard deviation of ln Y is defined as a based on the earthquake magnitude and is modelled as follows

Irinyemi A. Stephen
PhD in Geotechnical Earthquake Engineering (2021)
University of Manchester (UK)

Table 5.4. Computed weights for different GMPEs for the 3 seismic source zones.

Zone	M_{max}	TP2005	PEAL2018
A	6.8	0.46	0.54
B	4.8	0.49	0.51
C	5.2	0.48	0.52

5.5 Hazard results and discussions

The seismic hazard calculations were performed using the R-CRISIS software, a probabilistic seismic hazard analyses software developed by II-UNAM, the Instituto de Ingeniería at UNAM, México (Ordaz and Sagado-Gálvez, 2020). The software is available for free on the R-CRISIS website. The analysis was conducted on a 0.5-degree grids spacing under the following conditions: Hazard calculations was computed for rock site conditions for 0.5%, 2%, and 10% probability of exceedance in 50 years, corresponding to return periods of 475, 2475, and 9975 years, respectively. A minimum magnitude (M_{min}) of 4.0 was adopted.

Figure 5.7 shows the hazard maps in terms of mean PGA for 475, 2475, and 9975 years return periods prepared using the GIS ver. 3.18.3 software (https://www.qgis.org/en/site/). The results show that the highest levels of seismic hazard estimated are observed in northwest part of the country where the PGA values are 0.08g, 0.27 g and 0.56 g at 475, 2475, and 9975 years return periods, respectively.

We also determined seismic hazard curves and uniform hazard spectra for ten cities (see Figure 5.8). Table 5.5 lists PGAs for the 475, 2475 and 9975 years return periods of 10 cities within Guinea. The cities of Labé (second largest city in Guinea), Gauoal and Kindia are located in the northwest part of the country and their higher seismic hazard is reflected by the high values as shown in the UHS (Figure 5.8). The other cities have lower hazard with the lowest at Nzérékoré. Taking Conakry as an example, the largest city and capital of Guinea, the spectral acceleration (SA) at 0.1 s, is 0.11 g, 0.32 g and 0.71 g at 475, 2475 and 9975 years return periods, respectively.

Table 5.5. Peak ground acceleration (PGA) likely to be exceeded with probability of 10%, 2% and 0.5% corresponding to 475-year, 2475-year and 9975-year return periods, respectively for the selected sites within Guinea.

City	Latitude	Longitude	PGA (g)		
			475 Years	2475 Years	9975 Years
Conakry	9.509	-13.712	0.055	0.184	0.445
Kankan	10.383	-9.300	0.023	0.068	0.151
Siguiri	11.416	-9.166	0.023	0.066	0.144
Nzérékoré	7.750	-8.816	0.017	0.068	0.173
Labé	11.316	-12.283	0.080	0.272	0.570
Kindia	10.049	-12.854	0.080	0.268	0.570
Manéah	9.7333	-13.416	0.078	0.261	0.565
Gauoal	11.750	-13.200	0.080	0.270	0.570
Kamsar	10.650	-14.616	0.072	0.241	0.534
Kissidougou	9.1833	-10.100	0.022	0.070	0.169

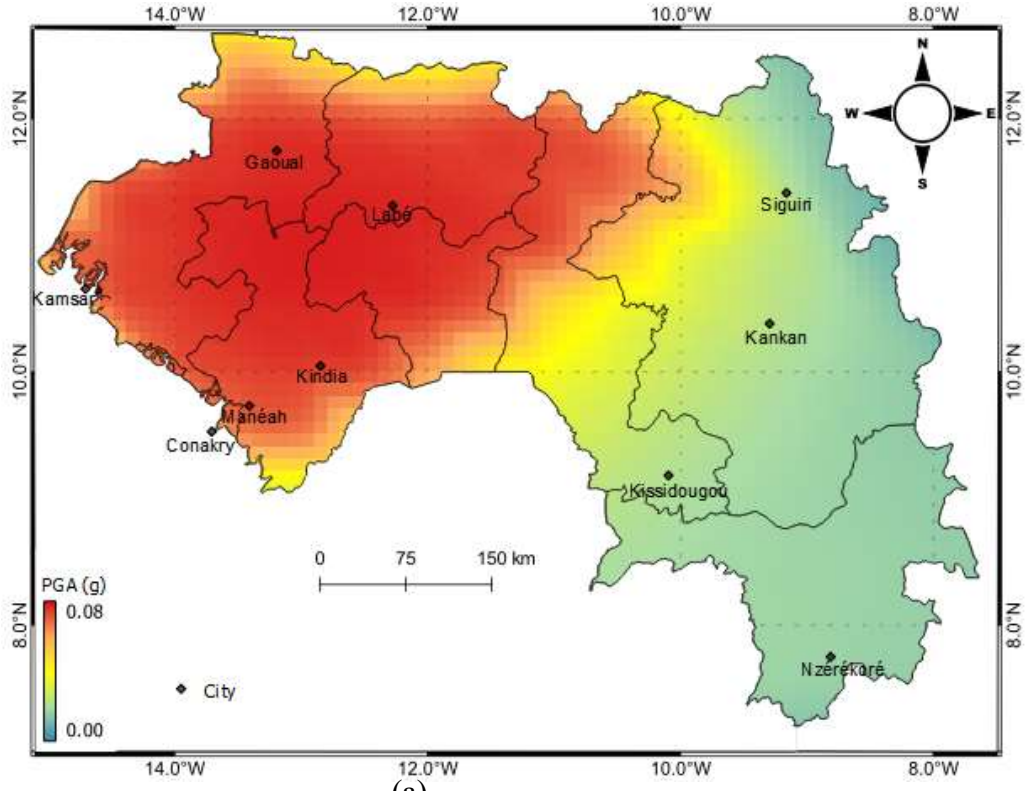

(a)

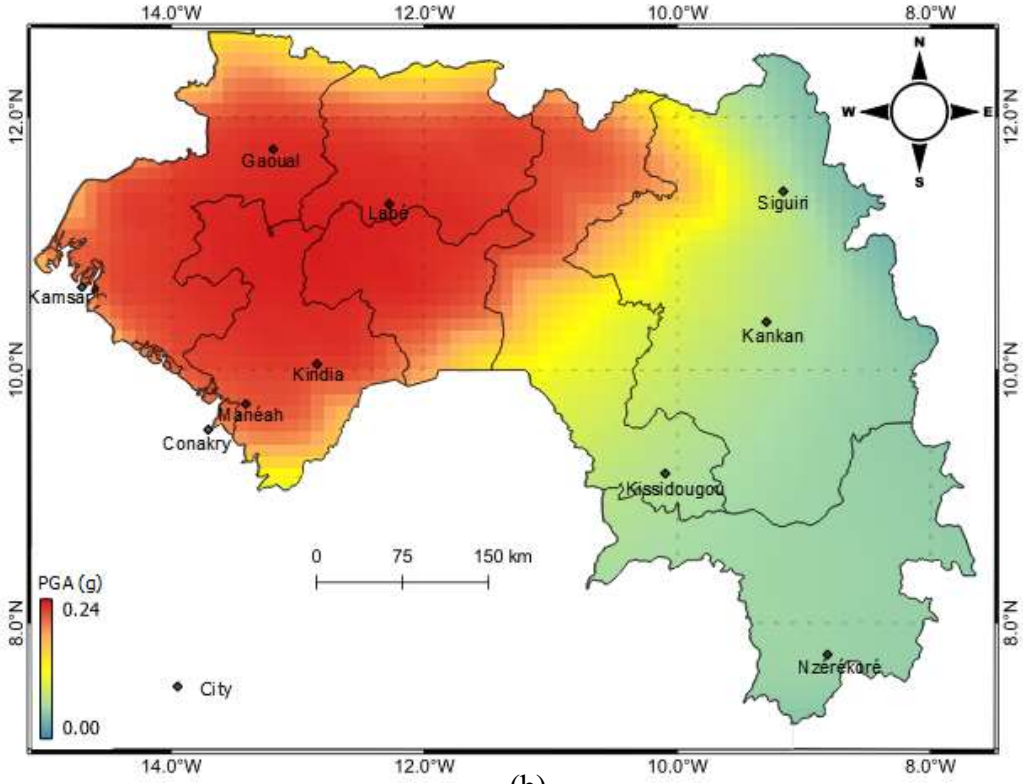

(b)

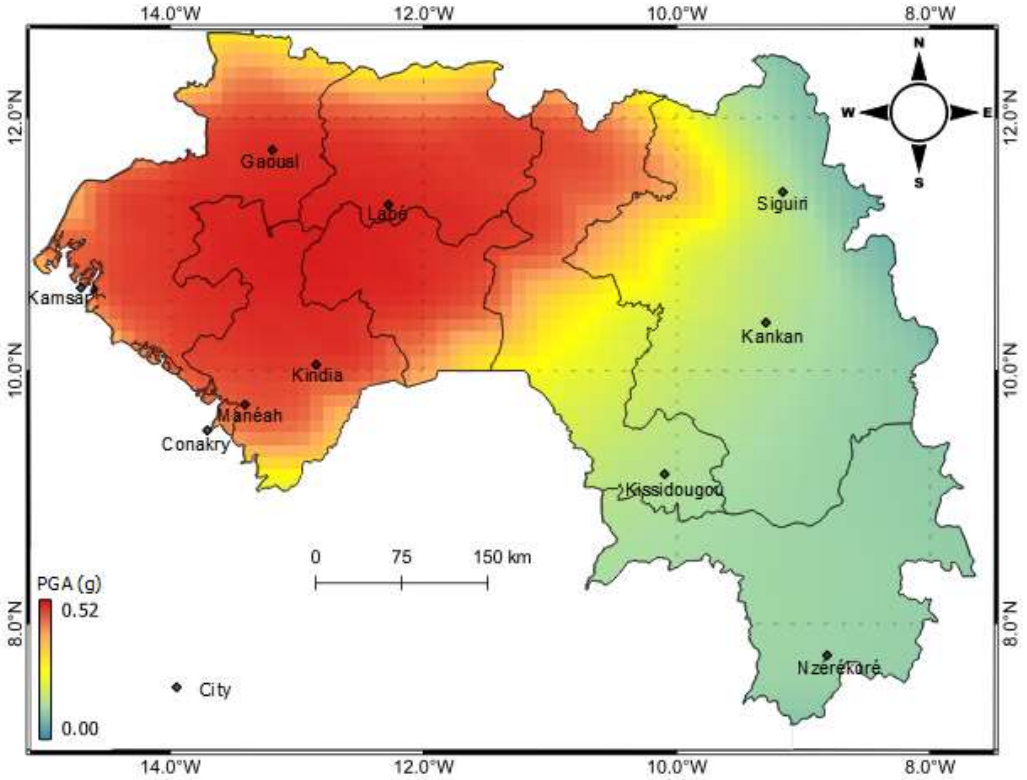

(c)

Figure 5.7. Seismic hazard maps at (a) 475-year (b) 2475-year (c) 9975-year, return periods.

Figure 5.9 shows the contour generated by QGIS Ver. 3.18.3. (https://www.qgis.org/en/site/) at the bedrock for four spectral accelerations (SA) at 0.1 s, 0.2 s, 1.0 s and 2.0 s for 475 years. The values are essential because different periods of ground motion influence buildings. In contrast, damage to a building is associated with a resonance between the natural building periods and the earthquake ground motion (Deif, 2011). The results show that the seismic hazard estimated for Guinea, West Africa, can be described as low to moderate at various sites selected. Following are the key observations from the results:

(a) Major seismic hazard in Guinea is observed at the North-western part, i.e., the Palaeozoic area, which has experienced some major earthquakes in the past.

(b) There is significantly less hazard in Archaean and Lower Proterozoic area as compared to the Palaeozoic area. The seismic hazard estimated reduces in the region around the Palaeozoic and decreases further at greater distances from the Palaeozoic itself.

(c) The north-western part of Guinea where the city of Gauoal, the epicentre of earthquake of 1983, shows higher hazard values 0.16 g, 0.11g, 0.02 and 0.008 for SA of 0.1s, 0.2s, 1.0s and 2.0 s, respectively.

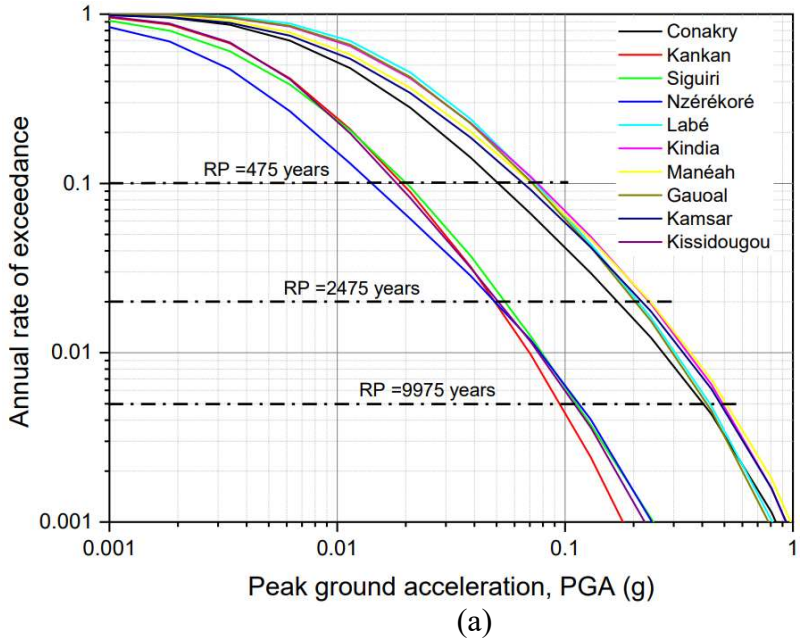

(a)

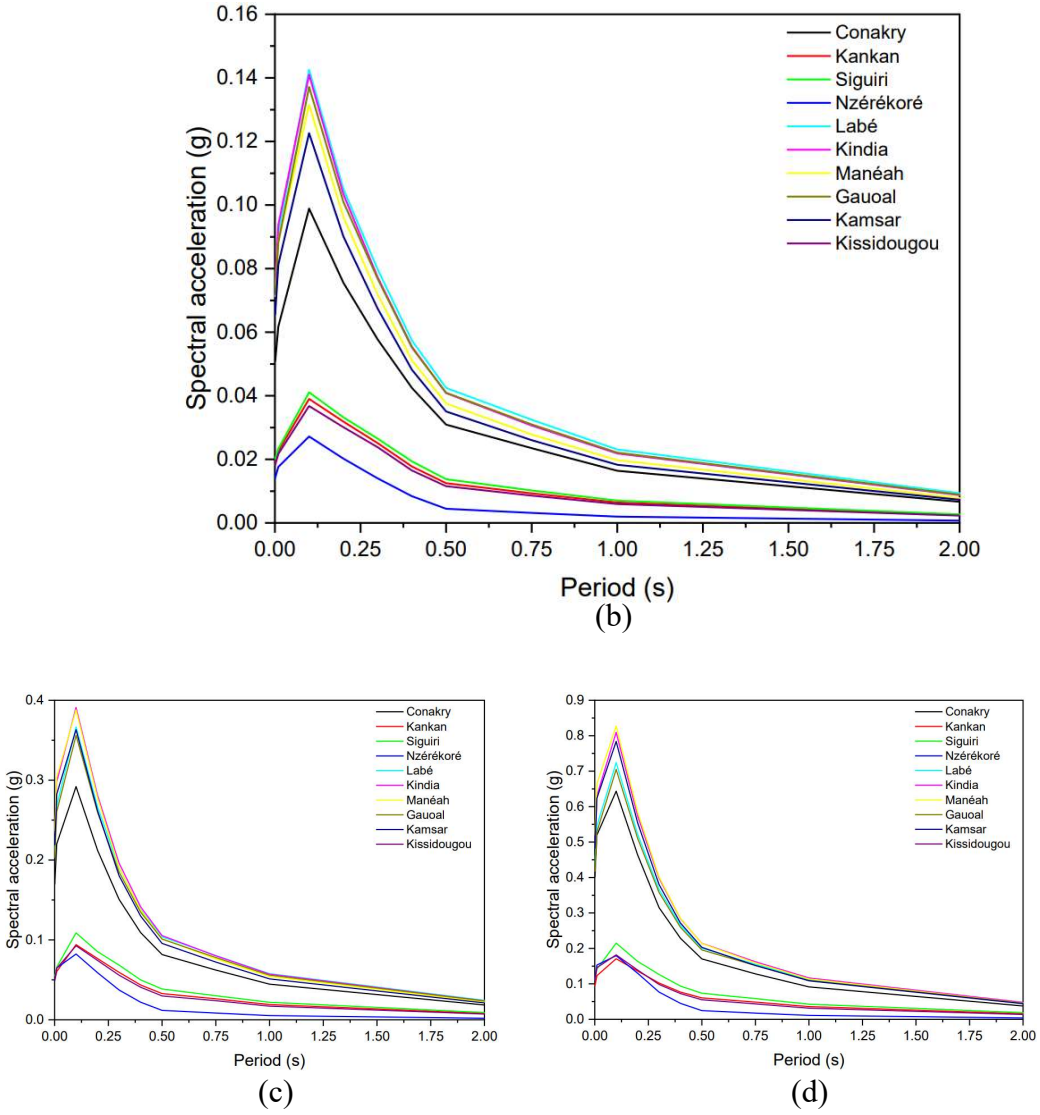

Figure 5.8. (a) Mean seismic hazard curves for PGA for ten analysed cities in Guinea. Uniform hazard spectra for selected ten cities within Guinea at (b) 475-year (c) 2475-years (d) 9975-year, return periods.

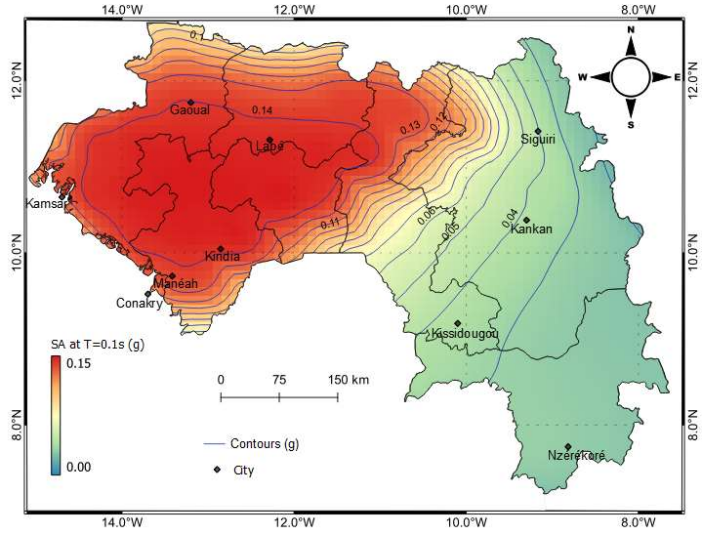
14.0°W
12.0°W
10.0°W
8.0°W
12.0°N
10.0°N
8.0°N
Gaoual
Labé
Siguiri
Kamsar
Kindia
Kankan
Mamou
Conakry
Kissidougou
Nzérékoré
SA at T=0.1s (g)
0.15
0.00
0
75
150 km
Contours (g)
City

(a)

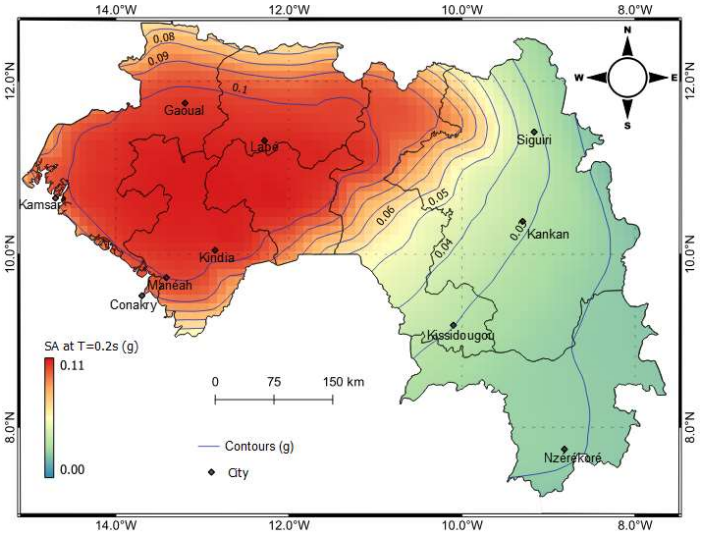
14.0°W
12.0°W
10.0°W
8.0°W
12.0°N
10.0°N
8.0°N
Gaoual
Labé
Siguiri
Kamsar
Kindia
Kankan
Mamou
Conakry
Kissidougou
Nzérékoré
SA at T=0.2s (g)
0.11
0.00
0
75
150 km
Contours (g)
City

(b)

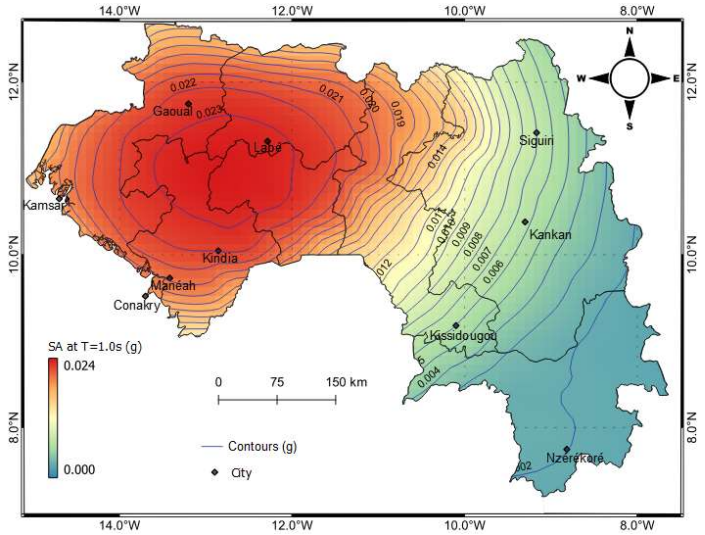
14.0°W
12.0°W
10.0°W
8.0°W
12.0°N
10.0°N
8.0°N
Gaoual
Labé
Siguiri
Kamsar
Kindia
Kankan
Mamou
Conakry
Kissidougou
Nzérékoré
SA at T=1.0s (g)
0.024
0.000
0
75
150 km
Contours (g)
City

(c)

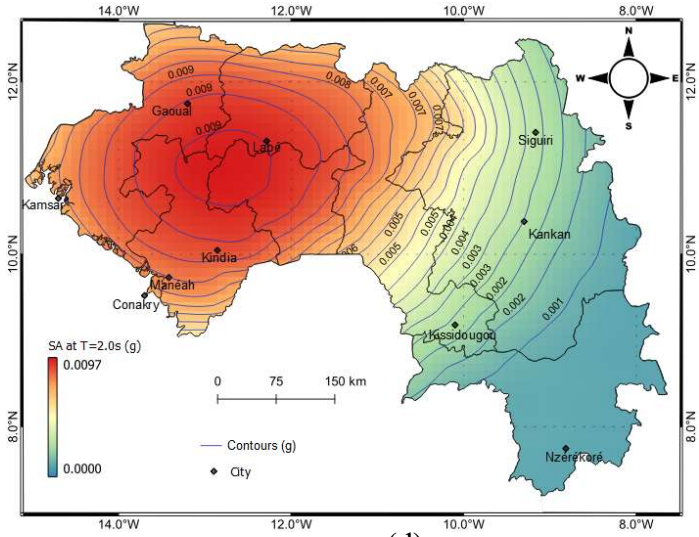

(d)

Figure 5.9. Seismic hazards on rock for spectral accelerations (SA) (a) 0.1, (b) 0.2, (c) 1.0 and (d) 2.0 s, respectively, (g) for 5% damping for a 475-year return period.

5.6 Summary

Probabilistic seismic hazard analysis for Guinea, West Africa, was performed based on an earthquake catalogue of duration of 100 years (1918-2018) estimated to be complete for magnitude M_w>4. The catalogue was compiled using data from three sources, the catalogue of Ambraseys and Adams (1986), ISC and USGS. The compiled catalogue was used to determine recurrence parameters and M_{max} values for three identified area seismic source zones. The seismic source zones were proposed based on geology and seismicity due to lack of information on local faults. The lack of strong ground motion records in this study means no GMPEs were developed specifically for the region. Therefore, the relations used in the study were adopted from those published for ENA, a SCR region as observed for the Guinea region.

Seismic hazard maps were produced for Guinea and seismic hazard curves for ten cities. The results show that at 475, 2475 and 9975 years return periods, there are significant seismic hazards in cities located in the north-western part of the country. From this study, six out of ten cities selected (Gaoual, Labé, Kindia, Kamar, Manéah and Conakry) fall within the high hazard levels for the new seismic hazard maps. The hazard levels estimated are critical since the ten cities are now seeing sizeable infrastructure

development. Therefore, the seismic risk associated with an increase in population and the expansion of the regional infrastructure can be significant. Thus, to protect the local population and to sustain the region's economic development, it is critical to mitigate against such risks, which, from the engineering design view, can be achieved by designing and building new infrastructure which take into account the seismic hazard maps proposed in this study.

CHAPTER 6

SEISMIC RISK ANALYSIS FOR LARGE DAMS IN WEST AFRICA REGION

Reformatted version of the following paper:

Paper title: **Seismic risk analysis for large dams in West Africa Region**

Authors**: Stephen A. Irinyemi, Domenico Lombardi & Syed M. Ahmad** (in preparation)

The author conducted the data analysis. Irinyemi designed the work, acquired and analysed the data, drafted the manuscript and prepared the Figures. Lombardi and Ahmad supervised the author.

Abstract

Dams are critical infrastructures, the failure of which would cause a catastrophic effect on a regional scale. West Africa has more than 150 large dams across the region, constructed in strategic locations which pose a potential risk for people and properties at the downstream paths. A method of seismic risk analysis for large dams within the West Africa region is discussed to evaluate the seismic hazard rating at the dam sites and the risk rating of its appurtenant structures. Although the study region is considered as a stable continental, two major earthquakes with casualty figures have been reported in Ghana and Guinea areas of the study basins in 1939 and 1983, respectively. This paper summarizes the procedures for analyses seismic risk and explain the seismic hazards of seventeen large dams selected within the study basins, based mostly on the significance of each dam and location of earthquakes in and around the dam sites. The results show the values of peak ground acceleration (PGA) at dam sites ranges from 0.02 g to 0.45 g. A hazard map of PGA indicating preliminary analysis of dam structures was developed for the study basins. Based on the results of these analyses, 59% of the analysed dams identified as high-risk dams, while the rest dams fall within the moderate-risk class.

These dams require further analyses for their safety to protect the populace and the built environments along the downstream paths.

Keywords: Dam; Seismic risk; Earthquake; peak ground acceleration; West Africa basins

6.1 Introduction

The seismic risk for large embankment dams of 15 m high or more from the foundation, and within 5 to 15 m whose reservoir capacity is more than 3 million cubic meters, were performed based on data of ICOLD, 2010. It assesses the seismic hazard at the dam site and the risk rating of dam and appurtenant structure differently. The method (Bureau, 2003) estimates the total seismic rating by combining the two factors. The analyses of the total risk for an existing and proposed dam structures depends on two factors: (1) the seismic hazard rating at the dam site (2) the risk rating of the dam and its accessory structures. The peak ground acceleration (PGA) estimated within the dam site represents seismic hazard for the dam structures. This study proposed a seismic zone map that estimates the seismic hazard within the dam sites. According to ICOLD (2010), the risk rating associated with a dam structure generally depends on the capacity of reservoir, evacuation requirements, dam height, and downstream damage factors. A method (Bureau, 2003) considered all the four listed factors to define the total seismic risk. The failure or loss of strength for embankment dams may be due to liquefaction or the dam itself. Method ICOLD (2010) explains safety about embankment dams due to earthquakes that involve loss of strength, instability of the dam, foundation materials or due to excessive deformations. Dam regulating bodies should ensure the safety of dam during seismic events and present minimum risk to people and properties within the dam vicinity.

Seismic activity in the study region has been at a relatively low level based on available recorded history. The first reported earthquake in Ghana was the 1615 with an estimated surface magnitude of 5.7 which caused damage along the coast and inland area (Ambraseys and Adams, 1986). On 22nd December 1983, the north-western Guinea experienced a damaging earthquake of 6.3 magnitude (M_w). The epicentre of earthquake was located in Gaoual, near the border with Guinea-Bissau. It resulted in approximately 10 km of surface rupture, which extensively damaged buildings, killing around 300 people and more 5,000 houses were destroyed (Langer et al., 1987; Langer and Bollinger,

1992). Evidence of dam damage by an earthquake has not been reported in the region. The 17 selected dams located in this study basins have shown moderate seismicity (Figure 6.1).

Seventen selected dams located in the Major basins of the West Coast and Niger River are studied. These dams have been designed to perform hydroelectric power generation and water supply, energy, irrigation, flood control and navigation and entirely constructed and fully operated (Table 6.1). The total area cover by the West Coast is 958,150 km^2, extended across 12 countries, from Senegal to the west and Nigeria in the east of this study basins. The Niger River has a drainage basin of 2,117,000 km^2. The source is taken from the forested mountainous plateau in central Guinea. It runs in a crescent through the border between Mali and Benin, discharging its source to the Gulf of Guinea in the Atlantic Ocean through Niger Delta in Nigeria. Seismic activities in Ghana part of the study region are being monitored by the National Digital Seismic Network Observatory (NDSO) beginning from 2012, established by the government of Ghana (Ahulu and Danuor, 2015). Nigeria established seismographic stations known as the Centre for Geodesy and Geodynamics (CGG), Toro, and became functional in 2008 to record events (Akpan et al., 2014).

This study evaluates the seismic hazard and determines the total seismic risk of these seventeen selected dams within the West Africa region (Figure 6.1) and will be used to set dam safety priority and maintain the dam structures to avoid seismic failure.

6.2 Seismo-tectonic setting in the study basins

The neotectonics of West Coast and Niger River Basins of the study region show five main structural elements (Figure 6.2): (1) Akwapim Fault Zone (AFZ), which is considered as the main seismotectonics in Ghana within the West Coast basin trends through northeastwards direction from the West of Accra and subjected to different faulting systems. Report shown that faults occurred through the ancient line of thrust in the boundary of Ghana and Togo (Ahulu et al., 2018). (2) The Coastal Boundary Fault (CBF) represents the northern boundary of basins during upper Jurassic era to recent age (Ahulu et al., 2018). CBF strikes approximately north of 60^0-70^0 in the east from 3 to 5

km in the direction of the Coast, where several kilometres block down throws to the south (Ahulu et al., 2018). (3) Romanche Fracture Zone (RFZ), which represents fault system that occurred offshore, is related to the opening of the Atlantic Ocean (Amponsah et al., 2012).

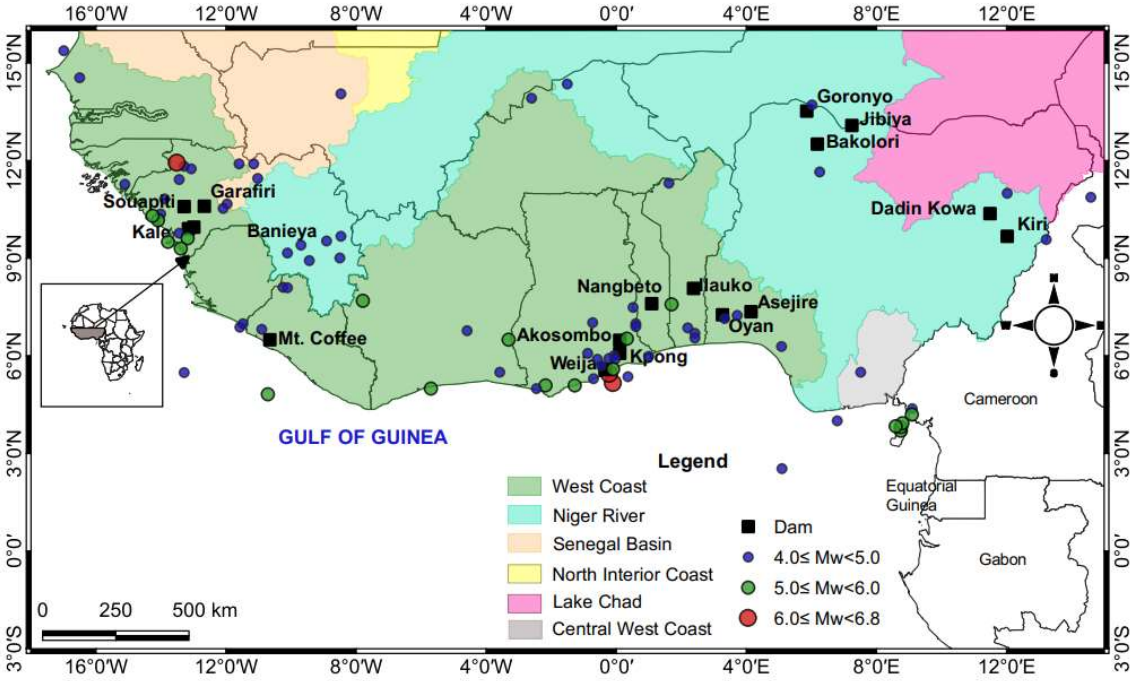

Figure 6.1. Location of dams and seismicity in the study basins.

RFZ is about 6-11 km wide parallel to the Coast (Amponsah et al., 2012). It is noted that the separation of Oceanic crust from the continental at the mid-Atlantic Ridge is represented by zone of inactive transform fault known as RFZ. (4) Saint Paul's Fracture Zone (StPFZ). The feature of StPFZ has been linked to the escarpment of the Liberia marginal plateau and the deep structural trend that merge the continental slope in the Côte d'Ivoire at the Western part of the Abidjan together with its alignment (Deiteil et al., 1974). The microearthquakes reported in Ghana are attributed to the reactivation of faults along the RFZ along the intersection of CBF and AFZ (Kutu, 2013). (5) Ifewara-Zungeru fault trends north-northeast to the south-southwest directions from the southwestern part of Nigeria (Awoyemi et al., 2017). Ifewara zone forms major part of the Schist belts within the Southwestern. The Nigeria Basement Complex which is found in Nigeria is part of African Crystalline structure (Adepelumi et al., 2008).

6.3 Method of analysis

A recommendation by (ICOLD, 2010) provides the simplified method to estimate the total risk factor associated with a specific dam. The method usually considers the calculation of both seismic hazard within the dam site and the risk rating of the dam structures separately. The method recommends four groups (low, moderate, high, and extreme) regardless of the type of dam into four to seismically assess the hazard at the dam site.

Table 6.1 Properties of dams considered for this study.

Dam	Country	Basin	River	Height (m)	Type[a]	Function[b]	Completed date	Reser. Cap. (× 1000 m^3)
Akosombo	Ghana	WT.Coast	Volta	134	RCF	EN	1965	147,960,000
Asejire	Nigeria	WT.Coast	Osun	26	ERF	WS	1969	32,913
Banieya	Guinea	WT. Coast	Samou	30	ERF	EN	1969	223,000
Bakolori	Nigeria	N. River	Sokoto	48	ERF	IR	1978	450,000
D.Kowa	Nigeria	N. River	Kano	42	RCF	IR+WS+EN	1988	2,855,000
Garafiri	Guinea	WT.Coast	Konkouré	80	ERF	EN	1999	1,600,000
Goronyo	Nigeria	N. River	Rima	21	ERF	IR	1984	976,000
Ilauko	Benin	WT.Coast	Ilauko	22	GRV	WS	1979	23,500
Jibiya	Nigeria	N. River	Katsina	22	ERF	IR+WS	1990	142,000
Kale	Guinea	WT.Coast	Samou	20	GRV	EN	1963	14,000
Kiri	Nigeria	N. River	Gongola	20	ERF	IR	1982	615,000
Kpong	Ghana	WT.Coast	Volta	20	RCF	EN+IR	1982	200,000
Mt. Coffee	Liberia	WT.Coast	St. Paul	19	RCF	EN	1966	238,600
Nangbeto	Togo	WT.Coast	Mono	52	ERF	IR+EN	1987	1,710,000
Oyan	Nigeria	WT.Coast	Oyan	30	GRV	IR+WS+EN	1983	270,000
Souapiti	Guinea	WT.Coast	Konkouré	117	GRV	EN	2019	6,300,000
Weija	Ghana	WT.Coast	Densu	17	RCF	WS+IR	1978	139,000

[a] GRV: gravity, ERF: earthfill, RCF: rockfill. [b] WS: water supply, EN: energy, IR: irrigation WT.Coast: West Coast; N. River: Niger River, D.Kowa: Dadin Kowa

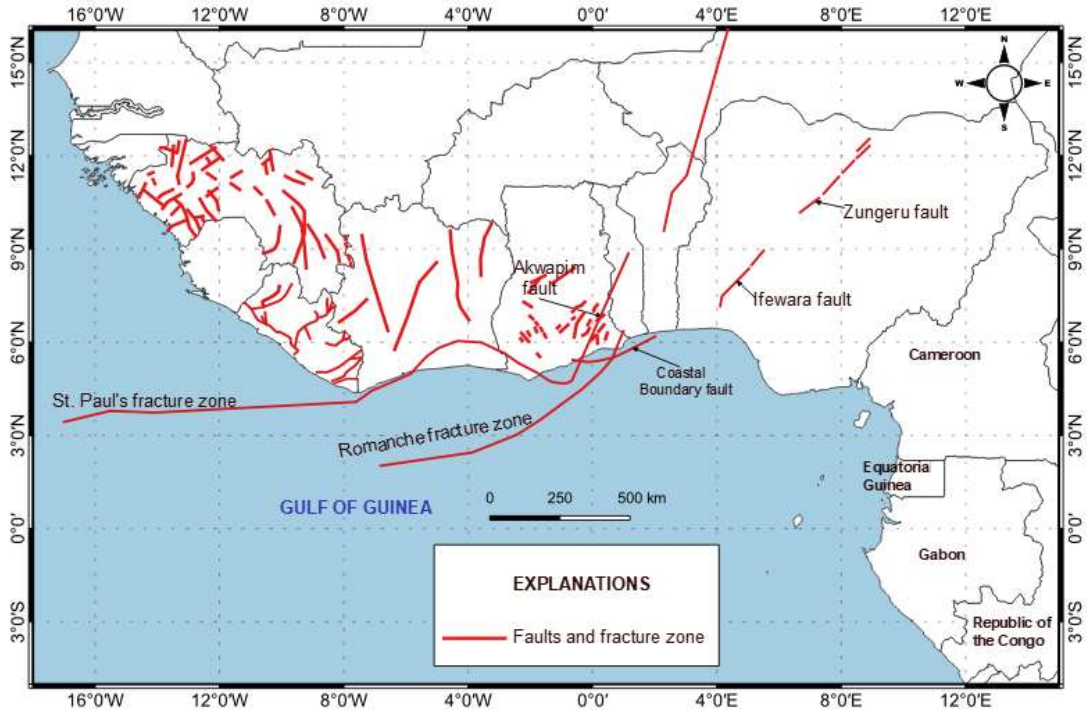

Figure 6.2. Main structural features for the study region.

6.3.1 Seismic hazards analysis

Determination of seismic hazard involves identify all possible seismic sources likely to cause ground shaking within a particular dam site. Extensive studies about the dam sites used the geological features and seismicity to quantify the seismic activity rate in the basins. Fourteen seismic zones separated the total area covering the basins. The seismic source zones defined for the hazard assessment are shown in Figure 6.3. Available Earthquake data were sourced from earthquake catalogues (Ambraseys and Adams, 1986; Amponsah et al., 2012; Musson, 2014), The United States Geological Survey (USGS) and International Seismological Centre (ISC).

The compiled catalogues (Appendix B) reported events in different magnitude units: local-magnitude (M_L), surface-magnitude (M_S), body-magnitude (m_b) and duration-magnitude (M_d), which were unified into moment-magnitude (M_w) using the expression of Scordilis and Grünthal et al. (Scordilis, 2006; Grünthal et al., 2009) in Equations (6.1-6.4).

$M_w = 0.85m_b + 1.03$, valid when m_b = (3.5- 6.2) (6.1)

$M_w = 0.67M_s + 2.07$, valid when M_s = (3.0- 6.1) (6.2)

$M_w = 0.85M_L + 0.65$, valid when M_L = (3.0- 6.1) (6.3)

$M_w = 1.47M_d - 1.49$ (6.4)

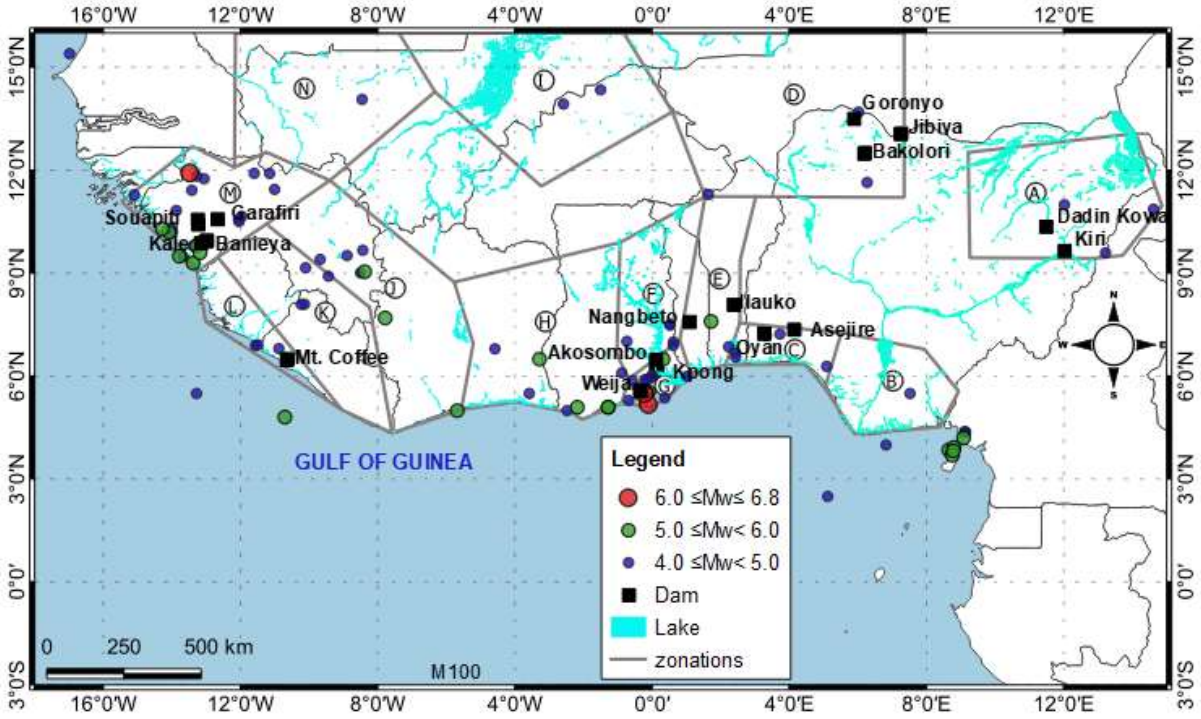

Figure 6.3. Seismic source zones and earthquake within the basins from 1615 to 2018 years

Throughout this study, considerations are given to seismic source zones and earthquakes reported within a radius of 300 km around the identified dam sites. The hazard analysis for this present study is based on the probabilistic framework (Cornell, 1968; McGuire, 1995).

Due to the lack of strong-motion records, various attenuation relationships were employed to estimate the maximum expected value of peak ground acceleration (PGA) acting at the identified dam sites. The determination of PGA values acting at the dam sites, considered five suitable Ground-motion prediction equations (GMPEs) (Pezeshk et al., 2011; Tavakoli andPezeshk, 2005; Abrahamson et al., 2014; Campbell and Bozorgnia, 2014; Chiou and Youngs, 2014).

Maximum credible magnitude (MCE) represents the deterministic event as the largest earthquake of event that occurred along an identified fault or defined from a tectonic

framework (Weiland, 2012; Tosun and Seyrek, 2010) and was calculated based on the method of Gupta (2002) due to limited seismic data, as given in Equation 6.5. The value of each PGA estimated for the identified dam sites (Table 6.2) represent the mean PGA values determined from five GMPEs. The recurrence parameters *b*-values and λ were calculated using the method of (Wiemer and Wyss, 2001) implemented in a research tool known as ZMAP (Wiemer, 2001). In the area with low-to-moderate seismicity activities, the same *b*-value can be estimated for all seismic source zones due to limited recorded data.

$$M_{max} = M_{obs}+0.5 \qquad (6.5)$$

The value of each PGA introduced for a dam site represents the means value obtained from five separate attenuation relationships, which was classified into several groups as shown in Appendix C. As a result, a unique *b*-value was obtained was classified into three groups and the *a*-value calculated are given (Appendix D). The λ-parameter varies from the different zones within a given area. It was estimated separately for each zone as the average of an annual number of magnitude events which are equal to or higher than the threshold magnitude ($M_{\min}$).

A PSHA program known as R-CRISIS (Ordaz and Sagado-Gálvez, 2017) determined the seismic hazards. The seismic analysis conducted on 0.5^0 x 0.5^0 grids. The PGA results calculated in the study region varies based on the geological setting in the basins.

A graphing and data analysis program, namely QGIS 3.14, as given in Figure 6.4 generated the seismic hazard in this study basins. The map showing the equivalent PGA were developed by the probabilistic seismic hazard analyses for seventeen identified dams within the basins. PGA values (Table 6.2) were estimated using a probabilistic approach based on regional-characteristic maximum credible magnitude ($M_{\max}$) values for large dams of 10,000 years return period (Wieland, 2012).

The most critical zone estimated based on this study is close to the Akwapim Fault zone in the Accra region of Ghana, where the maximum PGA values are evaluated. The 1939 M_w 6.4 Accra (Ghana) earthquake was also recorded in the area. This zone is significant for the three selected dams considered in Ghana part of this study. The dams are Akosombo, Kpong and Weija dams. The values of PGA obtained are within 0.39 g to

0.45 g for the dams. PGA values were estimated based on rock site conditions only. The most critical areas on the map (Figure 6.4) are those close to Guinea's Gulf in the Atlantic Ocean.

Table 6.2. Hazard class and rating for the selected dams within the study region

Dam	PGA*	Zone location	Hazard classification	Hazard rating
Akosombo	0.39	F	III	High
Asejire	0.12	C	II	Moderate
Banieya	0.24	M	II	Moderate
Bakolori	0.03	D	I	Low
Dadin Kowa	0.04	A	III	Low
Garafiri	0.24	M	II	Moderate
Goronyo	0.03	D	I	Low
Ilauko	0.06	E	I	Low
Jibiya	0.02	D	I	Low
Kale	0.24	M	II	Moderate
Kpong	0.44	G	III	High
Kiri	0.04	A	I	Low
Mt. Coffee	0.13	L	II	Moderate
Nangbeto	0.10	E	II	Moderate
Oyan	0.17	C	II	Moderate
Souapiti	0.24	M	II	Moderate
Weija	0.45	G	III	High

* PGA: Peak ground acceleration in g

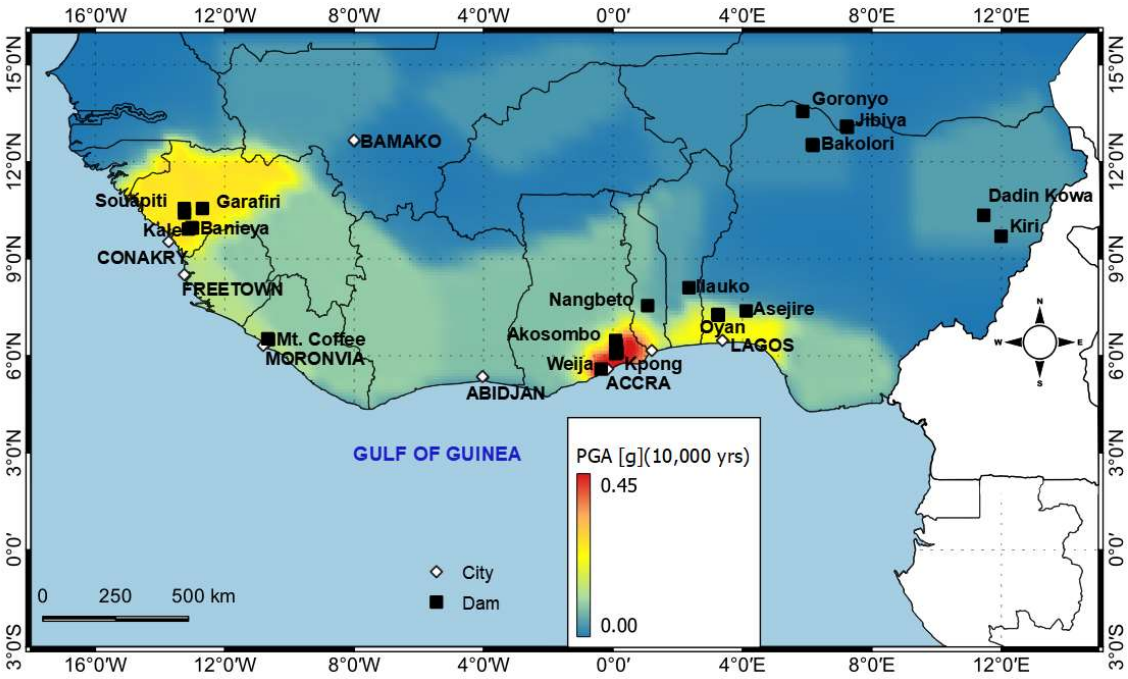

Figure 6.4. Seismic hazard map using MCE at the dam site for 10,000-return period.

6.3.2 Seismic risk analysis

The approach used Bureau (2003) recommendation, which provides different risk factors and weighting points to classify seismic risk for a particular dam on account of the age of dam, type of dam, reservoir capacity, downstream risk potential, and vulnerability of the dam coupled with the seismic hazard at the dam site as expressed in Equation 6 (Bureau, 2003; Singh et al., 2011). The Total risk factors (T_oRF) are classified as Extreme, high, moderate, or low.

$$T_oRF = [(C_aRF + H_iFR + A_gRF) + D_oHF] \times P_oDF \qquad (6.6)$$

where C_aRF represent the capacity of risk factor (Table 6.3), H_iFR is the risk factor for the dam height (Table 6.3) with the effect of causing significant flooding due to high and large reservoir storage. A_gRF is the age of dam risk factor indicating that the older the dams, the more vulnerable the dams due to deterioration effect, inadequate maintenance, outdated construction method or reservoir siltation (Table 6.4). Finally, D_oHF means the downstream hazard factor, while P_oDF indicates the predicted damage factor (Bureau, 2003). Dam structure influence is represented by the addition of three factors ($C_aRF + H_iFR + A_gRF$). The downstream hazard factor (D_oHF):

$$D_oHF = E_vRF + D_oRI \quad (6.7)$$

E_vRF is the Evacuation requirements factor that mostly depends on the number of people at downstream path and is defined in Equation 5.7, as provided in Table 6.5. The downstream damage risk index (D_oRI) which usually depend on government, industrial, commercial, or private properties located in the downstream paths are listed in Table 6.5. The values of D_oHF are determined from a combined factor taken from detailed dam breaches, economic studies and or preferably inundation mapping (Bureau, 2003). The values of DHF requires timely checking whenever latest information becomes available or when the dam is modified, raised, or repaired (Bureau, 2003). The D_oHF can be replaced by the downstream hazard potential rating of N_aID (National Inventory Dams) when it is difficult to determine both E_vRF and D_oRI from detailed studies, as shown in Table 6.6.

Table showing the numbers of people and values of properties at risk at the seventeen dam sites used to obtain the downstream hazard factor is shown in Appendix E.

Table 6.3. Dam site risk factor (Bureau, 2003)

Risk -Factor	Weighting points assigned to the Total Risk Factor in parentheses			
	Extreme	High	Moderate	Low
CRF/ (acre-feet)	Above 50,000 (6)	50,000-1000 (4)	1,000-100 (2)	Below 100 (0)
HRF/ (feet)	Above 80 (6)	80-40 (4)	40-20 (2)	Below 20 (0)

Table 6.4. Dam age rating factors (Bureau, 2003)

Risk Factor	<1900	1900-1925	1925-1950	1950-1975	1975-2000	>2000
A_gRF	6	5	4	3	2	1

Table 6.5. Downstream hazard factors (Bureau, 2003)

Risk Factors	Weighting points assigned to the Total Risk Factor in parentheses			
	Extreme	High	Moderate	Low
E_vRF	Above 1000 (12)	1000-10 (8)	100-1 (4)	None (0)
D_oRI	High (12)	Moderate (8)	Low (4)	None (0)

Table 6.6. Downstream hazard factors, based on N_aID (Bureau, 2003)

Downstream hazard potential rating (N_aID)	Loss of human lives	Economic, environmental, or lifeline losses	D_oHF
Low	None expected	Low, limited to owner's property	2
Significant	None expected	Yes	12
High	Likely, one or more expected	Yes, or probable but not strictly required	24

The vulnerability rating is a function of site-specific seismic assessment which is represented by the dam predicted damage factor (P_rDF) (Tosun and Seyrek, 2010). Each dam can be calculated using the in the Equation 8. P_oDI in the Equation 6.8 is the predicted damage index (P_rDI) and obtained through dam vulnerability curves (Tosun and Seyrek, 2010; Bureau, and Ballentine, 2002).

$$P_rDF = 2.5 \times P_oDI \qquad (6.8)$$

P_oDI, the potential damage index is primarily determined according to the type of dam and the seismic hazard at the dam site as expressed in terms of Earthquake Severity Index (ESI) (Bureau, 2003). The ESI is obtained from the scenario earthquake that produced the expected ground motion, as shown in Equation 6.9.

$$E_oSI = PGA \times (M_w - 4.5)^3 \qquad (6.9)$$

where (PGA) is the peak ground acceleration (g) for each specific site, M_w is the earthquake moment magnitude. Both Figure 6.5 and Equation 4.10 show the relationship between P_oDI and ESI (Hariri-Ardebili and Nuss, 2018).

$$P_oDI = \begin{cases} 1.08\ exp\ (0.297\ log\ (E_oSI)) & \text{Arch} \\ 1.28\ exp\ (0.296\ log\ (E_oSI)) & \text{Rockfill} \\ 1.69\ exp\ (0.139\ log\ (E_oSI)) & \text{Gravity} \\ 1.96\ exp\ (0.185\ log\ (E_oSI)) & \text{Earthfill} \\ 2.77\ exp\ (0.356\ log\ (E_oSI)) & HF - \text{tailings} \end{cases} \qquad (6.10)$$

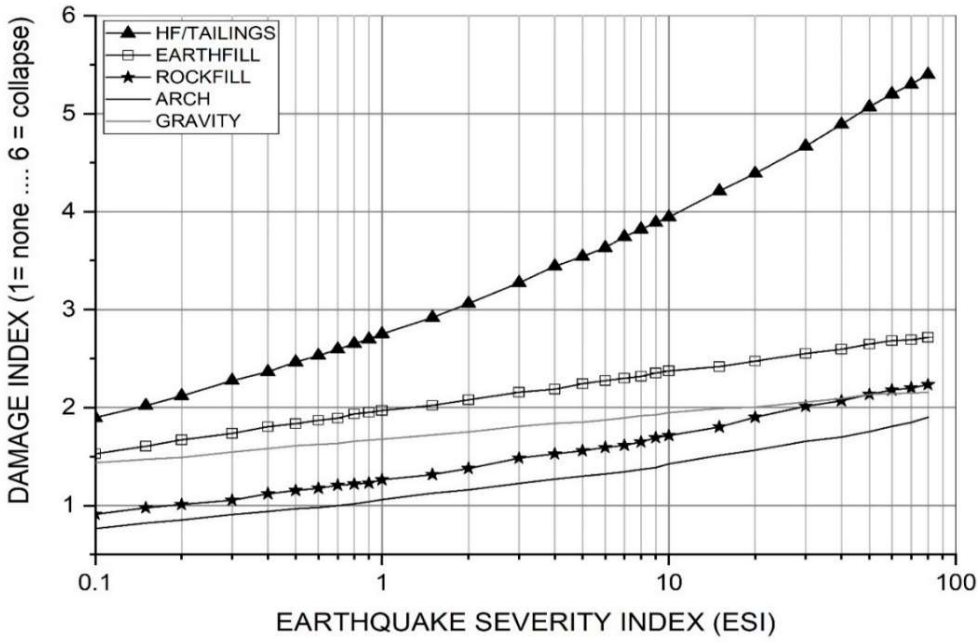

Figure 6.5. Predicted Damage Index (P_rDI) (Bureau, 2003).

6.4 Seismic risk results and discussions

The evaluation for the total risk factors for dam structures is done based on the seismic hazard rating at the dam site and the seismic risk rating of the dam structure. The (Bureau, 2003) approach, which considers the dam structure component, downstream hazard factors and evacuation requirements estimated the risk analyses of selected dams within the basins. The approach provided four individual classes of risks to assess the Total Risk Factor (TRF), as demonstrated in Table 6.7. Following the Bureau's method, all the seventeen selected dams in the basins are analysed as both moderate and high-risk classes.

The dam's total risk estimated across the West Coast and Niger River are shown in Table 6.8. and Figure 6.6. The TRF values obtained are within 68 to 166. The result means no dam is classified as IV and I within the basins.

Table 6.7. Dam risk class (Bureau, 2003).

Total Risk Factor (TRF)	Dam Risk Class (DRC)
2-25	I (low)
25-125	II (moderate)
125-250	III (high)
>250	IV (extreme)

Out of seventeen dams identified, seven are analysed as risk-class of II, and the rest ten dams fell into risk-class of III (Figure 6.6). This means 41% of selected dams shown risk-class of II while others identified as risk-class of III (Table 6.8).

The results indicated that dams with the high-risk rating are seen on the West Coast Basin close to the Gulf of Guinea. Out of the seven dams with moderate-risk rating, one is located on the south-eastern, and three on northern parts of Niger River basin. They have completely located on the secondary branches of Niger river.

This study identified some large important dams in the basins that can be re-analysed using appropriate seismic parameters. Three dam structures in this study region with PGA values, e.g., Akosombo (0.39g), Nangbeto (0.10g) and Souapiti (0.24) dams provide electricity for more than one country and may affect people and properties located in the downstream paths when they damage or fail.

The Akosombo dam is a 134-m rock-fill dam that has a storage capacity of 147,960,000 × 1000 m^3. It is located in Akosombo town in south-eastern Ghana and about 75 km southeast of Accra on the Volta River. The construction started in 1961 and was completed in four years in 1965. The dam was designed for maximum water level of 84.73 m, and a minimum water level of 73.15 m. It generates energy for industry usage with an upgraded capacity of 1,020 megawatts in 2006 (https://en.wikipedia.org/wiki/Akosombo_Dam). The seismic hazard estimated for the Akosombo dam shows that the dam can be critical in the basins. The seismic hazard analysis produced a PGA value of 0.39 g with a maximum credible magnitude of 6.9 with a high-risk rating. Numerical analysis should be performed for the Akosombo dam to determine the dam stability.

Table 6.8 The results of potential risk analyses of dams for the selected dams

Dam name	Site component		Structure component			Downstream component		TRF	Risk class	Rating
	M_{max}	PGA	C_aRF	H_iRF	A_gRF	E_vRF	D_oRI			
Akosombo	5.5	0.39	6	6	3	12	12	111	II	Moderate
Asejire	4.9	0.12	6	6	3	12	8	116	II	Moderate
Banieya	5.8	0.24	6	6	3	8	8	144	III	High
Bakolori	4.7	0.04	6	6	2	12	12	98	II	Moderate
Dadin Kowa	5.2	0.03	6	6	2	12	12	68	II	Moderate
Garafiri	5.8	0.24	6	6	2	8	8	140	II	High
Goronyo	4.8	0.03	6	4	2	12	12	100	II	Moderate
Ilauko	6.1	0.06	4	4	2	12	12	132	II	High
Jibiya	4.8	0.02	6	4	2	12	12	96	II	Moderate
Kale	5.8	0.24	4	4	3	8	8	110	II	Moderate
Kiri	5.3	0.04	6	4	2	12	12	129	III	High
Kpong	5.5	0.44	6	4	2	12	12	104	II	Moderate
Mt. Coffee	5.2	0.13	6	4	3	12	8	71	II	Moderate
Nangbeto	6.1	0.10	6	6	2	12	12	152	III	High
Oyan	4.8	0.17	6	6	2	12	8	108	II	Moderate
Souapiti	5.8	0.24	4	6	1	12	12	142	III	High
Weija	6.9	0.45	6	4	2	12	12	146	III	High

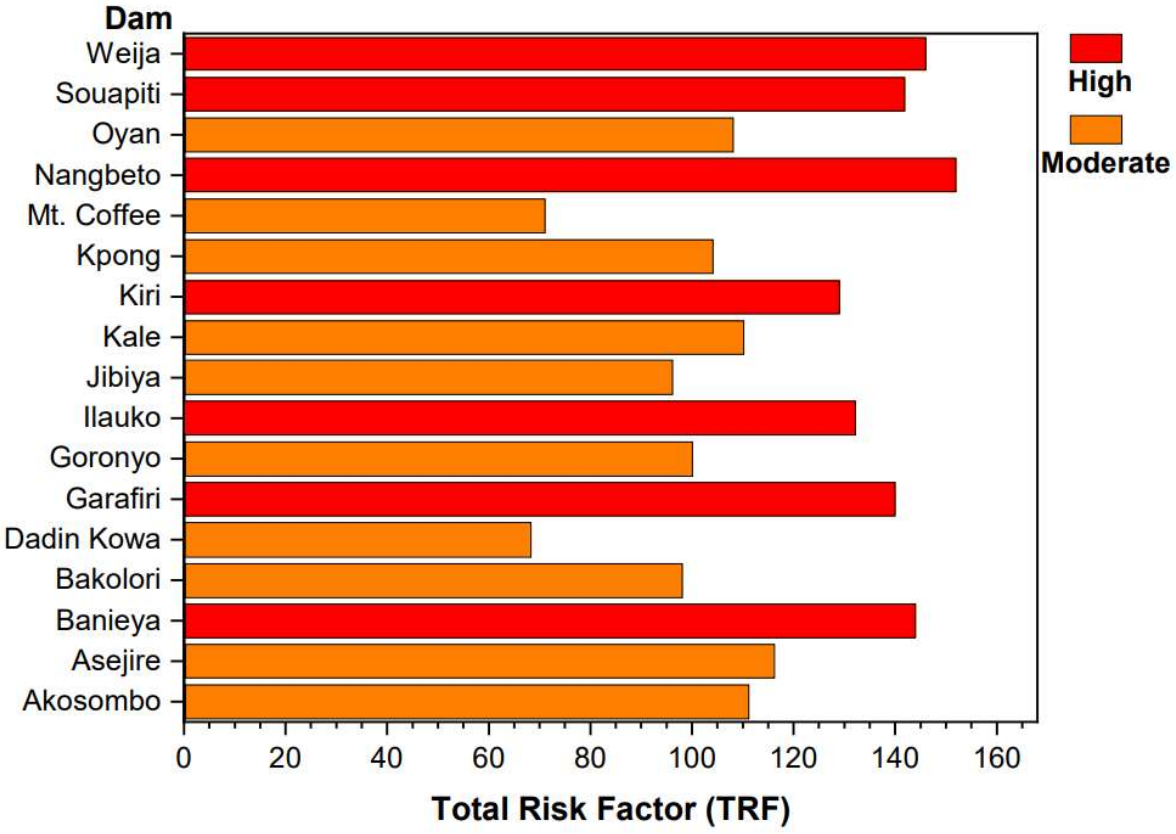

Figure 6.6. Total Risk Factor for the selected dams

Dadin Kowa and Asejire dams are located in Nigeria. The dams were estimated as hazard classes of II and III at PGA values of 0.03 g and 0.12 g, respectively (Table 6.2), and both dams having the same function in their locations as given in Table 6.1.

Weija Dam is a zoned earth-fill dam along Densu river in West Coast basin, located 18 km west from the state capital, Accra in Ghana. It has a 17 m from the riverbed. The reservoir capacity is 139,000 × 1000 m^3. The construction was completed in 1978. Its reservoir supplies large volume of water and provide irrigation services to Accra city and its environs. The dam is 43 years old but obviously cannot meet the latest seismic design standard. Thus, its seismic upgrade is needed since the estimated seismic risk is 146 and classified as a high-risk dam.

Banieya Dam is an earth-fill embankment dam on the Samou river, located 78 km north-east of Guinea capital, Conakry. The dam is 30 m high from riverbed and a storage capacity of 223,000 × 1000 m^3. Opening 51 years ago. It produces energy and supply

water to the Kindia region in Guinea with 5.2 MW capacity. 0.24 g PGA value was estimated based on the seismic hazard analysis and an MCE of 6.8. The dam is a high-risk rating with the highest value of 166 within the basins. Stability analysis can be performed for Banieya dam, which is about 226 km from the epicentre of the 1983 M_w of 6.3 Guinea earthquake.

Nangbeto Dam is an earth- fill embankment dam on the Mono River located in Togo, about 148 km in the northeast of Lomé, Capital of Togo. The dam is 52 m high, and the construction was completed in 1987 with a reservoir capacity of 1,710,000 × 1000 m^3. It was designed to provides hydroelectric power (65.5 MW) to both Togo and Benin as well as creating fisheries and supplying water for the purpose of irrigation. Based on the seismic hazard estimated for this study, the dam PGA and MCE are 0.10 g and 6.1, respectively. It is classified as a high-risk rating of 152. This dam should be assessed and analysed seismically to avoid future failure. Earthquake ground motions have some properties they can impose high seismic demand on the dam structures that may trigger their damage and failure. Failure of dams in this study region would result in social and economic losses of the region. So, the seismic vulnerability of dams located in West Africa region need to be investigated. Seismic vulnerability in this study is assessed by estimating the PGA and priories the seismic risk of the analysed dams.

6.5 Summary

For this study, seventeen selected dams located in the West Coast and Niger River Basins of West Africa were analysed to obtain their total seismic rating following the simplified method proposed by Bureau (2003).

i. The ten selected dams have identified as high-risk class at the value range (129-166.0). The PGA values obtained vary within 0.04-0.45 g (low to high-risk classes). Two destructive earthquakes documented within the study basins are the 6.4 Mw 1939 Accra (Ghana) earthquake and the 6.3 Mw 1983 Guinea earthquake. These earthquakes may have influenced the seismic results.

ii. Proper criteria should be selected to determine seismic analysis parameters due to the study basins. According to the results obtained, seven dams are estimated as high-risk

class. Thus, these dams should be re-visited for inspection, analysis seismically and redesigned if necessary.

iii. Implementation of dams in West Africa under the program known as National Dam Safety Program for dams and their accessory structures should be encouraged. The result of seismic risk analyses shows that Akosombo dam is classified as a moderate-risk class and the dam was designed to produce electricity for Ghana and the neighboring countries. The dam is identified as the dam with the largest reservoir capacity in West Africa region. This dam should be prioritized since the risk rating is moderate which could be critical to the dam.

iv. Further dam site assessments should include seismotectonic regime, surface rupture identification, local site effects, and reliability analysis.

6.6 Data and resources

Data sources for our assessment include that of the International Seismological Centre (ISC). The ISC catalogue, was searched through (http://www.isc.ac.uk/iscbulletin/search/catalogue/), (last accessed October 2020), and the United States Geological Survey -National Earthquake Information Centre (USGS – NEIC). (https://earthquake.usgs.gov/earthquakes/search/), (last accessed October 2020).

CHAPTER 7

SEISMIC RISK ANALYSIS FOR LARGE DAMS IN WEST COAST BASIN, SOUTHERN GHANA

Reformatted version of the following paper:

Paper 1 title: **Seismic risk analysis for large dams in West Coast basin, southern Ghana**

Authors**: Stephen A. Irinyemi, Domenico Lombardi & Syed M. Ahmad**

Published in: Journal of Seismology. (2021)

Research output: Contribution to journal › Article › peer-review

DOI: 10.1007/s10950-021-10045-w

Paper 2 title: **Seismic risk analyses for large dams in southern part of Ghana**

Authors**: Stephen A. Irinyemi, Domenico Lombardi & Syed M. Ahmad**

Accepted in: MACE PGR CONFERENCE. (2021)

Author contributions

The author (Irinyemi) conducted the seismic data analysis, designed the work, acquired and analysed the data and wrote the paper. Lombardi and Ahmad supervised the author.

Abstract

Dams are parts of the critical infrastructure of any nation. The failure of which would have a high-risk potential on the people and properties within the dam vicinity. Ghana is one of the most seismically active regions in West Africa and has at least 5 large dams across the region, constructed in strategic locations. The area is characterised by low-to-moderate seismicity, yet historical events suggest that major earthquakes with potentially damaging have occurred in the study basin. This paper summarise the method used to analyse seismic risk, discuss the seismic hazards of three large dams across the study

basin based on the seismicity at the dam sites and their risk due to structural properties and the location of each dam. The peak ground acceleration (PGA) values for the dam sites estimated are within the range of (0.31 g and 0.52 g) for 10,000 years return period. The study shows one large dam has a high-risk class in the basin. This dam should be inspected and analysed for its seismic safety and people's protection in the downstream paths.

Keywords: Seismic risk analysis. Peak ground acceleration. Earthquake. Dam. Ghana

7.1 Introduction

Dams are critical infrastructure in that they play a significant role in the region's economic, agricultural, and industrial developments. Ghana, located in Western Africa, covers an area of 238,540 km². 4.8% of the total area (11,400 km²) can be classified as cultivated land. Ghana can be divided into three basic drainage systems: the Volta River system, the southwestern river basins, and the coastal rivers. Out of the three studied dams, two are located on the river Volta system and globally considered the largest artificial lake by area in the world. The southwestern river system is deemed to be drained about one-fifth of the total land area of Ghana. Seismic risk analyses for three large dams in southern Ghana with a wall height of more than 15 m was performed. A simplified procedure based on Bureau (2003) approach assessed the potentially most vulnerable of the three dams. According to the (ICOLD, 1989) definition, dams with a wall high of 15 m or more and within 5 to 15 m whose reservoir capacity exceeding 1 million cubic meters are classified as large dams. The three selected dams (Table 7.1) located in the Major basin of the West Coast. The total area covered by the West Coast is 1,436,820 km^2, extended across 12 countries, from Senegal to the west and Nigeria in the east of West Africa basins. ICOLD (2020) method evaluates the seismic hazard of a dam site and the dam and accessory structure's risk rating separately. However, Bureau (2003) illustrated a procedure that combines the two factors to define the dam structures' total seismic risk. The analyses of the total risk for dam structures depends on two factors: (1) the seismic hazard rating at the dam site (2) the risk rating of the dam and its appurtenant structures.

The seismic hazard for the dam structures at various sites can be based on the peak ground acceleration (PGA). The values of PGAs obtained from the design earthquake produces the seismic loads. Dam type is an important parameter impacting the total risk factor (Bureau and Ballentine, 2002; Tosun and Seyrek, 2010). Seismic events in Ghana are monitored by the National Digital Seismic Network Observatory (NDSO) established by the government of Ghana. The database consists of natural and artificial seismic activities in 2012 (Ahulu and Danuor, 2015). The selected dams located in this study region have moderate seismicity (Figure 7.1). No accounts of damage to dams due to seismic activities have been observed within the study area. Ghana earthquakes of 1964 and 1969 were felt near the Akosombo dam and was subjected to induced seismicity (Musson, 2014). This paper evaluates the seismic hazard and determines the total seismic risk of these selected dams within the Ghana region and will be used to retrofit and investigate dam structures to avoid structural failure.

Table 7.1 Properties of dams considered for this study.

Dam	Basin	River	Height (m)	Type[a]	Function[b]	Completed date	Reservoir capacity (million m^3)
Akosombo	W.Coast	Volta	134	RF	E	1965	147960
Kpong	W.Coast	Volta	20	RF	E+I	1982	200
Weija	W.Coast	Densu	17	RF	WS+I	1978	139

[a] RF: rockfill, [b] WS: water supply, E: energy, I: irrigation, W.Coast: West Coast

6.2 Seismotectonic model of the dam sites in the basin

Figure 7.2 shows southern Ghana as part of continental West Africa and the equatorial Atlantic setting of the Gulf of Guinea and transform-fracture system. The first known seismic event in Ghana occurred as far back as 1615, where the fortress of Sao Jorge on the south coast of Ghana, in the present-day Elmina, collapsed (Ambraseys and Adams, 1986). Major seismic events have been reported in the southern part of Ghana: In December 1636, M_w 5.7 earthquake occurred along the north of Axim, where several buildings collapsed. On 10 July 1862, Mw 6.8 earthquake, which is still the most significant event reported in Ghana with an epicentre offshore, affected Accra's capital

city. The earthquake of 1939, with an epicentre located about 25 km offshore, and a moment magnitude of 6.4, has been the most destructive seismic event ever recorded in

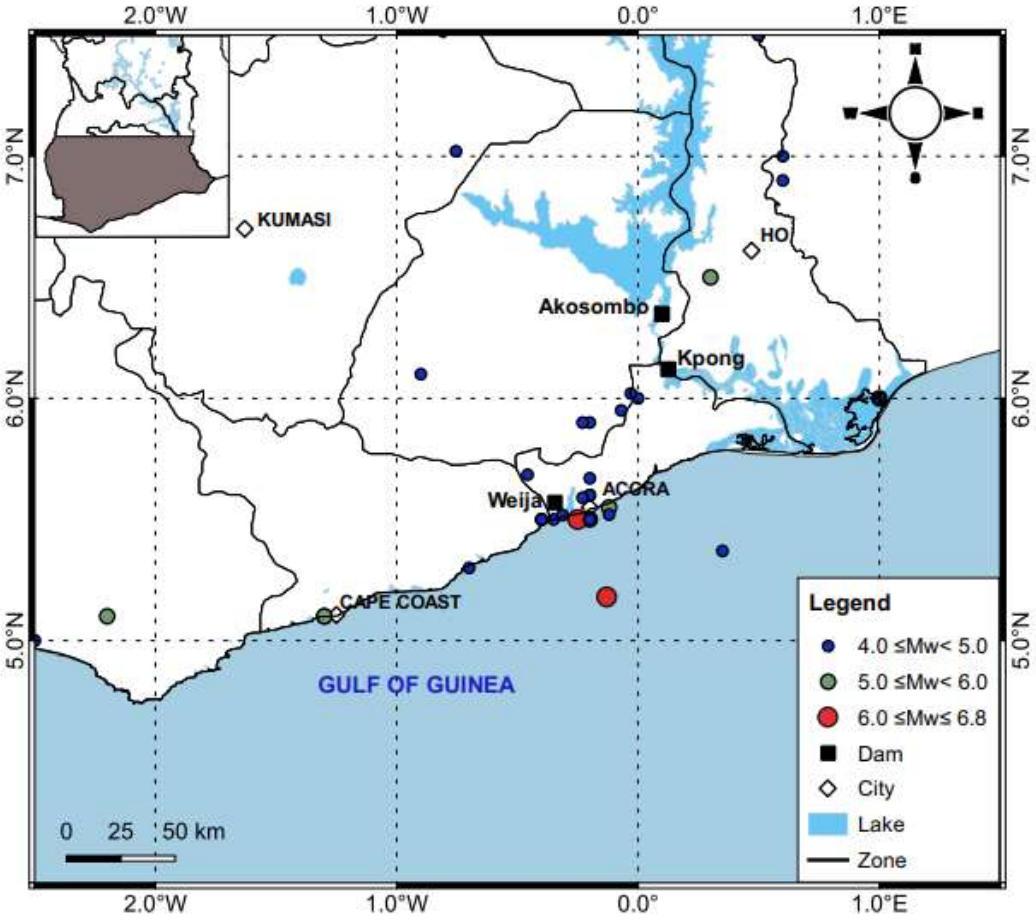

Figure 6.1. Location of dams and seismicity of the study region

Ghana. The mechanism studied of the earthquake of 1939 by Yarwood and Doser (1990) reported that strike-slip fault that occurred parallel to the Ghana coastline might have trigged the earthquake. Two major active faults governed the neotectonics of the West Coast basin in Ghana. They are: (1) the Akwapim fault, which is the main structural feature in the basin, (2) the Coastal boundary fault, which is a normal fault along the coastal line that strikes approximately north 60^0 E-70^0 E, at about 5 km from the coast.

The Volta passive margin basin in Ghana, Benin and Burkina Faso formed the Dahomeyide orogen foreland (Affaton et al., 1980). Upper Proterozoic covers Ghana to Late Palaeozoic sediments, which contains Early Proterozoic Birrimian rocks (Figure 7.2). Two transform-fracture systems found in the Gulf of Guinea are St. Paul's and

Romanche fracture zones and are located close to the coast of Ghana. The seismicity of southern Ghana is associated with the fault systems of the Romanche and St. Paul's fracture zones.

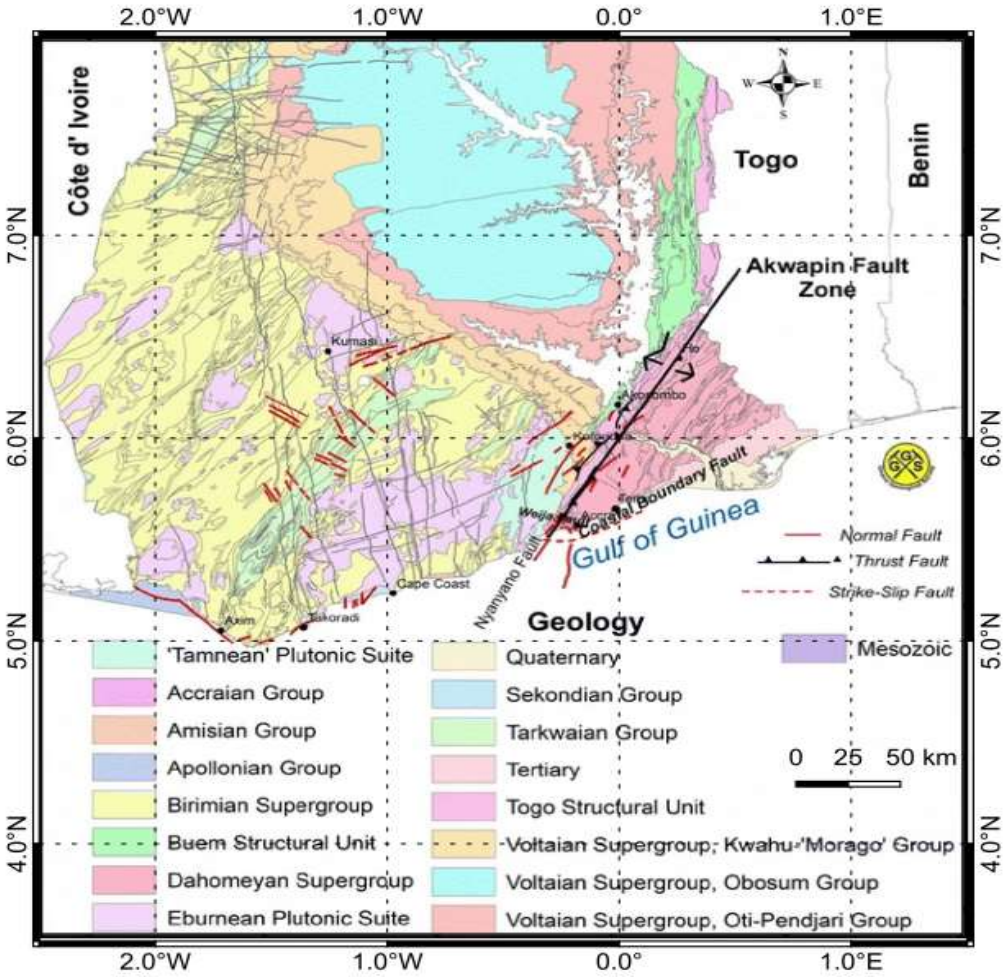

Figure 7.2 Geology and tectonic map of Southern part of Ghana. (Ahulu et al., 2018).

Accra's earthquakes are mainly attributed to the reactivation of faults in the Romanche fracture zone, specifically the Coastal Boundary fault and Akwapim fault (Kutu, 2013; Musson, 2014; Ahulu et al., 2018). The Coastal Boundary fault became tectonically active in Jurassic times and is still active (Ahulu et al., 2018). The Akwapim Fault Zone comprises a system of faults trending north-easterly from just west of Accra, along an ancient line of thrust boundaries in the Dahomeyan belt. The presence of neotectonics normal faults along the Akwapim range could mean that the tectonic movement is still

active, making faults from SW of the Akwapim within the Weija area likely active (Amponsah et al., 2012, Ahulu et al., 2018).

7.3 Method of analysis

According to the (ICOLD, 2010) approach, a dam's total risk is formulated and classified into four (low, moderate, high, and extreme). The hazard class of a dam site based on this method indicate the preliminary seismic evaluation requirements. Based on ICOLD (1989), the seismic risk (also known as "total risk") of dams depends on the structural and social-economics components. The structural component is based on the capacity of the reservoir and the height of the dam. The social-economics component depends on the evacuation requirements and potential downstream damage.

7.3.1 Seismic hazard analysis

For the seismic hazard analyses of the dam sites in the basin, all possible seismic sources that can produce significant ground shaking are identified. The study used geological features and seismicity to quantify the seismic activity rate. The historical and instrumental earthquake data were collected from earthquake catalogues (Ambraseys and Adams, 1986; Amponsah et al., 2012; Musson, 2014; the United States Geological Survey-National Earthquake Information Centre (USGS–NEIC); International Seismological Centre (ISC)) considering events with moment magnitudes, $M_w \geq 4.0$, recorded within the study area. The compiled catalogues produced events in different magnitude units: local magnitude (M_L), surface magnitude (M_S), body magnitude (m_b) and duration magnitude (M_d), which were homogenised to the moment magnitude (M_w) using the relationships by Scordilis (2006) and Grünthal et al. (2009) as expressed below.

$$M_w = 0.85m_b + 1.03 \quad \text{valid for } 3.5 \leq m_b \leq 6.2 \qquad (7.1)$$

$$M_w = 0.67M_s + 2.07 \quad \text{valid for } 3.0 \leq M_s \leq 6.1 \qquad (7.2)$$

$$M_w = 0.85M_L + 0.65 \quad \text{valid for } 3.0 \leq M_s \leq 6.1 \qquad (7.3)$$

$$M_w = 1.47M_d - 1.49 \qquad (7.4)$$

A catalogue completeness analysis method by Stepp (1972) determines the completeness of the compiled catalogue with respect to the magnitude and time. The Stepp method depends on the assumption that each magnitude sub-class represented as a point process in time, and the earthquake occurrence follows a Poisson distribution. The expression of the unbiased mean rate of occurrent of seismic events per unit time interval is given by,

$$\bar{\lambda} = \frac{1}{N}\sum_{i=1}^{N} \lambda_i \qquad (7.5)$$

$$\sigma_\lambda = \sqrt{\bar{\lambda}/T} \qquad (7.6)$$

where λ_i is the rate of occurrence of events per unit time interval for each subclass of the event set, N is the number of sub-classes, σ_λ is the standard deviation and T is the time interval.

Table 7.2 shows the completeness analysis at which the catalogue is complete for $M_w \geq 4$ between 1818 and 2018. Thus, all events with magnitude $M_w < 4.0$ were excluded from the compiled catalogue, with 35 events left in the working catalogue. The maximum curvature approach by Wiemer and Wyss (2001) determined the catalogue's completeness with respect to time. From Figure 6.3 and Figure 6.5, the compiled catalogue is complete for $M_w > 4$. The seismic hazard analysis used in the present study is based on the probabilistic framework proposed by Cornell (1968) and subsequently improved by McGuire (1995).

According to ICOLD, 2010, the maximum credible earthquake (MCE) is a deterministic event, which is the largest conceivable earthquake that is possible along a recognised fault or within a geographically defined tectonic framework (Tosun and Seyrek , 2010). The MCE is usually defined statistically with a typical return period of 10,000 years. Maximum Design Earthquake (MDE) is characterised by the level of motion equal to what is expected within the dam site from the occurrence of a deterministic evaluation of MCE (Tosun et al., 2007). Weiland (2012) specified that for large dams, the return period for the MDE ground parameters should be taken as 10,000 years based on a probabilistic seismic hazard analysis (PSHA).

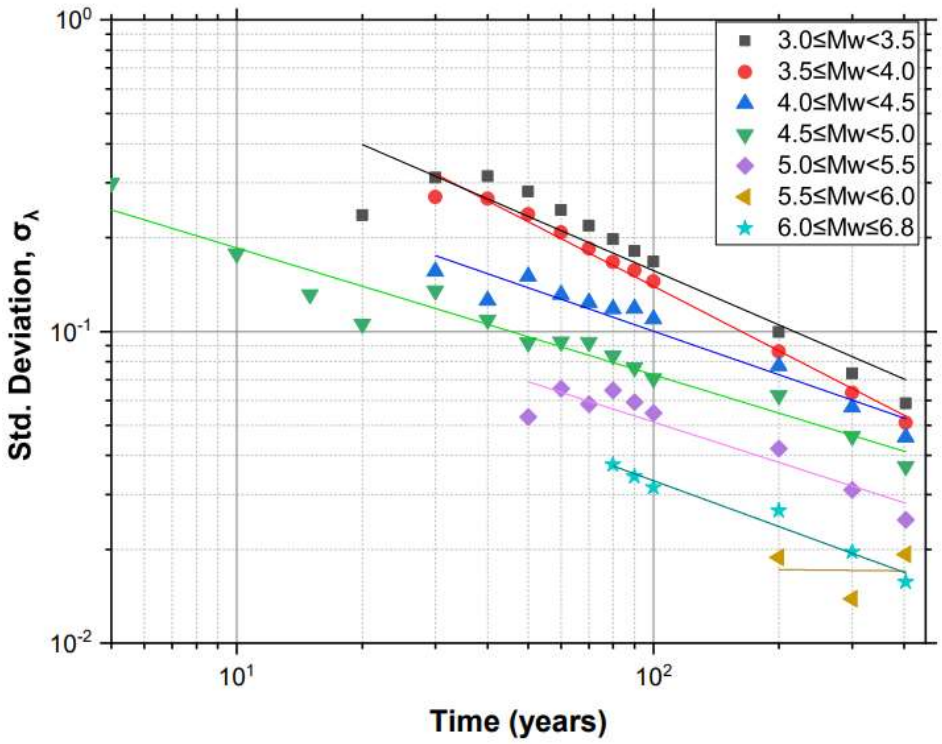

Figure 7.3. Completeness periods for different magnitude ranges using Stepp method (Stepp, 1972).

Table 7.2. Completeness periods for different magnitude classes

Magnitude class (M_w)	Completeness period	Completeness interval (years)
$3.0 \leq M_w < 3.5$	1918-2018	100
$3.5 \leq M_w < 4.0$	1818-2018	200
$4.0 \leq M_w < 4.5$	1818-2018	200
$4.5 \leq M_w < 5.0$	1718-2018	300
$5.0 \leq M_w < 5.5$	1718-2018	300
$5.5 \leq M_w < 6.0$	1615-2018	403
$6.0 \leq M_w \leq 6.8$	1718-2018	300

The assessment of maximum expected PGA at the dam sites estimated using a probabilistic approach based on the regional-characteristic maximum credible magnitude (M_{max}). For each dam site, M_{max} is determined from earthquakes within a radius of 100 km. It is noted the value of M_{max} is larger than the commonly used maximum credible earthquake for 10,000 years return period (Singh et al., 2011). Due to the lack of strong-motion records, the study adopted five different attenuation relationships to estimate the

expected peak ground acceleration (PGA) acting on the dam sites. They are (Pezeshk et al., 2011; Tavakoli and Pezeshk, 2005; Abrahamson et al., 2014; Campbell and Bozorgnia, 2014; Chiou and Youngs, 2014).

There are different approaches available to assess the maximum credible magnitude, M_{max}, (Kijko and Graham, 1998; Kijko, 2004). However, due to the paucity of recorded data for this study region, M_{max} was obtained from the largest observed magnitude M_{obs} in each zone by adding an arbitrary value of 0.5 as expressed by M_{max}, = M_{obs} + 0.5 (Gupta, 2002). Thus, other researchers have widely used this simple method in regions with limited data (Deif et al., 2011; Poggi et al., 2017; Ahulu et al., 2018). The PGA results are given in Table 7.3. It should note that each PGA value introduced for a dam site means the average weights of those obtained from five separate attenuation relationships.

According to Mavonga and Durrheim, (2009), where information on the location of potential faults that can cause a scenario earthquake is poorly documented, a seismic hazard assessment should be based on the available seismic and geological history of the study area. However, since no available literature correctly identifies this study region slip rates of faulting, fault geometries and fault segmentation lengths, area source zones (Figure 7.4) are used to define the seismic source zones. Three seismic zones used to estimate the seismic hazard of the dam sites are based on the geological and seismicity of the study region and in line with the seismic zones adopted by Alulu et al. (2018). Zone A is the offshore zone in the Gulf of Guinea representing the Jurassic era; both zone B (Accra region) and zone C (Ho region) are characteristic of the Neoproterozoic age. Calculated recurrence parameters of *b*-values and lambda (λ) for each zone used the maximum-likelihood method implemented in the computer programme ZMAP (Wiemer, 2001). It is common to use a unique *b*-value for all seismic source zones in low-to-moderate seismicity due to limited recorded data (Goitom et al., 2017; Ahulu et al., 2018). As a result, a uniform *b*-value was calculated and adopted for all the zones (Table 7.4) and Figure 7.5. The *a*-value calculated is given in Table 7.4. The λ-parameter varies significantly from the different zones within a given area. It was estimated differently for each zone by taking the average of an annual number of earthquakes with a magnitude equal to or higher than the minimum magnitude (M_{min}). The seismic hazards were estimated using computer program R-CRISIS Ver 20.0.0 (Ordaz and Salgado-Gálvez,

2018), developed with support from II-UNAM, the Instituto de Ingeniería at UNAM, México. The seismic analysis is conducted on a grid with dimensions 0.5^0 x 0.5^0. The estimated results show that PGA changes within a wide range based on the seismotectonic setting in the basin.

As a result of seismic hazard analyses performed for the dams within the basin, the maps showing the equivalent PGA were developed by a graphing and data analysis program, namely QGIS 3.18, as given in Figure 7.6.

Table 7.3 Hazard class and rating for the selected dams within the study region

Dam	Maximum PGA	Critical zone	Hazard class	Hazard rating
Akosombo	0.31	C	III	High
Kpong	0.41	B	III	High
Weija	0.52	B	III	High

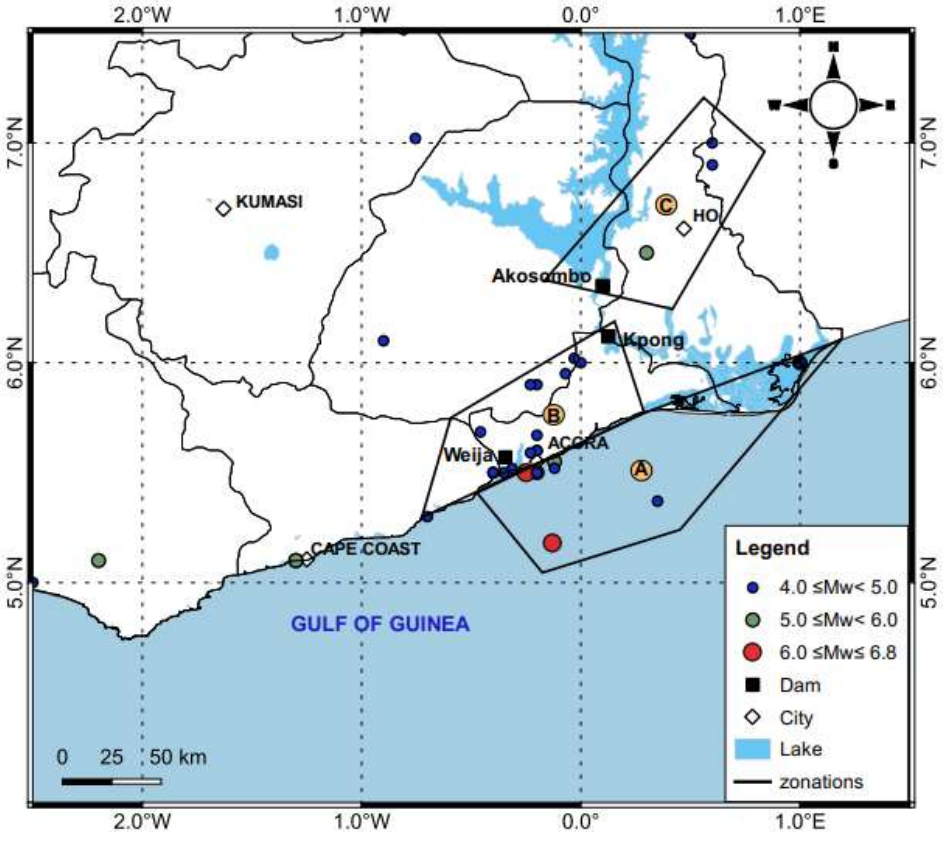

Figure 7.4. Seismic zones and earthquakes in the study region

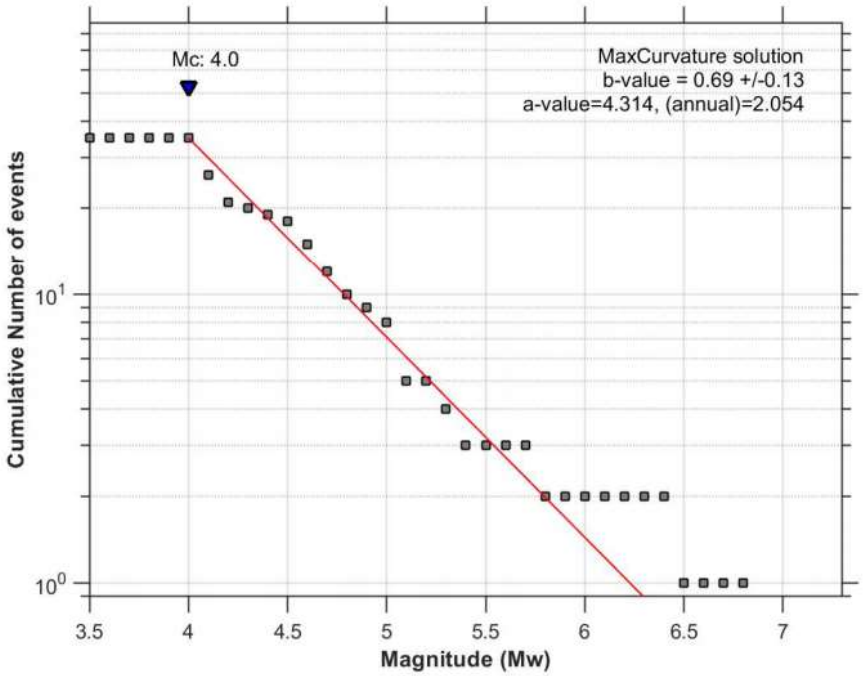

Figure 7.5 Frequency-Magnitude Distribution from 1818-2018 earthquake catalogue.

The map (Figure 7.6) shows that the most critical area in the basin is close to the Akwapim Fault zone in the Accra region of Ghana because the greater acceleration values are seen on this part. In addition, the 1939 *M*w 6.4 Accra (Ghana) earthquake was also recorded in the area. The three dams considered are Weija, Kpong and Akosombo dams. The estimated PGA values range from 0.31 g to 0.52 g for the dams for 10,000 years return period. Figure 7 plots the seismic hazard curves and the 5%-damped elastic spectra for different return periods within the dam sites. The highest hazard is located close to the Weija dam site in the Accra region, where the PGA attains the maximum value of 0.11g, 0.29g and 0.52g for the return period of 475, 2475, and 10,000 years, respectively. Figure 6.8 summarises the results from disaggregation for the three dam sites at the return period of 475, 2475, and 10,000 years. From Figure 7.8, the contributed hazard is dominated by earthquakes of magnitude 4.6-5.1 at distances less than 25 km.

Table 7.4 Recurrent parameters for each zone

Zone	M_{min}	M_{max}	$b \pm \sigma b$	a	λ
A	4.0	7.3	0.69± 0.13	4.314	0.045
B	4.0	5.4			0.070
C	4.0	5.5			0.015

7.3.2 Bureau (2003) method

The approach provides various risk factors and weighting points to assess the total risk factor (TRF) of any dam based on the type of dam, age, size, downstream risk, and vulnerability, which depend on the seismic hazard at the dam site given in Equation 7.7. Four risk factors are weighted separately as low, moderate, high, or extreme.

$$TRF = [(CRF + HFR + ARF) + DHF] \times PDF \quad (7.7)$$

Where CRF is a risk factor of capacity (Table 7.5), HFR is a risk factor of height (Table 7.5), ARF is the age rating factor (Table 7.6), DHF is the downstream hazard factor, and PDF is the predicted damage factor. The sum of the first three factors (CRF + HFR + ARF) represented the dam structure influence. The downstream hazard factor (DHF) is based upon the human population and the property's value at risk, as given in Table 7.7.

DRI is the downstream damage risk index. The downstream damage risk index (DRI) is based on the value of private, commercial, industrial or government properties in the potential flood path, given in Table 7.7. The DHF values should preferably be obtained from a combination of a clear dam breach, inundation mapping, and economic studies. When it is not cost-effective to determine both ERF and DRI from detailed studies, the DHF can be substituted by the downstream hazard potential rating of NID (National Inventory Dams), as provided in Table 7.8. Table 7.9 showed the numbers of people and values of properties at risk at the three dam sites and were used to obtain the downstream hazard factor. Note that the values in Table 7.7 and 7.8 was obtained through expert judgements.

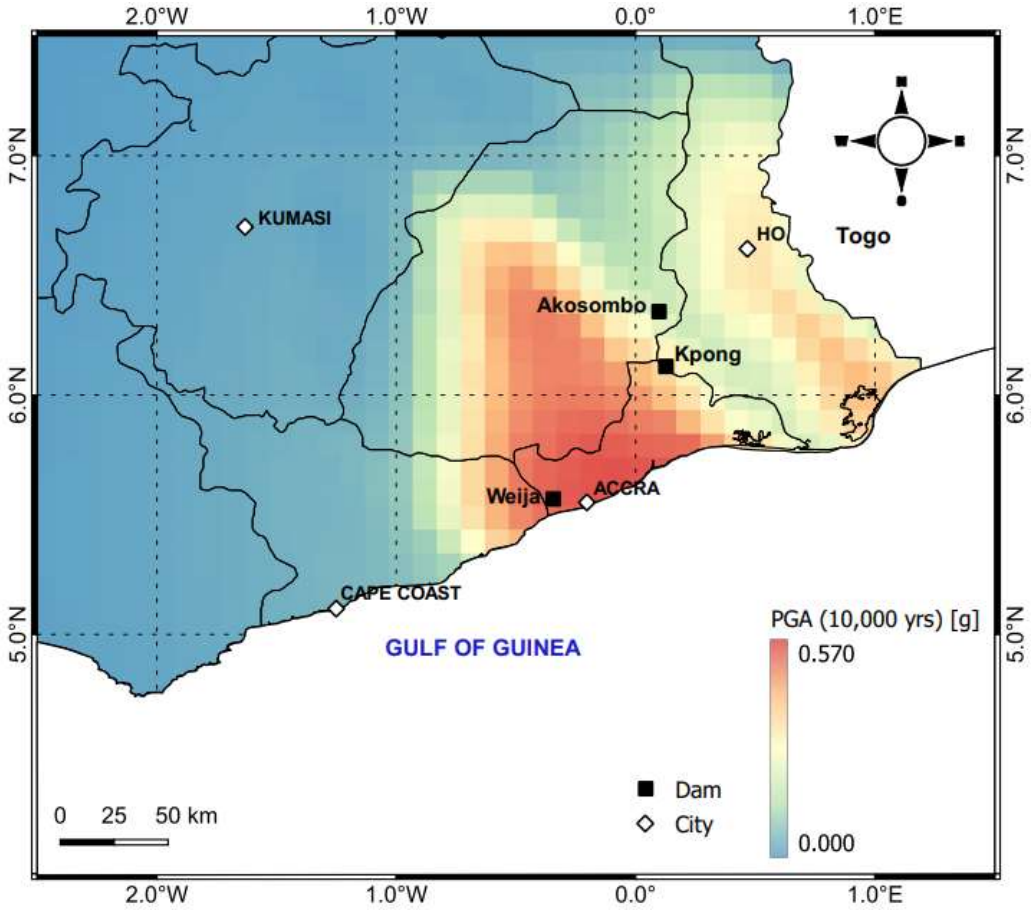

Figure 7.6. Seismic hazard map of the study basin as based on maximum design earthquake which represents dam site for 10,000-year return period.

Table 7.5 Definition of Dam site risk factor (Bureau, 2003)

Risk Factor	Contribution to Total Risk Factor (Weighting points)			
	Extreme	High	Moderate	Low
CRF/ (acre-feet)	>50,000 (6)	50,000-1000 (4)	1,000-100 (2)	< 100 (0)
HRF/ (feet)	>80 (6)	80-40 (4)	40-20 (2)	< 20 (0)

Table 7.6 Definition of dam age rating factors (Bureau, 2003)

Risk Factor	<1900	1900-1925	1925-1950	1950-1975	1975-2000	>2000
ARF	6	5	4	3	2	1

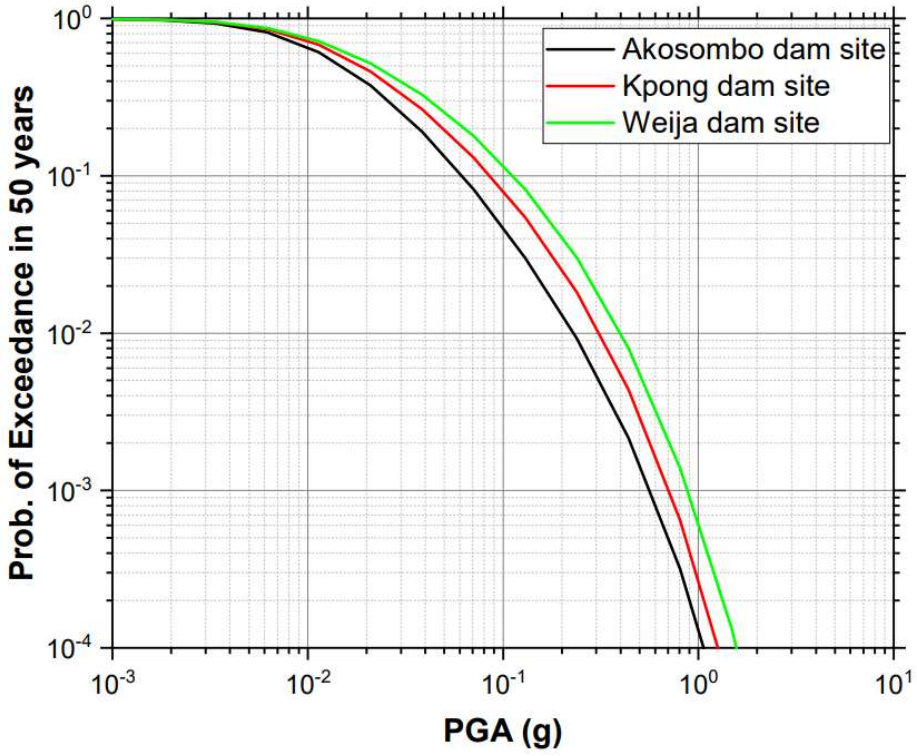
Akosombo dam site
Kpong dam site
Weija dam site
Prob. of Exceedance in 50 years
PGA (g)

(a)

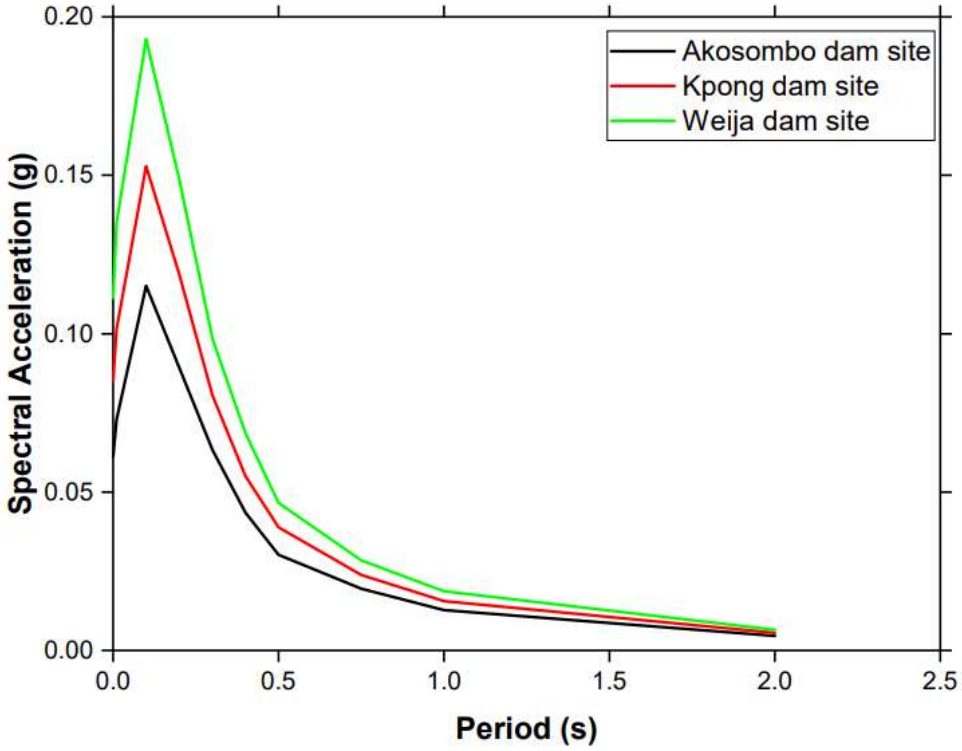
Akosombo dam site
Kpong dam site
Weija dam site
Spectral Acceleration (g)
Period (s)

(b)

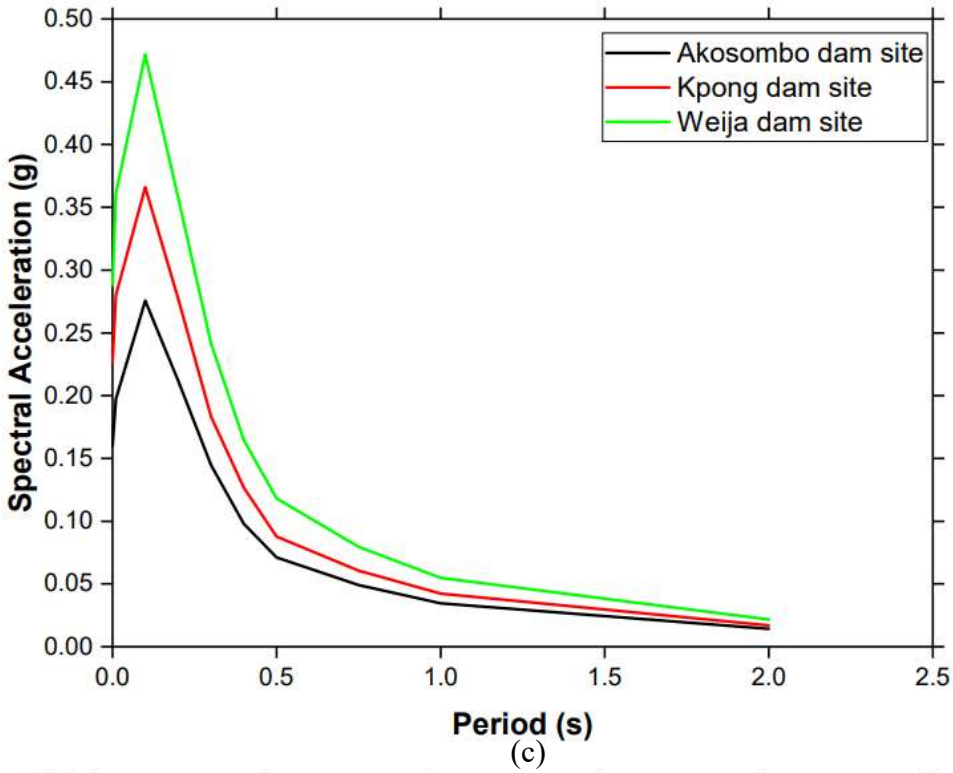

(c)

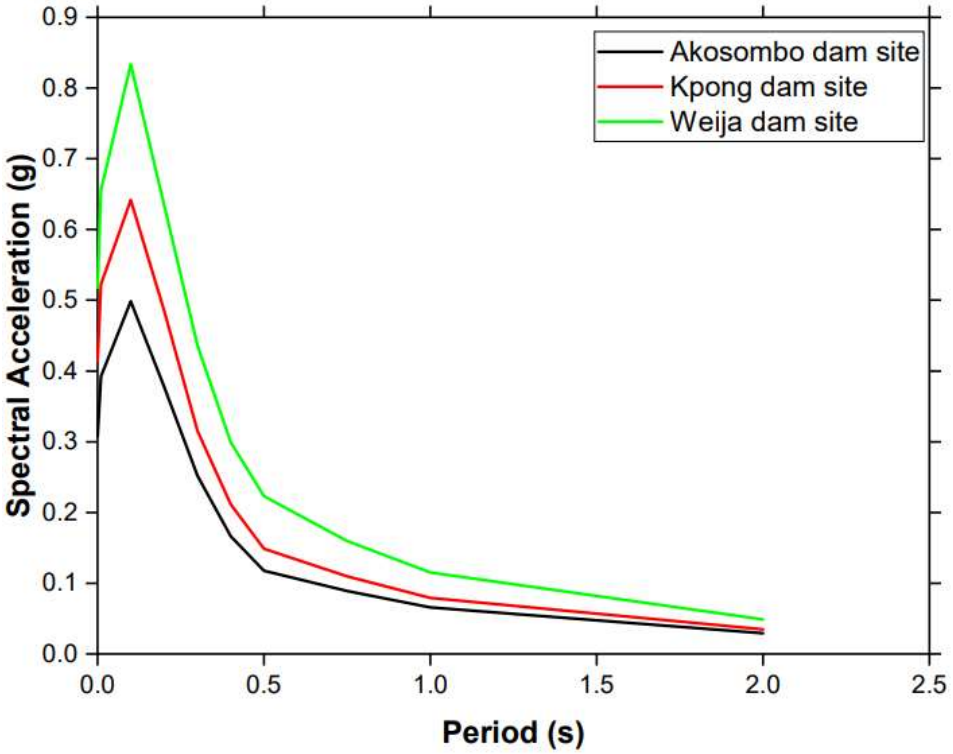

(d)

Figure 7.7. (a) Seismic hazard curves (b) Uniform hazard spectra for 475-year return period (c) Uniform hazard spectra for 2475-year return period. (d) Uniform hazard spectra for 10,000-year return period.

Table 7.7 Downstream hazard factors (Bureau, 2003)

Risk Factors	Contribution to Total Risk Factor (Weighting points)			
	Extreme	High	Moderate	Low
Evacuation requirements (persons) (ERF)	>1000(12)	1000-10 (8)	100-1 (4)	None (0)
Downstream damage risk index (DRI)	>High (12)	Moderate (8)	Low (4)	None (0)

Table 7.8 Definition of Downstream hazard factors, based on NID (Bureau, 2003)

Downstream hazard potential rating (NID)	Loss of human lives	Economic, environmental, or lifeline losses	DHF
Low	None expected	Low, limited to owner's property	2
Significant	None expected	Yes	12
High	Likely, one or more expected	Yes, or probable but not strictly required	24

Table 7.9 Numbers of people and values of properties at risk at various dam sites.

Dam	Human population	Values of property	Reference
Akosombo	18,142	3,703	Ntiamoa-Baidu et al. (2017)
Kpong	18,142	3,703	Ntiamoa-Baidu et al. (2017)
Weija	15,892	2,670	GSS (2014). Owusu-Ansah et al. (2019)

The predicted damage factor (PDF), the vulnerability rating, is a function of the site-dependent seismic hazard and similar dams' observed performance during earthquakes. The PDF can be defined by the predicted damage index (PDI) and calculated from the dam vulnerability curves provided by Bureau and Ballentine (2002) given in Equation 6.8.

$$PDF = 2.5 \times PDI \quad (6.8)$$

PDI depends on the dam type and the site seismic hazard and is expressed by the earthquake severity index (ESI). The seismic hazard represents the expected ground motion obtained at the dam site by the scenario earthquake considered, given in Equation 7.9.

$$ESI = PGA \times (M_w - 4.5)^3 \qquad (7.9)$$

where (PGA) is the peak ground acceleration in units of g for each site, M_w is the earthquake moment magnitude. PDI and ESI's relationship for different dam types obtained from geographical relationships are shown in Figure 7.9 and Equation 7.10 (Hariri-Ardebili and Nuss, 2018).

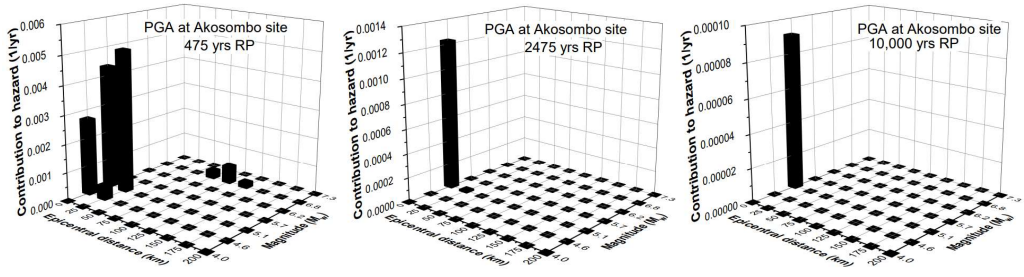

(a)

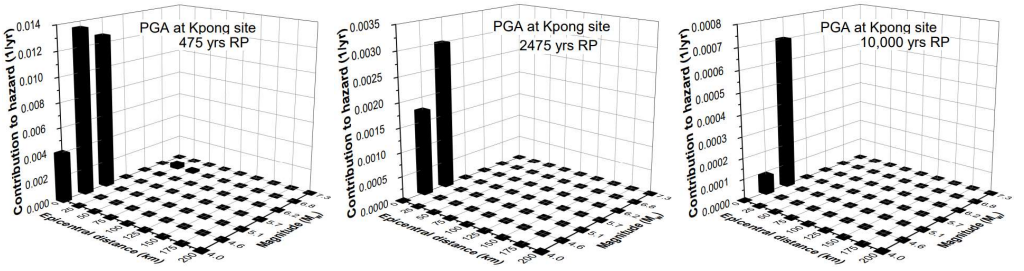

(b)

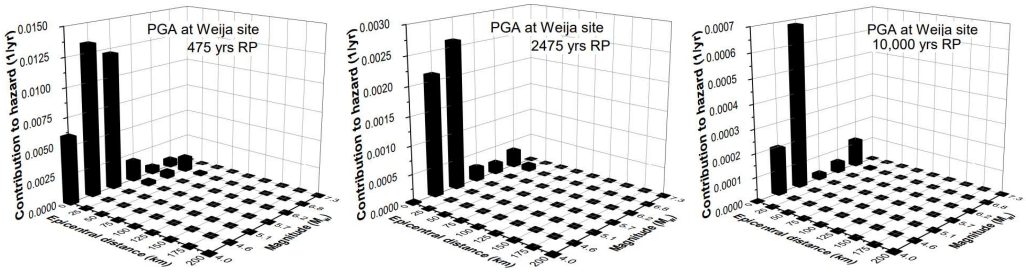

(c)

Figure 7.8 Disaggregation results for dam sites (a) Akosombo (b) Kpong (c) Weija for different return periods

$$\text{PDI} = \begin{cases} 1.08\ exp\ (0.297\ log\ (ESI)) & \text{Arch} \\ 1.28\ exp\ (0.296\ log\ (ESI)) & \text{Rockfill} \\ 1.69\ exp\ (0.139\ log\ (ESI)) & \text{Gravity} \\ 1.96\ exp\ (0.185\ log\ (ESI)) & \text{Earthfill} \\ 2.77\ exp\ (0.356\ log\ (ESI)) & \text{HF} - \text{tailings} \end{cases} \quad (7.10)$$

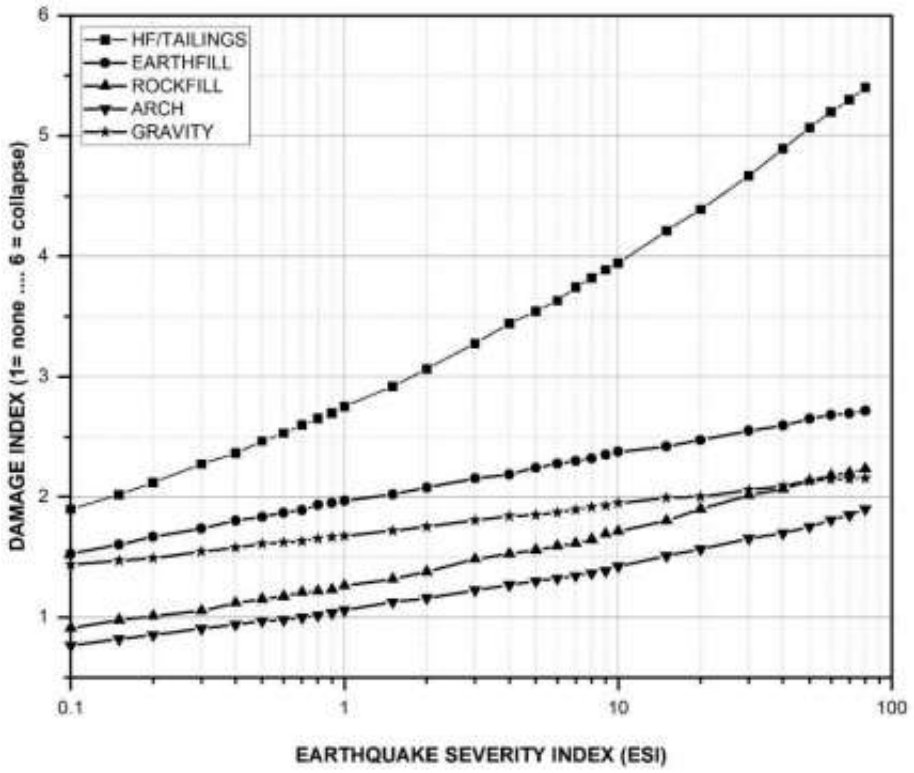

Figure 7.9 Predicted Damage Index (PDI) (Bureau, 2003)

7.4 Seismic risk analyses and discussions

The seismic risk for dam structures depends on the dam site's seismic hazard rating and the risk rating of the dam structure and its appurtenant structure. Therefore, the Bureau (2003) method, which considers the dam type, age, size, downstream damage potential and evacuation requirements, was used to determine the basin' risk analyses. The method recommends four separate risk classes ranging from I (low risk) to IV (extreme risk) as based on the Total Risk Factor (TRF) Table 7.10. Following the Bureau's method, all the three dams in the basin are classified in both II and III risk classes, representing moderate and high-risk rating.

Table 7.10 Definition of Dam risk class (Bureau 2003).

Total Risk Factor (TRF)	Dam Risk Class (DRC)
2-25	I (low)
25-125	II (moderate)
125-250	III (high)
>250	IV (extreme)

The results of total risk analyses of the dam within the West Coast are summarised in Table 7.11. The values of the TRF range from 102.7 to 148.4 This indicates that there is no dam having risk classes IV and I in the basin.

Figure 7.6 shows a map of equivalent PGA values due to seismic hazard analyses performed for the three large dams within the study basin. The PGA values were estimated using a probabilistic approach based on the maximum credible earthquake values for large dams of the return period of 10,000 years. The PGA values estimated are based on rock site conditions only. The most critical areas on the map (Figure 7.6) are those close to Guinea's Gulf in the Atlantic Ocean.

Table 7.11 The results of potential risk analyses of dams for the selected dams

Dam	Site influence[a]		Structure influence[b]			Downstream influence[c]		TRF[d]	Risk class	Rating
	M_{max}[a]	PGA	CRF	HRF	ARF	ERF	DRI			
Akosombo	5.5	0.31	6	6	3	12	12	107.4	II	Moderate
Kpong	5.5	0.41	6	4	2	12	12	102.7	II	High
Weija	6.9	0.52	6	4	2	12	12	148.4	III	High

[a]M_{max}- Maximum credible earthquake taken at 100 km radius of the dam site. PGA- Peak ground acceleration in g. [b]CRF- Capacity risk factor, HRF- Height risk factor, ARF- Age risk factor. [c]ERF- Evacuation requirement factor, DRI- Downstream damage risk factor. [d]TRF- Total risk factor.

This study identified one large dam of the basin, which must be reanalysed by selecting appropriate seismic parameters. Rehabilitation design and construction measures are

necessary in the study of the dam. The dam structures in this study region, e.g., the Weija dam with PGA of 0.52 g, provide water for the Greater Accra regions and affect people and properties located downstream paths when they damage or fail.

The Akosombo dam is the highest structure with 134 m from the riverbed and has the largest storage capacity of 147,960 × 10^6 m^3 in the study basin. Its construction was started in 1961 and entirely completed in 1965. It was designed to produce electricity with an installed capacity of 1,038 MW. Its TRF value is 107.4, and it is identified as risk class II, with a moderate risk rating. The dam is a rockfill embankment dam. This study's seismic hazard analyses will be subjected to a peak ground acceleration of 0.31 g with a maximum credible earthquake of 5.5.

Weija Dam is a zoned earth-fill with rock dam, constructed in 1978. The dam length is 375 m, and the crest height is 17.07 m. It is located 18 km west of Accra city on the Densu River. Its primary purpose is to supply water to many parts of the Greater Accra Metropolitan Area. The dam has a reservoir area of 20.5 km^2, with an average water level of 14.33 m. The design storage capacity of the dam is 113.5 × 106 m^3. The maximum designed water level and storage capacities are 15.25 m and 143.115 × 106 m^3, respectively. The dam identified as a risk class of III with the 2nd highest-risk rating of 148.4 within the basin. The seismic hazard analyses were performed throughout for this study show that the Weija dam can be a critical dam within the basins. It will be subjected to a peak ground acceleration of 0.52 g with a maximum credible earthquake of 6.9.

Kpong dam is a rockfill embankment dam on the lower Volta River, located 65 km northeast of Accra. It has a 20- m height from the riverbed and a reservoir capacity of 200 × 106 m^3. Its construction started in 1977 and was entirely completed in 1982. It was designed to generate 160 MW of electricity and to provide irrigation service to the host environment. Therefore, it will be subjected to a high PGA value (0.41 g) with a maximum credible earthquake of 5.5.

6.5 Summary

For dams with a wall high from 17 to 134 m in the West Coast Basin of Ghana, the seismic hazard and rating on three large dams were performed based on the Bureau (2003) methodology. As a result, the following results have been concluded:

i. The three selected dams have shown moderate to high-risk classes at the value range (102.7-148.4). The PGA values range from 0.31 g to 0.52 g (high classes). In this study, one destructive earthquake reported within the last 100 years is the 6.4 *M*w 1939 Accra (Ghana) earthquake. This earthquake may have influenced the seismic results. Therefore, dam implementation in Ghana by the National Dam Safety Program for dams and their appurtenant structures is encouraged.

ii. The three dams identified in the study region are old, and their age rise from 38 to 56 years: therefore, these dams should be inspected, analysed seismically and redesigned if necessary.

iii. Akosombo dam is identified as a risk class of II with the large reservoir on the main river and still under operation. Prioritise dams with a moderate to high-risk rating that provide electricity for more than one country in the study basin.

iv. A detailed assessment for the three dams in the future should include stability, reliability, and dynamic analyses to determine the possible dam failures.

7.6 Data and resources

Data sources for our assessment include that of the International Seismological Centre (ISC). The ISC catalogue, was searched through http://www.isc.ac.uk/iscbulletin/search/catalogue/), (last accessed October 2020), and the United States Geological Survey -National Earthquake Information Centre (USGS – NEIC) (https://earthquake.usgs.gov/earthquakes/search/) (last accessed October 2020).

CHAPTER 8

DYNAMIC RESPONSE AND STABILITY ANALYSES OF AKOSOMBO DAM USING NUMERICAL ANALYSIS

Reformatted version of the following paper:

Paper title: **Dynamic Response and Stability Analyses of Akosombo Dam Using Numerical Analysis**

Authors**: Stephen A. Irinyemi, Domenico Lombardi & Syed M. Ahmad**

Published in: International Journal of Advanced Research. 9 (2021) 639-655

Research output: Contribution to journal › Article › peer-review

DOI: 10.21474/IJAR01/13588

Author contributions

The author (Irinyemi) conducted the seismic data analysis, designed the work, acquired and analysed the data and drafted the paper. Lombardi and Ahmad supervised the author.

Abstract

Dams are very important in Ghana's economic development and environmental improvement. Although Ghana dams are seismically far from the active zone, accurately analysed dams should be evaluated since failure could severely impact the people in the flood environment and the region's economy on a large scale. This paper proposes a numerical procedure for the static, slope stability, and dynamic analysis of the Akosombo embankment dam. Nineteen horizontal acceleration time histories recorded data was used based on Maximum Design Earthquake (MDE), Maximum Credible Earthquake (MCE), Design Basis Earthquake (DBE) and Operating Basis Earthquake (OBE) data. The numerical results estimated showed that the Akosombo embankment dam is likely to experience moderate deformations during the different design earthquakes but will remain stable after the earthquakes. The result also indicated that non-linear analysis capable of capturing dominant non-linear mechanisms could be used to assess the stability of embankment dams. The factor of safety (FS) calculated was greater than 1.5

for high reservoir, rapid drawdown condition and low reservoir condition whereas, the FS values were found to be 1.42 for slow drawdown condition.

8.1 Introduction

Stability and crest displacements of embankment dams is a significant concern in every region. Seismic-induced deformations in a rockfill embankment dam may lead to overtopping and massive losses of built environments and people living along the dam paths. However, in recent years, the availability of seismic hazard maps and different design criteria have led to assessing the seismic safety of dams built without considering seismic-induced forces. Consequently, the designed remedies have posed a challenging problem for geotechnical engineers. A standard manual on world register dams provided by the International Commission on Large Dams (ICOLD) has about 95 member countries, including Ghana, which defined dams with a measured height of more than 15 m or between 5 and 15 m whose reservoir capacities greater than 3 million m^3 as "large dams". Presently about 60,000 large dams have been registered (Wang et al., 2021), and 1,949 are in Africa. Skinner et al. (2009) report showed that West Africa has over 150 large dams constructed on their region's river.

Akosombo Dam is the largest dam in West Africa located on the Volta River in Ghana, with a wall height of 134 m (4th in Africa) and a capacity of 150 billion cubic metres (3rd in Africa). Akosombo dam is a rockfill embankment dam, about 82 km north of Accra city in the southeast of Ghana (Figure 8.1). The dam has a crest length of 640 m, a crest width of 12.2 m, and a 114 m maximum structural height above the foundation level, completed in 1965. The reservoir is used for providing electricity for the host environment. The construction of embankment dams is more recognised globally with some advantages over other dams (Narita, 2000), i.e., the foundation does not require rigorous conditions. The embankment dams can be placed on alluvial deposits and pervious foundations. They can be constructed on the outskirts of the city area. The Knowledge of different specialists (engineering, hydrology, geophysics, geology, and soil mechanics) is required for the construction of an earth-fill (embankment) dam that can provide safety and constant critical surveillance of dam reservoir and foundation during its lifetime (Ebrahimian, 2011). However, the highest responsibility belongs to the seismic designers. Dams' failure can lead to a severe loss of human and properties.

The failures may be caused by structural deficiencies in the dam body due to poor design or construction, age of the dams, sliding of slope and instability, and overtopping (Shikhare et al., 2009). However, a record shown considerable numbers of embankment dams have been damaged in different countries due to earthquakes (Gosschalk, 1994). This call for a better method to enhance the stability of existing dams. The standard method used for the seismic design of earth dams was erroneous based on the assumption that dam bodies are fixed on a rigid foundation, thereby experiencing a uniform acceleration equal to the underlain-ground acceleration (Gazetas, 1985). However, research has shown that the response of dams under earthquakes depends on the constructed materials, the geometry, and the base motion's nature. Therefore, many studies have been conducted to understand the seismic behaviour of earth and rockfill embankment dams. Newmark (1965) was the first to conduct the effects of earthquakes on dams and embankments. He used a sliding block method to evaluate the performance of the earth and the embankment dam. Lin and Whitman (1986) assess earthquake-induced permanent displacement using sliding blocks. However, since the advent of more sophisticated and fast computer programmes, effective modelling, and testing, an increasing number of studies on earth (rockfill) dams using numerical methods such as finite element, finite difference, and boundary element methods with non-linear material models (Sengupta (2010); Albano et al. (2012) Afiri and Gabi (2018), performed seismic analysis on an existing bituminous faced rockfill dam in southern Italy using numerical analysis. The numerical simulation results compared to the small-scale centrifuge model of the dam. Selçuk and Terzi (2015) conducted a seismic response of the Ambar dam to a recorded earthquake. This study investigated the Ambar earth dam's dynamic response and earthquake resistance in the southeast part of Turkey using the non-linear dynamic time-history of Bingol (2003) earthquake and modal analysis methods. The dam was analysed under static conditions and dynamic analysis. The PGA responses caused by maximum design earthquake (MDE) applied to the dam body, impervious core, and foundation. They showed that the Ambar dam might experience moderate deformations during the design earthquake but stable after the earthquake. Afiri and Gabi (2018); Afiri et al. (2018) evaluated the slope stability analysis of Souk Tleta dam in north Algeria using the shear reduction method. They showed that large displacements occurred in the dam body and foundation at the end of construction and lowered during the reservoir

filling. Also, the result showed that the factor of safety in different conditions decreases when the reservoir water level increases. Finally, Jin and Chi (2019) conducted seismic fragility analysis on high earth-rockfill dams using various ground motion records. They used a program called DYNE3WAC in combination with the Pastor–Zienkiewicz–Chan model and Biot dynamic consolidation theory to determine the vertical deformation of the dams. Seismic behaviour of the El Infiernillo Dam which is similar to Akosombo dam was investigated. Important features of dam behaviour under seismic loading are calculated by coupled elastoplastic dynamic analyses, where analytical computation and experimental measurements are compared on the dam body during and after a past earthquake (Sica et al., 2002).

This paper investigates the dynamic response and earthquake resistance of the Akosombo embankment dam located in Asuogyaman Province, Ghana, using non-linear dynamic time histories. The dam was first analysed under static conditions and then performed acceleration-time histories of 19 earthquakes. The PGA responses caused by maximum design earthquake (MDE), Maximum Credible Earthquake (MCE), Design Basis Earthquake (DBE) and Operating Basis Earthquake (OBE) were applied to the dam body, impervious core, and foundation, and the factor of safety was calculated by drawdown reduction method. The drawdown reduction method was used by Athani et al. (2015) to determine seepage and stability analyses of earth dam using PLAXIS 3D Finite element method.

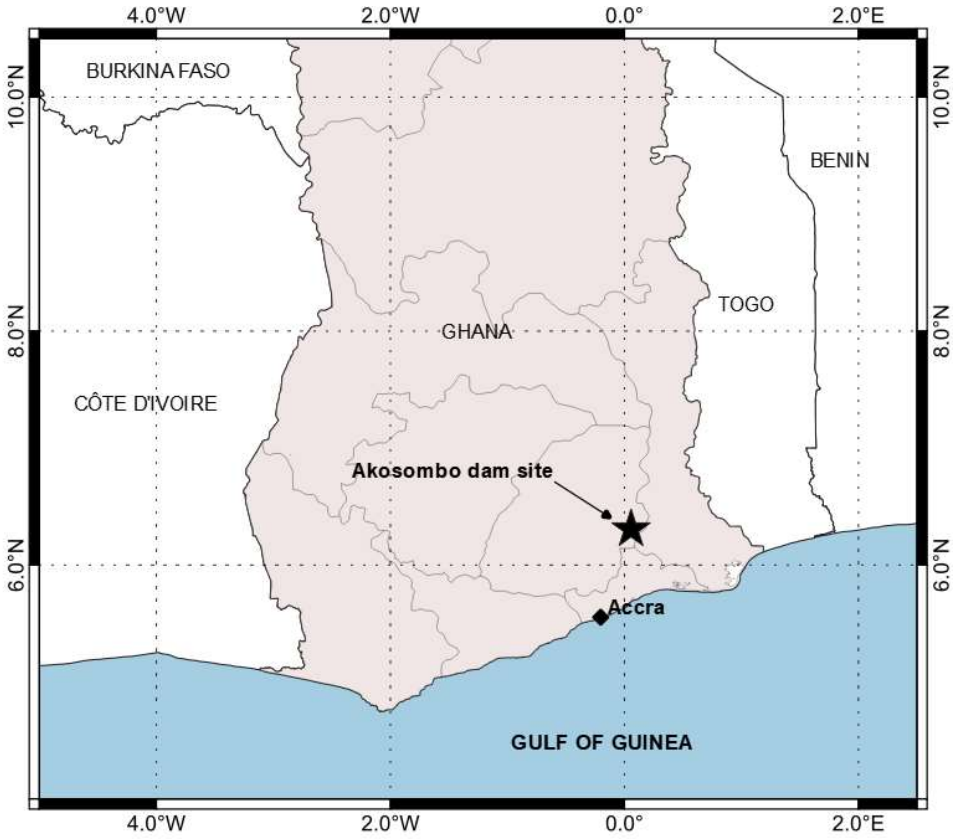

Figure 8.1 Location of Akosombo dam

8.2 Geology of the dam site

The geology of the dam bodies' foundation, lithology, stratigraphy, and soil parameters need to be assessed during analysis. A high degree of judgment is required to evaluate the soil characteristics through comprehensive field observation and laboratory tests (Ozkan et al., 1996; Selçuk and Terzi, 2015). To construct the cofferdams for Akosombo Dam, the entire bedrock surface was stripped of a thick deposit of sand alluvium using machine at a depth of 200 feet below the water surface. The upstream and downstream cofferdams formed by end dumping methods at depths varied from 30.48 m in the upstream to 60.96 m at the downstream. The clay core of Akosombo dam was compacted at moisture content slightly wet to 2 percent wet of optimum and compacted rockfill was sluiced at a water to cement ratio of 0.5 to 1.0. The field density of Akosombo core was put at 0.80 frequency of test at 764.555 m^3 (Wilson and Squier, 1984). The shell is made of compacted or dumped rockfill, while filter materials are of fine and coarse materials.

8.3 Geometry of the dam and soil properties

When assessing the safety threshold value of any structure, the most critical factor is the deformation that occurs under seismic effects at which the accelerations change at different locations. Therefore, an accurately designed dam should detect the accelerations at the critical area of the dam under investigation (Selçuk and Terzi, 2015). The geometrical features are provided in Table 8.1. The schematic cross-section of the Akosombo dam and the foundation layer used in this paper is shown in Figure 8.2. The geotechnical parameters of the slope layers are determined using engineering experience obtained from the literature. The necessary parameters for the slope stability analysis and design are presented in Table 7.2. Only the geotechnical parameters and properties that concern the dam's slope stability analysis are specified in this study. The permeability (k) of dam materials used the standard values were taken from the engineering perspective.

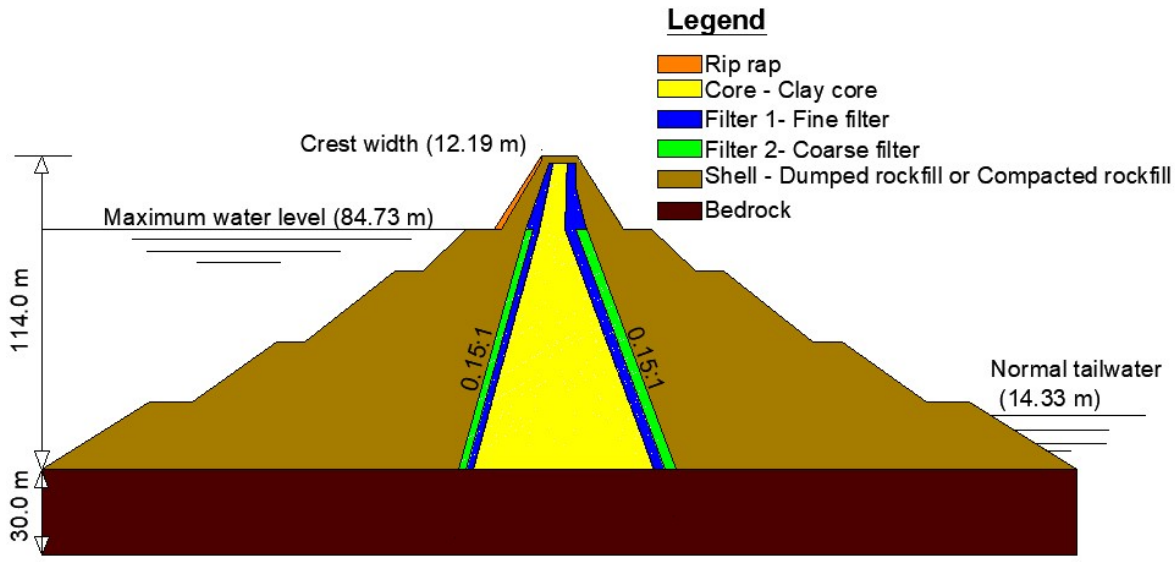

Figure 8.2 Geometry of the cross section of the Akosombo Dam

Table 8.1. Geometrical properties of Akosombo dam

Parameter	Value
Dam's height above ground level	114 m
Crest elevation	88.39 m
Dam width	366.0 m
Dam crest length	660.0 m
Dam crest width	12.20 m
Maximum water level	84.73 m
Tail water level	14.33 m
Area of watershed	8,502 km^2
Storage capacity	153,000 M m^3

8.4 Seismic activity in and around the dam site

Numerical estimation of permanent displacement of a proposed or existing earth/rockfill embankment dams requires an enormous task, mainly when information on field data is lacking. The seismic hazard assessment performed by probabilistic seismic hazard analysis (Cornell, 1968 and McGuire, 1995) considers all earthquake scenarios affecting the site. The seismic hazards estimated are represented by peak ground acceleration. Therefore, to assess the dynamic response of the Akosombo Dam, it is necessary to consider the seismic risk in and around the region.

Table 8.2. Parameters used for slope stability of Akosombo dam

Material type	Unit weight Υ_h (kN/m^3)	Saturated Unit weight Υ_{sat} (kN/m^3)	Internal angle of friction φ (^{0})	Cohesion of soil *c* (kPa)	Poisson's ratio υ	Young modulus E (MPa)	Permeability k (m/day)
Core clay	18	19	20	10	0.25	25	0.0000864
Filter 1	19	20	30	0	0.23	90	0.00864
Filter 2	17	19	30	0	0.27	80	0.00864
Shell	18	21	45	15	0.30	80	0.0864
Rip rap	20	21	30	0	0.24	60	0.000864
Bedrock	21	22	29	20	0.17	150	0.000001

Two major active faults governed the neotectonics of the southern Ghana. They are: (1) the Akwapim fault, which is the main structural feature in the basin, (2) the Coastal boundary fault, which is a normal fault along the coastal line that strikes north 60^0 E-70^0 E, at about 5 km from the coast.

No accounts of damage due to earthquakes have been observed within the dam area. However, Ghana earthquakes of 1964 and 1969 were felt near the Akosombo dam and was subjected to induced seismicity (Musson, 2014). Accra's earthquakes are attributed to the reactivation of faults in the Romanche fracture zone, specifically the Coastal Boundary fault and Akwapim fault (Kutu, 2013; Musson, 2014; Ahulu et al., 2018). The Coastal Boundary fault became tectonically active in Jurassic times and is still active (Ahulu et al., 2018). The Akwapim Fault Zone comprises a system of faults trending north-easterly from just west of Accra, along an ancient line of thrust boundaries in the Dahomeyan belt. Neotectonics normal faults along the Akwapim range could mean that the tectonic movement is still active, making faults from SW of the Akwapim active (Amponsah et al., 2012; Ahulu et al., 2018).

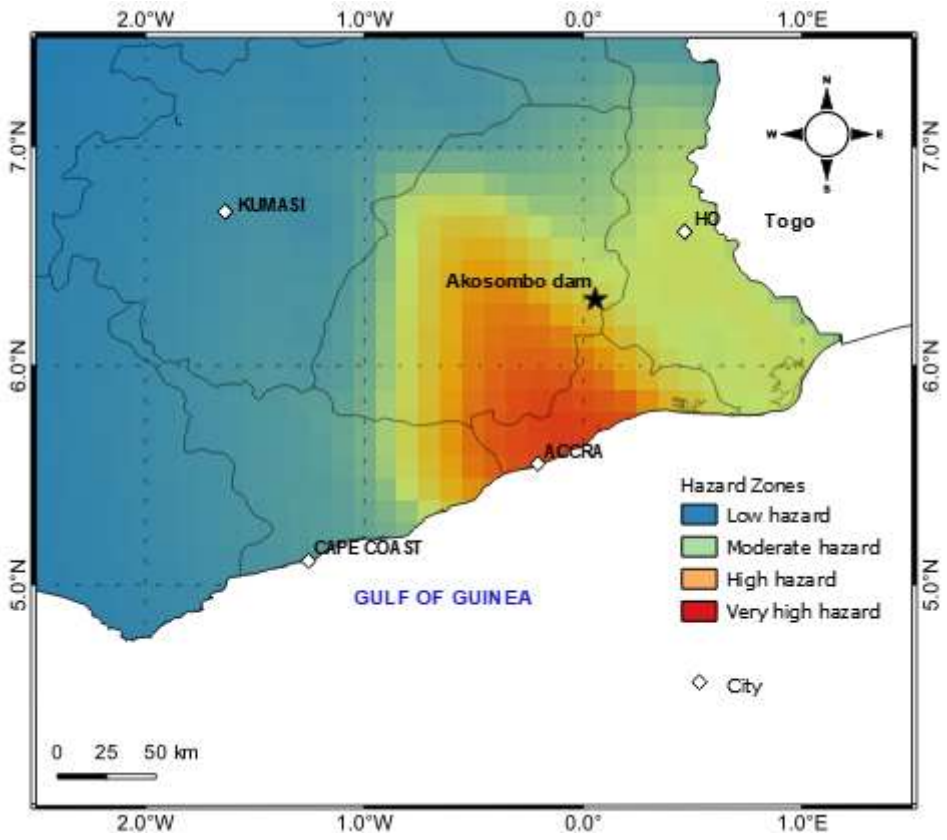

Figure 8.3. Proposed seismic hazard map for 475 years return period.

According to the available historical sources, about 35 earthquakes had occurred between 1818 and 2018 for $M_w \geq 4$. Based on this data, Ghana earthquake zoning Map was proposed (Figure 8.3), the map divides Southern Ghana into 4 risk zones, 70% of the total population of Ghana and 3 existing large dams currently in operations are in the proposed hazard zones. Based on the Earthquake Zoning Map; Figure 7.3 shows that the dam site is in Moderate Hazard Zone Area.

8.5 Numerical Analysis

The dynamic performance of dams using numerical analysis to estimate the crest settlement requires a more sophisticated approach (Kan and Taiebat, 2011). For the seismic design of the dams and its appurtenant structures, the following design earthquakes were considered as recommended by Wieland (2012).

1. Operating Basis Earthquake (OBE): The OBE design is used where earthquake damage to a dam project is limited, where the mean value of ground motion is determined from a probabilistic seismic hazard analysis (PSHA). According to ICOLD, 2010, the OBE should be designed at an average return period of 145 years (i.e., 50% probability of exceedance in 100 years).

2. Design Basis Earthquake (DBE): The DBE is designed for a return period of 475 years for dam and its appurtenant structures. The DBE mean value of ground motion parameters is estimated based on a PSHA. (i.e., the return period of the DBE usually determined based on the earthquake codes and regulations for buildings and bridges in any project region.). The ground motions for a 2% probability of exceedance within 50 years, which is equivalent to 2475 years of return period is also considered for the design earthquake in this study.

3. Maximum Credible Earthquake (MCE): The earthquake selected for dam structure whose return period is 2475 years. The earthquake that can expected to occur along a recognised fault or supported by known geologic and seismologic data. A hypothetical probabilistic earthquake is considered since the event is random, and its epicentral distance is determined mathematically by relationships of recurrence and magnitude for this study dam.

4. Maximum Design Earthquake (MDE): The MDE is designed for a return period of 10,000 for a large dam, where the ground motion parameters are estimated based on PSHA. The average mean values of the ground motion are also taken for the design.

Within all the frameworks of these assessments for the Akosombo seismic design considering the OBE, DBE and MDE, the peak ground acceleration earthquake coefficient was estimated as 0.03g, 0.08g, 0.21g and 0.39g respectively for 145, 475, 2475 and 10,000 years return periods. The input earthquake motions were compiled from a real accelerograms (Table 7.3) from online PEER Ground Motion Database - PEER Center (berkeley.edu), Strong motion virtual data Center (VDC) www.strongmotioncenter.org, and European Strong-Motion (ESM) Database, http://isesd.hi.is/. The real accelerograms (Figure 7.4) processed by Seism-Signal 2021, were used for the dynamic analysis using Plaxis 2D. The total displacement of the dam crest was chosen as Engineering Demand parameter (EDP). The response spectra estimated from the hard rock site conditions were compared with the 19 response spectra for the different return periods (Figure 8.5).

8.6 Dam stability analysis and drawdown conditions

PLAXIS 2D finite element software used Linear-elastic-perfectly plastic Mohr–Coulomb model for all layers of dam and foundation materials. The slope was modelled in the input module of PLAXIS, based on 15-nodded elements in a plane strain model. Drawdown conditions of stability of the reservoir were examined using a fully coupled flow-deformation analysis with time-dependent pore pressure. A fine mesh element of 2,009 and element nodes of 16,435 were generated in the simulation of slope stability analysis to estimate the least possible factor of safety (FOS). Figure 8.6 shows the 2D view for the finite element mesh of Akosombo dam and its foundation. The uses of Mohr–Coulomb model (linear elastic - perfectly plastic) in this study does not take into account effects of changes in density and consequently the effects such as softening cannot be modelled. The plane strain predictions of Mohr-Coulomb may be conservative.

Table 8.3. Properties of 19 real earthquakes used

Earthquake	Record station	M_w	D_{5-95}	a_{max}	T	I_a	EDA
Maximum Design Earthquake (MDE) 10,000 Years							
Friuli (Italy), 1976	Tolmezzo (000)	6.4	4.24	0.35	36.32	0.780	0.329
Imperial Valley (USA), 1979	USGS Station 5115	6.5	8.92	0.29	39.48	1.265	0.333
Kobe (Japan), 1995	Kakogawa (CUE90)	6.9	12.86	0.34	40.90	1.687	0.337
Loma Prieta (USA), 1989	CDMG (47381)	6.9	11.37	0.37	39.90	1.347	0.352
Duzce (Turkey), 1999	IRIGN (498)	7.1	12.26	0.39	35.00	2.196	0.391
Maximum Credible Earthquake (MCE) 2475 Years							
Kocaeli (Gebze Turkey), 1999	Yarimca (KOERI330)	7.4	15.62	0.22	34.96	1.318	0.327
Chi-Chi (Taiwan), 1999	TCU045	7.6	11.94	0.18	52.78	0.353	0.222
Hollister (USA), 1961	USGS Station 1028	5.9	16.53	0.19	39.93	0.257	0.194
Trinidad (USA), 1983	CDMG Station 1498	5.7	7.800	0.19	21.40	0.168	0.175
Design Basis Earthquake (DBE) 475 Years							
Manjil (Iran), 1990	Tonekabun S58E	7.3	18.87	0.10	35.49	0.409	0.100
Spitak (Armenia), 1988	Gukasian 90	6.7	7.480	0.17	20.01	0.299	0.171
Nahanni (Canada), 1985	Site 3, 360	6.9	5.915	0.15	9.545	0.229	0.150
Oroville-01 (USA), 1975	Oroville Station 37	5.9	3.415	0.08	12.19	0.032	0.082
Irpinia (Italy), 1980	Rionero In Vulture 0	6.9	24.55	0.09	37.16	0.349	0.090
Operating Basis Earthquake (OBE) 145 YEARS							
San Fernando (USA), 1971	Via Tejon PV 65	6.6	51.78	0.030	70.185	0.026	0.024
Morgan-Hill (USA), 1984	Apeel 1E-Hayward 0	6.2	34.25	0.027	59.98	0.024	0.040
Northern-Calif (USA), 1960	Ferndale City Hall 224	5.7	24.96	0.047	82.29	0.036	0.074
Helena-Montana (USA), 1997	Helena Fed. Building	6.0	0.555	0.034	21.09	0.0019	0.018
Umbria Marche (Italy), 1997	Aquilpark-Citta 90	5.7	33.19	0.005	99.835	0.0011	0.005

M_w = Moment magnitude, D_{5-95} = significant duration, a_{max}= peak ground acceleration (g), T = dynamic time (s), I_a = Arias intensity (m/s), EDA = Effective Design Acceleration (g)

Drawdown conditions for stability of the reservoir were examined under the following conditions, as listed below:

a. Steady state condition at High reservoir level of the Akosombo dam

b. Rapid drawdown in 5 days duration when the maximum water level is at 84.73 m

c. Slow drawdown in 30 days duration at water level of 84.73 m

d. Low water low at 34.73 m

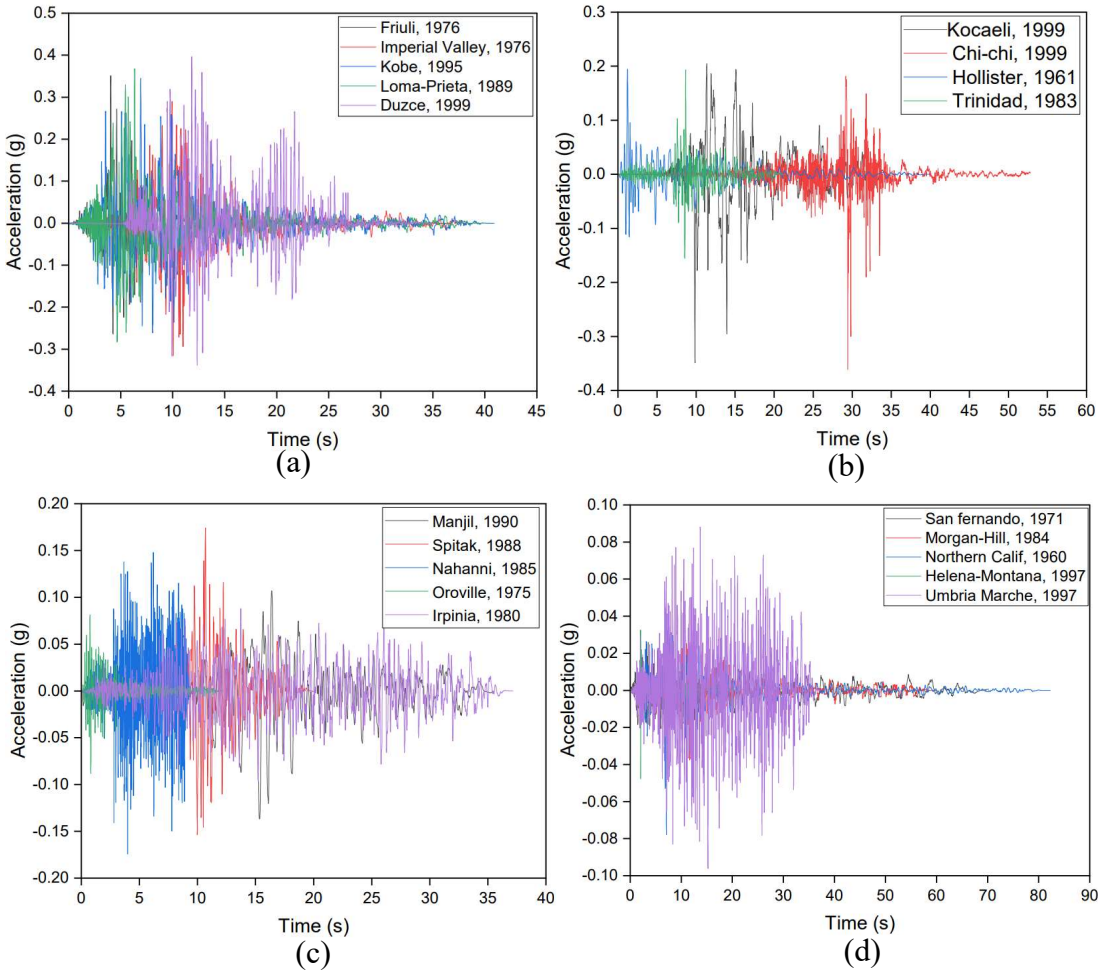

Figure 8.4. Horizontal acceleration-time history input data of nineteen earthquakes representing (a) 145-year (b) 475-year (c) 2475-year, (d) 10,000-year

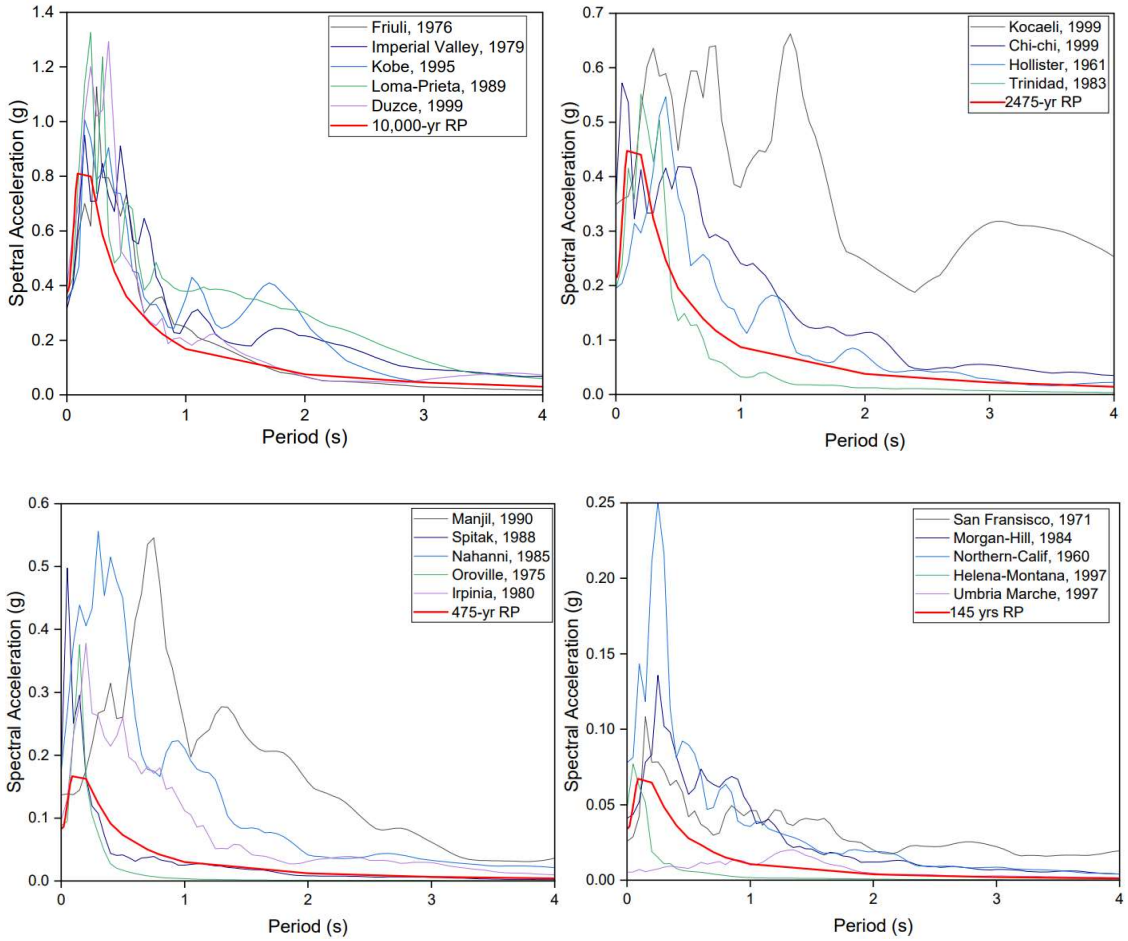

Figure 8.5. Comparison of acceleration response spectra of all the earthquakes and the site response spectrum for different return periods.

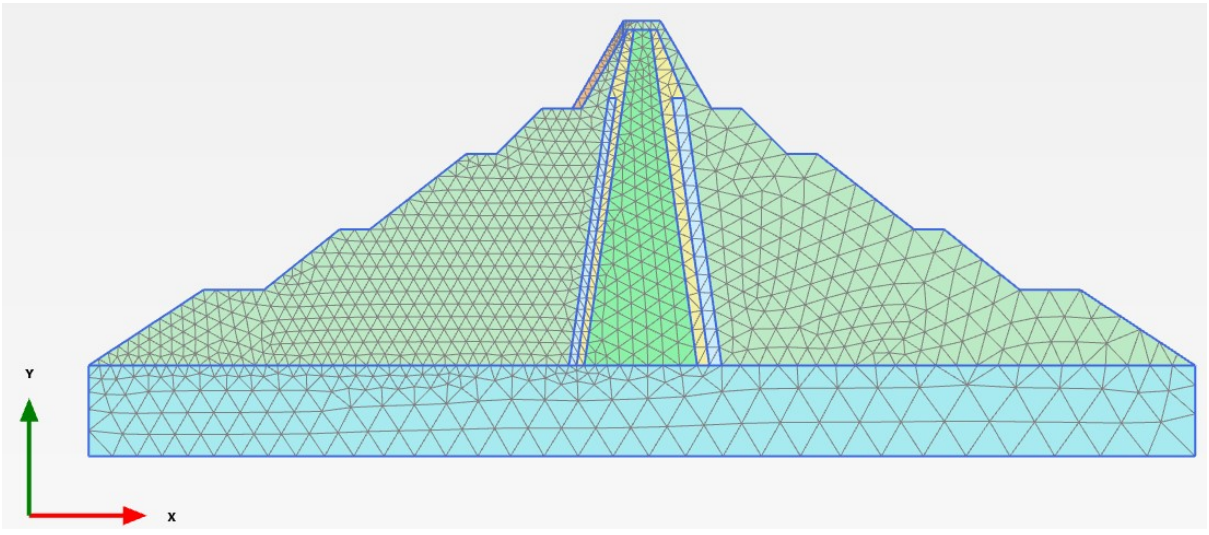

Figure 8.6. Connectivity plot of finite element mesh

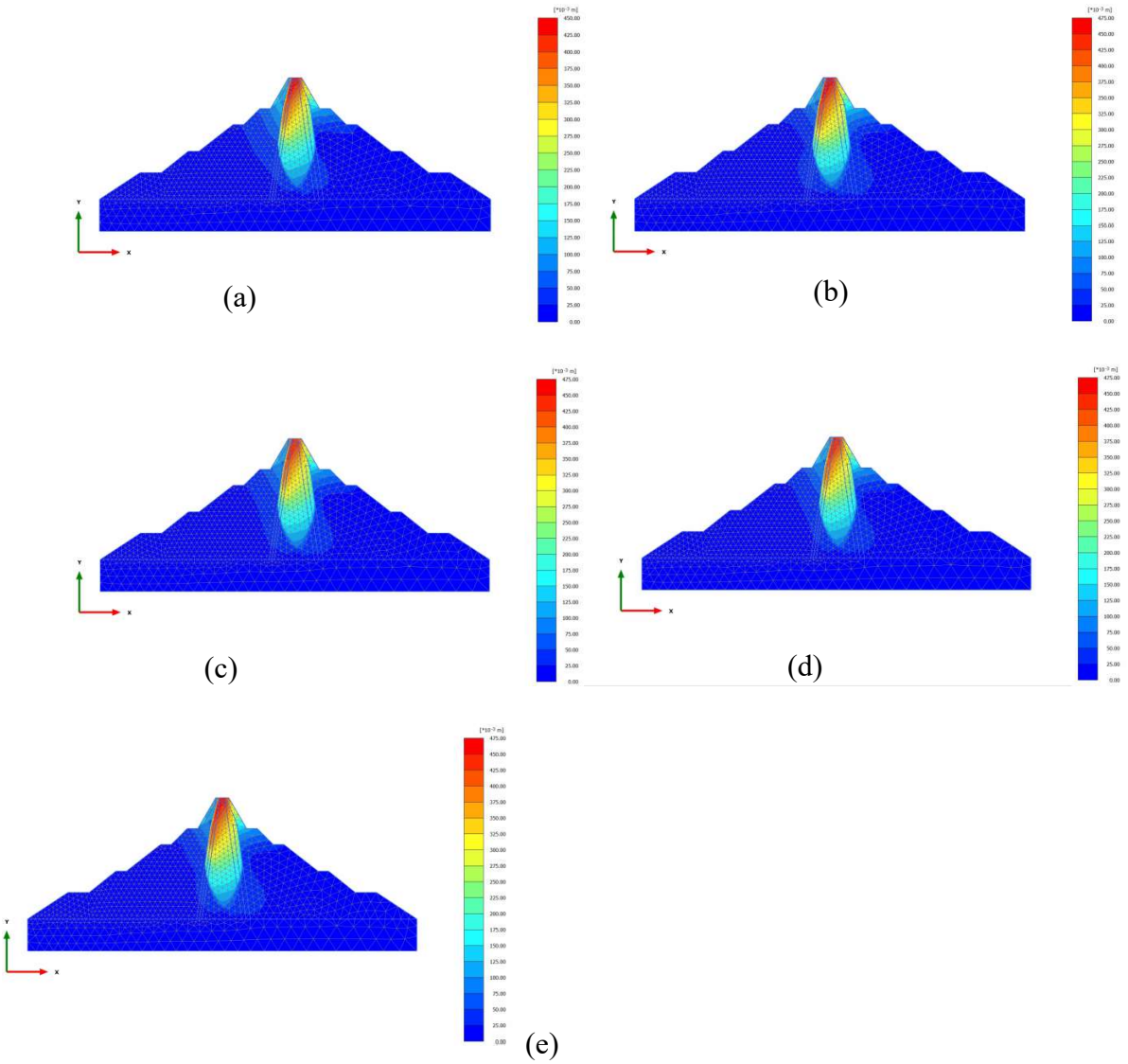

Figure 8.7. Earthquake induced deformation behaviour of Akosombo dam (a) using Friuli earthquake (b) using Imperial Valley earthquake (c) Kobe earthquake, (d) Loma-Prieta earthquake and (e) Duzce earthquake.

8.7 Dynamic analysis results

Dynamic deformation analysis was considered incremental stresses as a driving force for permanent deformation based on stress redistribution. According to Rampello et al. (2009), permanent displacements have resulted from plastic strains that accumulated during the earthquake because of progressive plastic loading, which are influenced by the duration of the strong motion. In the dynamic evaluations, the crest behaviour was selected as the parameter to represent earthquake-related deformations because it is the most frequently mentioned quantified measurement of damage presented in dam studies.

The amount of crest settlement is related primarily to two factors: the peak ground acceleration at the dam site and the magnitude of the causative earthquake (Selçuk and Terzi 2015). The computed total displacements along the dam body for MDE, DBE and OBE values are shown in Figure (8.7-8.10).

As seen in Figure (8.7-8.10), displacements increased with the increased height of the dam. When the dam section undergoes strong base excitation, a slump usually take place rather than failure along a discrete surface. Based on this study, permanent deformations are concentrated in the dam crest. In general, according to the literature, when earthquake shaking occurred in a dam site, the settlements at the crest of an embankment dam should not exceed 1 or 2% of the dam height. The dynamic analysis using nineteen values of PGA showed that the instability of the Akosombo dam took place along the crest where the maximum settlement occurred in the core of the dam. From the dynamic analysis, the analyses show the effect of deformation at the dam body. The estimated total displacements and displacement in horizontal directions of Akosombo dam are listed in Table 8.4.

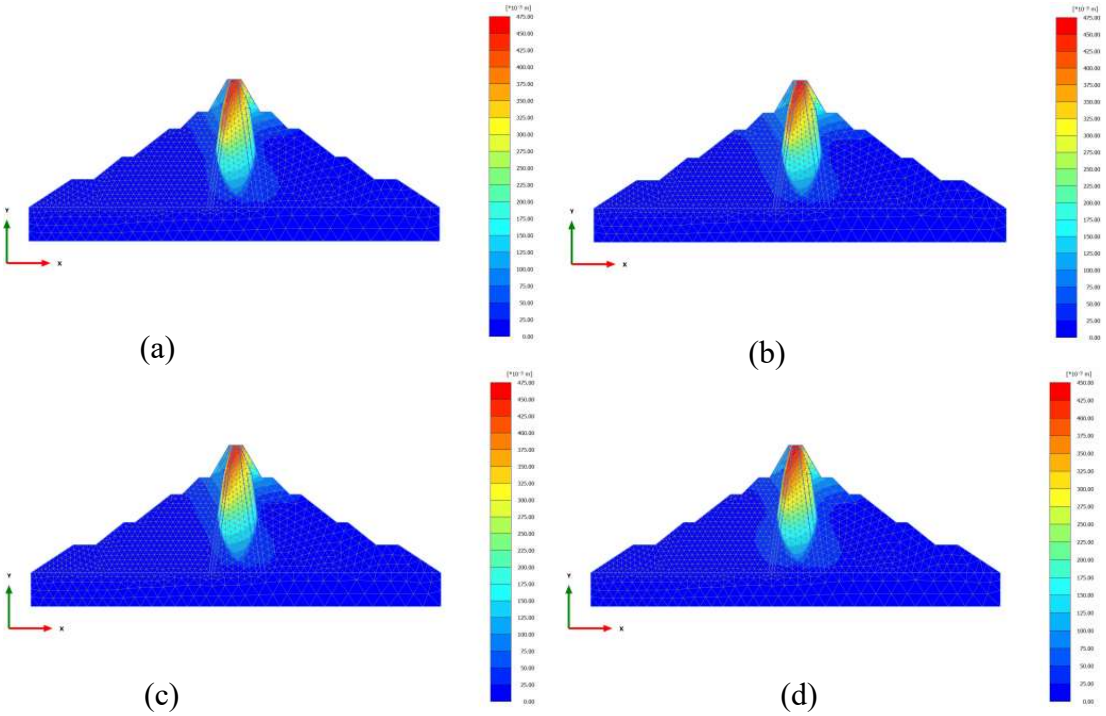

Figure 8.8. Earthquake induced deformation behaviour of Akosombo dam (a) Kocaeli earthquake (b) Chi-Chi earthquake, and (c) Hollister earthquake, and (d) Trinidad earthquake.

The effects of different 19 earthquakes (Table 8.3) on the total displacements at the crest of Akosombo dam with different horizontal peak ground accelerations are shown in Figure 8.11. The peak ground acceleration varied with the displacement. The total displacements and peak ground acceleration increase at the dam crest. The horizontal peak ground accelerations and numerical calculated horizontal displacements are shown in Figure 8.12. It can note that in Figure (8.11-8.12), the maximum peak ground acceleration does not lead to an increase in permanent displacement in the dam body. The total deformation is estimated larger (0.47 m) when the horizontal peak acceleration is 0.29 g for the Imperial Valley earthquake. Similarly, three earthquakes (Nahanni, Oroville, and Helena-Montana) are responsible for the large horizontal displacements in the numerical estimation of the Akosombo dam with the PGA values of 0.15 g, 0.08 g, and 0.034 g, respectively.

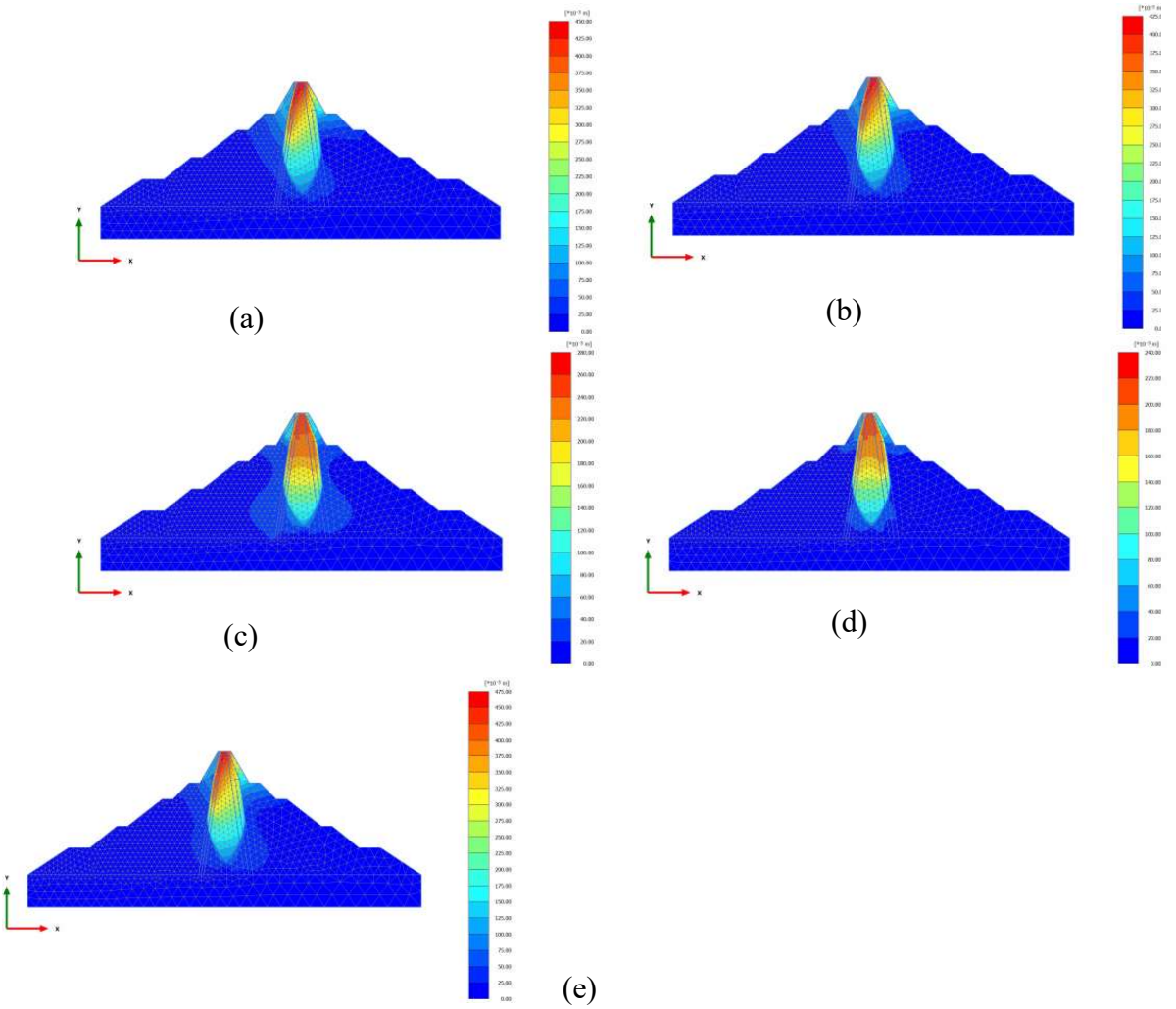

(a) (b) (c) (d) (e)

Figure 8.9. Earthquake induced deformation behaviour of Akosombo dam (a) using Manji earthquake (b) using Spitak earthquake (c) Nahanni earthquake, (d) Oroville earthquake and (e) Irpinia earthquake.

Table 8.4. Computed deformations from the numerical analysis of Akosombo embankment dam

Earthquake	Dam body (|U|) m	Dam body (U_x) m
Maximum Design Earthquake (MDE) 10,000 Years		
Friuli (Italy), 1976	0.4429	0.03218
Imperial Valley (USA), 1979	0.4704	0.03180
Kobe (Japan), 1995	0.4526	0.02986
Loma Prieta (USA), 1989	0.4530	0.03218
Duzce (Turkey), 1999	0.4648	0.03373
Maximum Credible Earthquake (MCE) 2475 Years		
Kocaeli (Gebze Turkey), 1999	0.4569	0.03330
Chi-Chi (Taiwan), 1999	0.4597	0.02914
Hollister (USA), 1961	0.4511	0.03212
Trinidad (USA), 1983	0.4313	0.02839
Design Basis Earthquake (DBE) 475 Years		
Manjil (Iran), 1990	0.4434	0.03191
Spitak (Armenia), 1988	0.4072	0.02984
Nahanni (Canada), 1985	0.2607	0.06174
Oroville-01 (USA), 1975	0.2216	0.06147
Irpinia (Italy), 1980	0.4604	0.03029
Operation Basis Earthquake (OBE) 145 YEARS		
San Fernando (USA), 1971	0.4457	0.02758
Morgan-Hill (USA), 1984	0.4482	0.02941
Northern-Calif (USA), 1960	0.4503	0.02762
Helena-Montana (USA), 1997	0.2216	0.06147
Umbria Marche (Italy), 1997	0.4604	0.03029

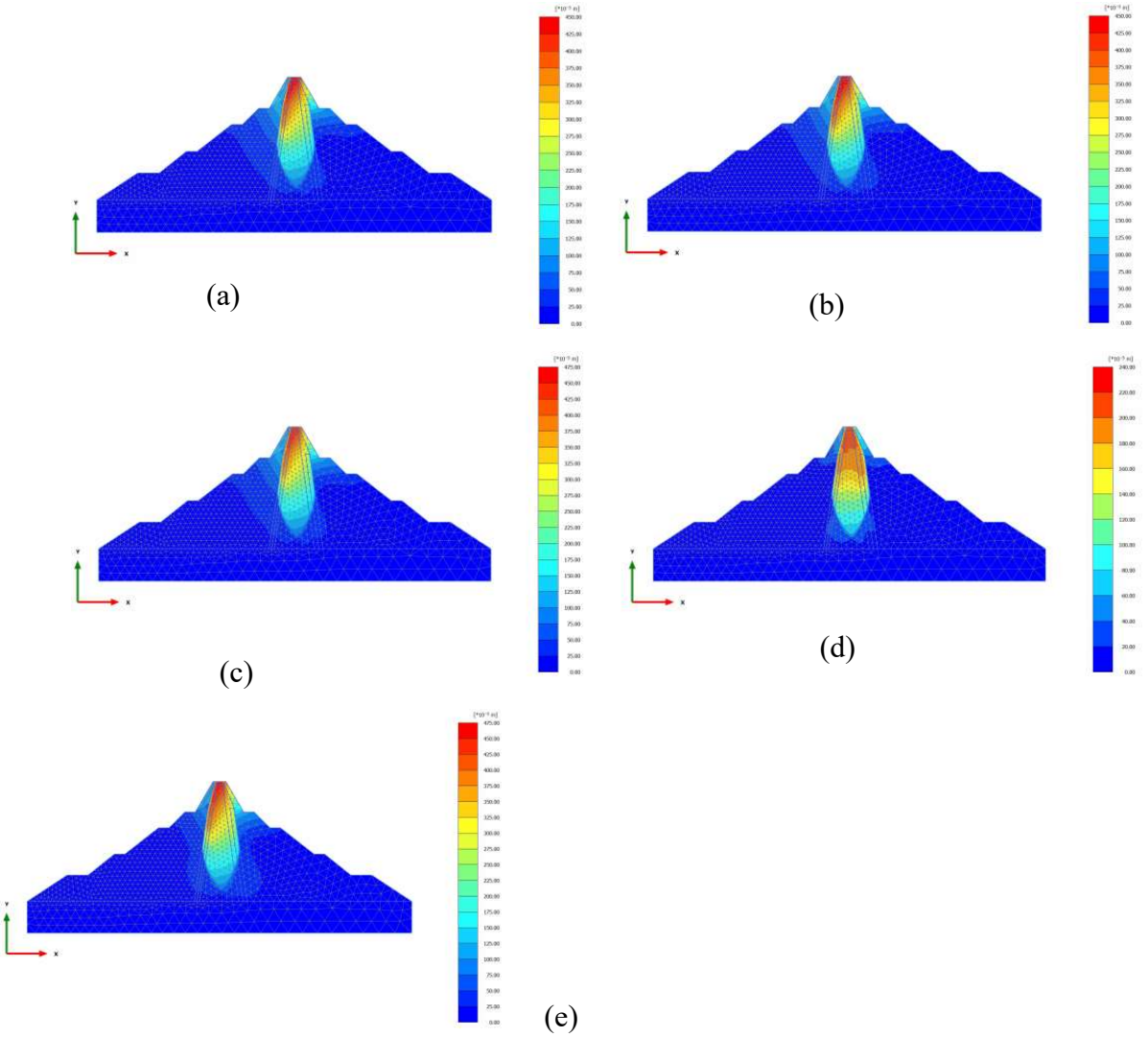

Figure 8.10. Earthquake induced deformation behaviour of Akosombo dam (a) using San Fernando earthquake (b) using Morgan-Hill earthquake (c) Northern-Calif earthquake, (d) Helena-Montana earthquake and (e) Umbria Marche earthquake.

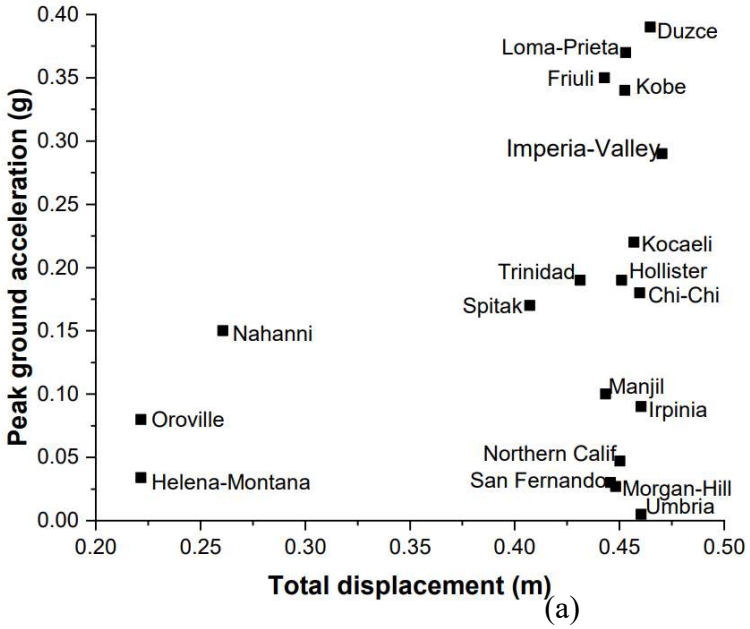

(a)

Figure 8.11. Peak ground acceleration at the dam crest versus permanent total displacements

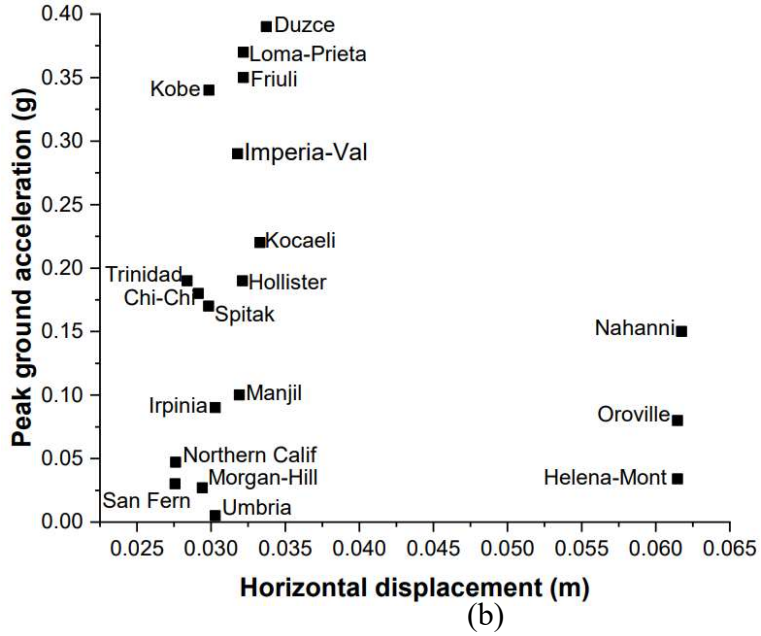

(b)

Figure 8.12. Peak ground acceleration at the dam crest versus permanent displacements (a) Total displacement (b) Vertical displacement

8.8 Slope stability analysis and results

The safety factor Akosombo dam was assessed for the dam cross section of the greater height and computed using the 'φ - c reduction' procedure. For each phase condition, appropriate slope stability analysis is computed based on shear strength reduction method using FEM Plaxis 2D.

The study computed the factor of safety as the ratio of the available shear strength to the strength at failure by summing up the incremental multiplier (M_{sf}) as expressed by:

$$FS = \frac{\text{available sterngth}}{\text{shear strength at failure}} = \text{value of } \Sigma Msf \text{ at failure}$$

The acceptable minimum value for safety for end of construction and multistage loading is around 1.3 (Afiri and Gabi, 2018). According to USBR (2019), if a static factor of safety against slope instability is greater than 1.5, it is regarded as less likely to damage deformation.

8.8.1 Steady state condition at high reservoir

In this first stage, stability analysis was performed for the slopes of the dam for two dam points, as shown in Figure 7.13, to optimize the volume of the dam body and materials. Gravity loading was used to calculate initial stresses and initial pressure of the dam under normal working condition. The slope analysis results under the steady state of high reservoir give a maximum safety factor of 1.72. For this study, the results of the finite element analyses are illustrated in Figure 8.14 (a-b).

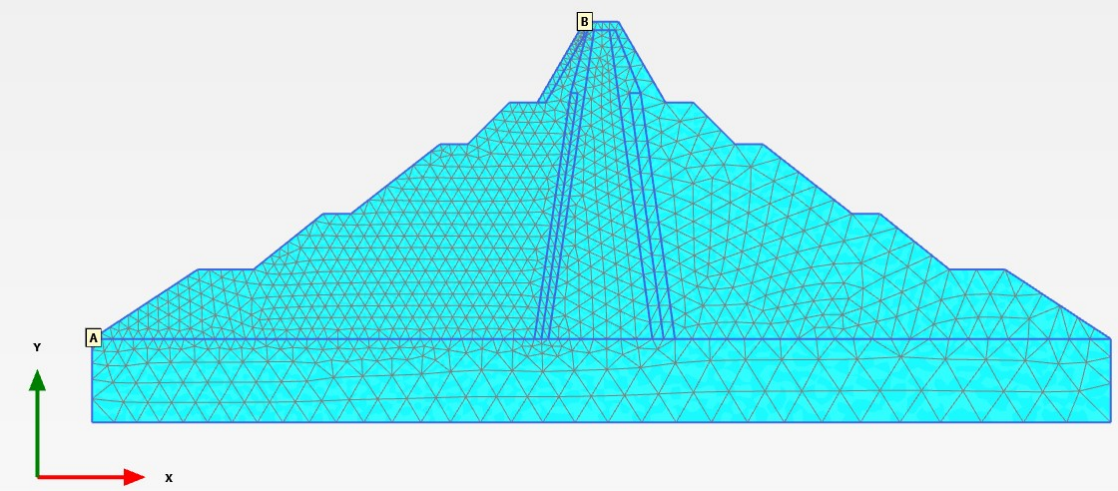

Figure 8.13. Location of point A and B for factors of safety calculations.

The dam body undergoes a maximum displacement of 2.2m due to the dead load of dam, and the settlement of different zones and foundation of the structure. The calculation of the displacements during this step is necessary because the imposed loads are very high which cause instability and even to a slope failure.

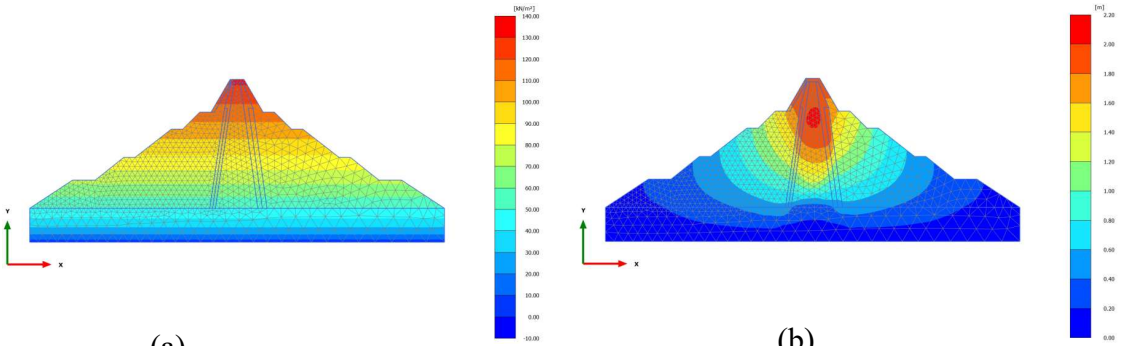

(a) (b)

Figure 8.14. (a) Pore pressure distribution, (p_{active}), for high reservoir (b) Total displacement (|U|) for high reservoir.

8.8.2 Rapid drawdown under the maximum water level

Rapid drawdown condition was used to compute the stability of the dam when the reservoir water level was at the maximum of 84.73 m. The water pressure distribution in the dam is calculated using fully coupled flow-deformation analysis by assigning 5 days value for the Time interval parameter with a reduced head water of 50 m. The computed groundwater for the pore pressure distribution after the rapid drawdown of the reservoir as well the displacement at the dam maximum water level is illustrated in Figure 8.15 (a-b). The slope analysis results under the rapid drawdown condition give a safety factor of 1.75.

8.8.3 Slow drawdown under the maximum water level

Slow drawdown condition was used to determine the stability of the dam when the reservoir water level was at 84.73 m. The water pressure distribution in the dam is also calculated by fully coupled flow-deformation analysis by assigning 30 days value for the Time interval parameter when the head water reduced to 50 m. When the reservoir filling at the maximum level, the lowest factor of safety of 1.42 is observed. The groundwater computed for the pore pressure distribution under the slow drawdown condition of the reservoir and the deformation estimated are shown in Figure 8.16.

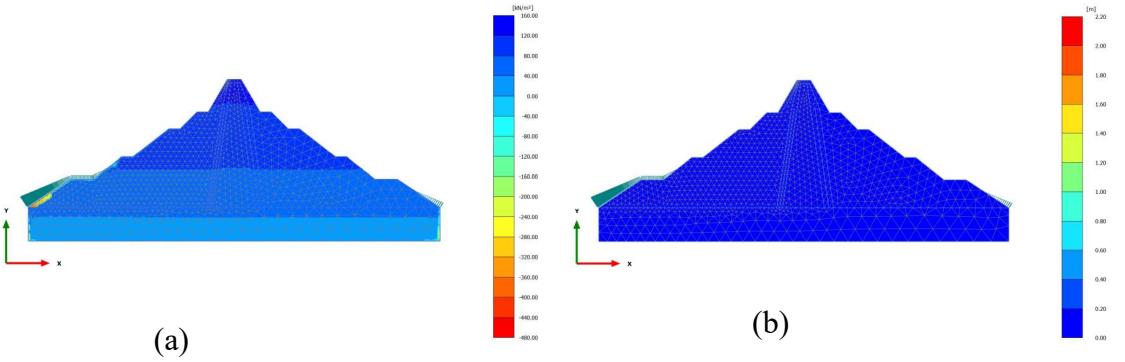

(a) (b)

Figure 8.15. (a) Pore pressure distribution, (p_{active}), for Rapid drawdown (b) Total displacement (|U|) for Rapid drawdown.

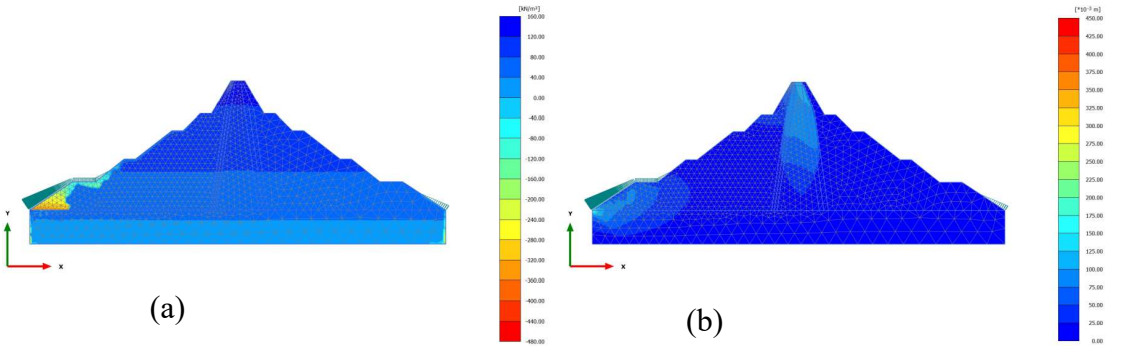

(a) (b)

Figure 8.16. (a) Pore pressure distribution, (p_{active}), for Slow drawdown (b) Total displacement (|U|) for Slow drawdown

7.8.4 Low water level

A long term situated was considered to estimate the stability of the Akosombo dam when the reservoir water level was at 34.73 m. The steady groundwater flow in the dam was calculated using plastic option. The numerical value under the water low level gives a safety factor of 1.74 for all the selected points. The groundwater computed for the pore pressure distribution under the low-level water reservoir and the maximum deformation experienced by the low level are illustrated in Figure 7.17.

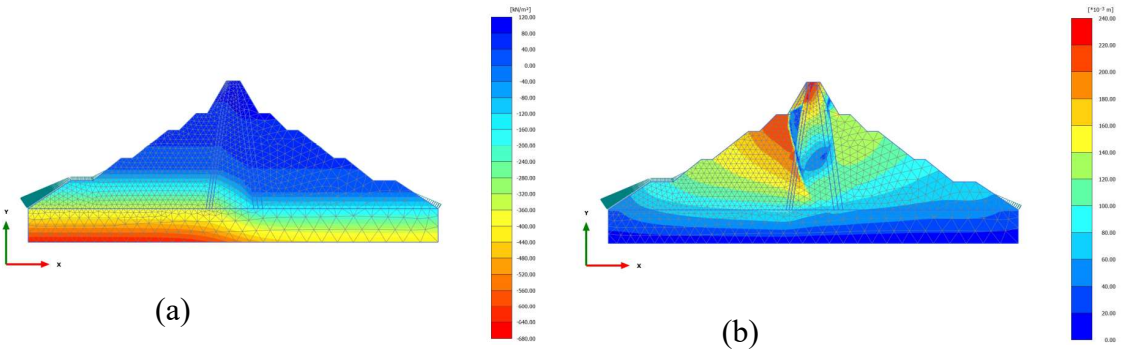

(a) (b)

Figure 8.17. (a) Pore pressure distribution, (p_{active}), for Low water level (b) Total displacement (|U|) for Low water level.

The behaviour of the Akosombo dam for all the conditions estimated, the displacements that occurred by water pressure in the dam body and foundation are observed. The maximum displacements are 2.2, 0.45, 2.2 and 0.24 for high reservoir under gravity loading, raid drawdown, slow drawdown, and lowest water level conditions, respectively. Factor of safety for all examined analysed conditions are shown in Figure 8.18. The results show that the safety factor of the dam decreased when the water level was in slow drawdown condition in the reservoir. The Factor of safety values under static condition are within 1.4 – 1.75, which means the slope is safe under static condition.

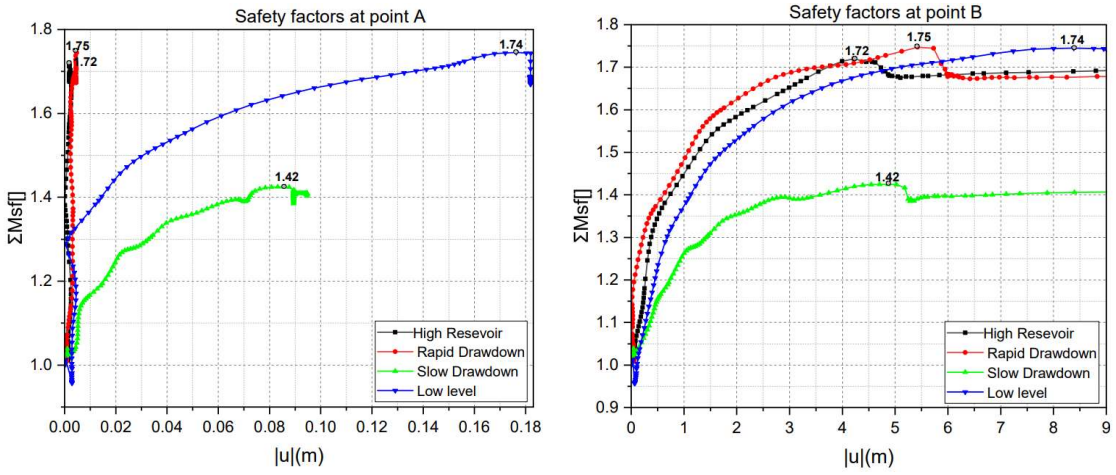

(a) (b)

Figure 8.18**.** Computed safety factors for different situations (a) point A at the base (b) point B at the crest.

8.9 Summary

A preliminary study of the dynamic response of the Akosombo dam was obtained by Plaxis 2D finite element analysis using 19 spectrum earthquake motions. According to the proposed seismic hazard map of southern Ghana, the site of Akosombo dam is situated in a moderate hazard.

The results obtained under the dynamic behaviour of the Akosombo dam provides an adequate basis for the deformations of the dam using different conditions of design earthquakes data. The results showed that deformations increased at the crest of the dam. The present study also aimed to numerically examine the slope stability of the Akosombo earth dam under the drawdown reduction method by Plaxis two-dimensional software. The strength for each load case combination of the dam is expressed through safety factors. Analysing the static stimulation of Akosombo dam using the drawdown principle, displacements and corresponding safety factors are obtained at the high reservoir, reservoir filling, and low water level conditions. The dam body and its foundation parameters used for the analysis are based on engineering properties determined from the literature. The total displacements are significant when studying most of the geotechnical problems. It is particularly recommended that laboratory tests be performed for the dam site conditions. The numerical results show that lower displacements occurred in the dam body and foundation through impounding. A factor of safety presents the primary key for slope stability analysis. The numerical results show that the drawdown reduction method used in the analyse effectively captures the progressive failure induced by reservoir dead load and water level fluctuations. Given the obtained results, when studying the problems related to slope stability in earth/rock-fill dams, it is recommended that inspections be conducted on the Akosombo dam during its service life.

CHAPTER 9

CONCLUSIONS AND FUTURE RESEARCH

9.1 Summary and conclusions

This thesis begins with a probabilistic seismic hazard assessment foundation for the West Africa region that estimated the hazard level for four significant cities (Accra, Conakry, Lagos, and Lomé) based on their population expansion and infrastructure level is developed (Chapter 4). The methodology used for the evaluation of seismic hazard is presented (Chapter 3). Next, this foundation forms the basis to estimate seismic hazards for ten cities in Guinea, West Africa (Chapter 5). Finally, examples of assessing the seismic risk for large dams in West Africa, in the Southern part of Ghana, performing non-linear time analysis and processing the results to determine the probabilistic framework are demonstrated (Chapter 6, 7 and 8).

9.1.1 Chapter 3: Probabilistic Seismic Hazard Assessment for West Africa Region

West Africa is currently undergoing very rapid infrastructural development. Previous studies regarding seismic hazards in West Africa have shown that the region presents low-to-moderate hazard levels across the region despite evidence of major earthquakes reported in the region. The first contribution of the chapter is a modified and updated catalogue for West Africa, obtained by sourced catalogues that span from 1615 to 2018, which included both historical and instrumental earthquakes. The seismic source model for the study region was divided into fourteen seismic source zones based on geological-tectonic features and spatial distribution of historical and instrumental events. To construct the ground motion model, five ground motion prediction equations (GMPEs) with the same tectonic setting as a target for the region. The seismic hazard estimates are presented in seismic hazard maps, seismic hazard curves, and response spectra for 475, 2475, and 9975 years.

The estimated results of the PSHA support the conclusion of some previous studies that the highest hazard level occurred in the Accra area of Ghana along the equatorial of West Africa. Therefore, it is advisable to protect the region against the potential risk of

seismic events by building earthquake-resistant structures using the hazard maps proposed for this study region. For a return period of 475, 2475 and 9975 years, the PGA values of 0.1g, 0.26 g and 0.45 g, respectively, were obtained for Accra. In particular, the seismic hazard deaggregation of the Accra area for PGA and SA for short and longer response periods is dominated by earthquakes of magnitudes 5.5–6.0 at distances less than 60 km.

9.1.2 Chapter 4: Seismic hazard Assessment in Guinea, West Africa Region

The level of seismic hazards in ten cities across Guinea, West Africa, was estimated using a probabilistic method. A homogenized 100-year catalogue sourced from three catalogues (Ambraseys and Adams (1986), USGS online catalogue and International Seismological Centre (ISC). All events with moment magnitudes of $M\mathrm{w} \geq 4.0$ are considered for the hazard assessment. The most devastating earthquakes reported in West Africa occurred in Guinea with over 300 casualties. The need to protect the region is necessary since seismic hazards across the cities have not been estimated. Three Seismic source zones are proposed based on geology and seismicity since information on local faults in Guinea is lacking.

The assessment results for hazard levels in 10 cities in Guinea are low and that, for structures of normal occupancy, seismic design may not be necessary. The exception is the Palaeozoic area of Guinea, where the hazard levels were a little higher. For a return period of 475 years, PGA values of 0.05, 0.023, 0.023, 0.017, 0.080, 0.080, 0.078,0.080, 0.072 and 0.022 g were obtained for Conakry, Kankan, Siguiri, Nzérékoré, Labé, Kindia, Manéah, Gauoal, Kamsar and Kissidougou, respectively.

9.1.3 Chapter 5: Seismic risk analysis for large dams in West Africa Region

To analyse the seismic risk associated with large dams within the West Africa region, A simplified method proposed by Bureau (2003) combined the evaluation of the seismic hazard of a dam site and the risk rating of a dam and appurtenant structure is presented. Seventeen large dams located in West Coast and Niger River basins in the West Africa region, having earthquakes of 300 km radius within the dam sites, were selected to analyse the total risk using the earthquake catalogue periods of 1615 to 2018. Five

prediction relationships were used since there are no available strong-ground motion records in West Africa to estimate the expected PGA values acting at the dam sites. First, a probabilistic approach determined peak ground acceleration (PGA) to represent the seismic hazard at the dam sites. Second, the seismic map proposed for the West Africa region estimates the seismic hazard at the dam site.

The risk rating within the dam sites depends on the reservoir's storage capacity, age, height, people, and properties at the downstream paths. The total risk for the seventeen large dams ranges from 68.0 to 152.0. This means that no dam is classified as risk class of IV and I in the region. Instead, the total risk results indicate that seven dams are classified as a high class while others show a moderate risk rating.

9.1.4 Chapter 6: Seismic risk analysis for large dams in West Coast basin, southern Ghana

Following the same criteria used to analyse the seismic risk for large dams in the West Africa region, ‘‘Seismic risk analyses for large dams in West Coast basin, in the southern part of Ghana’’ have been introduced to prioritise the risk rating of the three selected dams. Several studies have shown that southern Ghana recorded the most seismicity and highest seismic hazard level in West Africa. Akosombo dam is the largest dam with approximately 150 billion cubic metres and is located in Ghana. Three large dams (Weija, Kpong and Akosombo dams) located in the West Coast basin of southern Ghana, having earthquakes of 100 km radius around the dam sites, were used to estimate the total risk rating covering two century (1818-2018) earthquake catalogue. The seismic hazard map proposed by Alulu et al. (2018) is used for the hazard assessment. The results estimated for the three dams show that the risk ratings are moderate to high classes.

9.1.5 Chapter 7: Dynamic Response and Stability Analyses of Akosombo Dam Using Numerical Analysis

The numerical analysis procedure is used to estimate the dynamic response and stability analyses for the Akosombo dam. The dam is the largest in West Africa region, and it supplies energy for three countries (Ghana, Togo and Benin) within the region. 19 acceleration time-history recorded data used to compute for crest settlement of the dam

based on Maximum Design Earthquake (MDE), Maximum Credible Earthquake (MCE), Design Basis Earthquake (DBE) and Operating Basis Earthquake (OBE) data. The PGA coefficients estimated for 145, 475, 2475 and 10,000 years return periods are 0.03 g, 0.08 g, 0.21 g and 0.39 g, respectively. An analysis of the performance of the Akosombo dam using 19 recorded earthquake data shows that a numerical analysis procedure can be used to predict the crest deformation during a seismic event. The dynamic response of the Akosombo dam appears to provide a sufficient basis to assess the stability and deformation of the dam. The PLAXIS 2D finite element method shows that the maximum deformation occurs along with the dam's upper parts, while the deformation at the foundation level appears almost negligible.

Drawdown conditions are used to analyse the dam stability and compute safety factors (FS) for rapid drawdown, slow drawdown and low reservoir conditions. FS value reduced during slow drawdown (50 days duration) condition. The analyses for each section of the drawdown are essential because there is every chance of excess pore water pressure developing because of a sudden change in the water level. The FS is found to be greater than 1.5 for Rapid, High reservoir and low-level conditions.

9.2 Future Research

In light of these conclusions, the following recommendations are made for future research:

1. Once new geologic and tectonic information and more instrumental seismicity are available, a re-evaluation of the PSHA presented in the West Africa region is recommended. However, given the rate at which this information is made available, it is unlikely that any reassessment of the seismic hazard will yield markedly different results for some time to come. The notable exception would, of course, be the discovery of new seismic faults or evidence of the occurrence of major events within the sites considered.

2. Particularly in the Accra area, where more seismic activity has been observed in recent years, additional research needs to be conducted to assess the seismic potential of the geological structures in this region, such as Neotectonics, Paleoseismological studies and slip rate activities. These types of studies may provide valuable information,

in short to the medium term, that would enable an improved assessment of the seismic hazard in southern Ghana. However, as with most world areas, Paleoseismological investigations often do not result in amounts of data that allow activity rates to be constrained with much certainty. Therefore, a significant degree of epistemic uncertainty regarding the activity of these sources would remain.

3. The recently established seismological networks in some parts of the West Africa region (Ghana and Nigeria) needs to be extended to other parts of the area to increase the network's capabilities, particularly in Guinea, Senegal, and Togo. Such an expansion is perfectly feasible given the amount of investment that is pouring into the region. Moreover, estimates of the long-term activity rates would not change over the short term. Still, it would enable event locations to be resolved with greater accuracy, and the recorded motions would be extremely valuable for ground-motion modelling within the region.

4. Once enough recordings are available for the West Africa region, local ground-motion prediction models should be developed to reduce the epistemic uncertainty regarding selecting ground-motion models that fully dominate the current uncertainty in the seismic hazard results.
5. Research needs to be conducted to prove the existence or otherwise of an active tectonic structure running along the West Africa coast. Such as the Akwapim fault, the Coastal Boundary fault, St. Paul's fracture zone and the Romanche fracture zone. If such faults proved to exist, research-oriented to assess the seismic activity of the faults, such as fault mechanism, Exact location of the faults, length of slips should be conducted.
6. More research needs to be conducted to understand the implications of using different GMPEs in a PSHA within a logic tree framework and how selecting one equation influences seismic hazard results. Such research is primarily theoretical, and the optimal approach is likely to be identified within the next few years.
7. It is particularly recommended that laboratory tests be performed for all the dam site conditions to determine the properties of the dams.
8. A detailed assessment for all the selected dams in the future should include stability, fragility analysis, reliability, and dynamic analyses to determine the possible dam failures.

9. May consider utilizing spectrum compatible time history with the response spectrum which you have already developed.
10. May model the dam-foundation system with more details (such as radiation boundary, material specific plasticity model).

REFERENCES

Abrahamson, N. A. (2000b). State of the practice of seismic hazard assessment. Proceedings of GeoEng 2000, Melbourne, Australia. (1).659-685.

Adepelumi, A. A., Ako, B. D., Ajayi, T. R., Olorunfemi, A. O.,. Awoyemi, M. O., and Falebita, D. E. (2008). Integrated geophysical mapping of the Ifewara transcurrent fault system, Nigeria. *Journal of African Earth Sciences*, *52*(4–5), 161–166. https://doi.org/10.1016/j.jafrearsci.2008.07.002.

Affaton, P., Sougy, J., and Trompette, R. (1980). The tectono-stratigraphic relationships between the upper Precambrian and lower Paleozoic Volta Basin and the pan-african Dahomeyide orogenic belt (West Africa). *American Journal of Science* 280(3): 224-248. https://doi:10.2475/ajs.280.3.224.

Afegbua, K. U., Ezomo, F. O., Osahon, O. D., Yakubu, T. A., and Sanni, H. T. (2019). Probabilistic seismic hazard assessment for national planning and development in Nigeria. *Journal of Geodynamics*, *126*(November 2018), 46–55. https://doi.org/10.1016/j.jog.2019.03.004.

Afiri, R., and Gabi, S. (2018). Finite element slope stability analysis of Souk Tleta dam by shear strength reduction technique. *Innovative Infrastructure Solutions*, *3*(1): 1–10. https://doi.org/10.1007/s41062-017-0108-1.

Afiri, R., Abderrahmane, S. H., Djerbal, L., and Gabi, S. (2018). Stability Analysis of Souk-Tleta Earth Dam, North Algeria. *Sustainable Civil Infrastructures*, 1: 32–40. https://doi.org/10.1007/978-3-319-61905-7_4.

Aguilar-Meléndez, Armando, Mario G. Ordaz, Josep De la Puente, Lluis Pujades, Alex Barbat, Héctor E. Rodríguez-Lozoya, Marisol Monterrubio-Velasco, Jesús E. Escalante Martínez, and Amelia Campos-Rios. 2018. Sensitivity Analysis of Seismic Parameters in the Probabilistic Seismic Hazard Assessment (PSHA) for Barcelona Applying the New R-Crisis. *Computacion y Sistemas* 22(4):1099–1122. doi: 10.13053/CyS-22-4-3084.

Ahulu, S. T., Danuor, S. T., and Asiedu, D. K. (2018). Probabilistic seismic hazard assessment for the southern part of Ghana. *Journal of Seismology* 22: 539–557. doi.org/10.1007/s10950-017-9721-x.

Ahulu, S., and Danuor, S. K. (2015). Ghana's Experience in the Establishment of a National Digital Seismic Network Observatory. *Journal of Seismology* 19 (3): 667–683. https://doi.org/10.1007/s10950-015-9486-z.

Akpan OU, Isogun MA, Yakubu TA, Adepelumi AA, Okereke CS, Oniku AS, Oden MI. An Evaluation of the 11 th September, 2009 Earthquake and Its Implication for Understanding the Seismotectonics of South Western Nigeria. 2014; 542–550.

Albano, M., Modoni, G., Russo, G., and Croce, P. (2012). Performance Based Seismic Analysis of an Existing Rockfill Dam. 9: 1079–1090. Second International Conference on Performance-Based Design in Earthquake Geotechnical Engineering.

Aldama-Bustos, G. (2009). An Exploratory Study of Parameter Sensitivity, Representation

of Results and Extensions Of PSHA: Case Study – United Arab Emirates. Thesis. Imperial College, London.

Ambraseys NN,. Adams RD. Seismicity of West Africa. Annals of Geophysics 1986; 4 (B6): 679-702.

Ambraseys, N. N., and Melville, C. P. (1982). A history of Persian earthquakes. Cambridge University Press, Cambridge. pp. 212.

Ambraseys, N. N., Simpson, K. A., and Bommer, J. J. (1996). Prediction of horizontal response spectra in Europe. Earthquake Engineering & Structural Dynamics, 25(4): 371-400. https://doi.org/10.1002/(SICI)1096-9845(199604)25:4<371::AID-EQE550>3.0.CO;2-A.

Ambraseys, N. N., and Srbulov, M. (1994). Attenuation of earthquake-induced ground displacements. Earthquake Engineering & Structural Dynamics, 23(5): 467-487.

Abrahamson, N. A., and Bommer, J. J. (2005). Probability and uncertainty in seismic hazard analysis. *Earthquake Spectra* 21(2): 603-607. http://dx.doi.org/10.1193/1.1899158.

Amponsah, P., Leydecker, G., and Muff, R. (2012). Earthquake catalogue of Ghana for the time period 1615-2003 with special reference to the tectono-structural evolution of southeast Ghana. *Journal of African Earth Sciences* 75: 1–13. https://doi.org/10.1016/j.jafrearsci.2012.07.002.

Amponsah, P., Banoeng-Yakubo, B. K., Panza, G.F., and Vaccari, F. (2009). Deterministic Seismic Ground Motion Modelling of the Greater Accra Metropolitan Area, Southeastern Ghana. South African *Journal of Geology* 112 (3-4): 317-328.

Anon. (2018). Emergency plan of Action (EPoA) Togo: Flood Preparedness & Response.

Athani, S. S., Shivamanth, Solanki, C.H., and Dodagoudar, G. R. (2015). Seepage and Stability Analyses of Earth Dam Using Finite Element Method. *Aquatic Procedia*, *4*(December), 876–883. https://doi.org/10.1016/j.aqpro.2015.02.110

Awoyemi, M. O., Hammed, O. S., Falade, S. C., Arogundade, A. B., Ajama, O. D., Iwalehin, P. O, and Olurin, O.T. (2017). Geophysical investigation of the possible extension of Ifewara fault zone beyond Ilesa area, southwestern Nigeria. *Arabian Journal of Geosciences*, *10*(27): 1-14.

Babu, G. L. S., and Srivastava, A. (2009). Risk and Reliability Analysis of Stability of Earthen Dams. *Igc*, *Icold 1989*, 961–967.

Bacon, M., and Quaah, A. O. (1981). Earthquake Activity in Southeastern Ghana (1977-1980. *Bulletin of the Seismological Society of America* 71(3): 771-785.

Baker, J. W. (2013). Probabilistic Seismic Hazard Analysis. *White Paper Version 2.0.1*, pp 79.

Banson, J. K. A. (1970). Methods of studying seismicity at short range. MSc. Thesis, University of Edinburgh.

Bashir, A., and Basu, D. (2018). Revisiting probabilistic seismic hazard analysis of Gujarat: an assessment of Indian design spectra. *Natural Hazards*, *91*(3), 1127–1164. https://doi.org/10.1007/s11069-018-3171-9.

Baro, O., Kumar, A., Ismail-Zadeh,, A. (2018).Seismic hazard assessment of the Shillong plateau, India. Geomatics, *National Hazards Risk*. 9(1):841–61. https://doi.org/10.1080/19475705.2018.1494043.

Bazzurro, P., and Cornell, C. A. (1999). Disaggregation of seismic hazard. *Bulletin of the Seismological Society of America*, 89(2); 501-520. https://doi.org/10.1785/BSSA0890020501

BRRI (1990) Code for seismic design of concrete structures. Published by the Building and Road Research Institute, Kumasi, pp 45–46

Begg, G. C., Griffin, W. L., Natapov, L. M., O'Reilly, S. Y., Grand, S. P., O'Neill, C.J., and Hronsky J. M. A et al. (2009). The lithospheric architecture of Africa: Seismic tomography, mantle petrology, and tectonic evolution. *Geosphere* 5(1): 23-50. https://doi.org/10.1130/GES00179.1.

Binks, R. M., and Fairhead, J. D. (1992). A Plate Tectonic Setting for Mesozoic Rifts of West and Central Africa. In: P.A. Ziegler (Editor), Geodynamics of Rifting, Volume It. Case History Studies on Rifts: North and South America Africa. " *Tectonophysics* 213: 141-151. https://doi.org/10.1016/0040-1951(92)90255-5.

Bommer, J. J., and. Abrahamson, N. A (2006). Why Do Modern Probabilistic Seismic-Hazard Analyses Often Lead to Increased Hazard Estimates? *Bulletin of the Seismological Society of America* 96(6); 1967-1977. http://dx.doi.org/10.1785/0120060043.

Bommer, J. J., and Scherbaum, F. (2008). The use and misuse of logic trees in probabilistic seismic hazard analysis. *Earthquake Spectra*, 24(4); 997-1009. http://dx.doi.org/10.1193/1.2977755.

Bommer, J. J., Scherbaum, F., Bungum, H. Cotton, F., Sabetta, F., and Abrahamson, N. A. (2005). On the use of logic trees for ground-motion prediction equations in seismic-hazard analysis. *Bulletin of the Seismological Society of America*, 95(2); 377-389. https://doi.org/10.1785/0120040073.

Boore, D. M., Joyner, W. B., and Fumal, T. E. (1993). Estimation of response spectra and peak accelerations from western North America earthquakes: An interim report. U.S. Geological Survey. Open-file report 93-509. pp. 70.

Bureau, G. J. (2003). In: Chenh, W.F., Scawthorn, C. (Eds.). Dams and Appurtenant Facilities in Earthquake Engineering Handbook. CRS Press, Bora Raton, pp. 26.1–26.47.

Bureau, G.J., and Ballentine, G.D. (2002). A comprehensive seismic vulnerability and loss assessment of the State of South Carolina using HAZUS. Part VI. Dam inventory and vulnerability assessment methodology. 7th National Conference on Earthquake

Engineering, July 21–25, Boston, Earthquake Engineering Research Institute, Oakland, CA.

Campbell, K. W., and Bozorgnia, Y. (2014). NGA-West2 Ground Motion Model for the Average Horizontal Components of PGA, PGV, and 5% Damped Linear Acceleration Response Spectra. *Earthquake Spectra* 30(3): 1087–1114. https://doi.org/10.1193/062913EQS175M.

Cao, A. M., and Gao, S. S. (2002). Temporal variation of seismic b-values beneath northeastern Japan island arc, *Geophysical Research Letters*. 29(9): 1334. https://doi.org/10.1029/2001GL013775.

Celli, P. O., Lebedev, N. L., Schaeffer, A. J., and Gaina, C. (2020). African cratonic lithosphere carved by mantle plumes. *Nature communications* 11(1): 1-10.

Chen, Y., and Lin, P. (2018). The total risk analysis of large dams under flood hazards. *Water (Switzerland)*, *10*(2). https://doi.org/10.3390/w10020140.

Chiou, B. S. J., and Youngs, R. R. (2014). Update of the Chiou and Youngs NGA Model for the Average Horizontal Component of Peak Ground Motion and Response Spectra. *Earthquake Spectra* 30(3): 1117–1153. https://doi.org/10.1193/072813EQS219M.

Claridge, W.W. (1915), A History of Gold Coast and Ashanti, London, 4-90.

Cloetingh, S., and Burov, E. (2011). Lithospheric Folding and Sedimentary Basin Evolution: A Review and Analysis of Formation Mechanisms. *Basin Research* 23(3): 257–290.

Cornell, C. A. (1968). Engineering Seismic Risk Analysis. *Bulletin of the Seismological Society of America* 58(5): 1583-1606.

Cornell, C. A., and Vanmarcke, E. H. (1969). The major influences on seismic risk. Proceedings of the fourth world conference on earthquake engineering, Chile. (A-1): 69-93

Cornell, C. A., and Winterstein, S. R. (1988). Temporal and magnitude dependence in earthquake recurrence models. *Bulletin of the Seismological Society of America*, 78(4): 1522-1537.

Cosentini, R. M., Passeri, F. and Foti, S. (2020) A Simplified Methodology for the Assessment of the Seismic Risk Associated with Small Earth Dams, *Lecture Notes in Civil Engineering*. Springer International Publishing. doi: 10.1007/978-3-030-21359-6_10.

Coppersmith, K.J., Youngs, R.R., (1986). Capturing uncertainty in probabilistic seismic hazard assessments within intraplate tectonic environments. In: Proceedings of the Third U.S. National Conference on Earthquake Engineering. vol. 1. pp. 301–312. Cornell, C.A., 1968. Engineering seismic risk analysis. *Bulletin of the Seismological Society of America*. 18, 1583–1606.

Crowley, H. (2014) Earthquake Risk Assessment: Present Shortcomings and Future Directions. In: Ansal A. (eds) Perspectives on European Earthquake Engineering

and Seismology. Geotechnical, Geological and Earthquake Engineering, vol 34. Springer, Cham. https://doi.org/10.1007/978-3-319-07118-3_16

Dagne, Y., and Sandler, L. H. (2020). We're Leaving Everything Behind. The Impact of Guinea's Souapiti Dam on Dispaced Communities.

Deif, A., Hamed, H., Ibrahim, H. A., Elenean, K. A., and El-Amin, E. (2011). Seismic hazard assessment in Aswan, Egypt. *Journal of Geophysics and Engineering* 8(4): 531–548. https://doi.org/10.1088/1742-2132/8/4/006.

Delteil, J. R., Valery, P., Montadert, L., Fondeur, C., Patriat, P., and Mascle, J. (1974). Continental Margin in the Northern Part of the Gulf of Guinea. In: Burk C.A., Drake C.L. (eds). The Geology of Continental Margins. Springer, Berlin, Heidelberg. https://doi.org/10.1007/978-3-662-01141-6_22.

Delavaud, E., Scherbaum, F., Kuehn, N, and Riggelsen, C. (2009). Information-Theoretic Selection of Ground-Motion Prediction Equations for Seismic Hazard Analysis: An Applicability Study Using Californian Data. *Bulletin of the Seismological Society of America* 99(6): 3248–3263.

Douglas, J. (2006). Errata of and additions to Ground motion estimation equations 1964-2003'.Intermediary report, BRGM BRGM/RP-54603- FR. 103 pp., 2 tables.

Douglas, J. (2003). Earthquake ground motion estimation using strong-motion records: a review of equations for the estimation of peak ground acceleration and response spectral ordinates. Earth Sci. Rev. 61 (1–2), 43–104. https://doi.org/10.1016/S0012-8252(02)00112-5

Dong, W. M., Bao, A. B., and Shah, H. C. (1984). Use of maximum entropy principle in earthquake recurrence relationships. *Bulletin of the Seismological Society of America* 74(2): 725-737. https://doi.org/10.1785/BSSA0740020725.

Ebrahimian, B. (2011). Numerical analysis of nonlinear dynamic behavior of earth dams. *Frontiers of Architecture and Civil Engineering in China*, *5*(1): 24–40. https://doi.org/10.1007/s11709-010-0082-6.

Engdahl, E. R., Van der Hilst, R. D., and Buland, R. P. (1998). Global teleseismic earthquake relocation with improved travel times and procedures for depth determination. *Bulletin of the Seismological Society of America*, 88(3): 722-743.

Esteva, L., and Rosenblueth, E. (1964). Spectra of tremors at moderate and large distances, *Mexican Society of Seismic Engineering Bulletin* 2(1): 1-18.

Fell, R., Mac Gregor, P., Stapledon, D., and Bell, G. (2005). Geotechnical Engineering of Dams. A.A. Balkema Publishers, UK.

Freeth, S. J. (1978). Tectonic activity in West Africa and the Gulf of Guinea since Jurassic times—an explanation based on membrane tectonics. *Earth and Planetary Science Letters* 38(2): 298-300.

Gaina, C., Torsvik, T. H., van Hinsbergen, D. J. J, Medvedev, S.,. Werner, S. C, and Labails, C. (2013). The African Plate: A History of Oceanic Crust Accretion and Subduction since the Jurassic. *Tectonophysics* 604: 4–25.

Gazetas, G. (1987). Seismic response of earth dams: some recent developments. *Soil Dynamics and Earthquake Engineering*, *6*(1): 2–47. https://doi.org/10.1016/0267-7261(87)90008-X.

Giardini, D., Grünthal, G., Shedlock, K. M., and Zhang, P. (1999). The GSHAP global seismic hazard map. *Annal of Geophysical*, 42(6): 1225-1230. DOI**:** https://doi.org/10.4401/ag-3784.

Giardini, D., Wiemer, S., Fäh, D., and Deichmann, N. (2004). Seismic Hazard Assessment of Switzerland. *Swiss Seismological Service*. 82

Ghana Statistical Service. (2014). 2010 Population and housing census district analytical report; Ga South Municipality. Accra: http://www.statsghana.gov. und the Weija Dam near Accra, Ghana. www.statsghana.gov.gh.

Globig, J., Fernàndez, M., Torne, M., Vergés, J., Robert, A., and Faccenna, C. (2016). New insights into the crust and lithospheric mantle structure of Africa from elevation, geoid, and thermal analysis. *Journal of Geophysical Research* Solid Earth, 121(7): 5389-5424.

Goitom, B, Werner, M.J, Goda, K, Kendall, J. M, Hammond, J.O.S, Ogubazghi, and G, Oppenheimer et al. (2017). Probabilistic seismic-hazard assessment for Eritrea. *Bulletin of the Seismological Society of America* 107(3),1478–1494. doi:10.1785/0120160210.

Gosschalk, E. M., Severn, R. T., Charles, J. A., and Hinks, J. L. (1994). An Engineering Guide to Seismic Risk to Dams in the United Kingdom, and its international relevance. *Soil Dynamics and Earthquake Engineering*, 13(3): 163–179. https://doi.org/10.1016/0267-7261(94)90015-9.

Cramer, C. H., Petersen, M. D., Cao, T., Toppozada, T. R., and Reichle, M. (2000). A Time-Dependent Probabilistic Seismic-Hazard Model for California. *Bulletin of the Seismological Society of America* 90(1): 1-21.

Goda, K., Aspinall, W., and Taylor, C. A. (2013). Seismic hazard analysis for the U.K.: Sensitivity to spatial seismicity modelling and ground motion prediction equations. *Seismological Research Letters*, *84*(1), 112–129. https://doi.org/10.1785/0220120064.

Grunthal, G., Bosse, C., Sellami, S., Mayer-Rosa, D., and Giardini, D. (1999). Compilation of the GSHAP Regional Seismic Hazard for Europe, Africa and the Middle East. *Annali Di Geofisica* 42(6): 1215–1223.

Grünthal, G., Wahlström, R., and Stromeyer, D. (2009). The unified catalogue of earthquakes in central, northern, and northwestern Europe (CENEC) - Updated and expanded to the last millennium. *Journal of Seismology* 13: 517–541. https://doi.org/10.1007/s10950-008-9144-9.

Gutenberg, B., and Richter, C. F. (1944). Frequency of earthquakes in California. *Bulletin of the Seismological Society of America*, 34(4): 185-188.

Gupta, I. D. (2002). The State of the Art in Seismic Hazard Analysis. *ISET Journal of Earthquake Technology* 39(4): 311–346.

Hanks, T. C., and Kanamori, H. (1979). A moment magnitude scale. *Journal of Geophysical Research* 84: 2348-2350. https://doi.org/10.1029/JB084iB05p02348.

Hartnady C. J. H., and Benouar, D. (2007). African catalogue of earthquakes (ACE) project: Towards earthquake risk reduction in active plate-boundary zones. *Abstract, AfricaArray Workshop*, pp 17–18 July 2007, Johannesburg, South Africa.

Hariri-Ardebili, M.A., and Nuss, L. K. (2018). Seismic risk prioritisation of a large portfolio of dams. Revisited. Adv. Mech. Eng. 10(9), 1–20. https://doi.org/10.1177/1687814018802531.

Harmsen, S., Perkins, D., and Frankel, A. (1999). Deaggregation of Probabilistic Ground Motions in the Central and Eastern United States. *Bulletin of the Seismological Society of America*, *89*(1), 1–13.

Heine, C., Müller, R. D., Steinberger, B., and Torsvik, T. H. (2008). Subsidence in intracontinental basins due to dynamic topography. *Physics of the Earth and Planetary Interiors* 171(1-4): 252-264.

Helton, J. C., and Oberkampf, W. L. (2004). Alternative representations of epistemic uncertainty. *Reliability Engineering & System Safety* 85(1- 3): 1-10. DOI:10.1016/j.ress.2004.03.001.

ICOLD. (1989). Selecting parameters for large dams—guidelines and recommendations. ICOLD Committee on Seismic Aspects of Large Dams, Bulletin, vol. 72. 36 pp.

ICOLD. (2010). Selecting seismic parameters for large dams. Committee on Seismic Aspects of Dam Design, International Commission on Large Dams, Paris.

Jesse, E. E., Igbokwe, J. I., Esien, E., and Sumi, Y. L. (2019). Assessment of Water Level in Dadin Kowa Dam Reservoir in Gombe State Nigeria Using Geospatial Techniques. International Journal of Environment and Geoinformatics 6 (1): 115–130. https://doi.org/10.30897/ijegeo.487885.

Jin, C., and Chi, S. (2019). Seismic Fragility Analysis of High Earth-Rockfill Dams considering the Number of Ground Motion Records. *Mathematical Problems in Engineering* 2019(Im). https://doi.org/10.1155/2019/6958643

Junner, N.R. (1941). The Accra earthquake of 22nd June 1939. *Gold Coast Geological Survey Bulletin* 13: 3-17.

Kan, M. E., and Taiebat, H. A. (2011). Reliability of simplified methods for evaluation of earthquake-induced displacement in earth and rockfill dams. ICOLD 2011 Paper-Section 3A-4.

Kijko, A. (2004). Estimation of the maximum earthquake magnitude, mmax. Pure Apply Geophysics. 161(8): 1655–1681. https://doi.org/10.1007/s00024-004-2531-4.

Kijko, A., and Graham, G. (1998). Parametric-historic procedure for probabilistic seismic hazard analysis. Part I: Estimation of maximum regional magnitude m(max). *Pure and Applied Geophysics* 152: 413–442. https://doi.org/10.1007/s000240050161.

Kijko, A., and Sellevoll, M. A. (1989). Estimation of earthquake hazard parameters from incomplete data files. Part I. Utilization of extreme and complete catalogs with different threshold magnitudes. *Bulletin of the Seismological Society of America*

79:645–654.

Kramer, S. L. (1996). Geotechnical earthquake engineering. Prentice Hall, Upper saddle river, N.J.

Kramer, S. L., and Mitchell, R. A. (2006). Ground motion intensity measures for liquefaction hazard evaluation. *Earthquake Spectra* 22(2): 413-438. https://doi.org/10.1193/1.2194970.

Kulkarni, R. B., Youngs, R. R., and Coppersmith, K. J. (1984). Assessment of Confidence Intervals for Results of Seismic Hazard Analysis. *8th World Conference on Earthquake Engineering* 263–270.

Kumapley, N.K. (1996). Seismicity of southern Ghana: causes, engineering implications and mitigation strategies. Ghana Min J 2 (1), 33–41.

Kutu, J. M. (2013). Seismic and Tectonic Correspondence of Major Earthquake Regions in Southern Ghana with Mid-Atlantic Transform-Fracture Zones. *International Journal of Geosciences* 4: 1326–1332. http://doi:10.4236/ijg.2013.410128.

Langer, C.J, Bonilla, M.G, Bollinger, G.A. (1987). Aftershocks and Surface Faulting Associated With the Intraplane Guinea, West Africa, Earthquake of December 22. 1983. *Bulletin of the Seismological Society of America* 77(5): 1579–1601 https://doi.org/10.1785/BSSA0770051579.

Langer C.J., Bollinger G.A. (1992). The December 22, 1983, earthquake in Guinea, West Africa. In: Freeth S.J., Ofoegbu C.O., Onuoha K.M. (eds) Natural Hazards in West and Central Africa. International Monograph Series. Vieweg+Teubner Verlag, Wiesbaden. https://doi.org/10.1007/978-3-663-05239-5_4.

Latil-Brun MV., Flicoteaux, R., Blarez, E., Mascle, J., Bessis, F., Brunet, MF, (1988). Variation of subsidence along transform margin: the example of the Ivory Coast continental shelf. *Press and magazines Proceedings of the Academy of Sciences* 306(1): 83-88.

Lin, J. S, and Whitman, R. V. (1983). Decoupling approximation to the evaluation of earthquake-induced plastic slip in earth dams. *Earthquake Engineering and Structural Dynamics* 11(5), 667–678. https://doi.org/10.1002/eqe.4290110506.

Mavonga, T., and Durrheim, R. J. (2009). Probabilistic seismic hazard assessment for the Democratic Republic of Congo and surrounding areas. *South African Journal of Geology*. 112(3–4): 329–342. https://doi.org/10.2113/gssajg.112.3-4.329

McGuire, R. K. (1977). Seismic design spectra and mapping procedures using hazard analysis based directly on oscillator response. *Earthquake Engineering & Structural Dynamics*, 5(3): 211-234. https://doi.org/10.1002/eqe.4290050302.

McGuire, R. K. (1976). FORTRAN computer program for seismic risk analysis. *USGS Open-File Report*, 76-67.

McGuire, R. K. (1995). Probabilistic Seismic Hazard Analysis and Design Earthquakes: Closing the Loop. *Bulletin of the Seismological Society of America*. 85(5), 1275–1284. https://doi.org/10.1016/0148-9062(96)83355-9.

McGuire, R. K. (2008). Probabilistic seismic hazard analysis: Early history. *Earthquake Engineering and Structural Dynamics* (37): 329-338.

McGuire, R. K. (2004). Seismic hazard and risk analysis. *Earthquake Engineering Research Institute*, Oakland, CA. pp. 221.

McGuire, R. K., Cornell, C. A., and Toro, G. R. (2005). The case for using mean seismic hazard. *Earthquake Spectra* 21(3): 879-886.

Meghraoui, M., Amponsah, P., Ayadi, A., Ayele, A., Ateba, B., Bensuleman, A., Delvaux, D et al. (2016). The Seismotectonic Map of Africa. *Episodes Journal of international Geoscience, Seoul National University* 39(1): 9–18.

Midzi, V., Manzunzu, B., Mulabisana, T., Zulu, B. S., Pule, T., & Myendeki, S. (2020). Probabilistic seismic hazard maps for South Africa. *Journal of African Earth Sciences*, *162*(2020), 103689. https://doi.org/10.1016/j.jafrearsci.2019.103689

Musson, R. M. W. (2014). The Seismicity of Ghana. *Bulletin of Earthquake Engineering* 12(1): 157–169. https://doi.org/10.1016/0148-9062(96)83355-9.

Musson, R. M. W. (2005). Against fractiles. *Earthquake Spectra* 21(3): 887-891. https://doi.org/10.1193/1.1985445.

Narita, K. (2000). Design and construction of embankment dams. *Dept. of Civil Eng., Aichi Institute of Technology*, Lecture Notes. 0–17.

Nasir, A., Lenhardt, W., Hintersberger, E., and Decker, K. (2013). Assessing the completeness of historical and instrumental earthquake data in Austria and the surrounding areas. *Australia Journal of Earth Science* 106(1): 90–102.

Newmark, N. M. (1965). Effects of earthquakes on dams and embankments. *Geotechnique*, 15(2): 139–160. https://doi.org/10.1680/geot.1965.15.2.139.

Ntiamoa-Baidu, Y., Ampomah, B.Y., and Ofosu, E.A. (Eds.). (2017). Dams, Development and Downstream Communities : Implications for Re-Optimising the Operations of the Akosombo and Kpong Dams in Ghana. Digibooks Gh. Ltd., Tema, Ghana.

Oliveira, C. S., Roca, A., and Goula, X. (2006). Assessing and managing earthquake risk: geo-scientific and engineering knowledge for earthquake risk mitigation; developments, tools, techniques. Springer. 543 pp.

Ordaz, M., and Sagado-Gálvez, M. A. (2017). R-CRISIS Validation and Verification Document. ERN Technical Report. Mexico City, Mexico.

Ordaz, M., and Sagado-Gálvez, M. A. (2018). R-CRISIS Validation and Verification Document. ERN Technical Report. Mexico City, Mexico.

Owusu-Ansah, J. K, Dery, J.M., and Amoako, K. (2019). Flood Vulnerability and Coping Mechanisms around the Weija Dam near Accra, Ghana. GeoJournal 84 (6): 1597–1615. https://doi.org/10.1007/s10708-018-9939-3.

Oyedotun, T. D.T. (2011). Asejire Dam and the Host Communities. WIT Transactions on Ecology and the Environment 153, 501–511. https://doi.org/10.2495/WS110441.

Oyegoke, S., and Sojobi, A. (2012). Developing Appropriate Techniques to Alleviate the Ogun River Network Annual Flooding Problems. *International journal scientific &*

engineering research. 3(2), 1–7.

Özkan, M. Erdik, Y., M., Tunçer, M. A., and Yilmaz, Ç. (1996). An evaluation of Sürgü Dam response during 5 May 1986 earthquake. *Soil Dynamics and Earthquake Engineering*, 15(1): 1–10. https://doi.org/10.1016/0267-7261(95)00030-5.

Papazachos, B. C., Kiratzi, A. A, and Karacostas, B. G. (1999). Toward a homogeneous moment-magnitude determination for earthquakes in Greece and the surrounding area. *Bulletin of Earthquake Engineering*. 87(2), 474–483.

Petersen, M. D., Cao, T., Campbell, W. K., and Frankel, A. D. (2007). Time-independent and Time-dependent seismic hazard assessment for the state of California: Uniform California earthquake rupture forecast model 1.0. *Seismological Research Letters* 78(1): 99-109. https://doi.org/10.1785/gssrl.78.1.99.

Petersen, M. D., Frankel, A. D., Harmsen, S. C., Mueller, C. S., Haller, K. M., Wheeler, R. L., Wesson, R. L., Zeng, Y., Boyd, O. S., Perkins, D. M., Luco, N., Field, E. H., Wills, C. J., & Rukstales, K. S. (2010). Documentation for the 2008 update of the united states national seismic hazard maps. *Earthquake Research: Background and Select Reports*, 107–234.

Pezeshk, S., Zandieh, A., and Tavakoli, B. (2011). Hybrid Empirical Ground-Motion Prediction Equations for Eastern North America Using NGA Models and Updated Seismological Parameters. *Bulletin of the Seismological Society of America* 101(4): 1859–1870. https://doi.org/10.1785/0120050030.

Pezeshk, S., Zandieh, A., Campbell, K. W. and Tavakoli, B. (2018). Ground-motion prediction equations for central and eastern north America using the hybrid empirical method and NGA-west2 empirical ground-motion models. *Bulletin of the Seismological Society of America*. 108(4), 2278–304.

Pisarenko, V. F., Lyubushin, A. A., Lysenko, V. B., and Golubeva, T. V. (1996). Statistical estimation of seismic hazard parameters: Maximum possible magnitude and related parameters. *Bulletin of the Seismological Society of America* 86(3): 691-700. https://doi.org/10.1785/BSSA0860030691.

Poggi, V., R. Durrheim, G. M. Tuluka, G. Weatherill, R. Gee, M. Pagani, A. Nyblade et al. (2017). Assessing Seismic Hazard of the East African Rift: A Pilot Study from GEM and AfricaArray. *Bulletin of Earthquake Engineering* (15): 4499–4529. https://doi.org/10.1007/s10518-017-0152-4.

Quaah, A. O. (1980). Microseismicity, past seismic activity, and seismic risk in southern Ghana. Ph.D Thesis, University of London.

Rampello, S., Cascone, E., and Grosso, N. (2009). Evaluation of the seismic response of a homogeneous earth dam. *Soil Dynamics and Earthquake Engineering* 29(5): 782–798. https://doi.org/10.1016/j.soildyn.2008.08.006.

Reasenberg, P. (1985) Second-order moment of central California seismicity 1969-1982. *Journal of Geophysical Research* 90 (B7): 5479-5495.

Reid, H. F. (1910). The California earthquake of April 18, 1906. Report of the state earthquake investigation commission. Carnegie Institute, Washington DC.

Reiter, L., 1990. Earthquake Hazard Analysis: Issues and Insight. Columbia University Press, New York.

Richter, B. D., Postel, S., Revenga, C., Scudder, T., Lehner, B., Churchill, A., and Chow, M. (2010). Lost in Development's Shadow: The Downstream Human Consequences of Dams. Water Alternatives 3 (2): 14–42.

Rotondi, R., and Garavaglia, E. (2002). Statistical analysis of the completeness of a seismic catalogue." Natural Hazards, (25): 245- 258.

Rydelek, P. A. and Sacks, I. S. (1989). Testing the completeness of earthquake catalogues and the hypothesis of self-similarity. *Nature* (337): 251–253.

Sabetta, F., Lucantoni, A., Bungum, H., and Bommer, J. J. (2005). Sensitivity of PSHA results to ground motion prediction relations and logic-tree weights. *Soil Dynamics and Earthquake Engineering*, 25: 317-329. DOI:10.1016/j.soildyn.2005.02.002.

Schlüter, T. (2006). Geological Atlas of Africa: With Notes on Stratigraphy, Tectonics, Economic Geology, Geohazards and Geosites of Each Country. 2nd Edition, Springer-Verlag Heidelberg, pp. 307.

Schulte, S. M., and Mooney, W. D. (2005). An Updated Global Earthquake Catalogue for Stable Continental Regions: Reassessing the Correlation with Ancient Rifts. *Geophysical Journal International* 161: 707–721.

Shukla, J. and Choudhury, D. (2012) Estimation of seismic ground motions using deterministic approach for major cities of Gujarat, *Natural Hazards and Earth System Science*, 12(6); 2019–2037. doi: 10.5194/nhess-12-2019-2012.

Schwartz, D. P., and Coppersmith, K. J. (1984). Fault behaviour and characteristic earthquakes: Examples from the Wasatch and San Andreas fault zones. *Journal of Geophysical Research* 89(B7): 5681-5698. DOI:10.1029/JB089iB07p05681.

Scordilis, E. M. (2006). Empirical global relations converting M_S and m_b to moment magnitude. *Journal of Seismology* 10: 225–236. https://doi.org/10.1007/s10950-006-9012-4.

Selçuk, E. M., and Terzi, N.U. (2015). Seismic Response of Ambar Dam to Recorded Earthquake. 3(11): 979–993. *International Journal of Advanced Research* 11 (3): 979 - 994.

Sengupta, A. (2010). Estimation of permanent displacements of the Tehri dam in the Himalayas due to future strong earthquakes. *Sadhana - Academy Proceedings in Engineering Sciences* 35(3): 373–392. https://doi.org/10.1007/s12046-010-0011-3.

Shikhare, U. A., Maheshwari, B. K. and Paul, D. K. (2009). Seismic Analysis of an Embankment Dam Using Different Techniques. IGC 2009, Guntur, India, 793–797.

Sica, Stefania, Filippo Santucci de Magistris, and Filippo Vinale. 2002. "Seismic Behaviour of Geotechnical Structures." *Annals of Geophysics* 45(6): 799–815.

Singh, M., Kijko, A. and Van den Berg, L. (2011). Seismic risk ranking for large dams in South Africa. Acta Geophysica. 59(1): 72–90. https://doi.org/10.2478/s11600-010-0044-3.

Skinner, J., Niasse, M. and Haas, L. (eds.). (2009). Sharing the benefits of large dams in West Africa. Natural Resource Issues No. 19. *International Institute for Environment and Development*, London, UK.

Soro, A. M. (2016). Public Health Implications of Water Quality of the Kiri Reservoir, Adamawa State, Northeastern Nigeria. Thesis, American University of Nigeria.

Soumah, I. (2009). The future of Mining Industry in Guinea. Editions L'Harmattan. ISBN 978-2-296-21573-3.

Stepp, J. C. (1972). Analysis of Completeness of the Earthquake Sample in the Puget Sound Area and its effect on statistical estimates of earthquake hazard *Proceedings of the International Conference on Microzonation,* Seattle, USA (2): 897–910.

Stoneley, R. (1970). The History of the International Seismological Summary. *Geophysical Journal International*, 20(4): 343-349.

Stromeyer, D., Grünthal, G., and Wahlström, R. (2004). Chi-square regression for seismic strength parameter relations, and their uncertainties, with applications to an Mw based earthquake catalogue for central, northern and northwestern Europe. *Journal of Seismology*, *8*(1), 143–153. https://doi.org/10.1023/B:JOSE.0000009503.80673.51

Tavakoli, B., and Pezeshk, S. (2005). Empirical-Stochastic Ground-Motion Prediction for Eastern North America. *Bulletin of the Seismological Society of America* 95(6): 2283–2296. https://doi.org/10.1785/0120050030.

Thomas, G.A., and DiFrancesco, K. (2009). Rapid Evaluation of the Potential for Re-optimizing Hydropower Systems in Africa. The Natural Heritage Institute.

Toro, G. R. (2006). The effects of ground-motion uncertainty on seismic hazard results: examples and approximate results. Abstracts of the centennial meeting of the seismological society of America, San Francisco, USA.

Tosun, H., and Seyrek, E. (2010). Total risk analyses for large dams in Kizilirmak basin, Turkey. *Natural Hazards and Earth System Sciences*. 10(5): 979–987. https://doi.org/10.5194/nhess-10-979-2010.

Tosun, H., Zorluer, I., Orhan, A., Seyrek, E., Savaş, H., and Türköz, M. (2007). Seismic hazard and total risk analyses for large dams in Euphrates basin, Turkey. *Engineering Geolology*. 89(1–2): 155–170. https://doi.org/10.1016/j.enggeo.2006.10.003.

Tosun, H., Tosun, T. V. and Hariri-Ardebili, M. A. (2020). Total risk and seismic hazard analysis of large embankment dams: case study of Northwest Anatolia, Turkey, *Life Cycle Reliability and Safety Engineering*, 9(3): 329–338. doi: 10.1007/s41872-020-00113-4.

Tysdal, G. R. 1978. "Geology of the Juazohn Quadrangle, Liberia". Geological Survey Bulletin 1448. https://doi.org/10.3133/ofr74309.

Tysdal, R.G., and Thorman, C. H. (1983). Geological map of Liberia:1:1000000. U.S. Geological Survey Miscellaneous Investigations Series Map I-1480. https://doi.org/10.3133/i1480.

USBR. 2019. Seismic Risks for Embankments. Best Practices and Risk Methodology.

URS Corporation et al. (2002). Comprehensive Seismic Risk and Vulnerability Study for the State of South Carolina. Report of the South Carolina Emergency Preparedness Division (SCEPD) and HAZUS, CD-ROM.

Villeneuve, M., and Dallmeyer, R. D. (1987). Geodynamic evolution of the mauritanide, bassaride, and rokelide orogens (West Africa) . Precambrian Research 37(1): 19-28. https://doi.org/10.1016/0301-9268(87)90037-4.

Vick, S. G. (2002). Degrees of belief: Subjective probability and engineering. ASCE Publications. pp. 455

Wang, J., Walter, B. A., Yao, F., Song, C., Ding, M, Maroof, A. S., Zhu, J et al. (2021). GeoDAR: Georeferenced global dam and reservoir dataset for bridging attributes and geolocations, *Journal of Earth System Science.* Data Discuss. [preprint], https://doi.org/10.5194/essd-2021-58, in review, 2021.

Weatherill, G. (2010). A Monte Carlo Approach to Probabilistic Seismic Hazard Analysis in the Aegean Region. *Tectonophysics*, *492*(1–4), 253–278.

Wieland, M. (2012). 'Seismic Design and Performance Criteria for Large Storage Dams. 15th World Conference on Earthquake Engineering, Lisbon Portugal, 1999.

Wiemer, S. (2001). A software package to analyse seismicity: ZMAP. *Seismological Research Letters 72*(3): 373–382. https://doi.org/10.1785/gssrl.72.3.373.

Wiemer, S., and Wyss, M. (2001). Minimum Magnitude of Completeness in Earthquake Catalogs: Examples from Alaska, the Western United States, and Japan. *Bulletin of the Seismological Society of America* 90(4): 859–869.

Weichert, D. H. (1980). Estimation of the earthquake recurrence parameters for unequal observation periods for different magnitudes. *Bulletin of the Seismological Society of America* 70(4): 1337-1346. https://doi.org/10.1785/BSSA0700041337.

Wilson, D. S., and Squier, R. (1984). Earthquake and Rockfill Dams. State of-the-Art Report: International society for soil mechanics and Geotechnical engineering (ISSMGE), 137-220.

Woessner, J., and Wiemer, S. (2005). Assessing the Quality of Earthquake Catalogues: Estimating the Magnitude of Completeness and Its Uncertainty. *Bulletin of the Seismological Society of America* 95(2): 684–698.

Xie, X., and Heller, P. L. (2009). Plate Tectonics and Basin Subsidence History. *Bulletin of the Geological Society of America* 121(1–2): 55–64.

Yarwood, D.R., Doser, D. I. (1990). Deflection of oceanic transform motion at a continental margin as deduced from waveform inversion of the 1939 Accra, Ghana Earthquake. *Tectonophysics* 172(3-4): 341–349.

Youngs, R. R., and Coppersmith, K. J. (1985). Implications of fault slip rates and earthquake recurrence models to probabilistic seismic hazard estimates. *Bulletin of Earthquake Engineering* 75(4): 939-964. https://doi.org/10.1785/BSSA0750040939.

Zwahlen, R. (2012). Assessment, Social Impact, and Resettlement Action Plan. WEST AFRICAN POWER POOL (WAPP) Mount Coffee HPP ESIA and RAP Environmental and Social Impact Assessment and Resettlement Action Plan, no. 9.

APPENDIX A

Ground motion prediction equation developed by Chiou and Youngs (2014)

$$\ln(y_{refij}) = c_1 + \left\{c_{1a} + \frac{c_{1a}}{cosh(2.max(M_i - 4.5,0))}\right\} F_{RVi} +$$

$$\left\{c_{1b} + \frac{c_{1d}}{cosh(2.max(M_i - 4.5,0))}\right\} F_{NMi} + \left\{c_7 + \frac{c_{7b}}{cosh(2.max(M_i - 4.5,0))}\right\} \Delta Z_{TORi} +$$

$$\left\{c_{11} + \frac{c_{11b}}{cosh(2.max(M_i - 4.5,0))}\right\} (cos\delta_i)^2 + c_2 + (M_i - 6) + \frac{c_2 - c_3}{c_n} 1n(e^{c_n(c_M - M_i)}) +$$

$$c_4 \ln(R_{RUPij} + c_5 \cosh(c_6 . \max(M_i - c_{HM}, 0))) + (c_{4a} -$$

$$c_4)\ 1n\ (\sqrt{R_{RUPij}^2 + c_{RB}^2}) + c_8\ min(\frac{max\ (M_i - 40,0)}{30}, 0) +$$

$$\left\{c_{\gamma 1} + \frac{c_{\gamma 2}}{cosh(\ max(M_i -, c_{\gamma 3} 0))}\right\} R_{RUPij} + min(\frac{max\ (M_i - 5.5,0)}{0.8})\ e^{c_{8a}(M_i - c_{8b})\ \Delta DPP_i} j +$$

$$c_9 F_{HWij}\ cos\delta_i \left\{c_{9a} + (1 - c_{9a})\ tanh(\frac{R_{Xij}}{c_{9b}}\right\} \left\{1 - (\frac{\sqrt{R_{RUPij}^2 + Z_{TORi}^2})}{R_{RUPij} + 1}\right\} \quad \text{(A.1)}$$

where M_i = Moment magnitude for earthquake *i,* F_{RVi} = Reverse-faulting flag: 1 for 30° ≤ λ ≤ 150° (combined reverse and reverse-oblique), 0 otherwise; λ is the rake angle. F_{NMi} = normal faulting flag: 1 for −120° ≤ λ ≤ −60° (excludes normal-oblique), 0 otherwise, ΔZ_{TORi}= Z_{TOR} of centered on the *M*-dependent average Z_{TOR} (km), δ_i = Fault dip angle, R_{RUPij} = Closest distance to the ruptured plane(km), ΔDPP_{ij} = *DPP* centered on the site-

and earthquake-specific average *DPP*, *DPP* = Direct point parameter for directivity effect. R_{Xij} = Site coordinate measured perpendicular to the fault strike from the fault line, with the down-dip direction being positive(km). $c_1$to c_{11}, c_{HM}, c_n, c_M, c_{RB}, $c_{\gamma 1}$, c_{1a}, c_{4a}, c_{1b}, c_{7b}, c_{8a}, c_{9a}, c_{9b}, and c_{11b} are constant, are other variations reported by Chiou and Youngs (2014).

APPENDIX B

The list of updated earthquake catalogue for West Africa compiled from 1615 to 2018.

Table B.1: Compiled earthquake catalogue for West Africa from $M_{\mathrm{w}} \geq 4.0$

Day	Mon	Year	Hr:Mi	Lat.	Lon.	Depth	M_{w}	Reference
		1615		5.10	-1.30		5.5	A&A
18	Dec	1636	14:	5.10	-2.20		5.7	A&A
		1788		7.60	1.70		5.6	A&A
20	May	1795	22:	9.30	-13.40		5.2	A&A
	Jan	1818		12.1	-12.40		5.9	A&A
		1832		15.4	-17.0		4.1	A&A
	Dec	1836		5.10	-1.30		5.0	A&A
		1858		5.60	-0.20		4.5	A&A
		1861		6.00	0.00		4.5	A&A
23	Jul	1862	8:15	5.50	-0.25		6.8	A&A
23	Nov	1870	:12	5.30	-0.70		4.5	A&A
26	Jan	1871	:20	5.50	-0.40		4.6	A&A
14	Apr	1872	:23	5.50	-0.40		4.9	A&A
11	Feb	1879	:6	6.50	-3.30		5.7	A&A
13	Aug	1883	2:30	5.50	-0.40		4.6	A&A
5	Apr	1889	12:20	5.90	-0.20		4.0	A&A
		1889		6.80	-6.70		4.7	A&A
3	Nov	1892	22:	9.50	-13.70		4.0	A&A
		1894		5.50	-0.20		4.0	A&A

20	Nov	1906	:21	6.50	0.30		5.0	A&A
27	Feb	1907	22:15	6.10	-0.90		4.1	A&A
		1908		7.70	-7.80		5.7	A&A
25	Dec	1910		5.60	-0.20		4.0	A&A
2	Jan	1911	7:45	9.50	-13.80		5.3	A&A
17	Jun	1911	15:20	5.50	-0.20		4.0	A&A
		1912		5.50	-3.60		4.0	A&A
8	Feb	1914		10.20	-14.00		4.0	A&A
11	Jul	1927	11:30	9.80	-13.30		4.0	A&A
5	Apr	1928	8:2	9.80	-13.30		5.3	A&A
26	Mar	1930	20:30	10.20	-14.10		5.1	A&A
6	Jan	1933	:4	7.00	0.60		4.0	A&A
29	May	1935		6.90	0.60		4.0	A&A
17	Jul	1935	15:35	10.30	-14.30		5.6	A&A
26	May	1939	7:	9.60	-13.20		4.1	A&A
22	Jun	1939	19:19	5.18	-0.13	15	6.4	A&A
18	Aug	1939	4:51	6.2	-0.30		5.5	A&A
25	Dec	1939		11.10	-2.10		6.4	A&A
4	Apr	1950	22:9	6.80	-4.60		4.0	A&A
20	Oct	1950	15:21	7.50	0.50		4.0	A&A
4	Jan	1957	18:16	7:40	-12.50		5.7	A&A
2	Jul	1961		5.50	7.50		4.0	A&A
11	Mar	1964	12:45	5.90	-0.39		4.7	ISC
4	Nov	1967	11:15	11.00	12.00		4.8	A&A
9	Feb	1969	18:29	5.90	-0.39		5.2	ISC
10	Oct	1969	7:17	5.52	-0.12		4.3	MUS
		1975		12.40	8.50		4.0	A&A
22	Dec	1983	4:11	11.93	-13.50	11.3	6.3	A&A/USGS
28	Jul	1984	13:	7.34	3.71		4.0	A&A
	Dec	1984	13:	9.29	12.50		4.8	A&A
17	Jun	1985	4:11	11.36	-13.50	10	4.7	ISC
10	Jun	1987	20:2	11.38	-11.24	10	4.8	ISC
2	Nov	1987	18:7	11.44	-13.44	10	4.6	USGS/ISC
14	Jul	1970	4:3	13.70	6.00		4.1	A&A

6	Apr	1993	14:29	11.30	1.60	2	4.1	ISC
20	Oct	1995	14:6	5.81	-0.51	10	4.6	ISC
25	Nov	1995	0:4	6.77	-10.93	10	4.9	USGS/ISC
14	Feb	1997	23:29	6.98	-0.75	10	4.3	ISC
6	Mar	1997	15:16	5.59	-0.23	10	4.7	ISC
11	Jan	1999	18:1	13.97	-8.61	33	4.3	USGS
27	Mar	1999	18:4	3.96	8.65	10	4.6	ISC
28	Mar	1999	20:12	3.73	8.77	10	4.3	ISC
14	Dec	1999	22:48	13.92	-2.64	10	4.2	ISC
7	Mar	2000	15:53	6.29	5.07	10	4.7	ISC
17	Jan	2001	4:21	8.09	-10.24	10	4.8	USGS/ISC
2	Mar	2004	0:23	10.39	-14.08	10	4.7	USGS
2	Jul	2004	20:38	9.66	-13.55	10	4.3	ISC
26	Jan	2006	11:28	9.52	-8.91	10	4.3	ISC
11	Sep	2009	3:10	6.68	2.42	2	4.7	ISC
3	Nov	2011	13:2	14.35	-1.52	10	4.3	ISC
19	Mar	2012	2:26	9.41	-9.69	10	4.0	ISC
6	Aug	2012	14:29	9.33	-8.73	10	4.8	USGS
23	Aug	2012	22:3	11.79	-13.33	10	4.2	USGS
24	Jul	2014	19:58	5.87	-0.59	10	4.1	ISC
8	Aug	2015	15:31	6.86	2.21	10	4.3	ISC
12	Dec	2015	21:26	9.67	-8.45	10	4.2	ISC
17	Mar	2017	0:4	8.92	-9.45	10	4.1	ISC
12	Apr	2017	6:36	10.57	-12.07	10	4.5	ISC
5	May	2017	3:30	10.66	-11.98	10	4.3	ISC
19	Feb	2018	16:2	11.80	-11.95	13.66	4.8	USGS
22	Apr	2018	2:40	11.91	-11.17	10	4.0	ISC
21	Aug	2018	17:57	9.38	-10.15	10	4.2	ISC
3	Nov	2018	19:19	10.92	-13.83	10	4.3	ISC
9	Dec	2018	7:49	5.68	-0.45	10	4.7	ISC

A&A: Ambraseys and Adams, USGS: United States Geological Survey, ISC: International Seismological Centre.

APPENDIX C

Table C.1: Weights for different ground motion prediction equations for different seismic source zones.

Zone	M_{max}	TP2005	PEAL2011	ASK2014	CB2014	CY2014
G	7.3			0.53	0.37	0.10
M	6.8			0.48	0.41	0.11
A	5.3	0.57	0.43			
B	5.3	0.57	0.43			
C	5.3	0.57	0.43			
D	4.7	0.47	0.53			
E	6.1	0.58	0.42			
F	4.8	0.48	0.52			
H	6.2	0.59	0.41			
I	4.8	0.48	0.52			
N	4.8	0.48	0.52			
J	6.4	0.63	0.37			
K	5.3	0.57	0.43			
L	5.2	0.57	0.43			

APPENDIX D

Table D.1. Seismicity parameters used in the study model.

Zone		M_{obs}	M_{max}	$b \pm \sigma b$	a	λ
Group (1)	G	6.8	7.3	0.63± 0.13	3.916	0.156
Group (2)	M	6.3	6.8	0.60± 0.11	3.370	0.165
Group (3)	A	4.8	5.3	1.12± 0.29	6.584	0.015
	B	4.8	5.3			0.010
	C	4.8	5.3			0.030
	D	4.2	4.7			0.015
	E	5.6	6.1			0.004
	F	4.3	4.8			0.015
	H	5.7	6.2			0.020
	I	4.3	4.8			0.010
	N	4.3	4.8			0.010
	J	5.9	6.4			0.035
	K	4.8	5.3			0.020
	L	4.7	5.2			0.015

APPENDIX E

Table E.1. Numbers of people and values of properties at risk at various dam sites.

Dam	Human population	Values of property	Reference
Akosombo	18,142	3,703	Ntiamoa-Baidu et al., (2017)
Asejire	2,579	<1,000	Oyedotun (2011)
Banieya	<1,000	<1,000	
Bakolori	29,680	>1,000	Richter et al. (2010)
Dadin Kowa	26,000/30,690	>1,000	Jesse et al., (2019), Soro (2016)
Garafiri	<1,000	<1,000	
Goronyo	>1,000	>1,000	
Ilauko	>1,000	>1,000	
Jibiya	>1,000	>1,000	
Kale	<1,000	<1,000	
Kiri	33,627	>1,000	Soro (2016)
Kpong	18,142	3,703	Ntiamoa-Baidu et al., (2017)
Mt. Coffee	3,000	<1,000	Zwahlen (2012)
Nangbeto	16,000	>1,000	Anon (2018), Thomas and DiFrancesco (2009),
Oyan	1,280	<1,000	Oyegoke and Sojobi (2012)
Souapiti	16,000	>1,000	Dagne and Sandler (2020)
Weija	15,892	2,670	GSS (2014). Owusu-Ansah et al. (2019)

(This page is intentionally left blank)